Durham E-Theses

Chiral Interactions and Sensing at Liquid/Liquid Interface

LOPES, PAULA,CRISTINA,DIAS

How to cite:

Use policy

Chiral Interactions and Sensing at Liquid|Liquid Interface

Paula Cristina Dias Lopes

A thesis submitted in part fulfilment
of the requirements for the degree of
Doctor of Philosophy

Durham University

Department of Chemistry

Durham University

July 2012

Thesis accepted by:

Ritu Kataky, supervisor

Dr Sharon Cooper, internal examiner

Professor Frank Marken, external examiner

Department of Chemistry

Durham University

July 2012

Abstract

Chiral interactions of compounds with therapeutic interest and its study predicting and interpreting transport process across biological barriers represents one of the most important topics in research. This thesis is devoted to the study of chiral ion transfer at the interface between two immiscible electrolytes solutions (ITIES), as a promising method of simplifying chiral detection and separation.

As a proof of concept, for the study of chiral compounds at liquid|liquid interface, three different approaches were used: i) chiral stationary phases based on modified cyclodextrins, AcαCD and AcβCD, ii) chiral acute phase protein, α_1-acid-glycoprotein (AGP) and iii) thick film electrode modified with an ethylated cyclodextrin ferrocene (EtCDFc). The chiral selectors used, AcαCD, AcβCD, AGP and EtCDFc display complex three-dimensional structures that are capable of recognising specifically the enantiomers of a drug molecule, with different affinity. Cyclic voltammetry (CV) and differential pulse voltammetry (DPV) were used to investigate the enantioselective interaction between the chiral molecules.

In the study of chiral ion transfer using AcαCD and AcβCD, as a chiral organic phase, it was observed that the two lipophilic CDs facilitated the transfer of ephedrine ions by the formation of inclusion complexes. The enantioselectivity was achieved as the complexes between the protonated ephedrine ions and the CDs lead two different signal responses as a result of different affinities in the complex formation. Furthermore, the positive enantiomer $(+)EPH^+$ showed to be consistently the cation being transferred at less positive potentials suggesting that it binds preferentially with the chiral selectors, in

comparison with (-)EPH$^+$, indicating that its transfer is more facile. The difference in stability constant between the (+)EPH$^+$ and (-)EPH$^+$ complexes was found to be 1.41±0.1 for AcβCD and 1.20±0.1 for AcαCD.

When investigating the chiral interactions between the AGP and the three basic drugs (propranolol, lidocaine and procaine hydrochloride), it was found, that the plasma protein binds to the protonated drugs with clear different affinities. The formation of a complex between the drugs and AGP was shown as a decrease in the CV and DPV responses, corresponding to the reduction in the transfer of the cationic drugs, as only the unbound (free) drug was able to be transferred across the liquid|liquid interface. The bound and unbound drug concentration was estimated in a different range of concentrations based on the responses obtained in the presence and absence of the protein. The differences in current responses, observable in the measurements, lead to chiral discrimination between R- and S-propranolol. Scatchard analysis was employed to calculate the association constant and the number of binding sites of the drugs with AGP. The calculated association constants were 2.7×10^5 M^{-1} for S- and 1.3×10^5 M^{-1} for R-propranolol, which were significantly higher than those for lidocaine, 1.2×10^4 M^{-1}, and for procaine, 8.4×10^3 M^{-1}. This showed that AGP has more affinity for R- and S-propranolol than lidocaine or procaine hydrochloride.

A thick film modified electrode with a chiral redox probe, ethylated ferrocene cyclodextrin (EtCDFc) was used to study chiral ion transfer across the liquid|liquid interface coupled to a redox reaction. EtCDFc has a dual role, a redox active moiety and a cyclodextrin moiety which is able to form chiral complexes. Thus, the redox reaction of EtCdF was accompanied by the complexation of mandelic acid enantiomers with the cyclodextrin part of EtCDFc, with the two reactions mutually influencing each other. In addition the thick film ensured that the generated product of the molecular probe was within the

diffusion layer and away from the aqueous|organic solvent interface, so that the charge neutrality of the organic film was only maintained by the presence of ions from the aqueous phase.

Keywords: Liquid|liquid interface, chiral discrimination, ion transfer, cyclodextrins, α_1-acid-glycoprotein.

"Há quem passe a vida inteira lendo sem conseguir ir para além da leitura, ficam agarrados às páginas, não entendem que as palavras são só pedras colocadas para atravessarmos a corrente de um rio, e se estão ali é para podermos chegar à outra margem, pois o que importa é a outra margem."

"Some people spend their entire lives reading but never get beyond reading the words on the page, they do not understand that the words are merely stepping stones placed across a fast-flowing river, and the reason they are there is so that we can reach the farther shore, it's the other side that matters."

— José Saramago (1922-2010)

Portuguese novelist and man of letter, Nobel Prize for literature in 1998

Acknowledgements

First and foremost, I wish to thank my supervisor, Dr Ritu Kataky, for her support and encouragement over the last four years. Thank you for providing me the opportunity to work in the research area of electrochemistry, for sharing your scientific knowledge and experience. Also, for giving me the opportunity and confidence to write scientific papers and to participate in many international conferences. I personally want to say that 'your guidance and devoting care has made my working and learning experience a very special one. Thank you for everything.'

To the members of my supervisory committee, Professor Colin Bain, in the chemistry department and Professor David Wood, in the school of engineering and computing sciences, for their interesting and helpful scientific discussions, especially at the beginning of my PhD.

To Helen Riggs, in the chemistry department, for technical assistance with ESEM images.

To the staff in the department of chemistry, particularly: Jean, Tony, Elizabeth, Jeff, people in the glass, electrical and mechanical workshop. Thank you all for your help during these years.

Many thanks go also to the members, past and present, of the sensors group. Your positive attitude made the MC201/2 a good and pleasant place to work in.

Declaration

The research described in this thesis was undertaken in the Department of Chemistry of Durham University between October 2007 and March 2012. All work is my own, other than where stated otherwise. No part of this work has been submitted previously for a degree at this or any other university.

Aspects of chapters 4 and 5 are based on the following published work:

- Kataky, R, Lopes, P., Chem. Commun., **2009**, 1490-1492.

- Lopes, P., Kataky, R., Anal. Chem., **2012**, 84 (5), 2299–2304.

Statement of Copyright

The copyright of this thesis rests with the author. No quotation from it should be published in any format, including electronic and internet, without the author's prior written consent. All information derived from this thesis should be acknowledged appropriately.

Table of Contents

List of symbols and abbreviations

Symbol	Meaning	Value and/or Units
A	Interfacial area	μm^2
C	Concentration of the species	M
D	Diffusion coefficient	$cm^2 \, s^{-1}$
E	Potential difference	V
$E^{1/2}$	Half-wave potential	V or mV
F	Faraday constant	$96485 \, C \, mol^{-1}$
I_p	Peak current	A or nA
I_a	Anodic current	A or nA
I_c	Cathodic current	A or nA
j	Current density	$A \, cm^{-2}$ or $nA \, cm^{-2}$
k	Boltzmann constant	$1.38066 \times 10^{-23} \, J \, K^{-1}$
K_a	Association constant	-
K_d	Dissociation constant	-
K	Equilibrium constant	
R	Gas constant	$8.31451 \, K^{-1} \, mol^{-1}$
T	Absolute temperature	K
t	Time	
ϕ	Inner (or Galvani) potential	V
ϕ_i	Potential drop across the inner layer	V
$\Delta_o^w \phi$	Interfacial (Galvani) potential difference	V
$\Delta_o^w \phi_i^0$	Standard ion transfer potential	V
$\Delta_o^w \phi_i^{0\prime}$	Formal ion transfer potential	V

$\Delta G_{tr}^{0,w\rightarrow o}$	Standard Gibbs transfer energy of an ion i from the water (w) to the organic (o)phase	J mol^{-1}
ΔG	Gibbs free energy change in a chemical reaction	J mol^{-1}
μ_i^0	Standard chemical potential of the ion i	J mol^{-1}
$\tilde{\mu}_i$	Electrochemical potential of the ion i	J mol^{-1}
μ_i	Chemical potential of i	J mol^{-1}
I_{ss}	Steady-state current	A or nA
υ	Scan rate	V s^{-1} or mV s^{-1}
a	Radius of the tip	μm
$\emptyset$	Micropipette diameter	μm
γ	Activity coefficient	-
∇	Gradient	-
i	Species i	-
r^2	Regression coefficient of linear fits	-
P	Partition coefficient	-
J(x,t)	Flux at distance x and time t	mol cm^{-2} s^{-1}
ε	Permittivity	-
η	Solvent viscosity	Kg m^{-1} s^{-1}
z	Charge number	-
δ	Diffusion layer thickness	cm
τ	Time period	s

Abbreviation	Meaning
'TATP'	Teraphenylarsonium tetraphenylborate assumption
1,2-DCE	1,2-dichloroethane
a	Activity
ACT	Aqueous Complexation followed by Transfer
AcαCD	Hexakis(2,3,6-tri-O-Acetyl)-α-Cyclodextrin
AcβCD	Heptakis(2,3,6-tri-O-Acetyl)-β-Cyclodextrin
AH	Protonated acid
BH^+	Protonated base
CD	Cyclodextrin
CE	Counter electrode
CT	Charge transfer
CV	Cyclic voltammetry
DPV	Differential pulse voltammetry
e	Electron
ET	Electron transfer
EtCDFc	Ferroceneacetamido-6^A-deoxy-heptakis-(2,3-di-O-ethyl)-6^B,6^C,6^D,6^E,6^F-hexa-O-ethyl-β-cyclodextrin
Fc	Ferrocene
FIT	Facilitated ion transfer
FWD	Forward potential scan
HPLC	High performance liquid chromatography
IT	Ion transfer
ITIES	Interface between two immiscible electrolyte solutions
L	Ligand
LC	Liquid Chromatography
M	Ion
NB	Nitrobenzene
NMR	Nuclear magnetic Resonance

o	Organic or non-aqueous phase
OHP	Outer Helmoltz Plane
pzc	Potential of zero charge
RE	Reference electrode
REV	Reverse potential scan
SECM	Scanning Electrochemical Microscopy
TBA^+	Tetrabutylammonium cation
TEA^+	Tetrabuthylammonium cation
TIC	Transfer by Interfacial Complexation
TID	Transfer by Interfacial Decomplexation
TMA^+	Tetramethylammonium cation
TOC	Transfer by Organic Complexation
$TPAs^+$	Tetraphenylarsonium cation
TPB^-	Tetraphenylborate anion
tr	Transfer
w	Water or aqueous phase
WE	Working electrode

List of Figures

Page

3. Experimental methodology

4. Lipophilic cyclodextrins as chiral selectors at a liquid|liquid interface

6. Lipophilic cyclodextrins as chiral selectors at a liquid|liquid interface

Appendix

List of Tables

Chapter 1

Introduction

Chirality has always been an important issue for pharmaceutical research and industries, because most organic compounds and biological molecules, including many drugs and food additives, own chirality.[1] The presence of asymmetric centre(s) in chiral compounds gives rise to optical activity that can be responsible for the different properties of the enantiomers.

In pharmacology, chirality is an important fact in drug efficacy. About 56% of the drugs in use are chiral compounds, and about 88% of these chiral synthetic drugs are administrated as racemates.[2,3] Although the S or R isomers have the same substituent atoms or groups, qualitatively or quantitatively may have similar or different pharmacological effects, which may relate to their stereoselective pharmacokinetics or pharmacodynamics. The differences in the enantiomer pharmacodynamic activity and pharmacokinetic property are related to their different affinity or intrinsic activity at receptor site, thus the body exhibits different physiological responses to different enantiomers. One enantiomer may produce the desired therapeutic activities, while the other may be inactive or exhibit serious side effects. The elucidation of chiral interactions represents a significant challenge for a number of applications including drug interactions and toxicity measurements.

In recent years, chiral detection and separation has been achieved by a variety of methods such as: liquid chromatography (LC),[4–9] high pressure liquid chromatography (HPLC),[7-9] gas chromatography (GC),[13–17] capillary electrophoresis (CE),[18–21] nuclear magnetic resonance spectroscopy (NMR),[13,22–26] circular dichroism (CD)[27–29] and potentiometry.[30–33] While the chromatographic methods can be mostly used for the qualitative enatioanalysis,[34] enantioselective potentiometry and amperometry (potentiometric membrane electrodes and amperometric biosensors) can be used with a high reliability for the quantitative enantioanalysis.[35,36] All the enantioselective techniques share a common goal, to construct an effective chiral selective system by the presence of a chiral selector able to interact with both enantiomers although with different affinities. However, the selection of the chiral selector is still one of the most critical tasks in molecular recognition of enantiometric pairs.[1]

In my PhD work, I characterized dynamics of chiral ion transport in the presence and absence of recognition events using liquid-liquid interface approaches as a challenging alternative to the commonly used techniques. Interactions at a liquid|liquid interface studied by ion-amperometric measurements, rather than potentiometric measurements, are more sensitive, allow access to the estimation of enantioselective Gibbs free energies of transfer between an aqueous and a lipophilic phase and can be adapted to enable separation and detection.

The interface between two immiscible electrolyte solutions (ITIES) can be viewed as an artificial model of a cell membrane (Figure 1.1); it can be used to study phenomena of biological relevance by means of their electrochemical process. The unique properties of ITIES can be used to understand electrochemically controlled interfacial ion recognition and transfer, by the control of the interfacial potential.
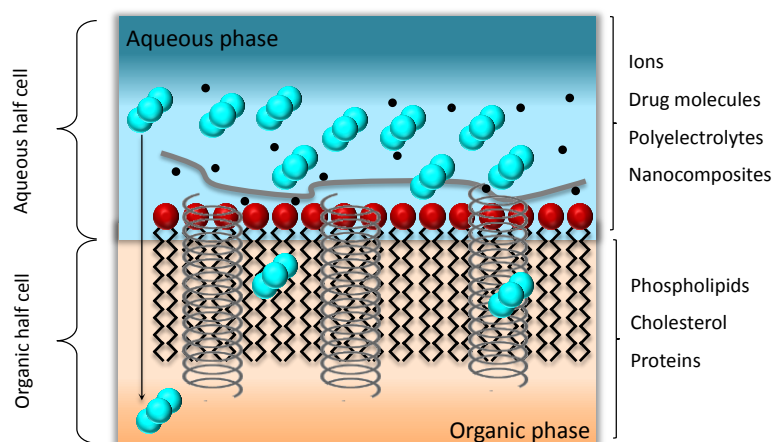
Figure 1.1 – A schematic illustration of a simple model of the biological membrane. Reproduced with permission from Santos et al.[37]

The purpose of the research presented in this thesis was to study the interaction between chiral molecules and ligands with high sensitivity, simplicity and low cost requirements, so that electrochemical approaches can be seen as an alternative method for the analysis of chiral compounds. Different chiral recognition events were examined qualitatively and quantitatively, demonstrating that the interfacial chiral interactions at liquid|liquid interface can be used as a sensing principle. Although, the focus of my research was primarily in the detection of mixtures of chiral enantiomers, the proof of concept was achieved with pure enantiomers.

In chapter 2 is described the general theory of the charge transfer reactions at the ITIES and the outline of various methodologies that electrochemistry at liquid|liquid interface can offer for analytical purposes. It focuses on the interfacial structure and kinetics as well as the various applications of ITIES and recent advances in the field, which serves as a background of the concepts that were employed in the research presented in this thesis.

Chapter 3 shows the experimental details of each of the experimental chapters. Materials, instrumentations and detailed experimental information are given. A description of the electrochemical techniques used is also given.

In chapter 4 the study of the discrimination between the enantiomers of a chiral molecule, ephedrine hydrochloride, is presented. Two different lipophilic chiral stationary phases, Hexakis(2,3,6-tri-O-Acetyl)-α-cyclodextrin (AcαCD) and Heptakis(2,3,6-tri-O-Acetyl)-β-cyclodextrin(AcβCD), to characterize the transfer of the chiral ions and the chiral interactions, were used.

Chapter 5 shows the transfer of the enantiomers of a β-blocker, propranolol hydrochloride in the presence and the absence of a chiral acute phase plasma protein, α_1-acid glycoprotein. The approach was extended to other molecules, anaesthetic drugs, lidocaine and procaine.

The study of a chiral acid, mandelic acid, at modified thick electrode is shown in Chapter 6. A modified thick electrode containing a cyclodextrin modified with ferrocene was used as a transducer to differentiate between the R- and S- enantiomers.

In chapter 7 of this thesis are presented general conclusions, together with possible future work. Suggestions of further directions and improvements for the study of chiral interactions at liquid|liquid interface are discussed.

References

(1)   Izake, E. L. *J. Pharm. Sci.* **2007**, *96*, 1659–1676.

(2)   Walther, W.; Netscher, T. *Chirality* **1996**, *8*, 397–401.

(3)   Rentsch, K. M. *Journal of Biochemical and Biophysical Methods* **2002**, *54*, 1–9.

(4)   Herráez-hernández, R.; Campins-Faco, P. *Anal. Chim. Acta* **2001**, *434*, 315–324.

(5)   Allenmark, S.; Bomgren, B.; Borén, H. *J. Chromatogr. A* **1983**, *264*, 63–68.

(6)   Singh, A. K.; Kedor-Hackmann, E. R. M.; Santoro, M. I. R. M. *Revi. Bras. Cienc. Farm.* **2004**, *40*, 301–308.

(7)   Noggle, F. T.; DeRuiter, J.; Clark, C. R. *Anal. Chem.* **1986**, *58*, 1643–1648.

(8)   Wang, Z.; Ouyang, J.; Baeyens, W. R. G. *J. Chromatogr. B* **2008**, *862*, 1–14.

(9)   Toyo'oka, T. *J. Biochem. Bioph. Meth.* **2002**, *54*, 25–56.

(10)   Armstrong, D. W.; Zhang, B. *Anal. Chem.* **2001**, *73*, 557 A–561 A.

(11)   Gubitz, G.; Schmid, M. G. *Biopharm. Drug Dispos.* **2001**, *22*, 291–336.

(12)   Fitos, I.; Visy, J.; Simonyi, M. *J. Biochem. Bioph. Meth.* **2002**, *54*, 71–84.

(13)   LeBelle, M. J.; Savard, C.; Dawson, B. A.; Black, D. B.; Katyal, L. K.; Zrcek, F.; By, A. W. *Forensic Sci. Int.* **1995**, *71*, 215–223.

(14)   Nie, M. Y.; Zhou, L. M.; Wang, Q. H.; Zhu, D. Q. *Anal. Sci.* **2001**, *17*, 1183–7.

(15)   Nie, M. Y.; Zhou, L. M.; Wang, Q. H.; Zhu, D. Q. *Chromatographia* **2000**, *51*, 736–740.

(16)   Schurig, V.; Nowotny, H.-P. *Angew. Chem. Int. Edit.* **1990**, *29*, 939–957.

(17)   Yu, Z.; Cui, M.; Yan, C.; Song, F.; Liu, Z.; Liu, S.; Zhang, G.; Zhang, H. *J. Mass Spectrom.* **2007**, *42*, 1106–1110.

(18)   Marusza, W.; Trojanowicz, M.; Margasińska, M.; Engelhardt, H. *J. Chromatogr. A* **2001**, *926*, 327–236.

(19)   Matchett, M.; Branch, S.; Jefferies, T. *J. Chromatogr. A* **1995**, *705*, 351–361.

(20)   Schmid, M. G.; Wirnsberger, K.; Jira, T.; Bunke, A.; Gubitz, G. *Chirality* **1997**, *9*, 153–156.

(21)   Liu, J.; Coffey, H.; Detlefsen, D. J.; Li, Y.; Lee, M. S. *J. Chromatogr. A* **1997**, *763*, 261–269.

(22)   Holzgrabe, U.; Mallwitz, H.; Branch, S. K.; Jefferies, T. M.; Wiese, M. *Chirality* **1997**, *9*, 211–219.

(23)   Alexander, J. M.; Clark, J. L.; Brett, T. J.; Stezowski, J. J. *PNAS* **2002**, *99*, 5115–5120.

(24)   Spisni, A.; Corradini, R.; Marchelli, R.; Dossena, A. *J. Org. Chem.* **1989**, *54*, 684–688.

(25)   Bates, P. S.; Kataky, R.; Parker, D. *J. Chem. Soc. Farad. T. 2* **1994**, 669–675.

(26)   Ndou, T. T.; Mukundan, S.; Warner, I. M. *J. Incl. Phenom. Macro.* **1993**, *15*, 9–25.

(27)   Li, S.; Purdy, W. C. *Anal. Chem.* **1992**, *64*, 1405–1412.

(28)   Krois, D.; Lehner, H. *J. Chem. Soc., Perkin Trans. 2* **1995**, 489–494.

(29)   Oravcová, J.; Bystricky, S.; Trnovec, T. *Biochem. Pharmacol.* **1989**, *38*, 2575–2579.

(30)   Gafni, A.; Cohen, Y.; Kataky, R.; Palmer, S.; Parker, D. *J. Chem. Soc. Farad. T. 2* **1998**, 19–24.

(31) Kaniewska, M.; Sikora, T.; Kataky, R.; Trojanowicz, M. *J. Biochem. Bioph. Meth.* **2008**, *70*, 1261–1267.

(32) Kataky, R.; Bates, P. S.; Parker, D. *Analyst* **1992**, *117*, 1313–1317.

(33) Bates, P. S.; Kataky, R.; Parker, D. *J. Chem. Soc., Chem. Commun.* **1992**, 153–155.

(34) Bojarski, J.; Aboul-Enein, H. Y.; Ghanem, A. *Curr. Anal. Chem.* **2005**, *1*, 59–77.

(35) Aboul-Enein, H. Y.; Stefan, R.-I.; van Staden, J. F. *Anal. Lett.* **1999**, *32*, 623–632.

(36) Stefan, R.-I.; van Staden, J. (Koos) F.; Aboul-Enein, H. Y. *Electroanal.* **1999**, *11*, 1233–1235.

(37) Santos, H. A.; García-Morales, V.; Pereira, C. M. *ChemPhysChem* **2010**, *11*, 28–41.

Chapter 2

Fundamental aspects of electrochemistry at the liquid|liquid interface

This chapter presents an introduction to electrochemistry at liquid|liquid interfaces, which is an important aspect of this thesis. The structure, types and the various charge transfer reactions at the interface are detailed.

2.1 Introduction

The interface between two immiscible liquids is a unique environment and has tremendous significance in the real world and life in general. The processes that occur at these interfaces underlie many important phenomena in chemistry and biology. The transport and exchange of mass across the liquid interface between lipid bilayer membranes and aqueous body fluids play key roles in life activity. All energy conversion processes in living organisms occur by nature at liquid interfaces.[1,2]

Liquid|liquid interfaces, also named Interfaces between Two Immiscible Electrolyte Solutions (ITIES) are formed between two liquid solvents of low (ideally zero) mutual miscibility.[3] One of these solvents is usually water, and the other is a polar solvent with moderate or high dielectric permittivity. The ITIES is by nature, a molecular interface characterised by very unique electrical, structural, dynamical and thermodynamic properties, which are different from those of the bulk liquids.[1,2,4]

Electrochemical studies at liquid|liquid interfaces have evolved into a well-established scientific field during the past decades. Many traditional electrochemical experiments and theoretical approaches of interfacial chemistry have contributed much to the actual understanding of the phenomena occurring at the ITIES.

The studies at liquid|liquid interfaces using electrochemical methods started in the beginning of the last century by Nernst and Riesenfeld,[5] who observed the transfer of ions during the passage of current through water-phenol-water interface. They were the first to investigate the effect of electric current flow across the ITIES.[3] The interest in the field spread when Cremer[6] pointed out in 1906 the analogy between water-oil-water systems with biological membranes and their surrounding electrolytes. The liquid|liquid interface became a model for the investigation of bioelectrical potentials and currents observed in

the living cells. In 1939, Verwey and Niessen[7] introduced the first theoretical study on ITIES regarding the electrical double layer and potential distribution. This study represented a physical model of the ITIES as two back-to-back Gouy-Chapman[8,9] diffuse layers.

The 1970s were marked by two key contributions that made the field of ITIES an integrant part of electrochemistry. The first was an experimental method by Gavach[10] for realizing that ITIES could be polarized and the Galvani potential difference between the two phases could be used as a driving force for the charge transfer reactions.[11] The second contribution was by Koryta[12] who has developed the concept of ideally polarized ITIES, demonstrating that the ITIES were polarisable in the same way as the interface between metallic electrodes and electrolyte solution. It was ensured that techniques commonly used for the measurement of electron transfer at solid|liquid interfaces could be applied in the study of ion transfer processes through ITIES, techniques such as: cyclic voltammetry,[13] chronoamperometry,[14] polarography,[15] differential pulse stripping voltammetry[16] and ac voltammetry.[17]

Another important milestone was added by Samec et al.[13,18–20] with the introduction of the four electrode potentiostat with iR drop compensation by means of a positive feedback loop. It opened a new route to use controlled potential techniques for the study of charge transfer reactions at the ITIES. Meanwhile, Koryta et al.[21] established the theoretical background for a series of electrochemical cells and pioneered the study of facilitated ion transfer by ionophores.

In 1986, Taylor and Girault[22] introduced the micro sized ITIES by means of supporting the interface at the tip of a glass of a micropipette. Another method of fabricating a micro-ITIES was developed by Campbell and Girault[23] in 1989, which developed a micro-hole, in a thin inert membrane using a UV laser photoablation to support the

interface. The micro-ITIES has been extensively employed in amperometric and potentiometric sensors.[24–26]

More recently work on modified liquid|liquid interface with lipids[27,28] and nanoparticles[29–31] have been reported. Droplet electrodes[32,33] and three-phase junctions[34] have made this field more popular and versatile. The electron transfer (ET) induced ion transfer (IT) reactions at three-phase junction have been employed to obtain a measure of lipophilicity (Log P) of different drugs at water-noctanol interfaces.[33]

The study of electrochemical processes at liquid|liquid interface has progressed in a remarkable way in the last 30 years, and is of continuing interest to many researchers, because their relevance to such diverse applications. Examples include ion transport across biological membranes,[35] drug delivery,[36] behaviour of ion-selective electrodes with liquid membranes and similar sensors,[37] extraction processes,[38] phase transfer catalysis,[39] pharmacology,[40,41] acid-base processes,[42] charge transfer,[43–46] adsorption-desorption,[35] complexation,[47] modelling of interactions at biological cell membranes,[48,49] solvation dynamics[50], fundamental studies of the nature of such interface,[51] and many applications in electroanalytical chemistry.[41,52–54]

2.2 Electrochemistry at ITIES

Electrochemistry at the ITIES differs from the conventional electrochemical experiments in that the reaction under study occurs at a liquid|liquid interface rather than at a typical electrode|electrolyte interface. In order to describe the charge transfer reactions at liquid|liquid interface, the process at an electrode|electrolyte interface must first be considered.

At an electrode|electrolyte interface, the interfacial potential difference arises from the difference in electronic energy between a redox couple present in solution and the

electrode. The metal can act as a source of electrons for the species in solution until the ionic levels of redox couple and the Fermi level[55] of the metal electrode are at equilibrium. The result is that the metal loses (or gains) electron density; when the equilibrium is reached, there will be a difference in charge and therefore a difference in potential between the metal electrode and the solution.

At liquid|liquid interface, the origin of the potential difference is due to the partitioning of the ions of a salt between the two phases. Girault and Schiffrin[56] made a full treatment of the interfacial potential where they demonstrate that the solvation energies of the salt under examination, the distribution (or partition) coefficients of the salt and the electrical potentials which arise from the ionic partitioning, are fundamental properties that must be considered. In any case, the interfacial regions should be electrically neutral.

The potential difference is the most characteristic feature of every interface and is highly dependent on the conditions of the thermodynamic equilibrium over the two phases.

The main advantage of studies at liquid|liquid interface in comparison with conventional electrochemical experiments is that the study of charge transfer processes is not limited to the study of the electron transfer reactions. These charge transfer can be classified in three main categories: (i) ion transfer (IT), (ii) electron transfer (ET), (iii) facilitated ion transfer (FIT) reaction. Thus, a large number of ion transfer reactions important to biological systems which would be impossible to explore with conventional metal electrodes, can be studied using liquid|liquid electrochemistry.

2.3 Charge transfer reactions at the ITIES

2.3.1 Ion transfer at the ITIES

When two different immiscible liquids are brought in contact, a potential is established from the dipoles orientation in the vicinity of the interface and due to the existence of excess free charges. The charge carries of the two immiscible liquids will partition between the two phases (aqueous: w and organic: o) by transferring across the interface (Figure 2.1).
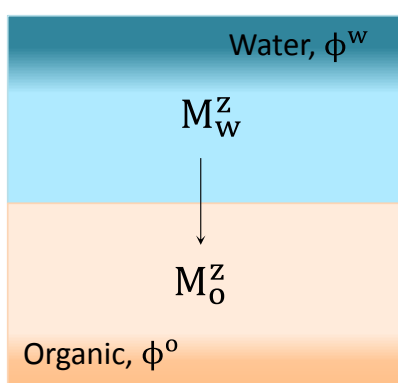
Figure 2.1 – Transferring of M^z ion from the aqueous to the organic phase. The ionic charge is transferred from the aqueous phase at the potential ϕ^w to the aqueous phase at the potential ϕ^o.

This generates an interfacial region, in which the electrical field strength differs from zero so that a Galvani potential difference is established across the interface between two phases:

$$\Delta_o^w\phi = \phi^w - \phi^o \qquad (2.1)$$

Where ϕ is the inner (or Galvani potential) of the respective phase. Thus, two back-to-back space charged regions known as electric double layers are formed, one with an excess of anions, the other with an excess of cations so that the overall interfacial

region is electrically neutral. At thermodynamic equilibrium, the equality of the electrochemical potential of species i in each phase is given by:

$$\tilde{\mu}_i^w = \tilde{\mu}_i^o \qquad (2.2)$$

The thermodynamic equilibrium is reached when the molar Gibbs energy for the species i is equal in both phases:

$$\Delta G_{tr,i}^{w \to o} = \tilde{\mu}_i^o - \tilde{\mu}_i^w = 0 \qquad (2.3)$$

The electrochemical potentials ($\tilde{\mu}_i^w$ and $\tilde{\mu}_i^o$), represent the work required to transfer the ion i, from the vacuum into a phase, and can be divided into a chemical and electrical part:

$$\tilde{\mu}_i^w = \mu_i^w + z_i F \phi^w \qquad (2.4)$$

with

$$\mu_i^w = \mu_i^{0,w} + RT \ln a_i^w \qquad (2.5)$$

where $\mu_i^{0,w}$ and μ_i^w are the standard and chemical potentials in the water phase. R is the gas constant, T is the temperature, z_i is the charge of the species i, F is the Faraday constant. ϕ^w is the bulk electrical potential of the water or inner potential (Galvani potential) and a_i^w is the activity of the species i in the electrified phase.

At the liquid|liquid interface, the equilibrium condition (Eq. 2.2) is fulfilled and the following relationship can be obtained:

$$\mu_i^{0,w} + RT \ln a_i^w + z_i F \phi^w = \mu_i^{0,o} + RT \ln a_i^o + z_i F \phi^o \qquad (2.6)$$

From Eq.(2.6) the difference in inner potential between the two phases can be expressed as:

$$\Delta_o^w \phi = \phi^w - \phi^o = \frac{1}{z_i F}\left(\mu_i^{0,o} - \mu_i^{0,w}\right) + \frac{RT}{z_i F} \ln\left(\frac{a_i^o}{a_i^w}\right) \qquad (2.7)$$

where the difference of standard chemical potentials $(\mu_i^{0,o} - \mu_i^{0,w})$ is equal to the standard Gibbs energy of transfer $(\Delta G_{tr,i}^{0,w\to o})$ defined by the difference between the standard Gibbs energy of solvation of the ion i in each phase:

$$\Delta G_{tr,i}^{0,w\to o} = \Delta G_{solv,i}^{0,o} - \Delta G_{solv,i}^{0,w} = \mu_i^{0,o} - \mu_i^{0,w} \qquad (2.8)$$

The equation (2.7) can be rewritten, taking into account the standard Gibbs energy of transfer, defined as follow:

$$\Delta_o^w \phi = \frac{\Delta G_{tr,i}^{0,w\to o}}{z_i F} + \frac{RT}{z_i F} \ln\left(\frac{a_i^o}{a_i^w}\right) \qquad (2.9)$$

$\Delta_o^w \phi_i^0$ represents the standard ion transfer potential, which is related to the standard Gibbs energy for the transfer of the ion i from the water (w) to the organic (o), defined through the equation:

$$\Delta_o^w \phi_i^0 = \frac{\Delta G_{tr,i}^{0,w\to o}}{z_i F} \qquad (2.10)$$

It is important to mention that an ion transfer is characterised by $\Delta_o^w \phi_i^0$ value, which is a measure of the ion's relative hydrophilicity/hydrophobicity. Substituting the equation (2.10) into the equation (2.9) leads to the Nernst equation for an ion transfer reaction across ITIES, which is analogous to the classical Nernst equation applicable for electron transfer reactions at an electrode|electrolyte solution interface,

$$\Delta_o^w \phi = \Delta_o^w \phi_i^0 + \frac{RT}{z_i F} \ln\left(\frac{a_i^o}{a_i^w}\right) \qquad (2.11)$$

For this reason, equation (2.11) is often called the Nernst equation for ion transfer at the ITIES, which governs the ions distribution at equilibrium between two electrified liquid phases. Since it is more convenient to work with concentrations rather than activities, equation (2.11) can be expressed in terms of concentrations. The standard transfer

potential $(\Delta_o^w \phi_i^0)$ can be replaced by the formal potential of transfer $(\Delta_o^w \phi_i^{0\prime})$ in which the activity coefficients, γ $(a_i = \gamma_i \times c_i)$, are included:

$$\Delta_o^w \phi = \Delta_o^w \phi_i^{0\prime} + \frac{RT}{z_i F} \ln\left(\frac{c_i^o}{c_i^w}\right) \qquad (2.12)$$

where the formal potential of transfer is expressed as a function of the standard potential of transfer:

$$\Delta_o^w \phi_i^{0\prime} = \Delta_o^w \phi_i^0 + \frac{RT}{z_i F} \ln\left(\frac{\gamma_i^o}{\gamma_i^w}\right) \qquad (2.13)$$

2.3.2 Electron transfer at the ITIES

Similar formalism can be applied to the case of heterogeneous electron transfer between redox couples across liquid|liquid interface. At the liquid|liquid interface electrons only can transfer from one chemical species located in one phase to a chemical species located in the other phase (Figure 2.2). In contrast to ion transfer reactions, electron transfer reactions are experimentally difficult to study at liquid|liquid interface because there are very few ideal systems.
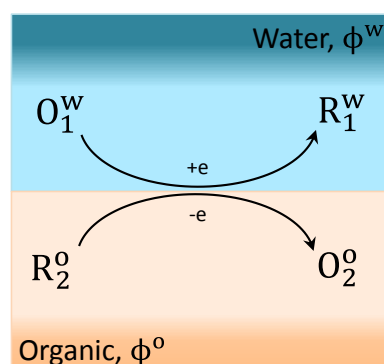
Figure 2.2 – Schematic diagram of a heterogeneous electron transfer reaction at the interface. The electronic charge is transferred from the organic phase at potential ϕ^o to the aqueous phase at potential ϕ^w.

There are normally two requirements for such systems, (i) the potentials of the redox couples in both phases cannot be very different; (ii) the reactants and the products in the organic phase cannot be dissolved in the aqueous phase, and will not be transferred across the interface in their ionic forms.

The electron transfer occurs either by external polarization of the interface or by the interfacial potential difference and can be represented by the following reactions:

$$O_1^w + n_1 e^- \rightleftarrows R_1^w \qquad (2.14)$$

$$R_2^o \rightleftarrows O_2^o + n_2 e^- \qquad (2.15)$$

$$n_2 O_1^w + n_1 R_2^o \rightleftarrows n_2 R_1^w + n_1 O_2^o \qquad (2.16)$$
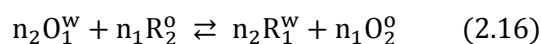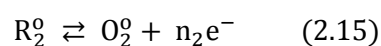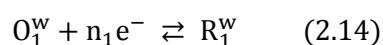
where O_1^w and R_2^o are the reactants in the aqueous and organic phases, respectively, and R_1^w and O_2^o are the corresponding products in the two phases, n is the number of electrons exchanged during the reaction. At the equilibrium, the electrochemical potentials of the reactants and products are equal[2]:

$$n_2 \tilde{\mu}_{O_1}^w + n_1 \tilde{\mu}_{R_2}^o = n_2 \tilde{\mu}_{R_1}^w + n_1 \tilde{\mu}_{O_2}^o \qquad (2.17)$$

The electrochemical potentials of the reactants and products are equal, so the Gibbs energy for the reaction (2.16), when the latter is electrically driven, is given by:

$$\Delta G_{tr,e}^{w \to o} = (n_2 \tilde{\mu}_{R_1}^w + n_1 \tilde{\mu}_{O_2}^o) - (n_2 \tilde{\mu}_{O_1}^w + n_1 \tilde{\mu}_{R_2}^o) = 0 \qquad (2.18)$$

As in the case of ion transfer, Eq. (2.6) can be written to express the electrochemical potentials of all chemical species, as follow:

$$n_2 \mu_{R_1}^{0,w} + n_1 \mu_{O_2}^{0,o} - n_1 \mu_{R_2}^{0,o} - n_2 \mu_{O_1}^{0,w} + RT\ln\left(\left(\frac{a_{R_1}^w}{a_{O_1}^w}\right)^{n_2}\left(\frac{a_{O_2}^o}{a_{R_2}^o}\right)^{n_1}\right) + n_2 F\phi^w + n_1 F\phi^o = 0 \qquad (2.19)$$

Equation (2.19) can be written to express the Galvani potential difference:

$$\Delta_o^w \phi = \phi^w - \phi^o = \frac{n_2\left(\mu_{R_1}^{0,w} - \mu_{O_1}^{0,w}\right) + n_1\left(\mu_{O_2}^{0,o} - \mu_{R_2}^{0,o}\right)}{n_1 n_2 F} + \frac{RT}{n_1 n_2 F}\ln\left(\left(\frac{a_{R_1}^w}{a_{O_1}^w}\right)^{n_2}\left(\frac{a_{O_2}^o}{a_{R_2}^o}\right)^{n_1}\right) \qquad (2.20)$$

where $n_2\left(\mu_{R_1}^{0,w} - \mu_{O_1}^{0,w}\right) + n_1\left(\mu_{O_2}^{0,o} - \mu_{R_2}^{0,o}\right)$ is equal to the standard Gibbs energy of reaction, which can also expressed in terms of standard redox potentials of O_1/R_1 couple in the aqueous phase and O_2/R_2 couple in the organic phase[57,58] respectively, as:

$$\Delta G_{tr,e^-}^{0,w\rightarrow o} = n_1 n_2 F(E_{O_2/R_2}^{0,o} - E_{O_1/R_1}^{0,o}) \qquad (2.21)$$

where $E_{O_1/R_1}^{0,o}$ and $E_{O_2/R_2}^{0,o}$ are required to be expressed in the same potential scale, for example the standard hydrogen electrode (SHE) in water.

Introducing the standard chemical potentials into Eq. (2.19), gives the Nernst equation for a heterogeneous electron transfer across the liquid|liquid interface:

$$\Delta_o^w \phi = \Delta_o^w \phi_{e^-}^0 + \frac{RT}{n_1 n_2 F}\ln\left(\left(\frac{a_{R_1}^w}{a_{O_1}^w}\right)^{n_2}\left(\frac{a_{O_2}^o}{a_{R_2}^o}\right)^{n_1}\right) \qquad (2.22)$$

where the standard electron transfer potential, $\Delta_o^w \phi_{e^-}^0$, is defined as:

$$\Delta_o^w \phi_{e^-}^0 = \frac{n_2\left(\mu_{R_1}^{0,w} - \mu_{O_1}^{0,w}\right) + n_1\left(\mu_{O_2}^{0,o} - \mu_{R_2}^{0,o}\right)}{n_1 n_2 F} = \frac{n_1 E_{O_2/R_2}^{0,o} - n_2 E_{O_1/R_1}^{0,w}}{n_1 n_2 F} \qquad (2.23)$$

The equation (2.22) governs the equilibrium concentrations of chemical species involved in an interfacial ET. Analogously to ion transfer reactions, Eq. (2.12) can be written in terms of concentrations:

$$\Delta_o^w \phi = \Delta_o^w \phi_{e^-}^{0\prime} + \frac{RT}{n_1 n_2 F}\ln\left(\left(\frac{c_{R_1}^w}{c_{O_1}^w}\right)^{n_2}\left(\frac{c_{O_2}^o}{c_{R_2}^o}\right)^{n_1}\right) \qquad (2.24)$$

2.4 Determination of Galvani potential differences

The Gibbs energy of transfer of a single ionic species is not directly accessible experimentally, therefore an extra-thermodynamic approach has to be introduced, to make $\Delta G_{tr,i}^{0,w \to o}$ amenable to direct measurement.

The standard Gibbs energy of transfer of a salt MX from water to organic phase, where MX is completely dissociated in both phases and M^+ and X^- are solvated, is written as:

$$\Delta G_{tr,MX}^{0,w \to o} = \left(\mu_{M^+}^{0,o} - \mu_{X^-}^{0,w}\right) - \left(\mu_{M^+}^{0,w} - \mu_{X^-}^{0,o}\right) \qquad (2.25)$$

This quantity can be expresses as the sum of the Gibbs energy of transfer of the ions M^+ and X^- by the following:

$$\Delta G_{tr,MX}^{0,w \to o} = \Delta G_{tr,M^+}^{0,w \to o} + \Delta G_{tr,X^-}^{0,w \to o} \qquad (2.26)$$

where $\Delta G_{tr,MX}^{0,w \to o}$ corresponds to the difference in the Gibbs energy of solvation of the neutral salt between the two phases and is, therefore, a measurable parameter.

To establish an ionic scale, many different assumptions have been suggested. The 'TATP' is the most commonly approach used, which is based on the assumption that the standard Gibbs transfer energies of tetraphenylarsonium (TPAs$^+$) cation and tetraphenylborate (TPB$^-$) anion in an arbitrary pair of solvents are equal due to their similar sizes and shapes.[59] The average radius of phenyl groups was found to be 4.2 A°.[60] As a result, their energies of solvation would be very similar, represented as follow:

$$\Delta G_{tr,TPAs^+}^{0,w \to o} = \Delta G_{tr,TPB^-}^{0,w \to o} = \frac{1}{2}\Delta G_{tr,TPATPB}^{0,w \to o} \qquad (2.27)$$

However, this assumption does not take into account the fact that the As-C and B-C bond lengths are not equivalent, which may result in different Gibbs energies of transfer.[61,62]

Girault and Schifrin[63] proposed another approach to define the absolute potential scale. They suggested that the potential of zero charge (pzc) of a polarized liquid|liquid interface can be used to define Galvani potential scales, since the dipolar contribution of the Galvani potential difference at the potential of pzc is negligible. Using this approach, Shao et al.[61] observed that the Gibbs energy of transfer of TPAs+ and TPB- were different, confirming that pzc assumption is more accurate than the 'TATP', thus allowing reasonable estimates of the Gibbs energy of transfer of ions between immiscible solvents. Despite that, the 'TATP' assumption is more widely used because the pzc approach should be determined for each system used to study the ITIES. Several authors have addressed experimental and theoretical approaches to evaluate standard Gibbs transfer energies of various ions transferring from water to different types of organic solvents.[64–66]

In the presented work, the tetraphenylarsonium tetraphenylborate ('TATP') approach was used for the evaluation of the formal Gibbs transfer energy of ions across the aqueous|organic interface, in terms of the voltammetric responses of ion transfer reactions.

2.5 Polarisation of liquid|liquid interfaces

When a potential difference is applied across a liquid|liquid interface, two extremes types of electrified interfaces can be distinguished, namely ideally polarisable and ideally non-polarisable.[2,3,21] In the case of ideally polarisable ITIES, a large change in the potential difference across the interface give rise to a small current passing across it, whereas for ideally non-polarisable ITIES, a relatively high current can be passed by applying only a small difference across the interface.

The polarisation of the ITIES is an ionic process, as ions are implicated in both regions which have a charge excess. One phase possesses an excess of positive charge which is

counterbalanced by an excess of negative charge, so the polarisability of the interface depends on the electrolytes for both phases. There are two ways to control the potential across the ITIES: (i) with an external circuit, when very hydrophilic and very hydrophobic electrolytes are present in aqueous and organic phases respectively (ideally polarisable interface), and (ii) by dissolving a single common ion in both aqueous and organic phases (non-polarisable interface).

2.5.1 Ideally polarisable ITIES

An ideally polarisable ITIES is when a strongly hydrophilic 1:1 electrolyte A_1B_1, dissolved in the aqueous phase and a strongly hydrophobic 1:1 electrolyte A_2B_2, in the organic phase respectively are used. The concentration of the hydrophilic salt in the organic phase is negligible compared with that of the hydrophobic salt and, conversely the concentration of the hydrophobic salt in water is negligible compared with that of the hydrophilic salt. Thermodynamically, the ideally polarized interface means that there is no common ionic species between the two phases and the polarisability of the ITIES depends on the Gibbs energy of transfer of the different salts. The interface is called polarised and the following system is considered:

$$RE_1|A_1B_1(w)\|A_2B_2(o)|RE_2 \qquad (2.28)$$
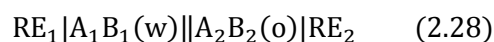
According to the hydrophobicity scale and in terms of potential, the system can be represented by the following equations:

$$\Delta_o^w\phi_{A_1^+}^0 \gg 0 \text{ and } \Delta_o^w\phi_{B_1^-}^0 \ll 0 \qquad (2.29)$$

$$\Delta_o^w\phi_{A_2^+}^0 \ll 0 \text{ and } \Delta_o^w\phi_{B_2^-}^0 \gg 0 \qquad (2.30)$$

ITIEs has been shown to behave nearly as an ideal condenser in the range of the potential differences, $\Delta_o^w \phi_{B_2^-}^0, \Delta_o^w \phi_{A_2^+}^0 \ll \Delta_o^w \phi \ll \Delta_o^w \phi_{B_2^-}^0, \Delta_o^w \phi_{A_1^+}^0$ [12,67] it is to be noted that the previous splitting of current is not straightforward matter when the ion participates in both the transfer reaction and adsorption. However, this problem can be circumvented by performing the measurement of a charge transfer reaction in the presence of an excess of the supporting electrolyte. The ions of the supporting electrolyte, in a general case, A_1B_1 in w and A_2B_2 in o, are not easily transferred into the other phase, and they both ensure the high electric conductivity of the phases and the charging of the electric double layer.

Under these conditions, the interface can be polarised using an external potential source without modifying the chemical composition of the adjacent phases. The application of a potential difference between the two phases demands a flow of an electrical current to establish a chemical equilibrium.

2.5.2 Ideally non-polarisable ITIES

An interface is termed non-polarisable when both phases have at least one common ion which is transferable across the interface. In this type of interface the current can pass in either direction but does not change the interfacial potential difference from the equilibrium value. This exists in the case of non-binary 1:1 electrolyte system $(A_3^+ B_1^- : A_3^+ B_2^-)$ and is represented:

$$RE_1 | A_3B_1(w) \| A_3B_2(o) | RE_2 \qquad (2.31)$$
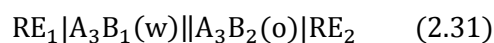
A_3^+ is the common ion and the anions B_1^- and B_2^- are sufficiently hydrophilic and hydrophobic to remain in their respective phases, so that A_3^+ is the only ion that can

transfer across the interface. As a result, the Galvani potential difference is only controlled by the activity of the ion A_3^+ in each phase:

$$\Delta_o^w \phi = \Delta_o^w \phi_{A_3^+}^0 + \frac{RT}{F} \ln \left(\frac{a_{A_3^+}^o}{a_{A_3^+}^w} \right) \qquad (2.32)$$

Considering the transfer of B_1 and B_2 negligible, the system can be described using the following equations:

$$\Delta_o^w \phi_{B_1^-}^0 \gg 0 \text{ and } \Delta_o^w \phi_{B_2^-}^0 \ll 0 \qquad (2.33)$$

$$\Delta_o^w \phi_{B_1^-}^0 \gg \Delta_o^w \phi_{A_3^+}^0 \gg \Delta_o^w \phi_{B_2^-}^0 \qquad (2.34)$$

The Galvani potential difference across the interface is independent of the electrolyte concentration, and therefore cannot be controlled by a potentiostat. These non-polarised liquid|liquid interfaces are commonly used as organic reference electrode because they can form ion selective electrodes for organic ions.

2.6 Potential window

As it was mentioned previously, at an ideally polarised liquid|liquid interface, no faradaic process occurs, since all the components of the system are considered to have infinite standard Gibbs energy of transfer (Eq. 2.29 and 2.30). As ionic species have finite solubility in any electrolyte phase, the ideally polarise liquid|liquid interface can be defined in a limited potential range, also called as 'polarisation range' (Figure 2.3), meaning that the range of potentials can be controlled by a potentiostat and that the current is small enough to be considered negligible. This region is also known as 'potential window' and is limited by the supporting salts.[68,69]
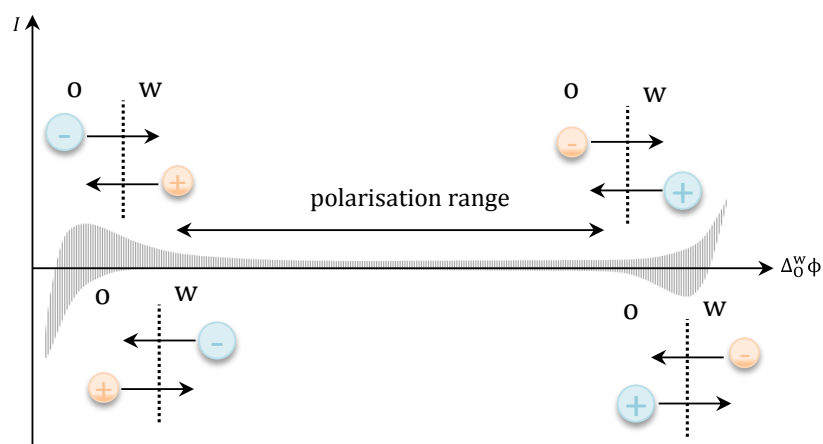
Figure 2.3 – Schematic representation of the polarisation window for an interface between two immiscible electrolyte solutions.

When the potential applied reaches high positive values, the cations A_1^+ or the anions B_2^- gain a sufficient energy to transfer in to the adjacent phases. Analogously, negative potentials provide enough energy for B_1^- or A_2^+ to transfer in the other phase. In the case of electrode|electrolyte interfaces, the faradaic transfer processes can be studied under potentiostatic control only within the polarisation range.

When an ion, whose formal transfer potential is intermediated between that of A_1^+ and B_2^-, is added to one of the phases, and a potential difference is applied, the transfer of this ion across the water|organic interface is induced. This flux of charges across the interface leads to a measurable current, which is recorded as a function of the applied potential. Such curves are called ionamperograms and are produced by reversible ion transfer reactions, similar to those obtained for electron transfer reactions at an electrode|electrolyte solution interface.

2.7 Interfacial structure and electrical double layers

Electrical double layers exist at all the boundaries between two ionic or electrical conducting liquid phases. At the liquid|liquid interface, the electrical double layer is an interacting electrical region involving two extended regions where ionic species are distributed. The liquid|liquid interface is a heterogeneous environment and therefore a molecular interface with its own dynamical properties. It is composed of a thin (i.e. about 1nm) mixed solvent layer and according to snapshots from molecular dynamics computer simulation, its local structure is greatly influenced by the presence of ionic charges.[50,70] The structure of the interface determines the distribution of the electrical potential in the interfacial region. In order to characterise the potential distribution at the ITIES, two models have been proposed, (i) the modified Verwey and Niessen[7] and (ii) the mixed solvent layer.[56]

2.7.1 Modified Verwey and Niessen model

The first model of interfacial structure was introduced by Verwey and Niessen.[7] The interfacial structure was represented by a space charge region in each phase, one containing an excess of the positive charge and the other phase an equal excess of negative charge. The space charge distribution was described by the Gouy-Chapman[71,72] as two diffuse back-to-back layers. Later Gavach et al.[73] revised the model of Verwey and Niessen[7], suggesting that the interface involves oriented dipoles of organic and water molecules. This description led to the concept of an ion-free compact layer at the surface of contact between the two immiscible phases. This compact layer is similar to inner layer existing at the electrode|electrolyte interface, which corresponds to the distance of the closest approach of the ions in solution, also called Outer Helmholtz Plane (OHP).[74] At the liquid|liquid interface, this inner layer separates the two planes of the closest approach

(outer Helmholtz planes, OHP) for both aqueous and organic sides of the interface, as depicted in figure 2.4.
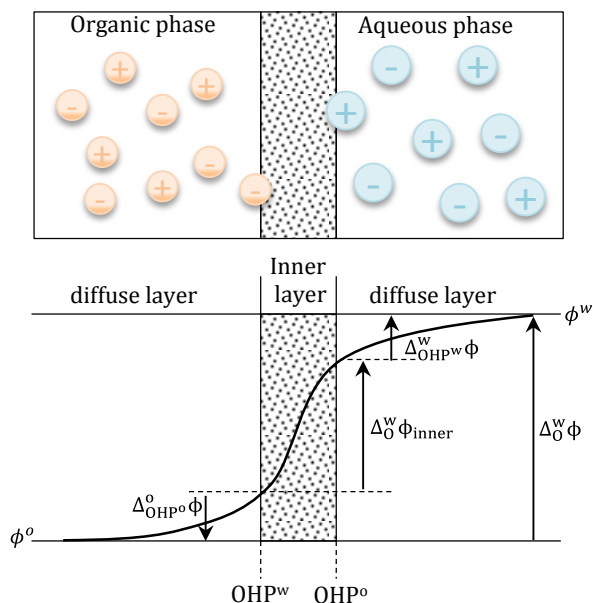
Figure 2.4 – Modified Verwey and Niessen model of the ITIES and potential distribution across the liquid|liquid interface. OHP^w and OHP^o are the positions of ions in planes of closest approach for the water and organic phase respectively.

In the modified Verwey and Niessen model, the Galvani potential difference $\Delta_o^w\phi$ between the two phases is split into three contributions, according to the following:

$$\Delta_o^w\phi = \phi^w - \phi^o = \Delta_{OHP^w}^w\phi - \Delta_{OHP^o}^o\phi + \Delta_o^w\phi_{inner} \qquad (2.35)$$

where $\Delta_{OHP^o}^o\phi = \phi^o - \phi(OHP^o)$ and $\Delta_{OHP^w}^w\phi = \phi^w - \phi(OHP^w)$ are the potential difference across the diffuse layers in the organic and aqueous phases respectively and $\Delta_o^w\phi_{inner}$ is the potential difference across the inner layer. The explanation of this model relies on drop weight interfacial tension measurements[73] which revealed that series of tetraalkylammonium ions showed no specific adsorption in the interfacial region. However, this was not the case for the tetrapentylammonium ion suggesting a specific adsorption of this species.

2.7.2 Mixed solvent layer model

Girault and Schiffrin[56] introduced the concept of the mixed solvent layer as a model to describe the ITIES. The authors suggested that a continuous change in composition from one phase to the other was a more representative picture than of ion-free layer at the ITIES. From measurements of the surface tension of non-polarisable ITIES in the presence of various aqueous salts, they showed that the thickness of the ion-free layer varied with ionic size of the species dissolved in the aqueous phase was dependent on the polarity of the organic solvent. They suggested that both, mixed ionic and solvent layer, no more than of two or three molecular diameter thickness, were responsible for this effect. The essential consequence of this model is that the Galvani potential difference is spread within the two back-to-back diffusion layers with a minimal potential drop across the mixed solvent region, whereas all the difference in chemical potential is developed across the mixed solvent layer (Figure 2.5).
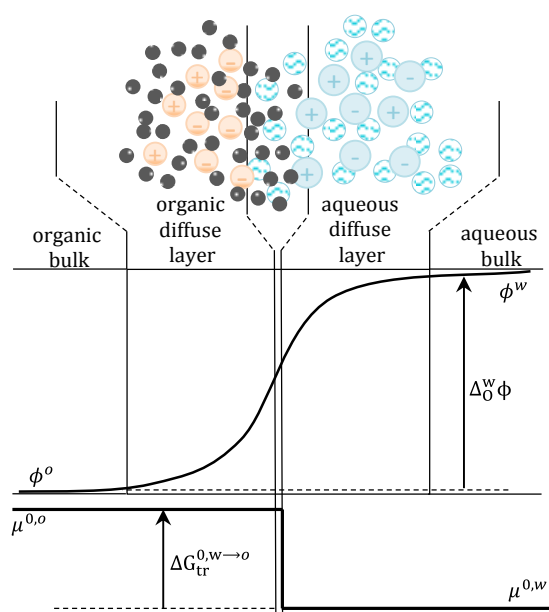
Figure 2.5 – Schematic representation of the mixed solvent layer model. The potential distribution across the interfacial region and the evolution of the chemical potential in terms of Gibbs energy.

The mixed solvent layer model also considers the penetration of ions in the interfacial region, the degree of penetration depending on the ion hydrophilicity. This assumption has been confirmed for aqueous solutions of alkali metal cations in contact with organic solvent using capacitance measurements.[75] Hydrophilic ions like potassium or chloride tend not to enter in the interfacial region as shown by positive excess concentration of water. On the other hand, at the interface between two electrolytes having a common hydrophobic cation, this cation will freely penetrate the interface to such an extent as to be specifically adsorbed. It is expected that the variation of standard chemical potential which represents the Gibbs energy of transfer takes place within the mixed solvent layer.[11,76]

2.8 Mass transport process for charge transfer reactions at ITIES

The similarity with the classical Nernst equation for redox reactions on an electrode, which is limited by the mass transfer of the reactants to the electrode, or by the products away from the electrode, the ion transfer reactions across the ITIES is limited by the mass transfer of ions to the interface or away from it. This implies that the mass transport differential equations and the boundary conditions of redox reactions at the electrode|electrolyte interface can be directly transposed to the study of ion transfer reactions at the ITIES.[52] As for electrode|electrolyte interfaces, three types of mass transport can occur at an ITIES, namely migration, convection and diffusion. In this manner, the mass transport of a species (i) is described by the Nernst-Plank equation:

$$J_i = J_{i,m} + J_{i,c} + J_{i,d} \qquad (2.36)$$

where the flux of i is equal to the sum of the migration flux ($J_{i,m}$), the convection flux ($J_{i,c}$) and the diffusion flux ($J_{i,d}$). For one dimension, the equation (2.36) has the following representation:

$$J_i(x,t) = -D_i \frac{\partial c_i(x,t)}{\partial x} - \frac{z_i}{RT} D_i c_i(x,t) \frac{\partial \phi(x,t)}{\partial x} + c_i(x,t)v(x,t) \qquad (2.37)$$

where $J_i(x,t)$ is the flux of ions, z_i, D_i, c_i are the charge, the diffusion coefficient and the concentration of the ion respectively. $\frac{\partial c_i(x,t)}{\partial x}$ is the concentration gradient (at a distance x and time t), $\frac{\partial \phi(x,t)}{\partial x}$ represents the potential gradient (at a distance x and time t) and $v(x,t)$ is the hydrodynamic velocity of the solution.

Migration corresponds to the displacement of charged species under the influence of an electrical potential. It is the main mechanism permitting the passage of charge across the solution when the current is flowing. As migration is purely electrostatic, the charge may be carried by any ionic species in solution. Consequently, with a large concentration of supporting electrolyte, only a negligible quantity of electroactive species is transported by migration. The term $-\frac{z_i}{RT} D_i c_i(x,t) \frac{\partial \phi(x,t)}{\partial x}$ in equation (2.37) can be neglected, when the species i is in the presence of concentrated supporting electrolytes.

Convection is the movement of species induced by the movement of the medium in which the species are present. This movement can be the result of temperature fluctuations or mechanical stirring. In most liquid|liquid interface experiments, the solutions are unstirred and the electrodes are static, so the movement of a species is not due to mechanical forces. The temperature is also constant in the time scale of the experiments, so that natural convection generally occurring in the bulk of the solution. Thus, the term $c_i(x,t)v(x,t)$ in equation (2.37) is also negligible.

Since migration and convection transports are negligible in most of the ITIES experiments, the movement of a species is limited to diffusion. This means that the

current, which is directly related to the flux J_i is thus governed by the arrival and removal of diffusing species at the interface. Accordingly, equation (2.36) becomes:

$$J_i = J_{i,d} \qquad (2.38)$$

This type of mass transport is predominant in the liquid|liquid electrochemical experiments, since a concentration gradient is induced during the transfer of ions from one phase to another, in other words the movement of species is due to a chemical potential gradient where the species will move down this gradient to reach homogeneity through the solution. In reversible ion transfer reactions, the mass transport at the proximity of the interface is diffusion controlled, given by Eq. (2.38). In the same manner, the Fick's second law describes the variation of the concentration of the species i at a location x with respect to time t, represented as follow:

$$\frac{\partial c_i(x,t)}{\partial t} = D_i \frac{\partial^2 c_i(x,t)}{\partial x^2} \qquad (2.39)$$

However the flux of species to an interface differs significantly with the geometry of this interface.

2.8.1 Influence of the interfacial Geometry

2.8.1.1 Macro ITIES

For a macroscopic ITIES (interfacial diameter greater than 50μm), the interface is considered as a flat semi-infinite plane. In this case the diffusion is linear (Figure 2.6) and the expression of the flux reduces to only one dimension:

$$J_i(x,t) = -D_i \frac{\partial c_i(x,t)}{\partial x} \qquad (2.40)$$

The Fick's equations explain that the response of the system stems from the resolution of the diffusion equations of the ion in the two adjacent phases:

$$\frac{\partial c_i^w}{\partial t} = D_i^w \frac{\partial^2 c_i^w}{\partial x^2} \quad \text{and} \quad \frac{\partial c_i^o}{\partial t} = D_i^o \frac{\partial^2 c_i^o}{\partial x^2} \qquad (2.41)$$

where D_i^w and D_i^o are the diffusion coefficients of species i in water and organic phase, respectively. By taking the interface as the origin, the current is then given by the flux of i across the interface of area A. The current is directly proportional to the flux according to:

$$I = z_i F A D_i^w \left(\frac{\partial c_i^w}{\partial x} \right)_{x=0} \qquad (2.42)$$

where the boundary conditions are given by the Nernst equation Eq. (2.11) and the equality of the fluxes yields to:

$$D_i^w \left(\frac{\partial c_i^w}{\partial x} \right)_{x=0} + D_i^o \left(\frac{\partial c_i^o}{\partial x} \right)_{x=0} = 0 \qquad (2.43)$$
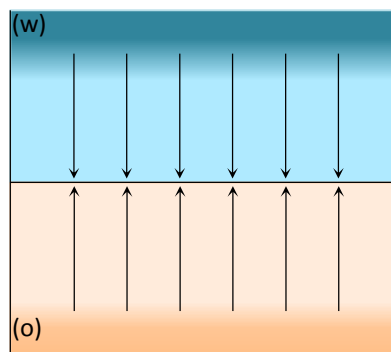
Figure 2.6 – Schematic representation of the linear flux across a large ITIES.

2.8.1.2 Micro ITIES

When the size of an interface is reduced to micrometre dimensions, the diffusion characteristics alter significantly. The passage of ions across the micro interfaces (Figure 2.7) is characterised by limiting diffusion currents such as those obtained for

metallic microelectrodes, the major difference being that the diffusion coefficients of the ion in the two adjacent phases are not the same. It changes from the linear to the nearly spherical diffusion due to edge effects. In the cases of micropipettes and micro-holes supported at a thick polymer film, the diffusion regime becomes asymmetric. If the interface is considered spherical, then the Fick's first law may be written in spherical coordinates:

$$J_i(x, t) = -D_i \frac{\partial c_i(r, t)}{\partial r} \qquad (2.44)$$

with r being the radial distance of the surface from the centre of the sphere.

Analogously to the macro interfaces, for a reversible charge transfer reaction, the distribution of the species i near the interface can also be obtained from the Fick's second law of diffusion in spherical coordinates, i.e:

$$\frac{\partial c_i(r, t)}{\partial t} = D_i \frac{\partial^2 c_i(r, t)}{\partial r^2} + \frac{2D_i}{r} \frac{\partial c_i(r, t)}{\partial r} \qquad (2.45)$$

The main consequence of the change in diffusional regime at a micro interface is the enhancement of the flux of species to the interface. In 1957, Reinmuth[77] presented a correction factor by which was possible to correct the current obtained from the planar diffusion solution for a spherical diffusion to a solid electrode. Due to the similarity between the types of diffusion found at spherical and microdisc electrodes, approximate solutions for the diffusion to microdisc electrodes are derived for spherical diffusion and made it possible to apply to the micro-hole interfaces (Figure 2.7 b).[78] It has thus been shown that the methodology developed for microdisc electrodes could be extended to the charge transfer reaction at micro-ITIES and that the current responses produced were of a steady-state type.[23,78]

The case of micro-ITIES supported at the tip of a micropipette, as depicted in Figure 2.7a) is rather interesting in the sense that the diffusion regime on both sides of the interface is asymmetric.[22] The diffusion regime of a species entering the pipette is spherical,[22,79] whereas the diffusion from the inside the pipette is restricted by the walls of the pipette, resulting in linear diffusion
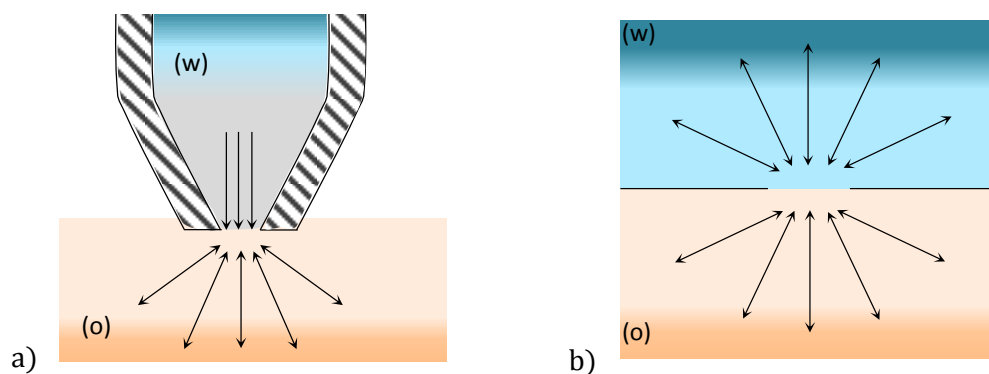
Figure 2.7 – Schematic illustration of spherical diffusion at micro-ITIES, a) hemispherical interface (micropipette type), b) spherical interface (micro-hole type).

This type of system has been a tool for the determination of the species limiting the potential window, and it has also been employed for supporting phospholipid monolayers[80] and for investigations on assisted ion transfer reactions[26,81] and its kinetics.[23,82]

2.9 Facilitated ion transfer at ITIES

The partition of ions in a two-phase system that contains lipophilic ligand in organic phase is a fundamental process in ion-selective electrode of liquid membrane type, solvent extraction, and carrier-mediated transport of ions across artificial as well as biological membranes.[83] At liquid|liquid interface, when an ion has relatively higher (or lower) Gibbs energy of transfer, its transfer normally appears outside of the potential window or very near the positive or negative end of the potential window. This can be the case of ions which are commonly used as a supporting electrolyte (e.g. Li^+), can be

difficult to study the simple IT reaction directly. Nevertheless, their transfer may become observable when they form a complex with a ligand (or ionophore) dissolved in either the organic or in the aqueous phase. Such a transfer is named an assisted or facilitated ion transfer (FIT), and the general reaction can be written as:

$$M^{z+}_{(w)} + nL_{(o)} \rightleftarrows ML^{z+}_{(o)} \qquad (2.46)$$
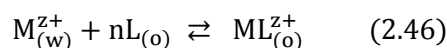
where M^{z+} represents the ion to be transferred and L the ligand.

The first study of assisted ion transfer reaction at polarised liquid|liquid interface was reported by Koryta in 1979.[21] He demonstrated that the decrease in an ion Gibbs energy of transfer (Eq. 2.47) is due to a selective complexation with a ligand.[2,21]

$$\Delta G^{w \to o}_{tr,M^{z+}} = RT\ln K_{ML^{z+}} \qquad (2.47)$$

where $K_{ML^{z+}}$ is the complexation constant between the ion and the ligand. According to Eq. 2.10, a decrease of $\Delta G^{w \to o}_{tr,i}$ yields the decrease of the transfer potential, as a result, the presence of the ionophore will shift the wave of a cation towards less positive potential, allowing the faradaic signal to be developed within the potential window. The effect of the ionophore on the ion transfer potential is shown in figure 2.8.
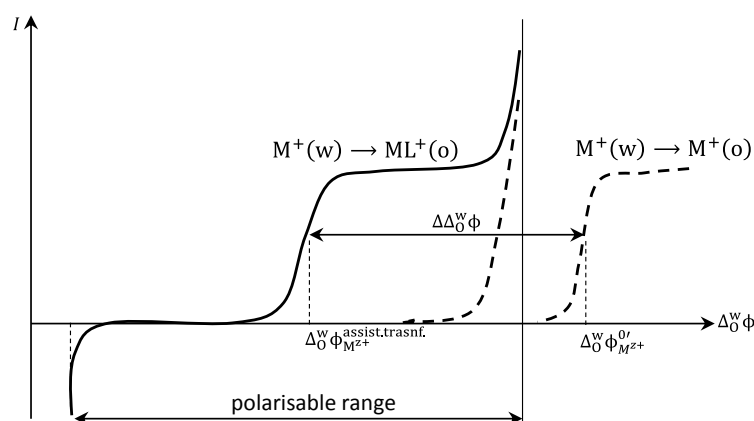
Figure 2.8 – Non-assisted (dashed line) and assisted (solid line) transfer of an aqueous ion.

Since the work of Koryta[21] various ionophores, natural or synthetic, such as valinomycin,[84,85] dibenzo-18-crown-6,[82,86] hydrophilic crown ethers[87,88] and lithium selective ionophore ETH1810,[87] have been used to facilitate cation transfer.[52,89] Recently anion transfers have also been study.[90,91] Molecules with acid-base properties can also be classified as undergoing a FIT reaction, the protonated base BH^+ can be regarded either as simple IT reaction or as a proton transfer facilitated by the conjugated acid.[52]

A considerable effort has been dedicated to explain the mechanisms of facilitated transfer reactions. In 1991, Girault et al.[81] proposed a new terminology for FIT reactions, which accurately describes the reaction mechanism. Depending on its nature, the ligand can be dissolved in the organic or in the aqueous phase, and four types of reaction mechanisms (Figure 2.9) can be distinguished:

TIC: Transfer by interfacial complexation

TID: Transfer by interfacial dissociation

TOC: Transfer followed by organic phase complexation

ACT: Aqueous complexation followed by the transfer of the complex

The mechanism of facilitated ion transfer reactions depends on many factors such as the relative concentration of both the ion and ionophore in the two phases and the association constant for the complexation equilibrium between the two phases. The ACT mechanism was proposed by Lin et al.,[92] who demonstrated that the assisted ion transfer reaction would occur via the diffusion of the ionophore, from the organic to the aqueous phase, followed by complexation in the aqueous phase and subsequent transfer. This mechanism is only viable if the ionophore is soluble in both phases. Samec and Papoff,[86] and Kakutani et al,[93] however, supported a TIC mechanism, which is favoured when the ratio of concentrations is such that the ion in the aqueous phase is in excess compared to

the ligand in the organic phase. Koryta[21] on the other hand supported a TOC mechanism where the ion transfer is followed by complexation in the organic phase. TID mechanism is known as the symmetric mechanism of TIC. A large majority of the reactions studied follows a mechanism of transfer by interfacial complexation/dissociation (TIC/TID),[81] applicable for highly hydrophobic ligands.

It is important to highlight that the type of mechanism involved depends mainly on the concentration ratios of the different species. For example, the assisted transfer reaction of an ion with an excess of ligand in the organic phase appears to follow a TIC mechanism than a TOC mechanism.
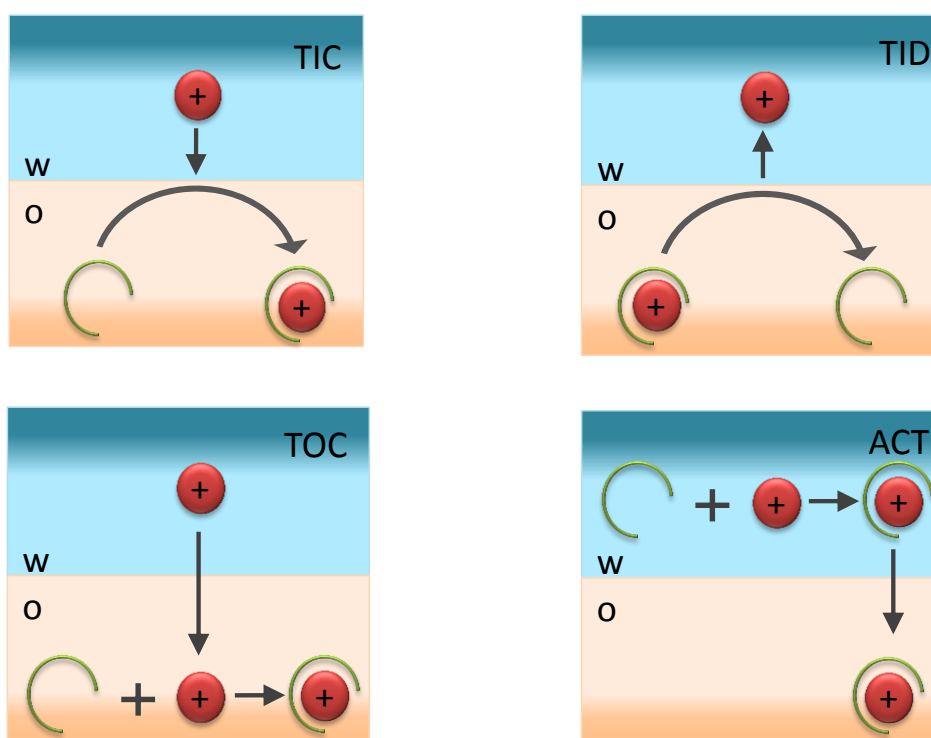
Figure 2.9 – Schematic representation of the different mechanisms for the FIT reactions at a liquid|liquid interface, (=ionophore (or ligand), =ion).

In 1991, Matsuda et al.[88] proposed a general theoretical equation for the polarographic response of reversible facilitated ion transfer reactions, leading to a prediction of the half-wave potential dependence on the initial concentrations of both ion and ionophore. The equations obtained are difficult to be applied directly even for the simplest case of 1:1 complexation. However they have been derived for two limiting cases: (i) $C_M \gg C_L$, where the mass transport is limited by that of the ligand, (ion concentration in excess), and (ii) $C_L \gg C_M$, where the limiting current observed is controlled by the diffusion of the ion so that the current is proportional to the concentration of the ion. For higher stoichiometries, the evolution of the half-wave potential has been given only in the case of ligand excess.

A model that describes the relation between the measured half-wave potential with the stoichiometry and the association constants of the reaction was recently proposed by Reymond et al.[94,95]

When compared to simple IT reactions, FIT can offer several advantages. This type of reactions can not only provide the stoichiometric information between the ion and the ligand, thermodynamic and kinetic parameters, but also applications in selective amperometric ion sensors, solvent extraction, and carrier-mediated transport of ions across artificial as well as biological membranes.[1,2,52]

2.9.1 Thermodynamics of assisted ion transfer at ITIES

From a thermodynamic point of view, the association constant of the complex, (represented in reaction (2. 46)) in the aqueous and organic phases (K_a^w and K_a^o) and also the distribution (partition) coefficient of the ligand (K_D) can be defined as follows:

$$K_a^w = \frac{a_{ML^{z+}}^w}{a_L^w a_{M^{z+}}^w} \qquad (2.48)$$

$$K_a^o = \frac{a_{ML^{z+}}^o}{a_L^o a_{M^{z+}}^o} \qquad (2.49)$$

$$K_D = \frac{a_L^0}{a_L^w} \qquad (2.50)$$

Considering that the diffusion coefficient of all the species are taken equal for each phase, and defining total concentrations of ion and ligand, respectively, the system can be defined according to Matsuda et al.[88]:

$$D_{M^{z+}}^{w,o} = D_{LM^{z+}}^{w,o} = D_L^{w,o} = D^{w,o} \qquad (2.51)$$

$$c_{M^{z+}_{tot}}^{w,o} = c_{M^{z+}}^{w,o} + c_{LM^{z+}}^{w,o} \text{ and } c_{L_{tot}}^{w,o} = c_L^{w,o} + c_{LM^{z+}}^{w,o} \qquad (2.52)$$

The mass balance equation can be expressed by:

$$\frac{\partial c_{M^{z+}_{tot}}^{w,o}}{\partial t} = D^{w,o} \frac{\partial^2 c_{M^{z+}_{tot}}^{w,o}}{\partial x^2} \text{ and } \frac{\partial c_{L_{tot}}^{w,o}}{\partial t} = D^{w,o} \frac{\partial^2 c_{L_{tot}}^{w,o}}{\partial x^2} \qquad (2.53)$$

These equations can be integrated and particular solutions for the total concentrations, $c_{M^{z+}_{tot}}^{w,o}$ and $c_{L_{tot}}^{w,o}$ obtained.

All the species involved in the complexation reaction may be present in both phases. For that reason, several assumptions can be made in order to simplify the reaction scheme.

(1) The ion concentration in the aqueous phase is in excess compared to that of the ionophore in the organic phase.

(2) The partition coefficient of the ionophore is small enough such that the ionophore concentration in the aqueous phase can be neglected.

(3) The complex formation in the organic phase is so high that the ion concentration in the organic phase can be neglected.

(4) Both the association constant and dissociation of ML^{z+} complex in the organic phase and the ion transfer reaction at the interface are very fast processes.

In the case of a 1:1 ion-to-ligand stoichiometry of facilitated ion transfer reactions at ITIES, the Galvani potential difference for a reversible ion transfer follows the same guidelines as in section 2.3.1. Hence, a Nernst equation for the transfer of 1:1 complex ML^{z+}, with a neutral ligand can be written as:

$$\Delta_o^w \phi = \Delta_o^w \phi_{ML^{z+}}^0 + \frac{RT}{zF} \ln\left(\frac{a_{ML^{z+}}^o}{a_{ML^{z+}}^w}\right) = \Delta_o^w \phi_{M^{z+}}^0 + \frac{RT}{zF} \ln\left(\frac{a_{M^{z+}}^o}{a_{M^{z+}}^w}\right) \qquad (2.54)$$

Using Eq.(2.54) and the formal transfer potential, the equation can be written in terms of concentrations:

$$\Delta_o^w \phi_{ML^{z+}}^{0\prime} = \Delta_o^w \phi_{M^{z+}}^{0\prime} + \frac{RT}{zF} \ln\left(\frac{c_{ML^{z+}}^o}{c_L^o K_a^o c_{M^{z+}}^w}\right) \qquad (2.55)$$

where $\Delta_o^w \phi_{ML^{z+}}^{0\prime}$ is the formal potential of the ionic species ML^{z+} defined as a function of the formal Gibbs energy of transfer and the activity coefficient of the ion in the adjacent phases, as:[95]

$$\Delta G_{tr,ML^{z+}}^{0\prime w \to o} = zF\Delta_o^w \phi_{ML^{z+}}^{0\prime} = \mu_{ML^{z+}}^{0,o} - \mu_{ML^{z+}}^{0,w} + \frac{RT}{zF} \ln\left(\frac{\gamma_{ML^{z+}}^o}{\gamma_{ML^{z+}}^w}\right) \qquad (2.56)$$

In the case where the ion concentration in the aqueous is in excess compared to that of the ligand, $C_M \gg C_L$, the current response, corresponds to the diffusion of the ligand to the interface and to the diffusion of the ion-ligand complex away from it. Since $M^{z+}(w)$ is in excess and its diffusion need not to be considered, the only diffusion species are $ML^{z+}(o)$ and $L(o)$. In this case, the half-wave potential depends on the ion concentration given as follows:

$$\Delta_o^w \phi_{1/2} = \Delta_o^w \phi_{M^{z+}}^{0\prime} + \frac{RT}{2F} \ln\left(\frac{D_L}{D_{ML^{z+}}}\right) - \frac{RT}{zF} \ln\left(K_a^o c_{M^{z+}}^w\right) \qquad (2.57)$$

At the half-wave potential of the FIT reaction, the following condition applies:

$$\left(\frac{c_{ML^{z+}}^{w}}{c_L^o}\right)_{x=0} = \left(\frac{D_L^o}{D_{ML^{z+}}^{w}}\right)^{1/2} \qquad (2.58)$$

where the index 0 indicates the concentration close to the interface. Eq. (2.57), then allows the calculation of the association constant ($\ln K_a^o$) in the organic phase from the plot of the half-wave potential ($\Delta_o^w\phi_{1/2}$) versus ($\ln c_{M^{z+}}^w$), assuming that $D_L = D_{ML^{z+}}$, which is considering similar sizes of the two species.[96]

On the other hand, when the ion transfer is assisted by the formation of 1:1 complex with the ligand present in the organic phase at an excess concentration, $C_L \gg C_M$, the half-wave potential shifts negatively by the value related to the stability constant, K_a^o, of the complex in the organic phase, which can be determined by the following equation,[54]

$$\Delta_o^w\phi_{1/2} = -\frac{RT}{zF}\ln(K_a^o c_L^o) \qquad (2.59)$$

Thus, the amperometric response of a series of ions can be tailored by selecting the suitable ligand yielding the most stable complex, which can be determined using Eq.(2.59)

It is important to mention that the study of FIT has been beneficial from well understood potentiometric sensors. For instance, the choice of the ligand in many FIT systems was based on reported potentiometric sensors. The study of FIT will be beneficial for the development of new potentiometric sensors, hence from a voltammetric response, many important thermodynamic parameters can be obtained, such as association constant, stoichiometric ratio between the ligand and ion, and Gibbs energy of transfer. Also, it can provide valuable information if a new synthesized ligand can be used for a novel potentiometric sensor or not. If the FIT reaction can be observed within the potential window, it is possible that the ligand can be used for the new sensor of the ion.

2.10 Overview of micro-ITIES

A micro-ITIES can be formed either at the tip of a pulled glass micropipette (the tip radius, r, typically of a few microns), single micro-hole or array of micro-holes in a thin polymer membrane.[22,23,97] Taylor and Girault[22] introduced the idea of miniaturization of liquid|liquid interfaces in 1986. They employed pulled glass micropipettes to support micrometre-sized liquid|liquid interfaces. Later, on the same group developed another approach to establish a micro-ITIES by fabricating a microhole in a thin inert membrane using an UV laser photoablation technique.[23]

Similarly to solid|liquid electrochemistry, which were revolutionized by the introduction of micrometre sized electrodes, important advantages were also obtained by replacing a large liquid|liquid interface with micro-ITIES. Girault and co-workers demonstrated that a voltammograms recorded at a micro interface had characteristics similar to those of usual redox voltammograms recorded at a solid microelectrode:[22–25,78,81,82,97,98]

(i)   The ohmic drop potential inherent in voltammograms measurement at the micro ITIES is very small, because the current flowing through the interface is much smaller than that at a conventional interface (1-10 mm in diameter). Due to the low ohmic drop, studies of charge transfer are possible even when the concentrations of supporting electrolytes are low. The reduced effect of solution resistance allows the study of systems which were previously inaccessible. With regard to kinetic measurements, the use of micro-ITES significantly increases the mass-transfer rate.

(ii)   The current that arises from the charge transfer is controlled by spherical diffusion of the ion,[99,100] which enhances the current hence improves the sensitivity of the voltammetry.

(iii)   The time required to achieve a steady-state is short and can be obtained at a fairly fast scan rate such as 50mV s^{-1}.

Additionally, a micro liquid|liquid interface of a quite high mechanical stability, a reproducible size and geometry and a good handling can be obtained in a quite simple way for the determination of thermodynamic parameters and kinetic investigations.[82]

The first study of ion (TEA$^+$) transfer at the micro interface supported by a micropipette tip was done by Girault et al.,[79] who also did simulations to explain the observed cyclic voltammograms and obtained a pseudo-analytical expression for the entire CV of a simple ion transfer at a micropipette. In the case of an ion transfer from outside to inside the pipette, the ingress takes place under steady-state conditions, similar to a redox reaction on a solid microdisc electrode. However, the egress occurs under linear diffusion due to size confined effect of the specific shape. The asymmetric diffusion field provides asymmetric voltammograms.

Assuming that the orifice of a micropipette is like a disc, the mathematical formulations of the diffusion patterns for a micropipette and a metal microdisc electrode are very similar when the charge transfer is controlled by essentially spherical diffusion in the outside solution. The following empirical equation can be used to calculate the steady-state diffusion limiting current:[82,101]

$$i_{ss} = AzFDCr \qquad (2.60)$$

where i_{ss} is the steady state current obtained from the difference between the background current and the current at the plateau region of sigmoidal voltammogram. D and C are the diffusion coefficient and the concentration of species responsible for the interfacial transfer process. F, z and r are the Faraday constant, transferred charge and radius of the micropipette, respectively. The value correspondent to the difference

between a metal microdisc and a micropipette is the value of factor A. For a metal microdisc electrode A is equal to 4, but for a micropipette A was found to be equal to 3.35π (for the water|1,2-dichloroethane interface) which is about 2.6 times bigger than that of a metal microdisc electrode. The large difference between this value and the factor 4 can be attributed to two factors. One is related to the nature of the glass pipette which is hydrophilic and the aqueous solution can escape from the pipette and form a thin layer on its outer wall near the orifice. This results in a significant increase of the effective area of the ITIES, which becomes much larger than the geometrical area of the pipette orifice and therefore an increase in the diffusion current can be observed.[101] This effect can be eliminated by making the outer pipette wall hydrophobic (section 3.1.2). Another factor contributing to the diffusion current to a pipette orifice is the additional flux from the back of the pipette due to small thickness of its wall, related to its unique shape.[53] The thickness of the insulation sheath is much smaller than that of a metal microdisc electrode, i.e., its RG (RG=Rg/r, where Rg is the glass insulator + r) is much smaller (Figure 2.10). Thus, the diffusion from the back of the pipette makes the additional contribution for the increase of current. A glass micropipette usually has RG $\leq$ 2 and metal microdisc electrode has RG $\geq$ 10.[102]
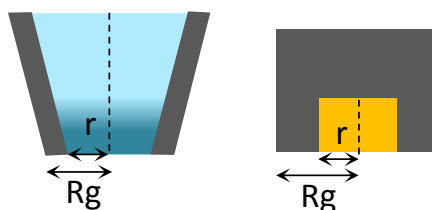
Figure 2.10 – Comparison of the thickness of the insulating sheath in a micropipette (left) and a metal microdisc electrode (right).

The peak-shaped voltammograms can be obtained for the egress of ions from the pipette because the ion transfer out the pipette is controlled by a semi-infinitive linear diffusion. The voltammetric behaviours are similar to those obtained at a macro liquid|liquid

interface and it obeys the Randles-Sevčik relationship. Its peak current is proportional to both the concentration and the square root of the scan rate.[79] On the other hand, in a FIT reaction, the mass transport regime will be completely analogous to a microdisc electrode if the concentration of the ligand (L) in the organic phase is much less than the concentration of the ion, e.g., $C_{M^{z+}} \geq 20C_L$, a steady-state voltammograms will observed. Another important aspect of the asymmetric diffusion field of the micropipettes and the corresponding asymmetric voltammograms is that they can elucidate about which ion is the limiting one for a potential window and also verifying the different mechanism of FIT is involved in the reaction.[53,97,103]

2.10.1 Application of micro-ITIES

The advantages of the micro-ITIES, mentioned previously, brought the ideal design for electrochemical sensors and circumvented problems associated with large ITIES. Due to their size and low current flow, sensors based on micro-electrodes do not destroy the sample being monitored. Also, the fast time responses enhance the mass transport allowing time independent currents to be measured. The micro-ITIES has found powerful applications in the detection of various ionic species including non-redox ions,[104,105] drugs[106] as well as pharmaceutical compounds.[107] Great improvements in the detection of hydrophilic ionic species including protons, alkali metal, heavy metal and other ions have been achieved by incorporating ionophores in one of the phases which selectively interact with the ions of interest.[54,108–110]

Micro sized liquid|liquid interfaces can offer several advantages in comparison to potentiometric electrodes, which can arise from the selectivity obtained from the control of the interfacial potential, with the measured current being proportional to the sample concentration. It has also been shown to possess useful properties when used as a

transducer to follow enzymatic reactions. Urea and creatinine have been successfully assayed using such methodology.[25] Several authors have also employed micro liquid|liquid interfaces as detectors for ion chromatography,[111] liquid chromatography and capillary electrophoresis.

2.11 Lipophilicity of ions

Lipophilicity (or hydrophobicity) is a molecular property expressing the relative affinity of solutes for an aqueous and an organic, water-immiscible solvent. For this reason, lipophilicity encodes most of the intermolecular forces that can take place between a solute and a solvent, and represents the affinity of a molecule for a lipophilic environment. Is one of the most important physicochemical parameters associated with chemical compounds, several studies have been carried out to understand, evaluate, and predict this parameter.[112]

Hydrophobicity governs numerous and different biological processes, such as, transport, distribution, and metabolism of biological molecules; molecular recognition; and protein folding. Therefore, the knowledge of a parameter that describes the behaviour of solutes (such as drugs) into polar and nonpolar phases is essential to predict their transport and activity. It has been traditionally accepted that ionisable compounds cross biological membranes only in their neutral form. However, recent studies[113-115] suggest a significant passive (i.e. diffusion controlled)[116] transfer of ions. As many drugs are organic compounds that are thus partially or largely ionized at physiological pH, membrane transport can be deeply affected by the lipophilicity of charged species.

In practice, at liquid|liquid interface, passive transfer simply means partition across an interface, mediated by a potential-driven process,[117] which is used to assess lipophilicity of ions. Thermodynamically, this parameter is defined as the ratio of the activity of the

species dissolved at equilibrium between two immiscible solvent phases, and it is often expresses on a logarithmic scale as logP, by the following:

$$logP = log\frac{a_i^o}{a_i^w} \qquad (2.61)$$

where the thermodynamic activity can be approximated by the concentration in diluted solutions. Therefore, logP reflects the difference in solvation energy between water and the organic adjacent phase, and it is directly related to the Gibbs energy of transfer. The interaction of a molecule of therapeutic interest with a biological membrane depends on the properties of both its charged and neutral forms. For neutral form of an ionisable compound (N), the partition depends only on the molecular structure of the solute and on the nature of the two solvents.[117,118] Its partition coefficient P is independent of $\Delta_o^w\phi$ and is simply related to its standard Gibbs energy of transfer as defined by Eq.(2.62)

$$logP_N = log\left(\frac{a_N^o}{a_N^w}\right) = -\frac{\Delta G_{tr,N}^{0,w\to o}}{RT} \qquad (2.62)$$

Although this quantity is constant for neutral solutes, in the case of ionic species, an additional condition is imposed by the electroneutrality condition of the two phases.[119,120] The partition coefficient of an ion, $logP_i$, depends on the Galvani potential difference across the interface.[117] Thus, $logP_i$ can be defined by:

$$logP_i = \frac{z_I F\left(\Delta_o^w\phi - \Delta_o^w\phi_i^0\right)}{2.3RT} = \frac{F\Delta_o^w\phi}{2.3RT} - \frac{\Delta G_{tr,i}^{0,w\to o}}{RT} = logP_i^0 + \frac{z_I F\Delta_o^w\phi}{2.3RT} \qquad (2.63)$$

where $logP_i^0$ is the standard partition coefficient of the species i.

The Eq. (2.63) shows that, contrary to the partition of neutral species for which $logP_N$ is a unique quantity related to its standard Gibbs energy of transfer, the partition of ionic species is potential dependent, and $logP_I^0$ represents the proportion of the ions present in each phase if the interface is not polarized. Thus, the formal transfer potential of an ion is

a direct measure of its partition coefficient. This quantity is thus directly related to the half-wave transfer potential of the ion, $\Delta_o^w \phi_{1/2}$, and it can be directly deduced from e.g. cyclic voltammetry experiments. However, there is a downside of electrochemistry at ITIES, which is the number of solvents systems to which it can be applied. In order to interpret the lipophilicity of ionisable drugs in pharmaceutical terms, the thermodynamic parameters obtained at 1,2-dichloroethane and nitrobenzene have to be correlated to the octanol|water (correspondence established),[121] because it is the system commonly used in pharmacology.

2.11.1 Ionic partition diagrams

The transfer behaviour of ionisable compounds depends on their degree of dissociation and hence on the pH of the aqueous phase. This potential-pH dependence can be presented by ionic partition diagrams, which consists in representing the domains of predominance of the various species as a function of applied potential and aqueous pH.

In the case of a monoprotic acid AH, the partition between two phases can be represented in an ionic partition diagram as displayed in figure 2.11.

$$A^- + H^+ \rightleftarrows AH \qquad (2.64)$$
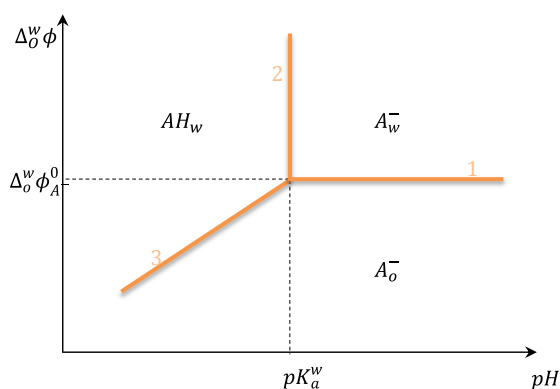
Figure 2.11 – Ionic partition diagram for a hydrophilic monoacid.

From Figure (2.11) it can be seen that the ionic form is dependent on the pH of the aqueous solution and the Galvani potential. At $pH > pK_a^w$, the anionic form is predominant. At Galvani potential more positive than the standard transfer potential, the anion is mainly in the aqueous phase, A_w^-, while at smaller values than the standard transfer potential it is mainly in the organic phase, A_o^-. The separation line 1 between these two zones is given by the Nernst equation for the anion:

$$\Delta_o^w \phi = \Delta_o^w \phi_{A^-}^0 - \frac{RT}{F} \ln \left(\frac{a_{A^-}^o}{a_{A^-}^o} \right) \qquad (2.65)$$

Its neutral form will be mainly in the aqueous phase, AH_w, and the separation line between the aqueous acid and the aqueous base (line 2) is given by:

$$pH = pK_a^w \qquad (2.66)$$

The separation line between the neutral acid in water and the base in the organic phase (line 3) can be obtained by including the acidic constant to the Eq.(2.65), which then gives:

$$\Delta_o^w \phi = \Delta_o^w \phi_{A^-}^0 + \frac{RT\ln 10}{F} (pH - pK_a^w) - \frac{RT}{F} \ln \left(\frac{a_{A^-}^o}{a_{A^-}^w} \right) \qquad (2.67)$$

For the case of a hydrophilic monobase, the ionic partition diagram can be represented as depicted in figure 2.12.

$$BH^+ \rightleftarrows B + H^+ \qquad (2.68)$$
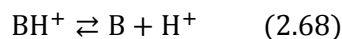
The corresponding acid dissociation constant in water is given by:

$$K_a^w = \frac{a_B^w a_{H^+}^w}{a_{BH^+}^w} \qquad (2.69)$$
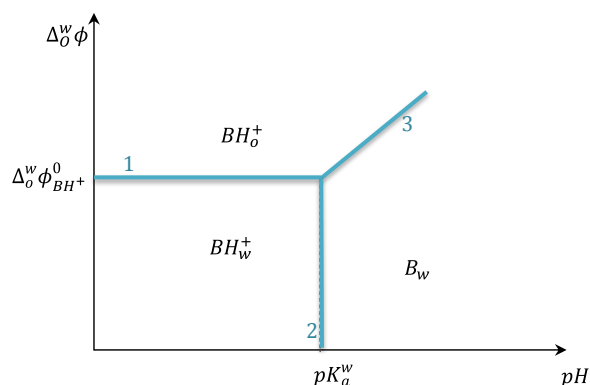
Figure 2.12 – Ionic partition diagram for a hydrophilic monobasic compound.

As in the case of a hydrophilic monoprotic acid, a hydrophilic monobasic compound B, which can be protonated in acidic solutions to form, BH^+, may be approached in the same way. The separation between aqueous and organic phases (line 1) is given by the Nernst equation:

$$\Delta_o^w \phi = \Delta_o^w \phi_{BH^+}^0 + \frac{RT}{F} \ln \left(\frac{a_{BH^+}^o}{a_{BH^+}^w} \right) \qquad (2.70)$$

As previously, line 2 is given by Eq. (2.66). At $pH < pK_a^w$, the only species present is BH^+.

The boundary between B_w and BH_o^+ (line 3), is defined by the neutral base in water and the acid form in the organic phase, and can be represented as follow:

$$\Delta_o^w \phi = \Delta_o^w \phi_{BH^+}^0 + \frac{RT\ln 10}{F} (pH - pK_a^w) + \frac{RT}{F} \ln \left(\frac{a_{BH^+}^o}{a_B^w} \right) \qquad (2.71)$$

Measurements performed on hydrophilic compounds at the ITIES, using cyclic voltammetry can provide accurate determination of the transfer potentials from one liquid phase to another and thus allowing the estimation of the standard partition coefficients of the ionic species. It is important to mention that drug molecules can have more than one acidic or basic group and thus given more difficult ionic partition diagrams.

References

(1)   Volkov, A. G. *Liquid Interfaces in Chemical, Biological, and Pharmaceutical Applications*; 1st ed.; CRC Press, 2001.

(2)   Volkov, A. G. *Liquid-liquid interfaces: theory and methods*; CRC Press, 1996.

(3)   Samec, Z. *Pure & Appl. Chem.* **2004**, *76*, 2147–2180.

(4)   Volkov, A. G. *Liquid Interfaces in Chemistry and Biology*; Wiley: New York, 1998.

(5)   Nernst, W.; Riesenfeld, D. L. *Ann. Phys.* **1902**, *7*, 600–608.

(6)   Cremer, M. Z. *J. Biol.* **1906**, *47*, 562–608.

(7)   Verwey, E. J. W.; Niessen, K. F. *Philos. Mag.* **1939**, *28*, 435–446.

(8)   Samec, Z. *Chem. Rev.* **1988**, *88*, 617–632.

(9)   Volkov, A. G.; Deamer, D. W.; Tanelian, D. L.; Markin, V. S. *Prog. Surf. Sci.* **1996**, *53*, 1–134.

(10)   Gavach, C.; Mlodnicka, T.; Guastalla, J. *C. R. Acad. Sci. C.* **1968**, *266*, 1196–1199.

(11)   Girault, H. H. *Electrochim. Acta* **1987**, *32*, 383–385.

(12)   Koryta, J.; Vanýsek, P.; Březina, M. *J. Electroanal. Chem.* **1977**, *75*, 211–228.

(13)   Samec, Z.; Mareček, V.; Weber, J. *J. Electroanal. Chem* **1979**, *100*, 841–852.

(14)   Kakutani, T.; Osakai, T.; Senda, M. *Bull. Chem. Soc. Jpn.* **1983**, *56*, 991–996.

(15)   Samec, Z.; Marecek, V.; Weber, J.; Homolka, D. *J. Electroanal. Chem.* **1979**, *99*, 385–389.

(16)   Mareček, V.; Samec, Z. *Anal. Chim. Acta* **1983**, *151*, 265–269.

(17)   Hundhammer, B.; Solomon, T.; Alemu, H. *J. Electroanal. Chem.* **1983**, *149*, 179–183.

(18)   Samec, Z. *J. Electroanal. Chem.* **1979**, *99*, 197–205.

(19)   Samec, Z. *J. Electroanal. Chem.* **1979**, *103*, 1–9.

(20)   Samec, Z.; Mareček, V.; Weber, J. *J. Electroanal. Chem* **1979**, *103*, 11–18.

(21)   Koryta, J. *Electrochim. Acta* **1979**, *24*, 293–300.

(22)   Taylor, G.; Girault, H. H. J. *J. Electroanal. Chem.* **1986**, *208*, 179–183.

(23)   Campbell, J. A.; Girault, H. H. *J. Electroanal. Chem.* **1989**, *266*, 465–469.

(24)   Silva, F.; Sousa, M. J.; Pereira, C. M. *Electrochim. Acta* **1997**, *42*, 3095–3103.

(25)   Osborne, M. D.; Girault, H. H. *Electroanalysis* **1995**, *7*, 714–721.

(26)   Ohkouchi, T.; Kakutani, T.; Osakai, T.; Mitsugi, S. *Anal. Sci.* **1991**, *7*, 371–376.

(27)   Santos, H. A.; García-Morales, V.; Pereira, C. M. *ChemPhysChem* **2010**, *11*, 28–41.

(28)   Tsionsky, M.; Bard, A. J.; Mirkin, M. V. *J. Am. Chem. Soc.* **1997**, *119*, 10785–10792.

(29)   Su, B.; Abid, J.-P.; Fermín, D. J.; Girault, H. H.; Hoffmannová, H.; Krtil, P.; Samec, Z. *J. Am. Chem. Soc.* **2003**, *126*, 915–919.

(30)   Quinn, B. M.; Liljeroth, P.; Kontturi, K. *J. Am. Chem. Soc.* **2002**, *124*, 12915–12921.

(31)   Quinn, B. M.; Kontturi, K. *J. Am. Chem. Soc.* **2004**, *126*, 7168–7169.

(32)   Ulmeanu, S.; Lee, H. J.; Fermin, D. J.; Girault, H. H.; Shao, Y. *Electrochem. Commun.* **2001**, *3*, 219–223.

(33)   Gulaboski, R.; Mirčeski, V.; Scholz, F. *Electrochem. Commun.* **2002**, *4*, 277–283.

(34)   Scholz, F.; Gulaboski, R. *ChemPhysChem* **2005**, *6*, 16–28.

(35)   Amemiya, S.; Yang, X.; Wazenegger, T. L. *J. Am. Chem. Soc.* **2003**, *125*, 11832–11833.

(36)   Mälkiä, A.; Liljeroth, P.; Kontturi, A.-K.; Kontturi, K. *J. Phys. Chem. B* **2001**, *105*, 10884–10892.

(37)   Dassie, S. A.; Baruzzi, A. M. *J. Electroanal. Chem.* **2000**, *492*, 94–102.

(38)   Lagger, G.; Tomaszewski, L.; Osborne, M. D.; Seddon, B. J.; Girault, H. H. *J. Electroanal. Chem.* **1998**, *451*, 29–37.

(39)   Forssten, C.; Strutwolf, J.; Williams, D. E. *Electrochem. Commun.* **2001**, *3*, 619–623.

(40) Gulaboski, R.; Cordeiro, M. N. D. S.; Milhazes, N.; Garrido, J.; Borges, F.; Jorge, M.; Pereira, C. M.; Bogeski, I.; Morales, A. H.; Naumoski, B.; Silva, a F. *Anal. Biochem.* **2007**, *361*, 236–243.

(41) Alemu, H. *Pure & Appl. Chem.* **2004**, *76*, 697–705.

(42) Gobry, V.; Bouchard, G.; Carrupt, P.; Testa, B.; Girault, H. H. *Helvetica Chim. Acta* **2000**, *83*, 1465–1474.

(43) Samec, Z.; Trojánek, A.; Langmaier, J.; Samcová, E.; Málek, J. *Electroanal.* **2000**, *12*, 901–904.

(44) Reymond, F.; Steyaert, G.; Pagliara, A.; Carrupt, P.; Testa, B.; Girault, H. *Helv. Chim. Acta.* **1996**, *79*, 1651–1669.

(45) Cui, R.; Li, Q.; Gross, D. E.; Meng, X.; Li, B.; Marquez, M.; Yang, R.; Sessler, J. L.; Shao, Y. *J. Am. Chem. Soc.* **2008**, *130*, 14364–14365.

(46) Cai, C.; Mirkin, M. V. *J. Am. Chem. Soc.* **2005**, *128*, 171–179.

(47) Caçote, M. *Electrochim. Acta* **2004**, *49*, 263–270.

(48) Yoshida, Y.; Maeda, K.; Shirai, O. *Journal of Electroanalytical Chemistry* **2005**, *578*, 17–24.

(49) Jänchenová, H.; Lhotský, A.; Štulík, K.; Mareček, V. *J. Electroanal. Chem.* **2007**, *601*, 101–106.

(50) Benjamin, I. *Ann. Rev. Phys. Chem.* **1997**, *48*, 407–451.

(51) Trojánek, A.; Langmaier, J.; Samec, Z. *Journal of Electroanalytical Chemistry* **2007**, *599*, 160–166.

(52) Reymond, F. *Electrochim. Acta* **2000**, *45*, 2647–2662.

(53) Liu, B.; Mirkin, M. V. *Electroanal.* **2000**, *12*, 1433–1446.

(54) Samec, Z.; Samcová, E.; Girault, H. H. *Talanta* **2004**, *63*, 21–32.

(55) Bard, A. J.; Faulkner, L. *Electrochemical Methods: Fundamentals and Applications*; 2nd ed.; John Wiley & Sons, 2001.

(56) Girault, H. H. J.; Schiffrin, D. J. *J. Electroanal. Chem.* **1984**, *170*, 127–141.

(57) Girault, H. H.; Schiffrin, D. J. *J. Electroanal. Chem.* **1988**, *244*, 15–26.

(58) Samec, Z.; Marecek, V.; Weber, J.; Homolka, D. *J. Electroanal. Chem.* **1981**, *126*, 105–119.

(59) Parker, A. J. *Electrochim. Acta* **1976**, *21*, 671–679.

(60) Grunwald, E.; Baughman, G.; Kohnstam, G. *J. Am. Chem. Soc.* **1960**, *82*, 5801–5811.

(61) Shao, Y.; Stewart, A. A.; Girault, H. H. *J. Chem. Soc Faraday Trans.* **1991**, *87*, 2593–2597.

(62) Hoffmann, K.; Weiss, E. *Journal of Organometallic Chemistry* **1974**, *67*, 221–228.

(63) Girault, H. H. J.; Schiffrin, D. J. *Electrochim. Acta* **1986**, *31*, 1341–1342.

(64) Samec, Z.; Langmaier, J.; Trojánek, A. *J. Electroanal. Chem* **1996**, *409*, 1–7.

(65) Samec, Z.; Mareček, V.; Colombini, M. P. *J. Electroanal. Chem.* **1988**, *257*, 147–154.

(66) Wandlowski, T.; Mareček, V.; Samec, Z. *Electrochim. Acta* **1990**, *35*, 1173–1175.

(67) Koryta, J.; Vanýsek, P.; Březina, M. *J. Electroanal. Chem.* **1976**, *67*, 263–266.

(68) Vanýsek, P.; Basáez Ramírez, L. *J. Chil. Chemi. Soc.* **2008**, *53*, 1455–1463.

(69) Vanysek, P. *Anal. Chem.* **1990**, *62*, 827A–835A.

(70) Reymond, F.; Girault, H. H. In *Encyclopedia of Analytical Chemistry*; John Wiley & Sons, Ltd, 2006.

(71) Chapman, D. L. *Philos. Mag.* **1910**, *25*, 475–481.

(72) Gouy, G. *C. R. Acad. Sci. C.* **1910**, *149*, 654–657.

(73) Gavach, C.; Seta, P.; D'epenoux, B. *J. Electroanal. Chem.* **1977**, *83*, 225–235.

(74) Brett, C. M. A.; Brett, A. M. O. *Electrochemistry: Principles, Methods, and Applications*; OUP Oxford, 1993.

(75)   Yufei, C.; Cunnane, V. J.; Schiffrin, D. J.; Mutomäki, L.; Kontturi, K. *J. Chem. Soc., Faraday Trans.* **1991**, *87*, 107–114.

(76)   Girault, H. H. J.; Schiffrin, D. J. *J. Electroanal. Chem.* **1985**, *195*, 213–227.

(77)   Reinmuth, W. H. *J. Am. Chem. Soc.* **1957**, *79*, 6358–6360.

(78)   Osborne, M. C.; Shao, Y.; Pereira, C. M.; Girault, H. H. *J. Electroanal. Chem.* **1994**, *364*, 155–161.

(79)   Stewart, A. A.; Taylor, G.; Girault, H. H.; McAleer, J. *J. Electroanal. Chem.* **1990**, *296*, 491–515.

(80)   Kontturi, A.-K.; Kontturi, K.; Murtomäki, L.; Quinn, B.; Cunnane, V. J. *J. Electroanal. Chem.* **1997**, *424*, 69–74.

(81)   Shao, Y.; Osborne, M. D.; Girault, H. H. *J. Electroanal. Chem.* **1991**, *318*, 101–109.

(82)   Beattie, P. D.; Delay, A.; Girault, H. H. *J. Electroanal. Chem* **1995**, *380*, 167–175.

(83)   *Handbook of Electrochemistry*; Zoski, C. G., Ed.; Elsevier Science, 2006.

(84)   Yoshida, Z.; Freiser, H. *J. Electroanal. Chem.* **1984**, *179*, 31–39.

(85)   Vanysek, P.; Ruth, W.; Koryta, J. *J. Electroanal. Chem* **1983**, *148*, 117–121.

(86)   Samec, Z.; Papoff, P. *Anal. Chem.* **1990**, *62*, 1010–1015.

(87)   Kudo, Y.; Takeda, Y.; Matsuda, H. *J. Electroanal. Chem.* **1995**, *396*, 333–338.

(88)   Matsuda, H.; Yamada, Y.; Kanamori, K.; Kudo, Y.; Takeda, Y. *Bull. Chem. Soc. Jpn.* **1991**, *64*, 1497–1508.

(89)   Liu, B.; Mirkin, M. V. *Anal. Chem.* **2001**, *73*, 670 A–677 A.

(90)   Shao, Y.; Linton, B.; Hamilton, A. D.; Weber, S. G. *J. Electroanal. Chem.* **1998**, *441*, 33–37.

(91)   Shioya, T.; Nishizawa, S.; Teramae, N. *J. Am. Chem. Soc.* **1998**, *120*, 11534–11535.

(92)   Sinru, L.; Zaofan, Z.; Freiser, H. *J. Electroanal. Chem.* **1986**, *210*, 137–146.

(93)   Kakutani, T.; Nishiwaki, Y.; Osakai, T.; Senda, M. *Bull. Chem. Soc. Jpn.* **1986**, *59*, 781–788.

(94)   Reymond, F.; Lagger, G.; Carrupt, P.-A.; Girault, H. H. *J. Electroanal. Chem.* **1998**, *451*, 59–76.

(95)   Reymond, F.; Carrupt, P.-A.; Girault, H. H. *J. Electroanal. Chem.* **1998**, *449*, 49–65.

(96)   Homolka, D.; Hung, L. Q.; Hofmanova, A.; Khalil, M. W.; Koryta, J.; Marecek, V.; Samec, Z.; Sen, S. K.; Vanysek, P. *Anal. Chem.* **1980**, *52*, 1606–1610.

(97)   Stewart, A. A.; Shao, Y.; Pereira, C. M.; Girault, H. H. *J. Electroanal. Chem.* **1991**, *305*, 135–139.

(98)   Shao, Y.; Mirkin, M. V. *J. Am. Chem. Soc.* **1997**, *119*, 8103–8104.

(99)   Wightman, R. M. *Anal. Chem.* **1981**, *53*, 1125A–1134A.

(100) Howell, J. O.; Wightman, R. M. *Anal. Chem.* **1984**, *56*, 524–529.

(101) Shao, Y.; Mirkin, M. V. *Anal. Chem.* **1998**, *70*, 3155–3161.

(102) Shao, Y.; Mirkin, M. V. *J. Phys. Chem. B* **1998**, *102*, 9915–9921.

(103) Liu, S.; Li, Q.; Shao, Y. *Chem. Soc. Rev.* **2011**, *40*, 2236–2253.

(104) Chen, Y. *Sci. China Ser. B* **2004**, *47*, 24–33.

(105) Yuan, Y.; Shao, Y. *J. Phys. Chem. B* **2002**, *106*, 7809–7814.

(106) Collins, C. J.; Lyons, C.; Strutwolf, J.; Arrigan, D. W. M. *Talanta* **2010**, *80*, 1993–1998.

(107) Ribeiro, J. A.; Miranda, I. M.; Silva, F.; Pereira, C. M. *Phys. Chem. Chem. Phys.* **2010**, *12*, 15190–15194.

(108) Rimboud, M.; Elleouet, C.; Quentel, F.; Kerbaol, J.-M.; L'Her, M. *J. Electroanal. Chem.* **2008**, *622*, 233–237.

(109) Benvidi, A.; Lanjwani, S. N.; Ding, Z. *J. Electroanal. Chem.* **2010**, *641*, 99–103.

(110) Faisal, S. N.; Pereira, C. M.; Rho, S.; Lee, H. J. *Phys. Chem. Chem. Phys.* **2010**, *12*, 15184–15189.

(111) Lee, H. J.; Girault, H. H. *Anal. Chem.* **1998**, *70*, 4280–4285.

(112) Masuda, T.; Jikihara, T.; Nakamura, K.; Kimura, A.; Takagi, T.; Fujiwara, H. *J. Pharm. Sci.* **1997**, *86*, 57–63.

(113) Davis, M. G.; Manners, C. N.; Payling, D. W.; Smith, D. A.; Wilson, C. A. *Journal of Pharmaceutical Sciences* **1984**, *73*, 949–953.

(114) Alcorn, C. J.; Simpson, R. J.; Leahy, D. E.; Peters, T. J. *Biochem. Pharmacol.* **1993**, *45*, 1775–1782.

(115) Smith, D. A.; Brown, K.; Neale, M. G. *Drug Metab. Rev.* **1985**, *16*, 365–388.

(116) Van Bree, J. B. M. M.; De Boer, A. G.; Danhof, M.; Breimer, D. D. *Pharmacy World & Science* **1993**, *15*, 2–9.

(117) Reymond, F.; Girault, H. H.; Steyaert, G.; Carrupt, P.; Testa, B. *Helvetica Chimica Acta* **1996**, *79*, 101–117.

(118) Berthod, A.; Mallet, A. I.; Bully, M. *Anal. Chem.* **1996**, *68*, 431–436.

(119) Reymond, F.; Steyaert, G.; Carrupt, P.-A.; Testa, B.; Girault, H. *J. Am. Chem. Soc.* **1996**, *118*, 11951–11957.

(120) Reymond, F.; Chopineaux-Courtois, V.; Steyaert, G.; Bouchard, G.; Carrupt, P.-A.; Testa, B.; Girault, H. H. *J. Electroanal. Chem.* **1999**, *462*, 235–250.

(121) Steyaert, G.; Lisa, G.; Gaillard, P.; Boss, G.; Reymond, F.; H, G. H.; Carrupt, P.-A.; Testa, B. *J. Chem. Soc., Faraday Trans.* **1997**, *93*, 401–406.

Chapter 3

Experimental methodology

The methods and materials used to produce the work presented in this thesis are reported in this chapter. The fabrication of the micropipettes that served as support for the liquid|liquid micro interfaces is described as well as the different set-up formats used. The three electrode system used with a working electrode modified by thick layer is also described in detail. The reagents and chemicals are listed together with the respective supplier and the preparation of the organic supporting electrolytes. Background information of the electrochemical techniques employed and details of the conditions used in the measurements performed for the study of charge transfer, are also reported.

3.1. Electrochemical apparatus for the study of ion transfer at the ITIES

The electrochemical measurements employed for the study of ion transfer were performed at a micro liquid|liquid interface. The micro dimension of the interface, formed by the tip of the micropipette, allows the electrochemical measurements to be made in a two electrode configuration (Figure 3.1),[1] as the currents are in the nanoampere range it does not disturb the potential of the reference electrode.
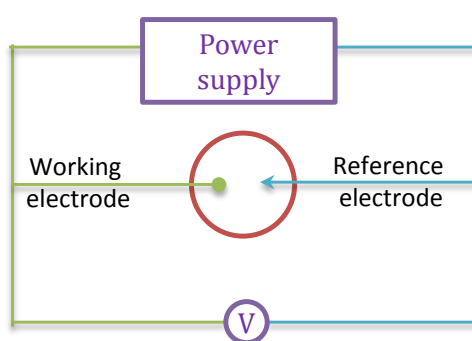
Figure 3.1 – Representation of a two electrode cell, (counter and reference are tied together).

The potential applied between the two electrodes was controlled using an IVIUM CompactStat (Ivium Technologies, Netherlands). All experiments were performed at room temperature (21±2°C) and inside a Faraday cage to minimise any background noise.

As a convention, positive currents are assigned to cations transferring from the aqueous to the organic phase or from anions transferring from the organic to the aqueous phase. Similarly, anions transferring from the aqueous to the organic phase and cations transferring from the organic to the aqueous phase are assigned as a negative current.

3.1.2 Micropipette electrodes

The pipettes of different radii were made from borosilicate capillaries of 1.5mm outer diameter and 1.0mm inner diameter (Harvard Apparatus Ltd, UK). The puller used in the

experiments was Flaming/Brown micropipette puller (model P-97, Sutter Instrument Co. Novato, US). The shape of the micropipette and the diameter of its orifice were controlled by proper choice of the Puller's parameters, which are: heat, pull, velocity, delay, time, and pressure. Since the ohmic resistance of a pipet is largely determined by the length of the narrow shaft leading to the orifice,[2–4] a pulling program (Figure 3.2) was develop to produce reproducible pipets with a short shank and a flat orifice in order to minimize the resistive potential drop inside the narrow shaft.
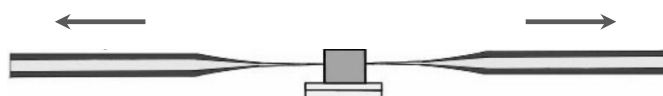
Figure 3.2 – Illustration of the pulling of a capillary glass, by controlling the different program settings (Heat, Pull, Time and Pressure).

The micropipette tips quality and geometry were inspected using an Environmental Scanning Electron Microscope (ESEM). The tip diameters were determined from the images taken (Figure 3.3) with an error of ±1µm.
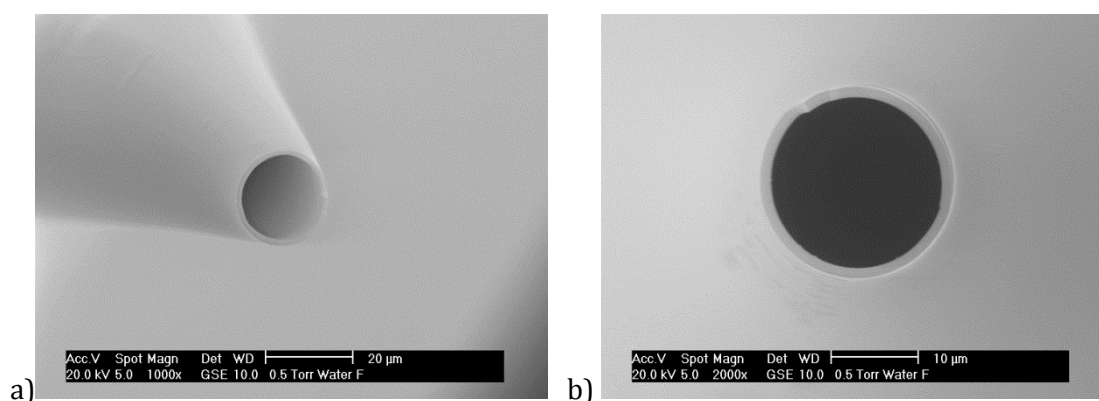
Figure 3.3 – ESEM images of a 10±1 µm radius micropipette tip, a) side view b) front view.

The micropipettes were filled by back-filling with a syringe and a fine needle, the tip of the pipette was previously filled by capillary action. The two different customised cells used where chosen in accordance to the filling solution of the micropipette.

3.1.2.1 Micropipettes filled with aqueous analyte solution

For experiments with aqueous solution inside the micropipette (Figure 3.4), the outer wall was silinized in order to prevent any escape of the filling solution.[5] This was done by immersing the tips in a solution of trimethylchlorosilane while a flow of argon was passed through the pipette from the back. In this procedure it is very important to avoid salinization of the inner wall of the pipette, otherwise, when performing the measurements, the outer solution (organic) can be drawn inside. The set-up to perform the measurements was composed of a glass U-tube, containing a small volume of organic phase in contact with the organic reference solution, similar to the one used by Beattie et al.[4]
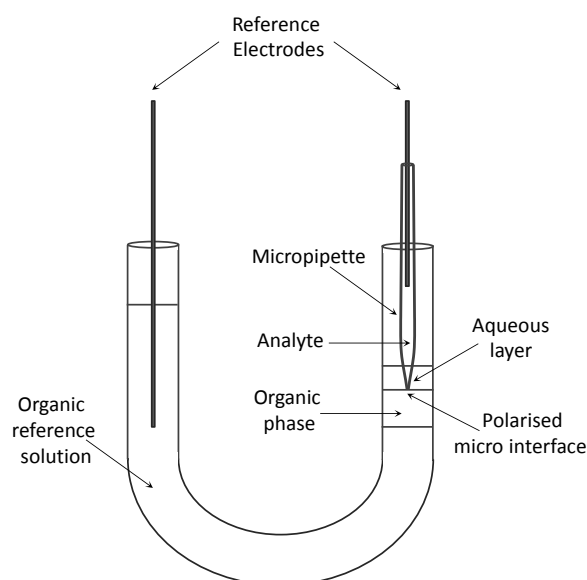
Figure 3.4 – Representation of the cell configuration used for studies at a micro liquid|liquid interface using a glass capillary filled with aqueous solution.

A layer of an aqueous solution was used to cover the organic phase to avoid evaporation during measurements. The tip was positioned as close as possible to the organic reference solution in order to minimise the ohmic drop effect from the organic phase. A micro liquid|liquid interface was thus formed at the entrance of the micropipette tip.

When an organic reference solution was not used in the experiments, the set-up is represented in figure 3.5. The potential was controlled with Ag|AgCl electrode placed inside the micropipette and a non-aqueous electrode, Ag|AgTPB, in the organic solution.
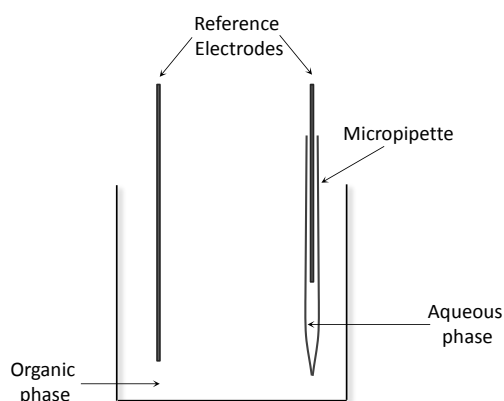
Figure 3.5 – Illustration of the set-up used for experiments without organic reference solution.

3.1.2.2 Micropipettes filled with organic solution

For experiments were the micropipette was filled with organic solution (Figure 3.6), its inner wall was silinized to make it hydrophobic. This was done by dipping the tip of the micropipette in a solution of trimethylchlorosilane, which penetrated inside the pipet. The solution was removed from the pipette after approximately 30 minutes using a small syringe, and the salinized pipet was allowed to dry in the air overnight. In this procedure, both inner and outer walls became salinized. Shao and Mirkin[5] have shown that the voltammetric responses of organic filled pipettes with inner walls or both inner and outer walls salinized were practically identical.
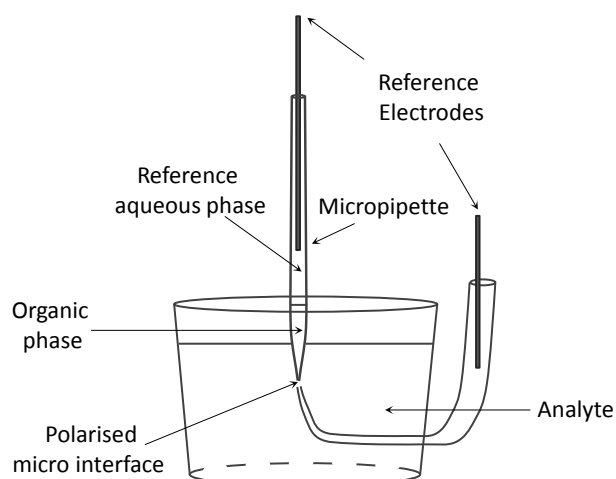
Figure 3.6 – Cell design for the micro ITIES experiments with micropipette filled with organic solution.

3.2 Electrochemical apparatus for the study of ion transfer using a modified thick layer electrode

The ion transfer studies using a thick film modified electrode were performed using an IVIUM CompactStat in a three electrode configuration (Figure 3.7).[6] As reference electrode, an Ag|AgCl (3M KCl, E=0.208V vs. SHE), a platinum flag was used a counter electrode and a glassy carbon (GC) as working electrode (area=0.07cm^2).
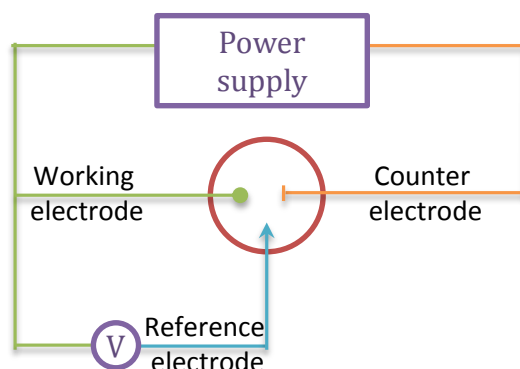
Figure 3.7 – Representation of a three electrode electrochemical cell.

The drop coating method was used to prepare the modified CG electrode. In order to deposit a steady thick film onto the electrode surface, a special design was required, as shown in figure 3.8. The GC electrode was surrounded with a silicon cap with a 2.2mm diameter and a 5mm depth. A small volume of 25μL of the organic solution containing the redox probe and the electrolyte was placed on the surface of a freshly polished working electrode with the help of an Eppendorf pipette. The electrode was then turned over and immersed immediately in an aqueous solution. Any air bubbles in the organic film were avoided by a careful dipping operation.
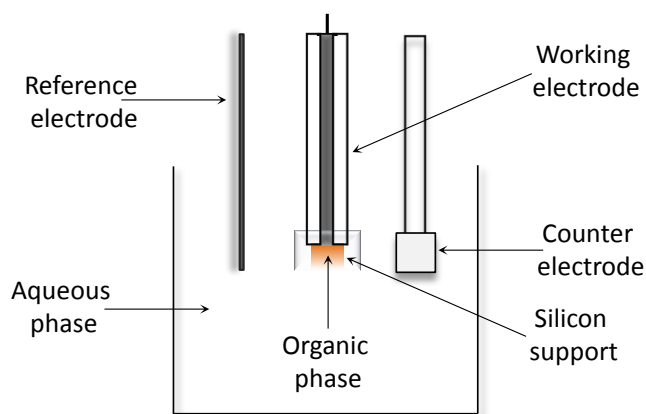
Figure 3.8 – Special design used for the measurement of ion transfer by a thick layer modified electrode.

Before used in the experiments the GC electrode surface was cleaned using alumina powder (0.3μm) solution, in an 8 figure pattern, for approximately two minutes. The electrode was rinsed with deionised water and dried under a slow stream of argon. The activation of the glassy carbon electrode was checked in a solution of 1mM ferrocyanide in 100mM KNO_3, as depicted in figure 3.9.
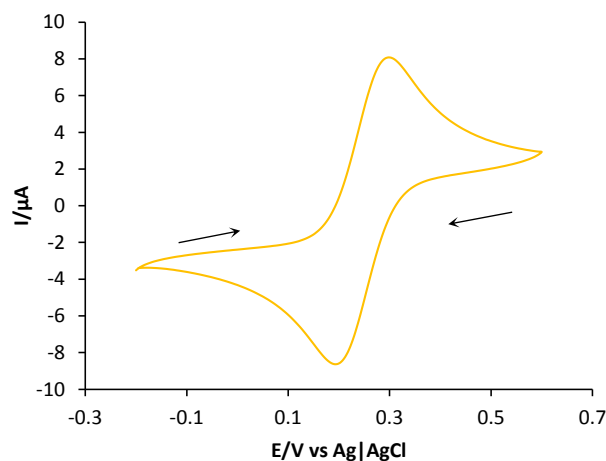
Figure 3.9 – Cyclic voltammogram of 1mM ferrocyanide in 100 mM KNO$_3$ with a freshly polished glassy carbon electrode. Scan rate: 50 mV s^{-1}.

3.3 Reference electrodes

By definition a reference electrode is an electrode for which the Galvani potential difference between the metal and the solution ($\phi^M - \phi^S$) is constant. For it to be stable, only a negligible current can be allowed to pass through the reference electrode, not to disturb the conditions for equilibrium.

The silver|silver chloride (Ag|AgCl) electrode is by far the most common type of aqueous reference electrode used in research and industry due to its simple construction, inexpensive design, and non-toxic components. The simplicity of the Ag|AgCl reference electrode lends itself to micro fabrication as well as incorporation in sensors. The potential is determined by the reaction

$$AgCl_{(s)} + e^- \rightleftarrows Ag_{(s)} + Cl^- \qquad (3.1)$$
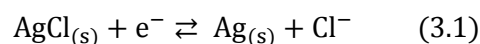
and calculated as follows:

$$E_{Ag|AgCl} = E^{\circ}_{Ag|AgCl} - \frac{RT}{F}\ln a_{Cl^-} \qquad (3.2)$$

The Ag|AgCl reference electrodes, placed inside the pipettes, for the studies at liquid|liquid, were made of high-purity silver wire with 0.25mm diameter (99.9%, Sigma UK) by anodic AgCl coating. A cleaned silver wire was chlorodised by placing it in a solution of KCl 3M and applying a potential of 2V for approximately 30 minutes. The resultant current flow produces an insoluble layer on the silver wire with a brown colour. The Ag|AgCl reference electrodes were rinsed and directly plunged in aqueous solution containing chloride, to ensure that the potential of interface was maintained constant.

The reference electrodes for the organic phase were constructed as follows: an Ag|AgCl electrode was immersed in an aqueous solution of chloride, which is in contact with the organic phase, known as the organic phase reference solution. This reference solution contained a cation which was common in the organic phase, as well. In this study the cation in the reference solution was TBA^+ or $BTPPA^+$ which coincides with the cation of the organic electrolyte salt TBA^+TPB^- or $BTPPA^+TPBCl^-$ respectively, containing similar concentrations of the corresponding anion as supporting electrolyte. Where the reference solution and organic phase meet, a reference interface forms, the common ion to both solutions equilibrates between the two phases and produces an interfacial potential. Therefore, the potential applied by the potentiostat corresponds to the sum of the interfacial potential, the potential of the two reference electrodes and the potential of the reference interface.

In the case where reference electrodes were directly inserted in organic solution, i.e. without the use of organic reference solution, silver wires were coated with AgTPB via anodization in aqueous solution of KTPB at +1.0V vs. Ag|AgCl for approximately 30 minutes, according to published procedures.[7,8]

3.4 Chemicals

All salts and drugs used were of reagent grade and used as received unless indicated otherwise. The material safety data sheet (MSDS) for each compound was read prior to use and appropriate precautions were taken where necessary. All aqueous solutions were prepared using deionized water (Sartorius Arium 611 ultrapure water system (resistivity of not less than 18.2 MΩ cm), from a Milli-Q system (Watford, UK).

3.4.1 Electrolytes

The supporting electrolyte ions have two roles in electrochemical experiments: 1) they carry charge, which is beneficial as migration can be neglected when solving the corresponding transport problem for ion transfer across the interface; 2) they set the limits for the applicable, polarisable range, $\Delta_o^w \phi$, which is called the potential window. The potential window increases with increasing hydrophobicity of the organic base electrolyte ions for a given aqueous base electrolyte. The study of ion transfer reactions is limited to those that occur within the potential window (see section 2.8).

3.4.1.1 Aqueous Supporting Electrolytes

The aqueous salts used as electrolytes were bis(triphenylphosphoranylidene) ammonium chloride (99% BTPPACl, Aldrich), potassium tetrakis(4-chlorophenyl-borate) (99% KTPBCl, Fluka), lithium chloride (98% LiCl, Fluka), tetrabuthylammonium chloride (98% TBACl, Sigma).

3.4.1.2 Organic Supporting Electrolytes

The organic salts used as electrolytes were tetrabuthylammonium tetraphenylborate (99% TBATPB, Sigma) and bis(triphenylphosphoranylidene) ammonium tetrakis

(4-chlorophenyl)borate (99.9% BTPPATPBCl). BTPPATPBCl was prepared by metathesis of equimolar quantities of potassium tetrakis(4-chlorophenyl-borate) (KTPBCl) and bis(triphenylphosphoranylidene) ammonium chloride (BTPPACl).[9] The two salts were dissolved separately in a 2:1 methanol/water mixture and then gently mixed together. The resulting precipitate was filtered under vacuum, washed with water and placed in the dessicator to dry overnight. The salt was then recrystallized by its dissolution in acetone and dried under vacuum before use.

3.4.2 Cyclodextrins

Hexakis(2,3,6-tri-O-Acetyl)-α-cyclodextrin(AcαCD), (99% Cyclolab), Heptakis(2,3,6-tri-O-Acetyl)-β-cyclodextrin(AcβCD), (99% Cyclolab). The structures of the two macrocycles are presented in figure 3.10.

a)   b)
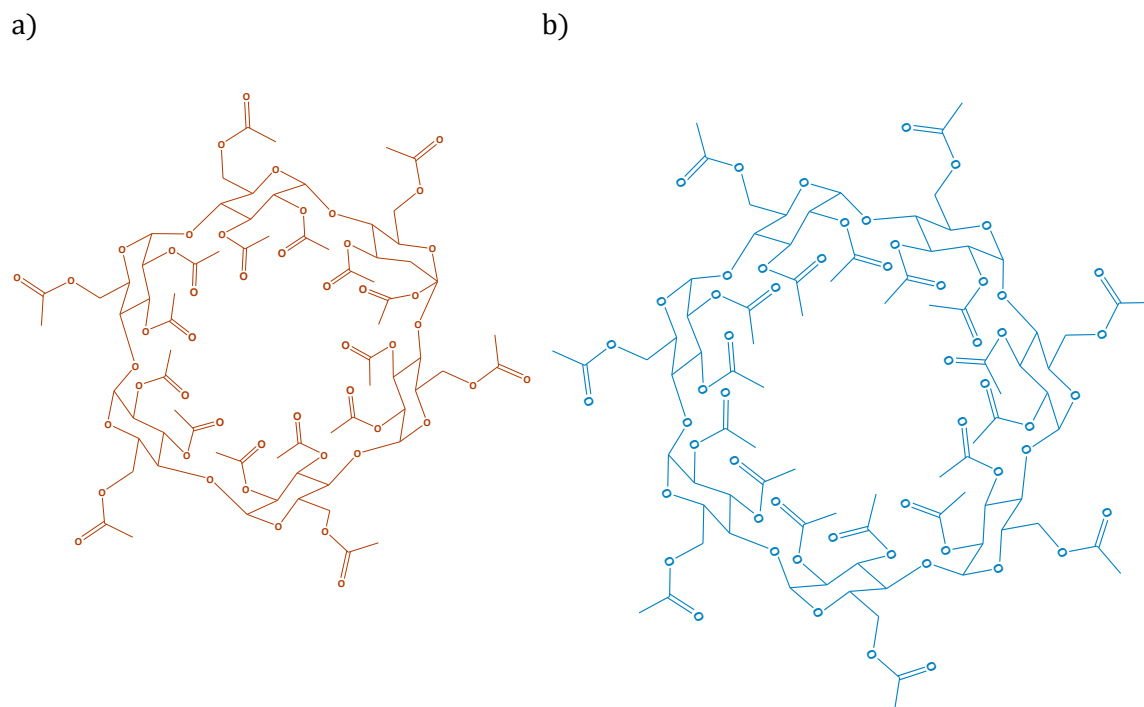
Figure 3.10 – Planar structure of a) AcαCD and b) AcβCD.

Ferroceneacetamido-6[A]-deoxy-heptakis-(2,3-di-O-ethyl)-6[B],6[C],6[D],6[E],6[F]-hexa-O-ethyl-β-cyclodextrin, (EtCDFc), was synthetized in department of chemistry at Durham University.[10] The structure of EtCDFc is presented in figure 3.11.
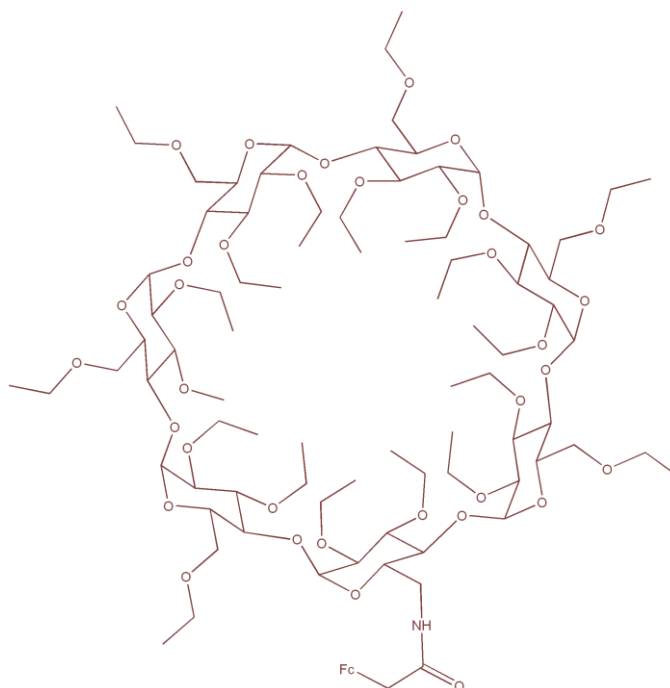
Figure 3.11– Planar structure of EtCDFc.

3.4.3 Other chemicals

Trimethylchlorosilane (Sigma), potassium chloride (99.5% KCl, Sigma), potassium phosphate dibasic (Sigma), potassium phosphate monobasic (Sigma), hydrochloric acid (37% HCl, Sigma), sodium hydroxide (98% NaOH, Sigma), lithium hydroxide (98% LiOH, Sigma).

3.4.4 Solvents

There are large numbers of solvents that have been tested for their suitability for liquid|liquid phase experiments. In order to choose the appropriate solvent for the ITIES studies there are three requirements, which have been commonly considered:

(i)   The solubilities of the solvent in water must be very small,

(ii)   The solvent must be sufficiently polar to promote sufficient dissociation of the supporting electrolyte and thus keeping enough conductivity of the solution,

(iii)   The density of the solvent should differ significantly from that of aqueous phase in order to get a physically stable liquid|liquid interface.

At the present, the most commonly used organic solvents for performing the studies of charge transfer at liquid|liquid interface are nitrobenzene (NB) and 1,2-dichloroethane (1,2-DCE), even though the first is a carcinogenic and is the latter is highly toxic. The current alternatives to 1,2-DCE and NB are o-NPOE (relatively expensive), o-dichlorobenzene (not carcinogenic, but very toxic) and the ketones of Cheng et al.[11,12] which has the advantage of being low in toxicity but has an unsatisfactory potential window for various studies, such as drug transfer, where a wide potential window is needed. o-NPOE has also some disadvantages, which is a density very close to that of water (1.041g.cm^{-3})[13] which makes it difficult to form a well-defined interface in a standard four electrode cell. Also the high viscosity (12.35-13.8 mPa s) in comparison with NB (1.795 mPa s) and 1,2-DCE (0.779 mPa s) may difficult the diffusion of species and thus decreasing the rate of the interfacial process.[13]

In this work, 1,2-DCE[14] was the organic solvent chosen and was handled with all necessary precautions, to avoid any inhalation or skin contact.

3.5 Experimental techniques

There are various electrochemical techniques that can be used for the detection of analytes, all of which have advantages and disadvantages. This section outlines the electrochemical techniques used, cyclic voltammetry (CV) and differential pulse voltammetry (DPV).

3.5.1 Cyclic voltammetry

Cyclic voltammetry (CV) is known to be a useful and powerful technique for the investigation of the electrochemical behaviour of a system. It is often the first experiment performed in electroanalytical studies due to its simplicity, speed and relatively simple interpretation, which makes it a very versatile technique. CV is part of the potential-sweep techniques group. These involve varying the applied electrode potential as a function of time (Figure 3.12), at a particular rate, while measuring the resulting current.
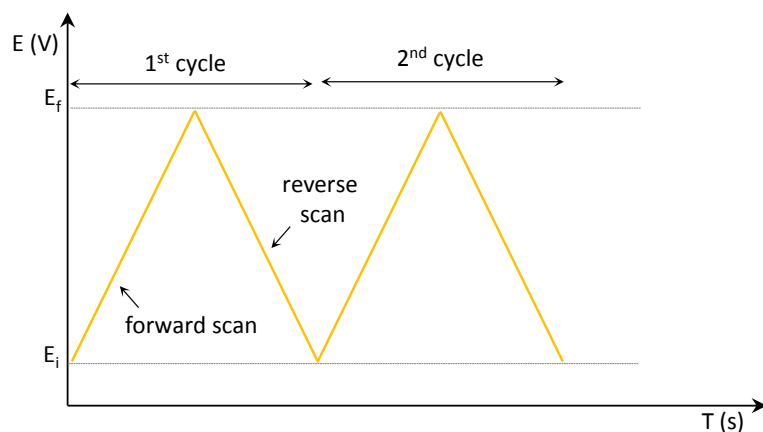
Figure 3.12 – Triangular potential waveform of cyclic voltammetry.

3.5.1.1 Large ITIES

CV was first used for the investigation of charge transfer at liquid|liquid interfaces by Samec et al.,[15] who successfully employed a four electrode system with IR drop compensation, in the study of the tetraalkylammonium ion transfer.

The cyclic voltammograms of a reversible ion transfer reaction (Figure 3.13) exhibits similar features to a reversible electron reaction process at a metal electrode|electrolyte interface.[15–17] When the potential that is applied approaches the formal transfer potential of the ionic species, the flux of ions across the interface increases, resulting in a rise of the

current. When higher potentials are reached, the interfacial/surface concentration drops nearly to zero; the mass transfer of species reaches a maximum and then it declines as the depletion effect sets in. This results in a peaked current-potential curve, as shown in figure 3.13. The current follows a decrease of $t^{1/2}$ as given by the Cottrell equation (Eq. 3.3).[6]

$$i(t) = \frac{zFAD^{1/2}C}{\pi^{1/2}t^{1/2}} \qquad (3.3)$$

When the sweep is reversed, the same phenomena occurs, resulting in a curve of same appearance of the forward scan but with a negative current, as the direction of the ionic flux is inverted compared to the forward scan. All this processes yields a voltammogram, the shape of which is dependent on the size of the interface: a peak shape in the case of large interfaces or a sigmoidal shape for micro interfaces (see sections 2.7.1.2 and 2.13). The current measured during this process can be normalised to the interface area and referred to as the current density, which is then plotted against the applied potential.
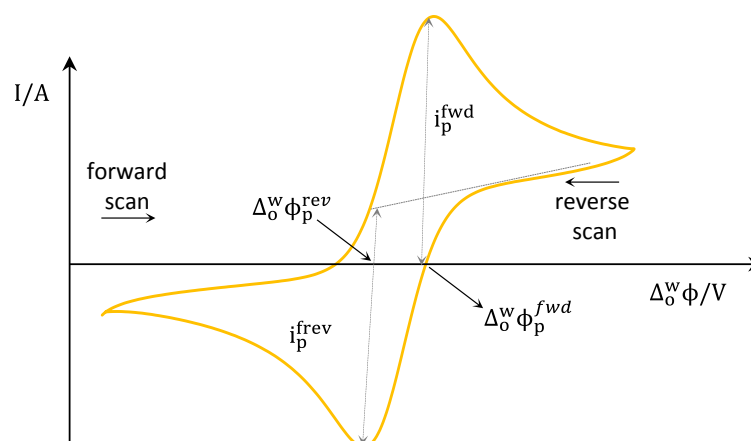
Figure 3.13 – Theoretical cyclic voltammogram for a single charged ion transfer reaction across a macro liquid|liquid interface. $\Delta_o^w \phi_p^{fwd}$ and $\Delta_o^w \phi_p^{rev}$ correspond to the forward and reverse potentials and i_p^{fwd} and i_p^{rev} are the forward and reverse peak currents respectively.

From the sweep-rate dependence of the voltammetric data, several quantitative properties of the charge-transfer reaction can be determined. However, it is in qualitative mechanistic investigations that sweep techniques like cyclic voltammetry are most useful. This technique is very convenient for determining whether a simple electrochemical reaction is limited by diffusion (reversible systems) or limited by kinetics (irreversible systems) or partially limited by kinetics (quasi-reversible systems).[6] The diagnostic test for a reversible transfer process is the separation of forward and reverse peak currents (E_p^a and E_p^c respectiely), ΔE_p, given by:

$$\Delta E_p = E_p^a - E_p^c = \frac{59}{n} \, mV \, (at \, 25°) \qquad (3.4)$$

n is the number of electrons exchanged or the charge of ions to be transferred. The analysis of ion transfer process is similar to that of redox reactions, and the expression of the peak current for ion transfer reactions is given by the Randles-Sevcik equation,[6]

$$i_p = 0.4463 \times 10^{-3} (nF)^{3/2} A(RT)^{-1/2} D^{1/2} C \upsilon^{1/2} \qquad (3.5)$$

which at 298K can be simplified to:

$$i_p = (2.69 \times 10^5) n^{3/2} \upsilon^{1/2} D^{1/2} AC \qquad (3.6)$$

where i_p is the peak current (A), A is the area of the ITIES (cm^2), R and F are the gas and Faraday constants, z, C and D, are the charge, the bulk concentration (mol cm^{-3}) and the diffusion coefficient of the ion (cm s^{-1}), respectively, T is the absolute temperature (K), υ the scan rate (V s^{-1}), and t, the time (s). By varying the scan rate and maintaining all the other factors constant, the Eq. (3.6) allows then the evaluation of the diffusion coefficient of the transferring ion.[18]

It is also important to note that the applied potential difference between two reference electrodes depends on the nature of the electrodes used. It is therefore necessary to convert the scale of applied potential (ΔE) to the Galvani scale. This can be achieved by internally referencing each measurement with transferring ions such as TMA^+ for which the formal transfer potential is already known in most solvent systems:

$$\Delta E = \Delta_o^w \phi + E_{ref} \qquad (3.7)$$

An essential application of CV at the ITIES is the determination of the formal transfer potential of ions, $\Delta_o^w \phi_i^{0\prime}$. For a reversible ion transfer reaction at a large planar interface, the formal potential can be expressed in terms of the half-wave potential, $\Delta_o^w \phi_{1/2,i}$ by:

$$\Delta_o^w \phi_i^{1/2} = \Delta_o^w \phi_i^{0\prime} + \frac{RT}{z_i F} \ln \left(\frac{D_i^w}{D_i^o} \right)^{1/2} \qquad (3.8)$$

The $\Delta_o^w \phi_{1/2,i}$ differs substantially from the standard transfer potential as the diffusion characteristics of the ion are different in the aqueous and the organic phase. Experimentally, $\Delta_o^w \phi_{1/2,i}$ is considered equal to the mid-peak potential and is directly deduced from the voltammograms:

$$\Delta_o^w \phi_i^{1/2} = \Delta_o^w \phi_{p,i}^{fwd} - \left(\frac{\Delta_o^w \phi_{p,i}^{fwd} - \Delta_o^w \phi_{p,i}^{rev}}{2} \right) = \Delta_o^w \phi_{p,i}^{fwd} - \frac{\Delta \Delta_o^w \phi_{p,i}}{2} \qquad (3.9)$$

where $\Delta \Delta_o^w \phi_{p,i}$ corresponds to the peak-to-peak separation.

Concerning the ratio of the diffusion coefficients in both phases (Eq. 3.6), this term is usually approximated to the inverse ratio of the solvents viscosities, η, by the application of Walden's rule,[6] since the diffusion coefficients in the organic phase are rarely known due to experimental difficulties.

$$\frac{D_i^o}{D_i^w} = \frac{\eta^w}{\eta^o} \qquad (3.10)$$

For the experiments reported in this thesis, two reference ions were used, TMA[+] and TEA[+]. The formal potential of TMA[+] and TEA[+] has been determined as +160 mV[9,19] and +52 mV[9] respectively, using the 'TATP' assumption (see section 2.4), TMA[+] or TEA[+] where added to the water phase after each experiment in order to reference all the observed reversible half-wave potentials, $\Delta_o^w \phi_i^{1/2}$, deduced from the voltammograms. The logarithm of the ratio of the diffusion coefficients in both phases is neglected in this study. When using TMA[+] ions as an internal reference, the measured half wave potential and the formal transfer potential for the ion under study and the reference are simply related using Eq. 3.11.

$$\Delta_o^w \phi_i^{o'} = \Delta_o^w \phi_{TMA^+}^{o'} - \Delta_o^w \phi_{TMA^+}^{1/2} + \Delta_o^w \phi_i^{1/2} \qquad (3.11)$$

3.5.1.2 Micro ITIES

The cyclic voltammogram presented in Figure 3.14 yields the current flowing through a micro interface supported at a micropipette tip in response to the applied potential, associated with the electrochemical cell (scheme 2.1). With 1,2-DCE as organic solvent, a potential range of approximately 0.8V is obtained when the electrolytes LiCl and BTPPATPBCl are used in the water and organic phases, respectively. The interface is considered polarised within this potential range, where only little current flows, mostly due to the charging current of the interface.

Ag'|AgCl	10mM LiCl 1mM BTPPACl	10mM BTPPATPBCl 1,2-DCE	10mM LiCl	AgCl|Ag
RE'	Organic reference solution	Organic phase	Aqueous phase	RE
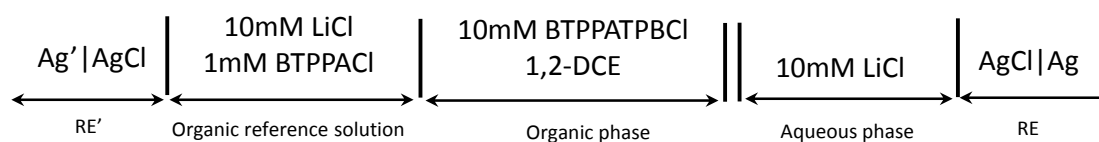
Scheme 2.1 – Schematic representation of the blank electrochemical cell.

The current rise is associated with the transfer of Li+ and TPBCl- at positive potentials and Cl- or BTPPA+ at negative potentials. The relative contribution of the lipophilic anion and hydrophilic cation depends on the racking of these ions on the scale of the Gibbs energies of transfer.[20] Since both are similar, both ions contribute to the observed background current, (Figure 3.14, dashed line).
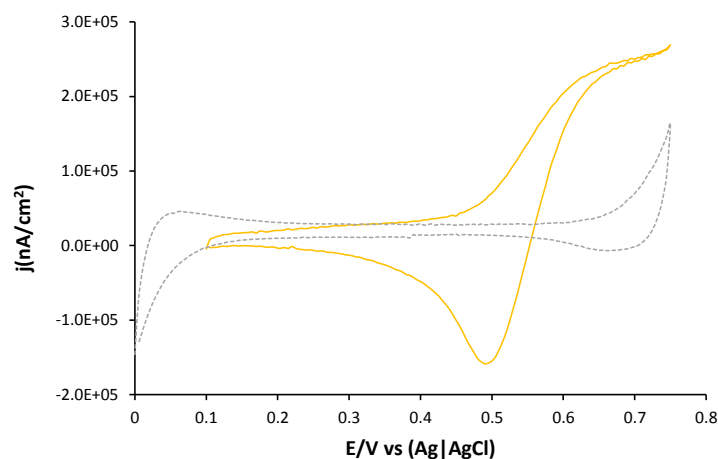
Figure 3.14 – Cyclic voltammograms in the absence (dashed line) or in the presence (full line) of TMA+ at a aqueous|1,2-DCE interface supported at a micropipette tip (radius=20.1±1μm).

Several salts can be used as aqueous and organic electrolytes, yielding various potential windows, meaning that the potential window can be expanded by using a more hydrophobic and hydrophilic supporting electrolytes in the organic and aqueous phase, respectively.

3.5.2 Differential pulse voltammetry

In order to increase speed and sensitivity, many forms of potential modulation have been tried over the years. Differential pulse voltammetry (DPV), normal pulse voltammetry (NPV) and square wave voltammetry (SWV) are the most commonly used pulse techniques. The basis of all pulse voltammetric techniques is the difference in the rate of

the decay of the charging and the faradaic currents following a potential step, also known as pulse. The ultimate aim of the pulse techniques is to lower the detection limit of the voltammetric measurements by increasing the ratio between the faradaic and non-faradaic current. DPV, particularly, has become widely used because of its high sensitivity and general applicability,[21] as its operation results in a very effective correction of the charging background current. In this technique, the potential wave consists of small pulse of constant amplitude superimposed upon a staircase wave form (Figure 3.15).
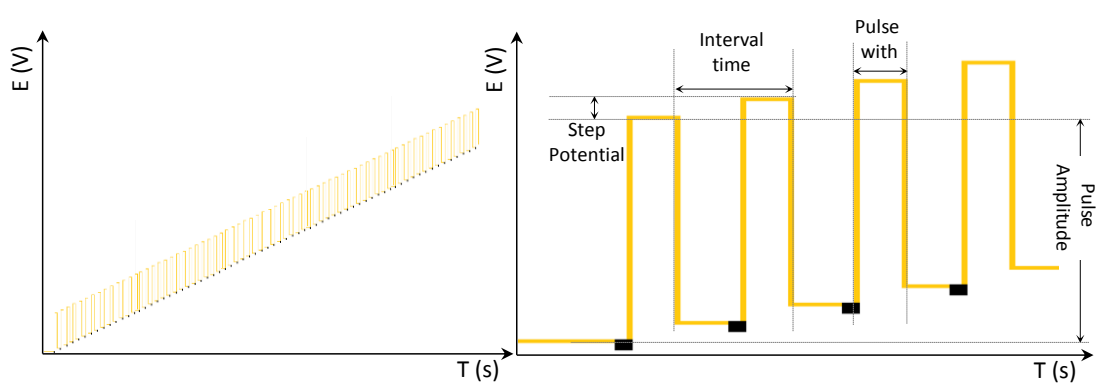
Figure 3.15 – Potential-time waveform of DPV. Orange trace corresponds to the applied potential. The black squares indicate the first and second points, where the current sampled. a) Full waveform, b) Zoom of the waveform.

Unlike normal pulse voltammetry, with which it can be compared, the current is measured at two points for each pulse, the first point just before the application of the pulse (τ') and the second at the end of the pulse (τ). These sampling points are selected to allow for the decay of the non-faradaic current. The difference between the current measured at these points for each pulse is determined, $\Delta i = i(\tau) - i(\tau')$, and plotted against the base potential (Figure 3.16).
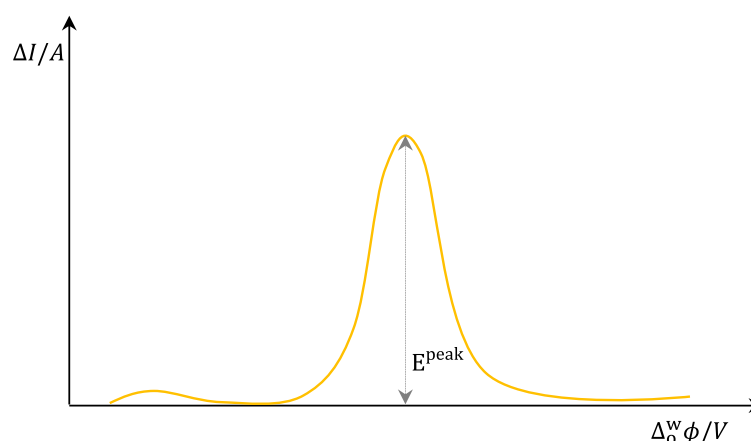
Figure 3.16 – Representation of a differential pulse voltammogram.

The resulting differential pulse voltammogram consists of current peaks with the height of the peak current directly proportional to the concentration of the analyte. The peak current (I^{peak}) and potential (E^{peak}) parameters, of a differential pulse voltammogram are defined by Eq. 3.12 and Eq. 3.13, respectively.[6]

$$I_{DPV}^{peak} = nFA \left(\frac{D}{\pi(\tau - \tau')} \right)^{1/2} C \left(\frac{1 - \sigma}{1 + \sigma} \right) \qquad (3.12)$$

$$E^{peak} = E^{1/2} - \frac{\Delta E}{2} \qquad (3.13)$$

where n is the number of electrons, F the Faraday's constant, A the electrode area (cm^2), D the diffusion coefficient ($cm\ s^{-1}$), C the concentration of the analyte ($mol\ cm^{-3}$), ΔE is the pulse amplitude, τ' and τ are the first and second current sampling time respectively.

The maximum value for the quotient $(1 - \sigma)/(1 + \sigma)$ is obtained for large pulse amplitudes and is the unity, σ is expressed by Eq. 3.12.

$$\sigma = \exp \left(\frac{nF\Delta E}{2RT} \right) \qquad (3.12)$$

The peak current also increases with the pulse amplitude, $\Delta E = E_2 - E_1$, but in a complicated linear fashion. For this reason, in practice, amplitudes greater than 100mV are not used, since the peaks broaden and the resolution is significantly inhibited. The characteristics of DPV are symmetrical peaks for reversible reactions and asymmetrical peaks for irreversible reactions.

References

(1) Liu, S.; Li, Q.; Shao, Y. *Chem. Soc. Rev.* **2011**, *40*, 2236–2253.

(2) Wei, C.; Bard, A. J.; Nagy, G.; Toth, K. *Anal. Chem.* **1995**, *67*, 1346–1356.

(3) Stewart, A. A.; Taylor, G.; Girault, H. H.; McAleer, J. *J. Electroanal. Chem.* **1990**, *296*, 491–515.

(4) Beattie, P. D.; Delay, A.; Girault, H. H. *J. Electroanal. Chem* **1995**, *380*, 167–175.

(5) Shao, Y.; Mirkin, M. V. *Anal. Chem.* **1998**, *70*, 3155–3161.

(6) Bard, A. J.; Faulkner, L. *Electrochemical Methods: Fundamentals and Applications*; 2nd ed.; John Wiley & Sons, 2001.

(7) Horrocks, B. R.; Mirkin, M. V. *Anal. Chem.* **1998**, *70*, 4653–4660.

(8) Clarke, D. J.; Schiffrin, D. J.; Wiles, M. C. *Electrochim. Acta* **1989**, *34*, 767–769.

(9) Reymond, F.; Chopineaux-Courtois, V.; Steyaert, G.; Bouchard, G.; Carrupt, P.-A.; Testa, B.; Girault, H. H. *J. Electroanal. Chem.* **1999**, *462*, 235–250.

(10) Kataky, R.; Dell, R.; Senanayake, P. K. *Analyst* **2001**, *126*, 2015–2019.

(11) Cheng, Y.; Schiffrin, D. J. *J. Electroanal. Chem.* **1997**, *429*, 37–45.

(12) Cheng, Y.; Schiffrin, D. J. *J. Electroanal. Chem.* **1996**, *409*, 9–14.

(13) Samec, Z. *Pure & Appl. Chem.* **2004**, *76*, 2147–2180.

(14) Sebelius, K. *12th Report on Carcinogens*; 2011; pp. 145–147.

(15) Samec, Z.; Mareček, V.; Weber, J. *J. Electroanal. Chem* **1979**, *100*, 841–852.

(16) Samec, Z.; Mareček, V.; Weber, J. *J. Electroanal. Chem* **1979**, *103*, 11–18.

(17) Homolka, D.; Hung, L. Q.; Hofmanova, A.; Khalil, M. W.; Koryta, J.; Marecek, V.; Samec, Z.; Sen, S. K.; Vanysek, P. *Anal. Chem.* **1980**, *52*, 1606–1610.

(18) Reymond, F.; Girault, H. H. In *Encyclopedia of Analytical Chemistry*; John Wiley & Sons, Ltd, 2006.

(19) Wandlowski, T.; Mareček, V.; Samec, Z. *Electrochim. Acta* **1990**, *35*, 1173–1175.

(20) Behr, B.; Gutknecht, J.; Schneider, H.; Stroka, J. *J. Electroanal. Chem.* **1978**, *86*, 289–299.

(21) Pelzer, J.; Scholz, F.; Henrion, G.; Nitschke, L. *Electroanalysis* **1989**, *1*, 437–440.

Chapter 4

Lipophilic cyclodextrins as chiral selectors at a liquid|liquid interface

In this chapter, work is described that demonstrates conclusively that size matched cyclodextrins, such as lipophilic acetylated α- and βCD (AcαCD and AcβCD) common chiral stationary phases, can be used in a non-aqueous phase to differentiate chiral molecules, such as ephedrine hydrochloride. Facilitated ion transfer of ephedrine enantiomers and racemate by the lipophilic cyclodextrins was investigated at the aqueous|1,2-dichloroethane micro interface using electrochemical approaches (cyclic voltammetry and differential pulse). The interaction of the ephedrinium ions with AcαCD and AcβCD was studied varying the concentration of the ephedrine ions and the ligand. The results suggest that the transfer of the ephedrine chiral ions facilitate by AcαCD and AcβCD are controlled by the diffusion of the ligands. Differences in the half-wave potential and current intensities show that chiral discrimination occurs both between the enantiomers and ligands. The difference in stability constant between the (+)EPH[+] and (-)EPH[+] complexes was found to be 0.83±0.1 for AcβCD and 0.71±0.1 for AcαCD.

4.1 Introduction

It has long been recognized that many molecules exist in two mirror images. Despite the emphasis that has been placed on the recent advances in chiral chemistry, optical isomers have been known for many years. In fact, the discovery of chirality in chemistry can be traced back to more than 200 years ago. In the early 1800s, Jean Biot[1,2] observed optical activity in mineralogical samples such as quartz, in which an asymmetrical crystalline form was macroscopically observable.[3] At that time the crystals pair which are mirror images of each other were called "enantiomorphous" crystals (from the Greek enantios and morphe) which means opposite form. The existence of optical isomers was established by the work of Pasteur in 1848.[2,4] Pasteur separated an optically inactive sample of a tartaric acid salt into optically active dextrorotatory and levorotatory components by physically segregating the enantiomorphous crystalline forms. He showed that what had been thought to be a pure substance (racemic acid) was a mixture of two compounds: the natural, dextrorotatory tartaric acid and a substance that, although identical to the first compound identified in all of its other chemical properties, was yet opposite in its solid state structure and in its observed rotation of polarised light. Furthermore, he advanced the field by studying the influence of one chiral compound upon another and introduced the technique of resolution via diastereoisomer formation, which became the basis of many modern chromatographic separations.[3,5]

The existence of the asymmetric carbon atom and the explanation of optical rotation was proposed by both van't Hoff[2,6] and Le Bel.[2,7] However, it was Emil Fisher,[2,8] who made the first serious attempts to relate the absolute stereochemistry of optical isomers and determined the configuration of (+)-glucose for which he received the Nobel prize. The discovery that the respective physiological activity of the isomers of a drug could differ radically initiated a new interest in chiral substances, particularly chiral drugs. This was

found to be true for many physiologically active compounds and, in particular, physiologically active biotechnology products. However, the major stimulation for chiral studies arose from the unfortunate birth defects initiated by one of the enantiomers of thalidomide. This drug was manufactured and sold as a racemic mixture of N-phthalylglutamic acid imide. However, the desired physiologically activity was found to reside solely in the R-(+)-isomer and it was discovered, too late, that the corresponding S-(-)-enantiomer was teratogenic and caused serious fetal malformations. The thalidomide disaster evoked the need to test the different enantiomers of a drug and the appropriate analytical procedures to separate and quantitatively assay them.

Chiral analysis and separation has therefore become an important topic in pharmaceutical analysis and bioanalysis for the screening of drugs, drug impurities, synthetic precursors, side products, and metabolites.[9,10] Cyclodextrins (CDs), native or modified, are numbered among the most popular and most frequently used chiral agents for enantiomeric resolution.[10,11] Harada et al.[12] were the first to introduce the CDs as chiral separation agents and, in 1980, Armstrong[13] used the CDs as mobile phase additives for chiral separations by thin-layer chromatography. Since then, the use of CDs for chiral molecular recognition in separation sciences has undergone with growth as they can discriminate between positional isomers, functional groups, homologous and enantiomers.[14]

4.1.1 Cyclodextrins

CDs also known as cycloamyloses, cyclomatoses and Schardinger dextrins,[15] are chiral by essence,[16] they are cyclic (α-1,4)-linked oligosaccharides of α-D-glucopyranose containing a relatively hydrophobic (lipophilic) cavity and hydrophilic outer surface. Owing to lack of free rotation about the bonds connecting the glucopyranose units (in chair formation), the CDs are not perfectly cylindrical molecules but are toroidal or cone shaped. Based on this

architecture, the primary hydroxyl groups are located on the narrow side of the torus while the secondary hydroxyl groups are located on the wider edge (Figure 4.1). The cavity is lined by the hydrogen atoms and the glycosidic oxygen bridges, respectively.[17] The three dimensional structures of the CDs make them attractive because of the differential reactivity of their alcohol functions, which allow regioselective chemical modification either at the primary or at the secondary rim.[16]
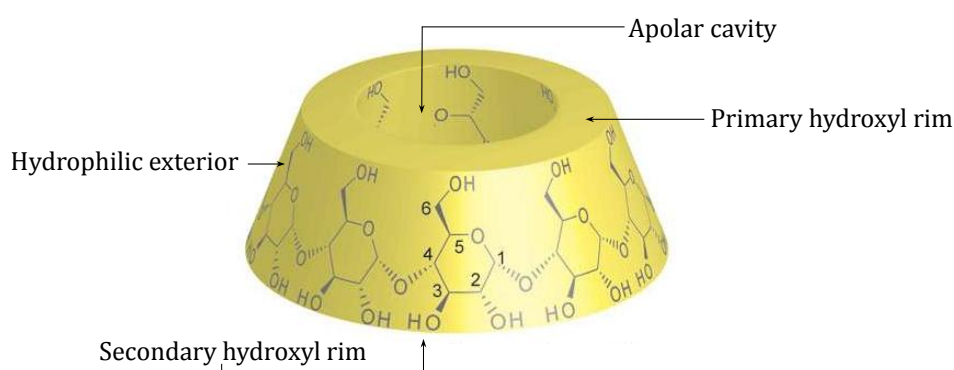
Figure 4.1 – 3D structure of a native cyclodextrin, illustrating the comical shape of the cyclodextrin molecules and both primary and secondary hydroxyl groups. Reproduced with permission from Ogoshi and Harada.[18]

The naturally occurring CDs are α-, β- and γ-CD which consist of six, seven and eight glucopyranose units, respectively (Figure 4.2). CD molecules are relatively large with a number of hydrogen donors and acceptors and, thus in general they do not permeate lipophilic membranes. CDs are generally soluble in water and in most organic solvents. This property is attributed to the presence of primary and secondary hydroxyl groups that are on the outside of the CDs. The cavity of the CD ring consists of a ring of C-H groups and a ring of glycosidic oxygen atoms. This renders the cavity of the CD rings less polar than the outside.
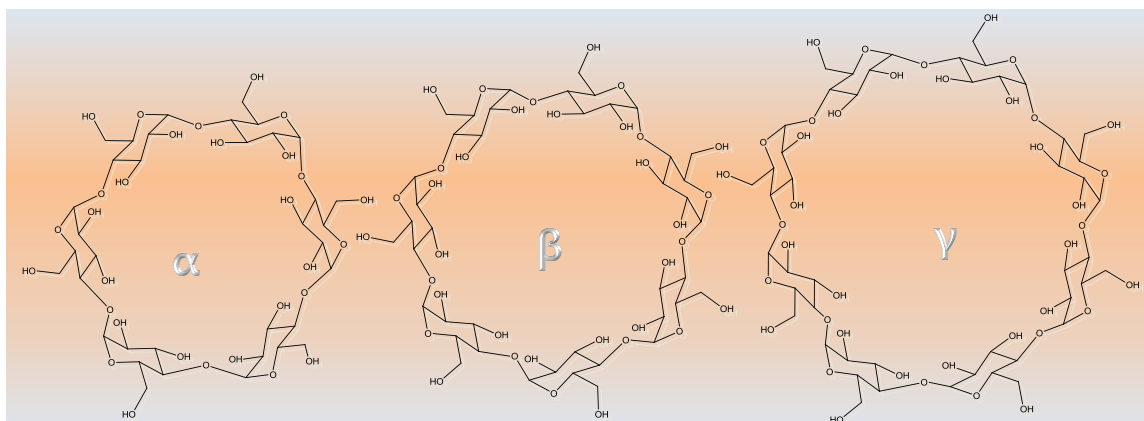
Figure 4.2 – Chemical structure of the host α-, β- and γ-cyclodextrin.

While is thought that, due to steric factors, CDs having fewer than six glucopyranose units cannot exist, CDs containing nine, ten, eleven, twelve and thirteen glucopyranose units, which designated $\delta-, \in -, \xi-, \eta -$, and θ-CD, respectively have been reported.[19] Of these large-ring CDs only δ-CD has been well characterized. The chemical and physical properties of the three most common CDs are quite different, e.g., width of the cavity, solubility, molecular mass etc., however they possess the same depth.[15] The main characteristics are summarized in table 4.1.

Table 4.1 – Physical properties of α-, β-, and γ-CD[15,20]

	α-CD	β-CD	γ-CD
Number of glucose units	6	7	8
Molecular weight (g/mol)	972.86	1135.01	1297.15
Water solubility (g/100mL :25°C)	14.5	1.85	23.2
Internal diameter (Å)	4.0-5.3	6.0-6.5	7.5-8.3
Height of torus (Å)	7.9	7.9	7.9
Cavity volume (Å³)	174	262	427
Substitutable hydroxyl groups	18	21	24

Based on published data it seems that the cavity of βCD is appropriate for hosting a wide number of chemical compounds especially of pharmaceutical interest. CDs are widely used as "molecular cages" in the pharmaceutical, agrochemical, food and cosmetic industries.[21] In the pharmaceutical industry they are used as complexing agents to increase aqueous solubility of poorly soluble drugs and to increase their bioavailability and stability.[19,22] In short, CDs act as a drug delivery system and are potential drug delivery candidates in many applications because of their ability to alter the physical, chemical and biological properties of guest molecules through the formation of inclusion complexes.[23] In addition, CDs can be used to reduce gastrointestinal drug irritation, convert liquid drugs into microcrystalline or amorphous powder and prevent drug-drug and drug-excipient interactions.

CDs can also play a major role in environmental science in terms of solubilisation of organic contaminants, enrichment and removal of organic pollutants and heavy metals from soil, water and atmosphere. They are applied in water treatment to increase the stabilizing action, encapsulation and adsorption of contaminants. High toxic substances can be removed from industrial effluent by inclusion complex formation.[24] Currently, chiral separations seem to be one the most significant areas of application in the use of CDs and their derivatives.[10]

4.1.1.1 Cyclodextrins for chiral sensing

The five chiral carbon atoms in each glucopyranose unit are the source of the enantioselectivity of CDs.[25] The shapes of the glucose units do not repeat from unit to unit, as a result, different chiral recognition sites are present between glucopyranose units of the same CD. Furthermore, CDs can change their shape upon interacting with analytes, in which they can experience included-fit interactions, which can broaden the chiral

selectivity of CDs.[26] Because of their unique properties CDs have been utilised for chiral resolution for a long time and are becoming increasingly popular, however the exact nature of the interaction between the CD and the chiral ligand which leads to enantiomeric discrimination is still not known in detail. CDs serve as ideal selector by chiral molecular recognition and are therefore used in various types of separations. In capillary electrophoresis (CE),[27–30] hydrophilic CDs have been frequently used as buffer modifiers to effect chiral separation of drugs.[30] CDs are also widely used in the separation of enantiomers by high-performance liquid chromatography (HPLC),[2,28,31] or gas chromatography (GC).[32] The stationary phases of these columns contain immobilized CDs. Other analytical applications can be found in CE[27–30] and spectroscopic methods. In nuclear magnetic resonance (NMR) studies[33–35] they can act as chiral shift agents and in circular dichroism[36] as selective (chiral) agents altering spectra.

CDs have been used for their ability of enantiospecific molecular recognition in the liquid phase. Parker and co-workers[37,38] have demonstrated that highly lipophilic αCDs, per-octylated at both rims, are suitable receptors for chiral sensing of ephedrine, pseudoephedrine and norephedrine in the liquid phase, using potentiometric electrodes. In these experiments CDs derivatives have been incorporated into PVC membranes using o-nitrophenyl octyl ether (oNPOE) and bis(butylpentyl) adipate (BBPA) as plasticizers. Potentiometric electrodes have also been used by Stefan and co-workers[39] to design enantioselective sensors. They used membrane electrodes based on graphite paste (graphite powder and paraffin oil) impregnated with 2-hydroxy-3-trimethyl-ammoniopropyl-β-CD. They showed that molecules that possess at least one hydrophobic cyclic part could presumably be included in the hydrophobic cavity of the CD receptor. Polar functions of the guest molecule are then in close contact with eventual polar

functions of the receptor and then could interact to improve the stability and the enantioselectivity of the complex.[40]

In order to enhance the chiral resolution power, a variety of derivatized CDs have been introduced. Due to the availability of multiple reactive hydroxyl groups, the functionality of CDs is greatly increased by chemical modification. Most of the modified CDs are mixtures characterized by an average degree of substitution in varying locations. It follows that increased chiral discrimination can be expected with modified CDs where, through the modification, the degree of asymmetry of the cyclodextrin has been increased and there is the possibility of greater interaction between chiral portions of the cyclodextrins and those of the guests. Modifying CDs and their complexing characteristics usually involves substitution of one or more of the C-2, C-3 and C-6 hydroxyl groups (Figure 4.3).
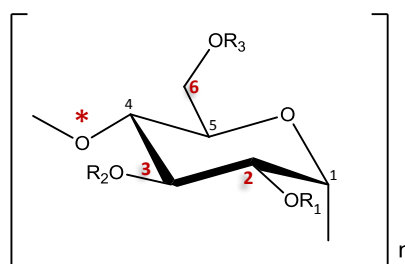
Figure 4.3 – Schematic representation of the glucose unit showing in red the positions susceptive of modification on the CDs, (* represents the α-1,4-type glycosidic linkage).

The modifications may be divided into two categories. In one, the hydroxyl groups are substituted in a symmetric fashion to give a single modified cyclodextrin (e.g. all the hydroxyl groups may be substituted) or at random to give a complex mixture of cyclodextrins in which the average effect is that of a symmetric substitution. A single substituent or a specific combination of substituents can also be done to obtain a modified cyclodextrin. There are 18, 21 and 24 hydroxyl groups in α-, β- and γ-CD, respectively, that can be modified by a wide variety of groups like: alkyl-, hydroxyalkyl-, aminothio-,

glucosyl-, maltosyl-, methyl-, hydroxyethyl-, hydroxypropyl-, acetyl-, etc. This derivatisation may induce substantial changes in the asymmetry of the CD and result in additional and more specific interactions between the chiral area of the guest and the asymmetry of the host, which restrict the geometry of binding, leading to greater enantioselectivity.[10,20,41]

Acetylated CDs, the ones used in this work consist of CD molecules in which the secondary hydroxyl groups in positions 2 and 3 and all available primary hydroxyl groups in positions 6 are acetylated. This functionality acts as hydrogen bond acceptor, which can interact with the analyte hydroxyl or amine groups. The acetyl group can also act as rigid π-electron system for the steric interactions, and it has effect of the extending the mouth of the cyclodextrins cavity to include larger molecules. This is especially advantageous when the chiral analyte, upon the biding to the cyclodextrins protrudes from the cavity and the chiral centre is not in close proximity to the rim of the CDs. For these molecules, the acetylated CDs will enhance the enantioselectivity compared to native CDs.[42]

In any case the major reason for the preparation of CD derivatives are generally the modification of solubility, modification of complexation abilities (stability constant, guest selectivity), or introduction of specific groups with specific functions.

4.1.1.2 Formation of cyclodextrin inclusion complexes

Inclusion complexation refers to a molecular phenomenon where one molecule of guest and one molecule of the host come into contact and form a complex.[13,45-48] CDs can undergo molecular inclusion with a variety of low molecular weight compounds from aliphatic non-polar molecules to polar acids and amines. In these complexes, a guest molecule is held within the cavity of the CD host molecule.[10,43]

As early as 1952, Dalgliesh[44] pointed out that at least a three-point interaction should take place between the analytes and the chiral selector. For instance, the analyte should contain an α-amino-group or carboxyl group (hydrogen bonding), an aromatic ring (hydrophobic interaction) and the ring should contain one or more substituents allowing a closer fit within the cavity of the CD and hence a greater interaction with one of the enantiomers than with the other. Armstrong et al.[45] mentioned that some of the requirements for the chiral recognition by CDs are: (i) formation of an inclusion complex, (ii) relatively tight fit between the analyte and the CD and (iii) a chiral centre or a substituent at the chiral centre must be near and interact with the mouth of the CD cavity.

 The lipophilic cavity of the CD molecules provides a hydrophobic microenvironment into which appropriately sized non-polar moieties can enter to form inclusion complexes.[19,22] However, no covalent bonds are broken or formed during formation of the inclusion complex. The binding strength depends on how well the 'host–guest' complex fits together and on specific local interactions between surface atoms.[14] Inclusion in CDs exerts a profound effect on the physicochemical properties of guest molecules as they are temporarily locked or caged within the host cavity giving rise to beneficial modifications of guest molecules, which are not achievable otherwise.[10]

The ability of a CD to form an inclusion complex with a guest molecule can be explained by steric and thermodynamic factors. The steric factors involved depend on the relative size of the CD to the size of the guest molecule and certain key functional groups attached to the guest. If the guest's size is too large or too small it will not fit into the CD (i.e. geometric compatibility).[15,17,46] Analytes can also fit either completely or with their hydrophobic part into the CD cavity entering through one of the openings, primary and secondary rims.

For an inclusion complex to be thermodynamically favourable there must be a favourable net energetic driving force that pulls the guest into the CD. A favourable net energetic change for the formation of an inclusion complex could involve several processes.[10] The release of polar water molecules from the apolar CD cavity, the formation of a larger amount of hydrogen bonds between water molecules that are released from the cavity, a decrease in the amount of repulsive interactions between hydrophobic guests and an aqueous environment and an increase in hydrophobic interactions as the guest moves into the apolar CD cavity can contribute to a favourable net energetic change for the formation of an inclusion complex.[10,43,46,47] Various explanations for the favourable energy changes that occur in the formation of inclusion complexes ultimately show that the complexation mechanism is neither simple nor universal for all combinations of cyclodextrins, guests and solvents.

Complex formation is usually associated with a large, negative ΔH and a ΔS that can either be positive or negative. However, classical hydrophobic interactions, which are based on the hydrophobic effect, are associated with a slightly positive ΔH and a large, positive ΔS and have been shown to drive CD complexation in certain cases.[10] Other factors involved in complex formation include the release of ring strain in the glucopyranose units composing the CD, van der Waal's forces, hydrogen bonding and the flexibility, or degrees of freedom of a guest. Thus, it is accepted that various forces contribute to the complex formation.[33]

The most frequent complex formed is a 1:1 ratio where one CD molecule includes one organic guest molecule and the binding process is not fixed or permanent but rather is a dynamic equilibrium. The 1:1 interaction is usually described by Eq. (1) or as figure 4.4, although higher complexes have been postulated.[11]

$$\mathrm{Guest_{free} + CD_{free} \rightleftarrows [CD - Guest]_{complex}} \qquad (4.1)$$
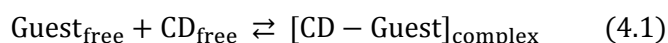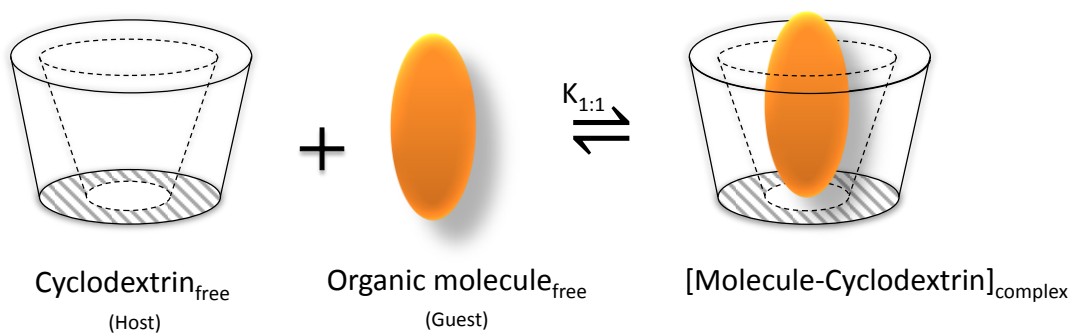
Figure 4.4 – Formation on and inclusion complex of a CD with an organic guest molecule.[20] where, $K_{1:1} = \frac{[Guest-CD]}{[Guest][CD]}$.

The complexation of enantiomeric pairs of guest molecules with CDs typically involves small differences between the thermodynamic quantities describing the complexation of each enantiomer. For example, differences in $\Delta G°$ that are typically less than 1 kJ mol^{-1} are reported for the complexations of mono(6-anilino-6-deoxy)-βCD with enantiomeric pairs of various amino acids and for the complexations of α- and βCDs with enantiomeric ephedrines and pseudoephedrines. Often, enantioselectivity is attributed to a larger $\Delta S°$ value for the complexation reaction involving the preferred enantiomer compared to the complexation reaction involving the less preferred enantiomer. The larger $\Delta S°$ value is a consequence of greater conformational freedom of the favoured enantiomer inside of the CD cavity and the classical hydrophobic effect in which there is more extensive desolvation of the cyclodextrin cavity in the system with the preferred enantiomer.[46]

4.1.2 Chiral Analyte

Ephedrine and ephedrine derivatives (e.g., methylephedrine and norephedrine) are sympathomimetic amines known to have central nervous system stimulating properties,[48] producing excitement and euphoria and increasing motor activity,[49] which has direct effects on the regulations of the World Anti-Doping Agency (WADA). Ephedrine has

become a valuable precursor as it serves as a starting material for two powerful and popular stimulants, methamphetamine and methcathione.[50] Ephedrines are also used as a major active component in medications for the treatment of nasal congestion,[51] asthma and obesity.[52] Each ephedrine exists as a pair of enantiomers (Figure 4.5), which may differ in pharmacological activity as well as in the rate of their metabolism. For example, the stimulant effect of the (1S,2R)-(+)-ephedrine enantiomer amounts to 80% of the activity of the (1R,2S)-(-)-ephedrine.
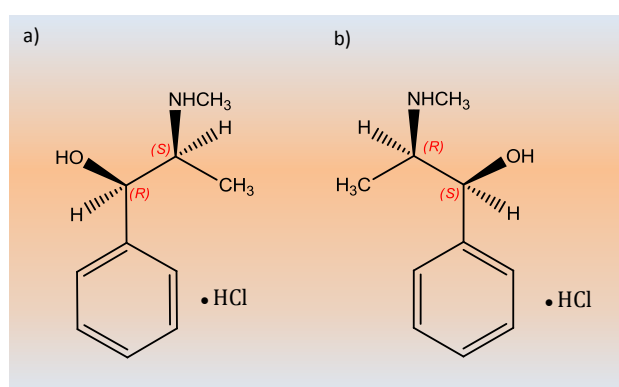
Figure 4.5 – Chemical structure of ephedrine hydrochloride enantiomers. a) (1R,2S)-(-)-ephedrine hydrochloride, b) (1S,2R)-(+)-ephedrine hydrochloride. IUPAC name (R*,S*)-2-(methylamino)-1-phenylpropan-1-ol (pK_a=9.39).[53]

As a consequence of a widespread use of ephedrine, it has been necessary to develop analytical techniques for their reliable detection. The enantiomer composition (qualitative or quantitative) can be useful in order to identify the synthetic pathways of clandestine ampethamine samples.[54] For these reasons, the development of chiral methods of analysis for ephedrines is receiving increasing attention in the clinical, toxicological and pharmaceutical fields. In this respect, the chiral discrimination of ephedrine has been reported by a number of techniques, including, liquid chromatography (LC),[28,55] gas chromatography (GC),[50] capillary electrophoresis (CE)[56,57] and NMR spectroscopy.[33,34]

It has been stated by several authors, that 1:1 complexes can be formed with βCD and modified βCDs with the enantiomers of the ephedrine.[28,33,34,55,56] The aromatic moiety of the ephedrine is included in the cavity of the CD, composed of seven glucose units, whereas the said chain is located at the wider rim (secondary rim). This type of inclusion allows the formation of hydrogen bonds with the OH or the amino group of the ephedrine molecule with the acetyl groups in the rim of the CD. Holzgrabe et al.[33] studied the chiral discrimination of ephedrine induced by βCD, heptakis(2,3-di-O-acetyl)β-CD, heptakis(6-O-acetyl)β-CD using one- and two- dimentional NMR techniques. He found different inter- and intramolecular nuclear overhauser effects (NOEs) for the enantiomers with βCD and heptakis(2,3-di-O-acetyl)β-CD which reflected the ability of these CDs to discriminate between (+)- and (-)-ephedrine. No differences could be found between the enantiomers using 6-acetylated CD. Furthermore, indications that the ^{1}H-^{1}H-coupling constants of the enantiomers did not change upon complexation with both CDs suggested that is a different orientation of the enantiomers rather than a different conformation of the cavity that causes the chiral recognition. These findings were also reported by several authors.[34,53,58] Mularz et al.[58] proposed that hydrogen bonding between the ligands and the secondary hydroxyls in the 2- and 3-positions of the CD is essential for the discrimination of ephedrine and pseudoephedrine enantiomers. Li and Purdy[59] reported on the necessity of side chain interactions between native βCD and substituted amino acids to discriminate between the optical isomers.

The recognition of ephedrine enantiomers has also been done by potentiometry using enantioselective sensors based on lipophilic CDs (α- and 2,6-di-O-dodecyl-βCD).[38,60-62] It was established that it was the configuration of the amino group in the ephedrine molecules which determined the sense of enantiodifferentiation in CD inclusion complexes. The (+)-enantiomer of ephedrine was found to be the more strongly bound

and in the (2S)-(-)-complex it was proposed that there was an unfavourable steric interaction between the 2-Me group and the H_3 proton of the CD host that inhibited a favourable $\overset{+}{N}H \ldots O$ hydrogen bonding interaction. Furthermore, it was demonstrated that CDs in which the OH have been alkylated showed no difference in the stability of the diastereoisomers complexes with (-)- and (+)-ephedrine.[61] It was shown that complete alkylation of the 3-OH group in αCD derivatives removed the enantioselectivity in binding ephedrine and its stereoisomers.[37,38]

4.2 Results and Discussion

4.2.1 Transfer of ephedrinium ions assisted by AcαCD without organic reference solution

Preliminary studies for the chiral discrimination of ephedrine, using liquid|liquid interface approach, were performed in the presence of AcαCD, as chiral ligand, in the organic phase. The interaction between the ephedrinium ions and AcαCD can be represented by the following reaction:

$$Ac\alpha CD_{(o)} + EPH^+_{(w)} \rightleftharpoons [\,Ac\alpha CDEPH^+\,] \qquad (4.2)$$

where EPH$^+$ stands for the two enantiomers of ephedrine hydrochloride, (+)EPH$^+$ (-)EPH$^+$, and the racemate ($\pm$)EPH$^+$. AcαCD is the abbreviation for hexakis(2,3,6-tri-O-Acetyl)-α-Cyclodextrin (see section 3.4.2, Figure 3.5). Outer silanised micropipettes were filled with solutions of ephedrine hydrochloride, enantiomers and racemate, and dipped in a 1,2-DCE solution containing the chiral selector (see section 3.1.2, Figure 3.10). The electrochemical cell employed for the study the of ephedrinium ions transfer facilitated by AcαCD is represented in scheme 4.1.

$$\text{Ag}\,|\,\text{AgTPB}_{(s)} \left|\begin{array}{c} \text{10 mM TBATPB} \\ \text{25 mM Ac}\alpha\text{CD}_{\,(1,2\text{-DCE})} \end{array}\right|\left|\begin{array}{c} \text{10 mM KCl} \\ \text{5 mM EPH}^{+}_{(aq.)} \end{array}\right| \text{Ag}\,|\,\text{AgCl}_{(s)}$$

Scheme 4.1 – Cell configuration for the facilitated chiral transport of EPH$^+$ ions using AcαCD.

All the potentials were calculated using TBA$^+$ as the internal reference, according to Eq.(4.3); the transfer potential of the reference[63–65] ion TBA$^+$ was measured by using 10mM of TBACl inside the pipette instead EPH$^+$. The $\Delta_o^w \phi_{(\text{Ac}\alpha\text{CDEPH}^+)}^{o'}$ values were calculated in accordance with the 'TATB' assumption in the form:

$$\Delta_o^w \phi_{(\text{Ac}\alpha\text{CDEPH}^+)}^{o'} = E_{(\text{Ac}\alpha\text{CDEPH}^+)}^{1/2} - \left(E_{\text{TBA}^+}^{1/2} - \Delta_o^w \phi_{\text{TBA}^+}^{o'} \right) \qquad (4.3)$$

where $\Delta_o^w \phi_{\text{TBA}^+}^{o'}$ represents the value of the transfer potential of the TBA$^+$ ion, $E_{(\text{Ac}\alpha\text{CDEPH}^+)}^{1/2}$ and $E_{\text{TBA}^+}^{1/2}$ are the experimental half-wave potentials of the charge transfer reactions and TBA$^+$ transfer, respectively. As reference for our measurements the value of $\Delta_o^w \phi_{\text{TBA}^+}^{o'}$ =-230 mV[66] was used.

Figure 4.6 shows the DPV voltammograms (background subtracted) obtained for the assisted transfer of the ephedrinium ions by AcαCD. As it can be seen from the same figure, the (+)-EPH$^+$ enantiomer transfers at 142±2mV (Figure 4.6, red curve) whereas the (-)-EPH$^+$ transfers at 117±2mV (Figure 4.6, purple curve). For the racemate, the transfer was observed at an intermediate potential of 122±2mV (Figure 4.6, blue curve). In the absence of the chiral selector, no transfer across the liquid|liquid interface was observed, within the potential window. TBA$^+$ is also known to form weak association complex with AcαCD. The facilitated transfer of TBA$^+$ by AcαCD (Figure 4.6, grey curve) occurs at approximately 265±2mV mV. As the concentration of the ligand in the organic phase is in

excess, the current measured is proportional to the concentration of species in the aqueous phase.
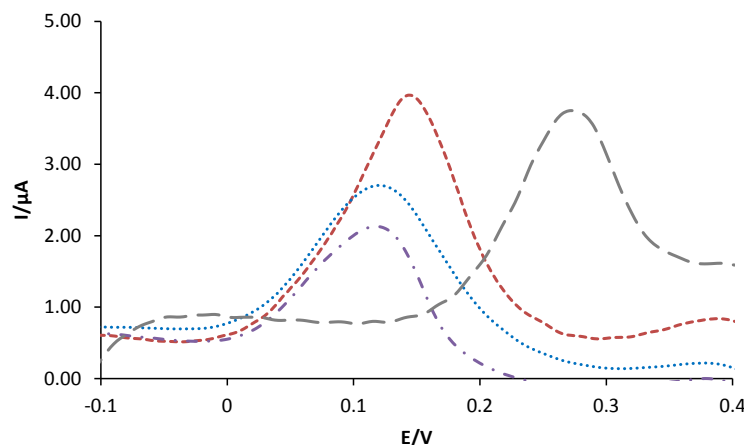
Figure 4.6 – DPV voltammograms for the assisted transfer of ephedrine ions (in red: (+)EPH[+], blue: (±)EPH[+], purple: (-)EPH[+]) and TBA[+] (in grey) by AcαCD across the liquid|liquid interface. DPV conditions: pulse height: 0.0025 V, pulse with: 0.1 s, step height: 0.005 V, step time: 1 s, pipette radius was ∼50μm.[67]

The difference observed in the half-wave potential of transfer between the (+)-EPH[+] and (-)-EPH[+] reflects the difference in chiral Gibbs free energy of the two enantiomers from the aqueous to the organic phase. This difference was found to be -2.47 kJ mol^{-1} (Table 4.2). A peak of higher current intensity for the (+)-EPH[+], suggest that this enantiomer is more facile to transfer in comparison to (-)-EPH[+]. Reharsky and co-workers[53] using titration calorimetry, to measure equilibrium constants of ephedrine and related substances with αCD, reported K values, of 18.0±0.9 and 17.0±0.9 for (+)- and (-)-EPH[+], at 298K, respectively. These values were based on a 1:1 binding model and a single binding site. The same authors suggested that the interactions between ephedrines and CDs can be qualitatively understood in terms of steric effects, hydrophobic interactions and hydrogen bonding.

Table 4.2 – Enantioselective differentiation of ephedrine enantiomers and the racemate using AcαCD at a aqueous|1,2-DCE interface.

	(+)-EPH$^+$	(-)-EPH$^+$	Racemate
$E^{1/2}_{(AcαCDEPH^+)}$/mV	142±3 mV	117±3 mV	122±3 mV
$\Delta(\Delta G)_{chiral}$/kJ mol^{-1}		-2.47	
ΔK		0.5±0.1	

4.2.2 Transfer of ephedrinium ions assisted by AcαCD and AcβCD with organic reference solution

In order to extend the preliminary results obtained for the chiral differentiation of ephedrine enantiomers at liquid|liquid interface, an additional chiral stationary was used, AcβCD, and the experimental set-up refined (see section 3.1.2, Figure 3.4).

Before comparing the enantiomeric resolution of the two ligands, experiments were focused on the electrochemical response only in the presence of the lipophilic CDs in the organic phase, i.e. in the absence of ephedrinium ions in the aqueous phase, to observe any possible complexation between the ligands and the electrolytes. Figure 4.7 compares the CV and DPV voltammograms at the aqueous|1,2-DCE interface, according to scheme 4.2.

$$Ag|AgCl_{(s)} \left| 10\text{ mM TBACl}_{(aq.)} \right| \genfrac{}{}{0pt}{}{10\text{ mM TBATPB with/without}}{1\text{ mM AcαCD or AcβCD}_{(1,2\text{-DCE})}} \left|\left| 10\text{ mM LiCl}_{(aq.)} \right| Ag|AgCl_{(s)} \right.$$
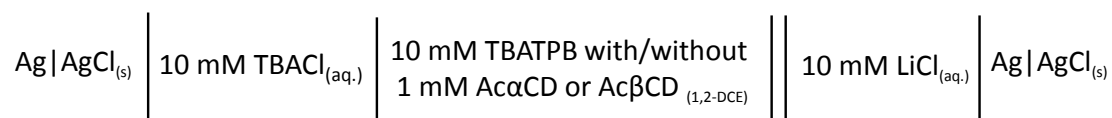
Scheme 4.2 – Cell configuration for the study of ion transfer in the absence of ephedrinium ions.
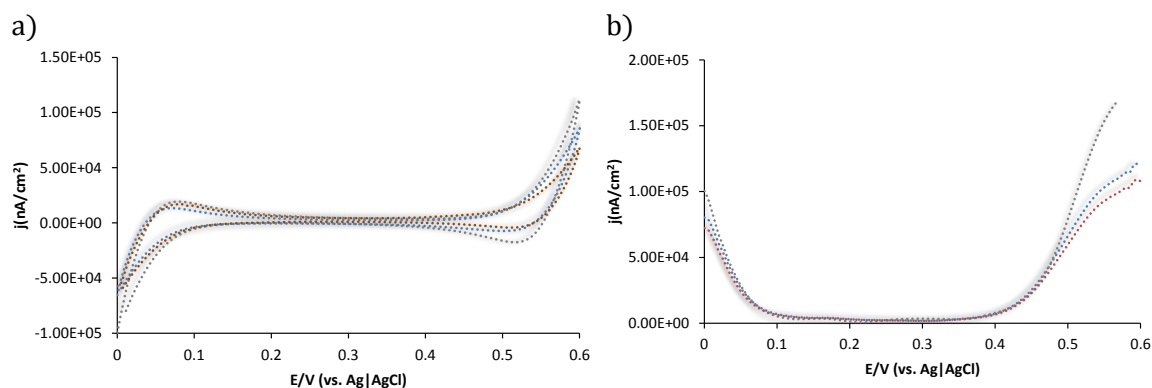
Figure 4.7 – CV and DPV response obtained at the aqueous|1,2-DCE interface in the absence of ephedrinium ions. The grey dotted line represents the response of the background electrolytes, in blue and red in the presence of AcαCD AcβCD (1mM) in the organic phase, respectively. Scan rate:10mV s^{-1}; pulse amplitude 0.05 V, sampling with 0.060 s, step hight 0.005 V. Micropipette tip radius 7±1 μm.

As it can be seen from figure 4.7, in the presence of AcαCD and AcβCD in the organic phase, the background electrolytes response does not alter significantly. The polarised potential window is approximately 400mV, limited by the background electrolytes transfer at the extremes of the potential window. At positive potentials, the potential window is limited by the egress of Li$^+$ from water to the organic phase or by the ingress transfer of TPB$^-$ ion from the organic to aqueous phase. Conversely at negative potentials, the window is limited by either TBA$^+$ (from the aqueous to the organic) or Cl$^-$ (from the organic to the aqueous phase) transfer at the negative side of the potential window. The transfer of the protonated drug (EPH$^+$) ions was also studied in the absence of ligands in the organic phase. The electrochemical cell used is presented in scheme 4.3.

$$\text{Ag}|\text{AgCl}_{(s)} \left| \begin{array}{c} \text{10 mM TBACl}_{(aq.)} \end{array} \right| \begin{array}{c} \text{10 mM TBATPB}_{(1,2\text{-DCE})} \end{array} \left\| \begin{array}{c} \text{10 mM LiCl} \\ \text{5 mM EPH}^+_{(aq.)} \end{array} \right| \text{Ag}|\text{AgCl}_{(s)}$$
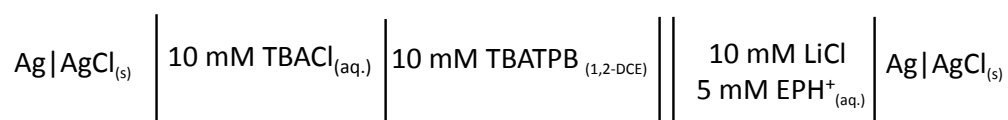
Scheme 4.3 – Cell configuration for the study of ephedrinium ion transfer in the absence of ligands (AcαCD and AcβCD) in the organic phase.

In figure 4.8 are presented the CV and DPV voltammograms obtained for the unassisted transfer of ephedrinium ions from aqueous to organic phase.
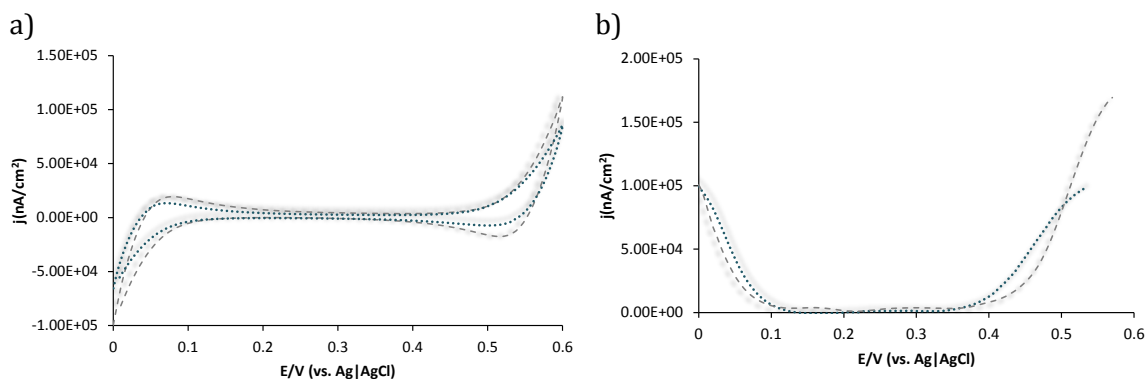
Figure 4.8 – a) CV b) DPV responses obtained at the aqueous|1,2-DCE micro interface in the absence (dashed line) and in the presence (dotted line) of ephedrinium ion, [EPH$^+$]=5.0mM). Scan rate:10 mV s^{-1}; pulse amplitude 0.05 V, sampling with 0.060 s, step hight 0.005 V. Micropipette tip radius 7±1 μm.

In the absence of chiral ligands in the organic phase, no voltammetric waves of the unassisted transfer of EPH$^+$ from the aqueous phase, inside the micropipette, to the organic solution, containing only supporting electrolyte (TBATPB), could be seen. The results were almost undistinguishable from those obtained in the absence of ephedrine in the aqueous phase. The steeply rising currents at the positive and negative limits of the potential window are due to the transfer of the supporting electrolyte ions from the pipette to the 1,2-DCE phase and from the organic to the aqueous solution inside the pipette. EPH$^+$ is therefore transferred to the organic phase at potentials more positive than the positive limit of the potential window. The presence of a ligand in the organic phase is therefore needed to assist the transfer of the ephedrine cations.

4.2.2.1 Influence of the bulk concentration of ephedrinium ions on the facilitated transfer by the chiral ligands.

The study of the assisted transfer of ephedrine chiral ions is represented in the following scheme.

$$\text{Ag}\,|\,\text{AgCl}_{(s)} \left| \begin{array}{c} \text{10 mM TBACl}_{(aq.)} \end{array} \right| \begin{array}{c} \text{10 mM TBATPB} \\ \text{0.5 mM Ac}\alpha\text{CD or Ac}\beta\text{CD}_{(1,2\text{-DCE})} \end{array} \left|\left| \begin{array}{c} \text{10 mM LiCl} \\ \chi \text{ mM EPH}^{+}_{(aq.)} \end{array} \right| \text{Ag}\,|\,\text{AgCl}_{(s)}$$
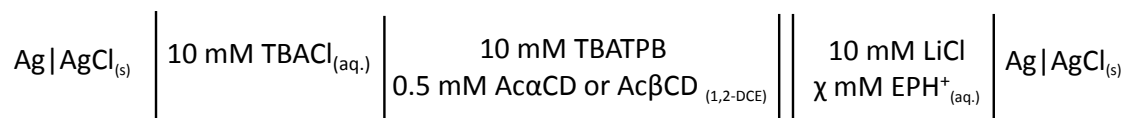
Scheme 4.4 – Cell configuration used for the study of the ephedrine cations assisted by AcαCD and AcβCD. EPH$^+$ represents the protonated enantiomers and racemate forms of ephedrine hydrochloride, χ=5, 10, 15, 20 mM.

From the previous results (Figure 4.8), it is clear that the facilitated ion transfer of ephedrine involves complexation of its cations ((+)EPH$^+$, (-)EPH$^+$, ($\pm$)EPH$^+$) which are initially present in the aqueous solution (inside the micropipette), to the lipophilic CDs, contained in the outer organic solution. With the pipette biased at a sufficiently positive potential and the concentration of EPH$^+$ ions much higher than the concentration of the ligands, [EPH$^+$]$_{(w)}$>>[CD]$_{(o)}$, the limiting current is controlled by the diffusion of the ligand, AcαCD or AcβCD, from the bulk organic solution (outside of the pipette) to the pipette orifice. This process coincides with a TIC mechanism (see section 2.9) at the exclusion cavity of the CDs.

Figures 4.9 to 4.12 and Figures 4.13 to 4.16 show the responses obtained for the transfer of ephedrine cations assisted by AcαCD and AcβCD, respectively. As it can be seen from the figures, the current response for the transfer of the complex cations of ephedrine back to the aqueous phase is a steady-state wave, which suggests that the complexed ions do not cross the interface. If this was the case, the return wave should be peaked indicating linear diffusion of the complexed ion within the pipette back to the interface.

Furthermore, the solubility of both chiral ligands (AcαCD and AcβCD) in water is very low, thus it is expected that the transfer is dissociative, i.e. transfer by interfacial dissociation (TID). Upon dissociation the free ligand diffuses away from the interface in a spherical diffusion, whereas the ephedrine cations diffuse away linearly inside the pipette.

The relationship between the experimental half-wave potential and the logarithm of the ephedrinium ions concentration is shown in Figures 4.9c, 4.10c and 4.11c. The plots indicate that the half-wave potential of the assisted transfer undergoes a shift towards less positive potentials, while the current is reasonable unchanged, when the concentration of ephedrine cations is varied. The slopes of the linear graphs yielded values of 40, 55 and 49 mV per decade for $(+)EPH^+$, $(-)EPH^+$ and $(\pm)EPH^+$, respectively. These values are close to the theoretical value of 59 mV $decade^{-1}$ for monovalent ions, indicating that the facilitated transfer is of reversible nature.[68,69] For comparison, in figure 4.12 is shown the responses obtained for the transfer of the two enantiomers and racemate cations of ephedrine assisted by AcαCD.
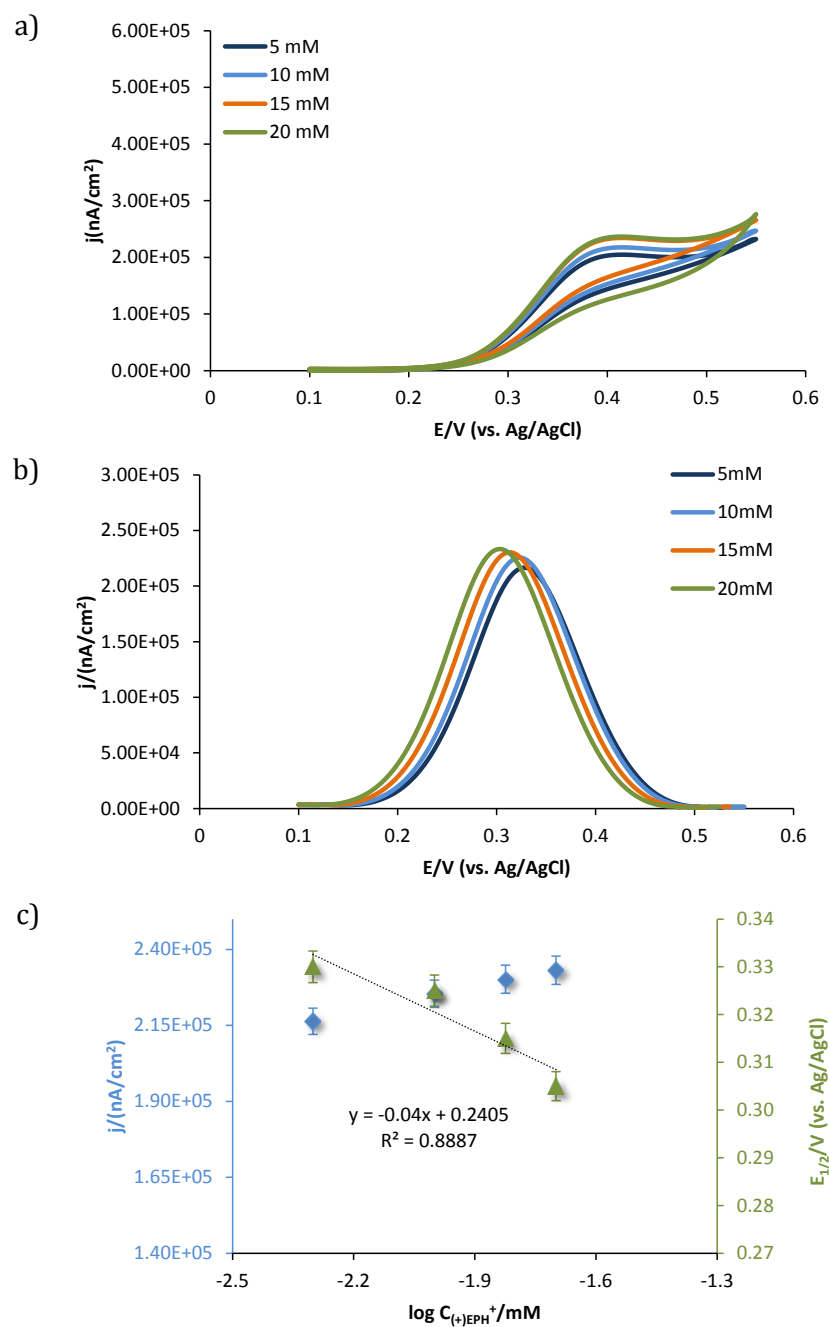
Figure 4.9 – a) CV and b) DPV voltammograms of the (+)EPH$^+$ ion transfer facilitated by AcαCD (0.5 mM) for different ion concentrations, c) dependence of current density and half-wave potential of [AcαCD(+)EPH$^+$] complexes on the variation of the logarithm of the concentration. Scan rate:10 mV s^{-1}; pulse amplitude 0.05 V, sampling with 0.060 s, step height 0.005 V. Micropipette tip radius 7±1 μm.
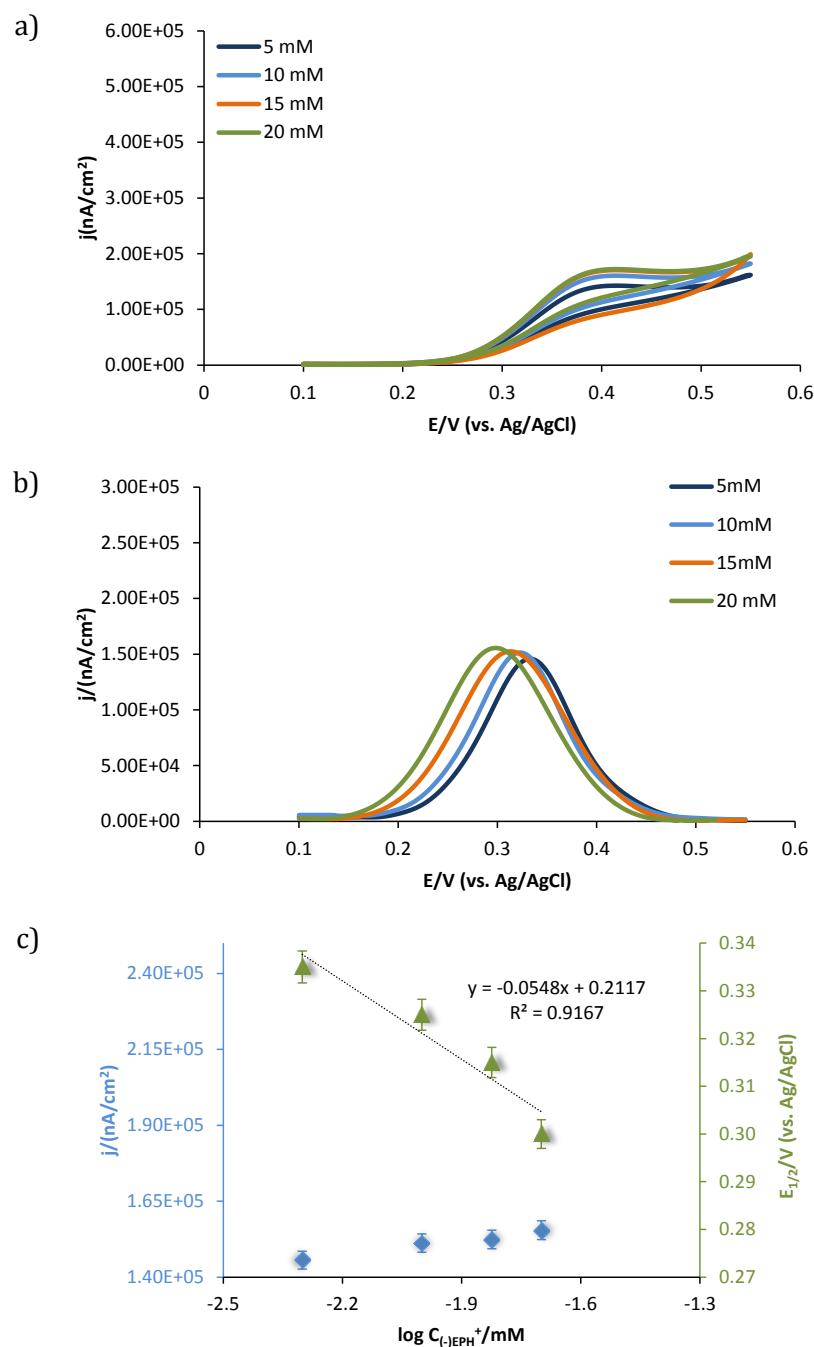
Figure 4.10 – a) CV and b) DPV voltammograms of the (-)EPH+ ion transfer facilitated by AcαCD (0.5 mM) for different ion concentrations, c) dependence of current density and half-wave potential of [AcαCD(-)EPH+] complexes on the variation of the logarithm of the concentration. Scan rate:10 mV s-1; pulse amplitude 0.05 V, sampling with 0.060 s, step height 0.005 V. Micropipette tip radius 7±1 μm.
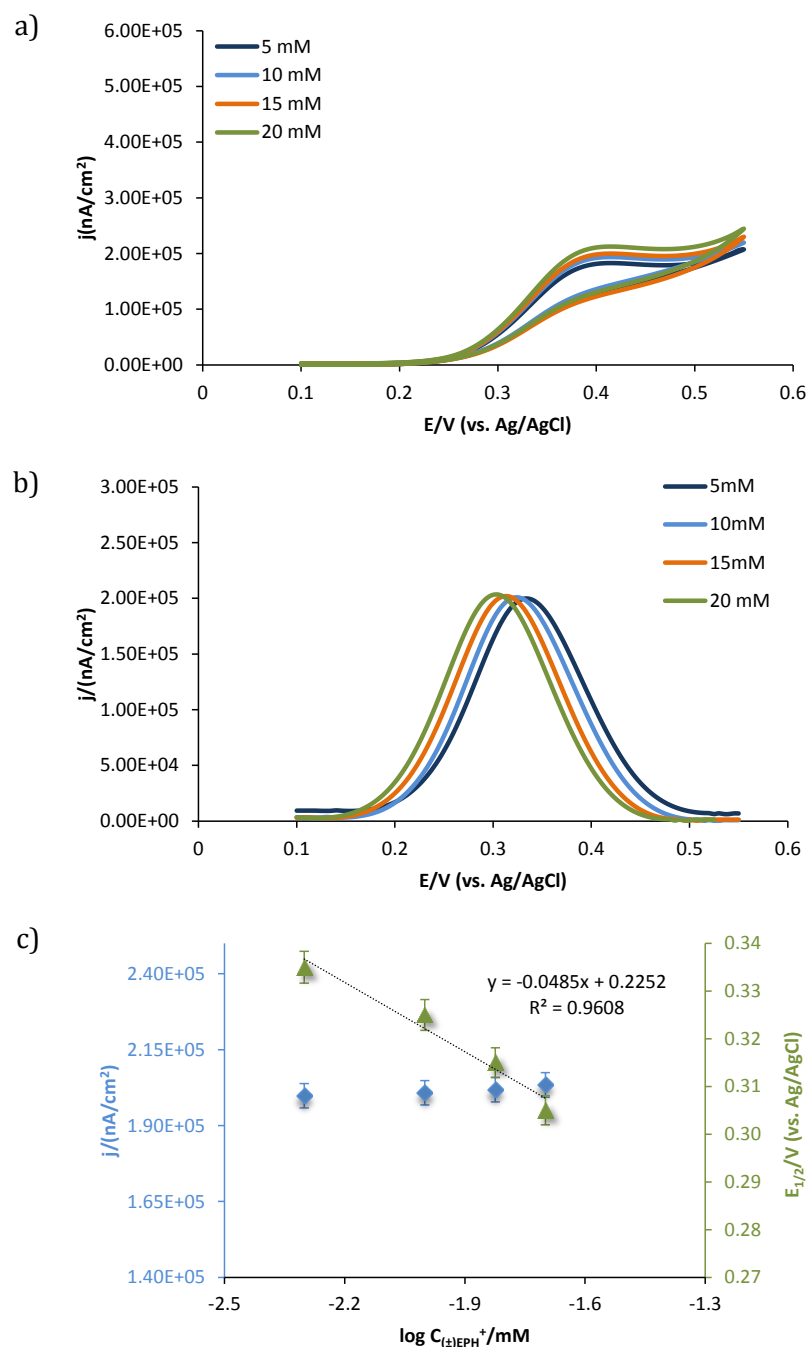
Figure 4.11 – a) CV and b) DPV voltammograms of the $(\pm)EPH^+$ ion transfer facilitated by AcαCD (0.5 mM) for different ion concentrations, c) dependence of current density and half-wave potential of $[AcαCD(\pm)EPH^+]$ complexes on the variation of the logarithm of the concentration. Scan rate:10 mV s^{-1}; pulse amplitude 0.05 V, sampling with 0.060 s, step height 0.005 V. Micropipette tip radius 7±1 μm.

Figure 4.12 – a) CV and b) DPV comparison voltammograms of the two enantiomers and the racemate EPH$^+$ (10 mM) transfer of assisted by AcαCD (0.5 mM). Scan rate:10 mV s^{-1}; pulse amplitude 0.05 V, sampling with 0.060 s, step height 0.005 V. Micropipette tip radius 7±1 μm.

The fact the current intensities are higher for (+)EPH$^+$ suggests that the transfer of this enantiomer assisted by AcαCD is more facile when compared to (-)EPH$^+$. As the complex formation between (+)EPH$^+$ and AcαCD seems to be more favourable, the number of uncomplex CDs at the interface is smaller given rise to a higher current. Also, the response of the racemate being closer to the positive enantiomer further supports the idea that the chiral selector has more affinity with (+)EPH$^+$. The difference observed in the responses can be attributed to more suitable interactions between the (+)EPH$^+$ enantiomer and the cavity of the CD. The different fit within the cavity of the CD is related with the formation

of intermolecular hydrogen bonding between the hydroxy or amino group of the ephedrinium ions and the acetyl groups of the CD. Although the differentiation between the racemate and the enantiomers of ephedrine using AcαCD is modest, it is plausible that the (+)EPH$^+$ changes its conformation somewhat upon complexation with the CD, in a different manner from the (-)EPH$^+$ enantiomer, in order to maximise its interaction. Bates and co-authors[62] have suggested that the enantioselectivity interaction between the ephedrinium ions and a lipophilic αCD ('per'-O-octyl-α-CD) may depend upon the orientation of the C-methyl group with respect to the CD cavity. They have proposed two different models for the binding process. In the case of (+)EPH$^+$, the methyl group is oriented away from the glycosidic region of the CD, whereas the (-)EPH$^+$ is orientated towards the H^3 and relatively close to H^5 in the cavity of the CD, which lead to an unfavourable steric interaction. It seems likely that it is the different orientation of the ephedrine enantiomers in the cavity of the CD that is responsible for the enantioselection.

Figures 13 to 16 show the assisted transfer of ephedrinium ions by AcβCD, according to the cell presented in scheme 4.4.
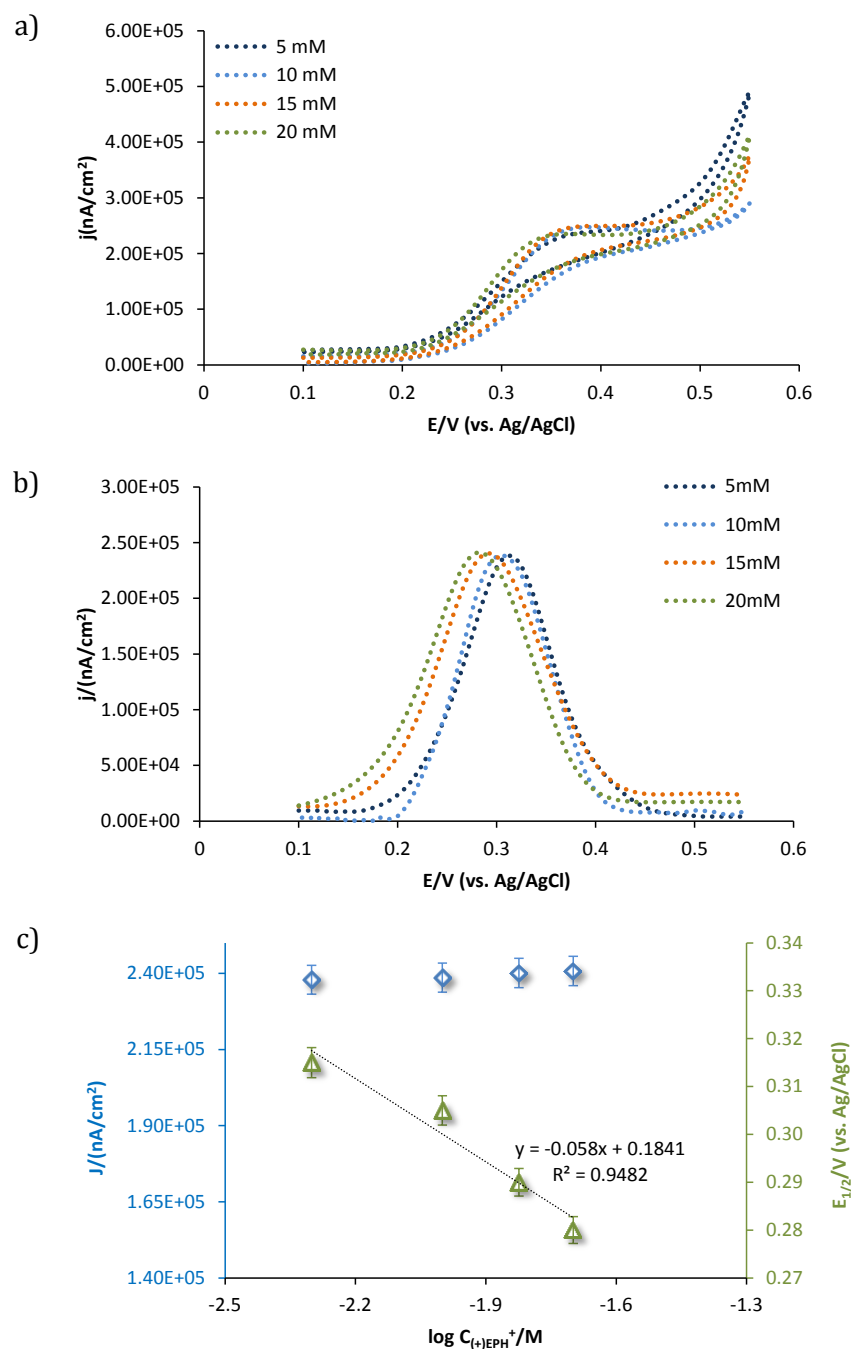
Figure 4.13 – a) CV and b) DPV voltammograms of the (+)EPH+ ion transfer facilitated by AcβCD (0.5 mM) for different ion concentrations, c) dependence of current density and half-wave potential of [AcβCD(+)EPH+] complexes on the variation of the logarithm of the concentration. Scan rate:10 mV s-1; pulse amplitude 0.05 V, sampling with 0.060 s, step height 0.005 V. Micropipette tip radius 7±1 μm.
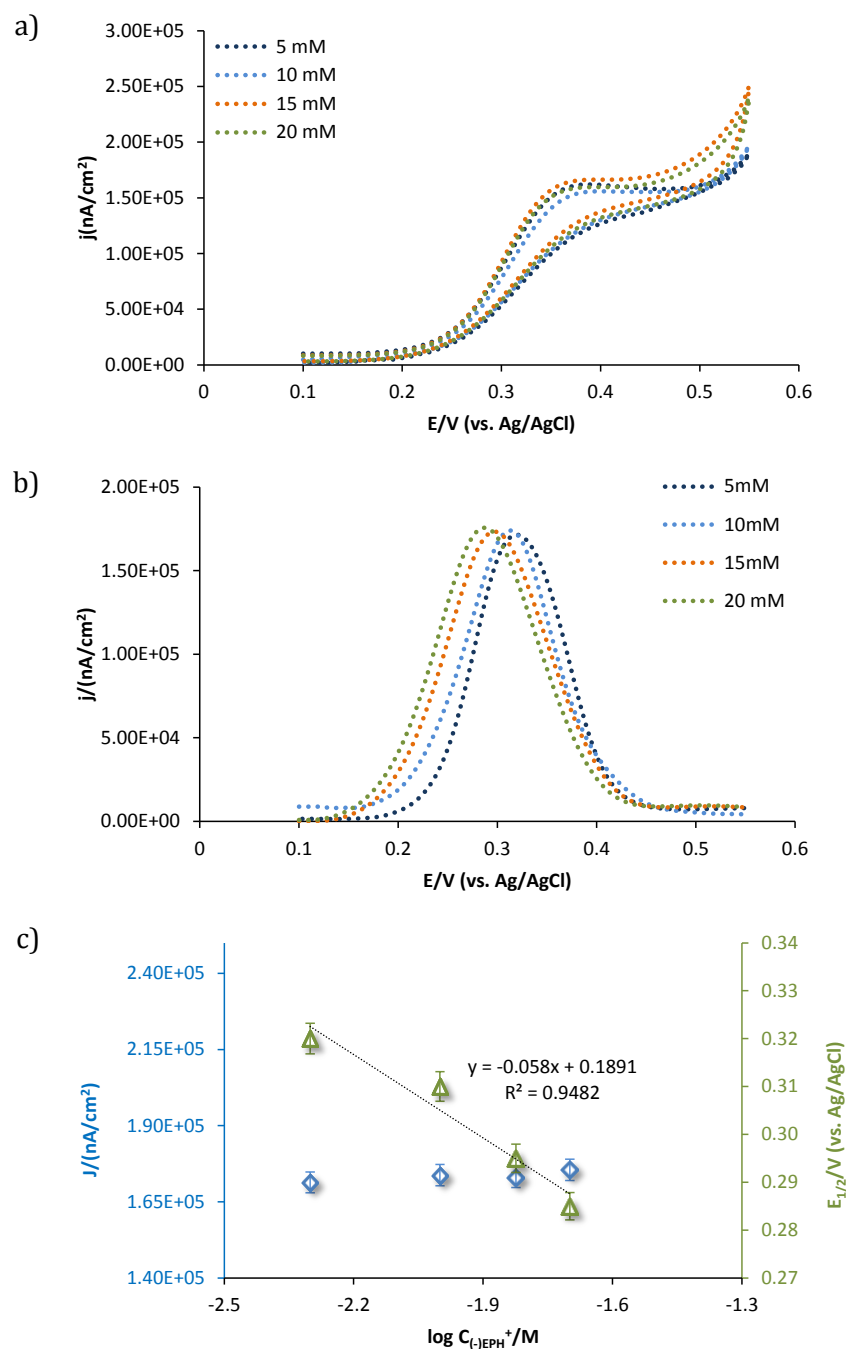
Figure 4.14 – a) CV and b) DPV voltammograms of the (-)EPH+ ion transfer facilitated by AcβCD (0.5 mM) for different ion concentrations, c) dependence of current density and half-wave potential of [AcβCD(-)EPH+] complexes on the variation of the logarithm of the concentration. Scan rate:10 mV s-1; pulse amplitude 0.05 V, sampling with 0.060 s, step height 0.005 V. Micropipette tip radius 7±1 μm.
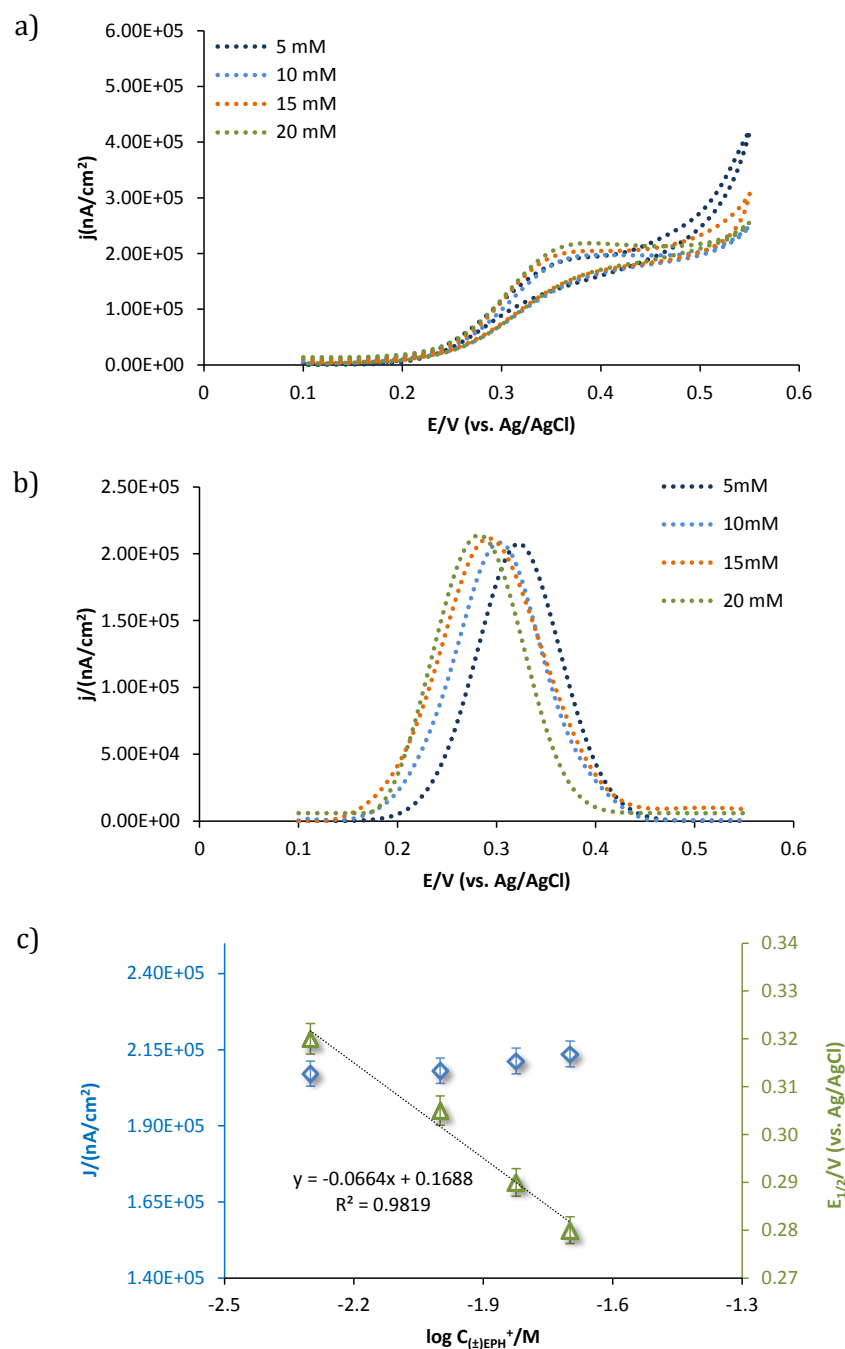
Figure 4.15 – a) CV and b) DPV voltammograms of the (±)EPH$^+$ ion transfer facilitated by AcβCD (0.5 mM) for different ion concentrations, c) dependence of current density and half-wave potential of [AcβCD(±)EPH$^+$] complexes on the variation of the logarithm of the concentration. Scan rate:10 mV s^{-1}; pulse amplitude 0.05 V, sampling with 0.060 s, step height 0.005 V. Micropipette tip radius 7±1 μm.

Figures 4.13c, 4.14c and 4.15c show that, like in the case of the assisted transfer by AcαCD, linearity was obtained when experimental half-wave potential was plotted against the logarithm of the concentration of ephedrinium ions. The experimental half-wave potential is shifted towards less positive potentials which are due to a decrease in the Gibbs energy of EPH+ transfer from aqueous to organic phase.[69] Similarly to the transfer assisted by AcαCD no significant changes were observed in the current response. The slopes of plots yielded values of 58, 58 and 66mV decade[-1] for (+)EPH+, (-)EPH+ and (±)EPH+, respectively, which are in agreement with the theory.[68,69] The comparison of the responses for (+)EPH+, (-)EPH+ and racemate cations using AcβCD is shown in figure 4.16.
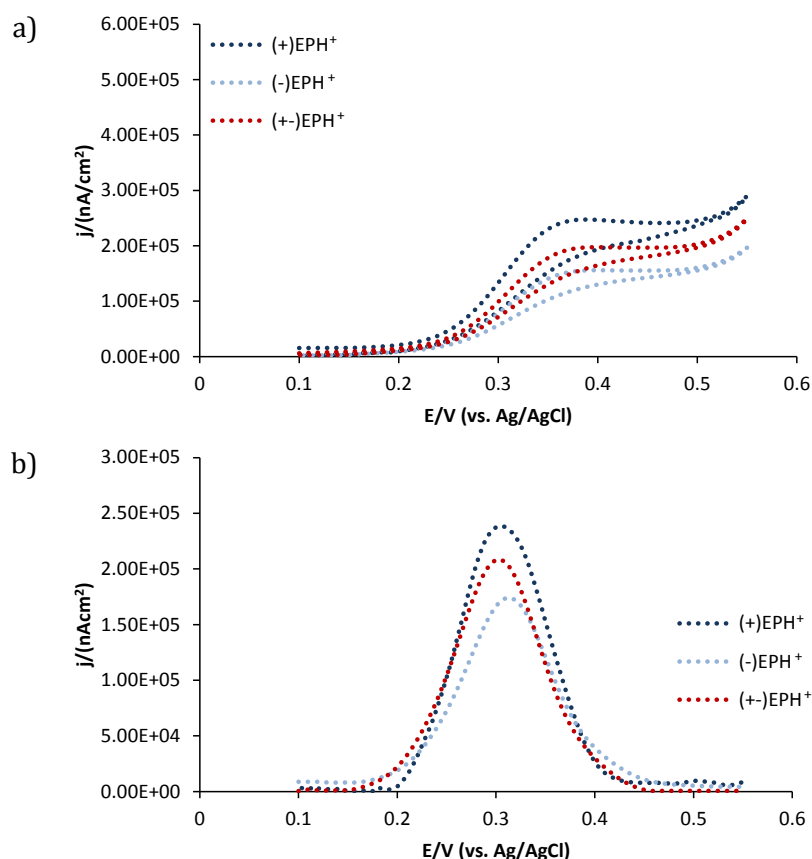
Figure 4.16 – a) CV and b) DPV comparison voltammograms of the two enantiomers and the racemate of EPH+ (10 mM) transfer of assisted by AcβCD (0.5 mM). Scan rate:10 mV s^{-1}; pulse amplitude 0.05 V, sampling with 0.060 s, step height 0.005 V. Micropipette tip radius 7±1 μm.

Since the the steady-state wave appears only when EPH+ is present in the aqueous phase and one of the chiral selectors is in the organic phase, it is obvious that the ion transfer process involves both species. Figure 4.8 illustrates the concept of the ephedrinium ion transfer by the formation of a hydrophobic complex between the ephedrinium ions and the lipophilic CDs at the aqueous|organic solution interface. The ephedrinium ion is sequestered within the structure of the CD which improves its solvation in the organic phase and then transported to the organic phase.
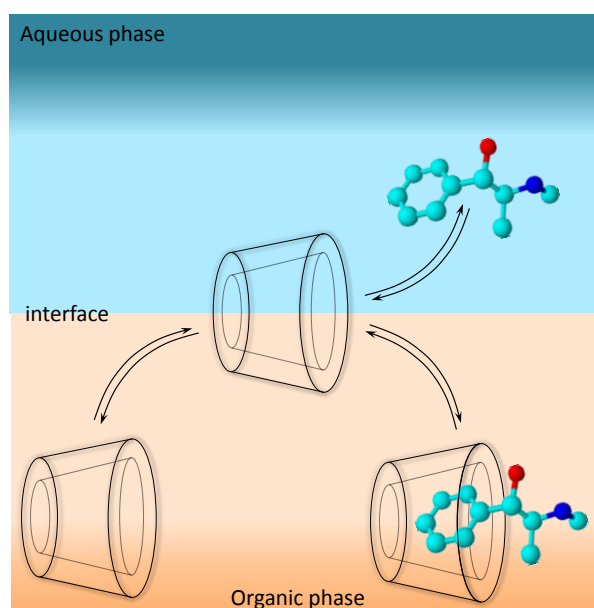
Figure 4.17 – Schematic illustration of the proposed mechanism for the assisted transfer of the ephedrinium ions at the aqueous|1,2-DCE micro interface by lipophilic CDs.

4.2.2.2 Influence of the bulk concentration of chiral ligands on the facilitated transfer of ephedrinium ions.

At the liquid|liquid interface, if the concentration of the ion is greater than of the ionophore/ligand (schemes 4.4 and 4.5), the observed limiting current is proportional to the concentration of the ligand; the same phenomenon was observed in this system. In these conditions, the equation for limiting current of the facilitated chiral ion transfer by

AcαCD and AcβCD across the aqueous|1,2-DCE micro interface at a micropipette (see section 2.13), is written as:

$$i_{ss} = 3.35\pi zFD_{CD}C_{CD}r \qquad (4.4)$$

where i_{ss} is the limiting current, D_{CD} the diffusion coefficient of the chiral ligands, z is the charge number, F is the Faraday constant, C_{CD} is the bulk concentration of the ligand and r is the radius of the micropipette.

In the investigation of the variation of the chiral ligands concentration the following cell was employed:

$$\text{Ag}\,|\,\text{AgCl}_{(s)} \left| 10\text{mMTBACl}_{(aq.)} \right| \begin{array}{c} 10\text{mMTBATPB} \\ \varkappa\ \text{mM AcαCD or AcβCD}_{\,(1,2\text{-DCE})} \end{array} \left|\left| \begin{array}{c} 10\text{mMLiCl} \\ 5\ \text{mM EPH}^+_{\,(aq.)} \end{array} \right| \text{Ag}\,|\,\text{AgCl}_{(s)}$$
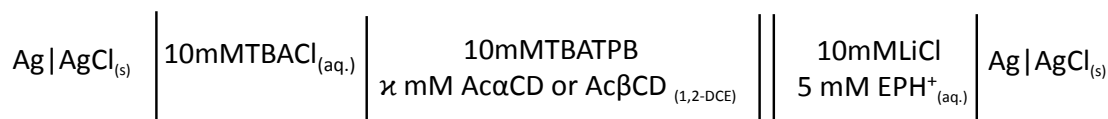
Scheme 4.5 – Cell configuration used for the study of AcαCD and AcβCD diffusion controlled process. $\varkappa$= 0.5, 1, 2.5 and 5 mM.

The obtained CVs and DPVs for the ephedrinium ions transfer facilitated by AcαCD and AcβCD, varying the ligands concentration, are shown in figures 4.18 and 4.19, and in figures 4.20 and 4.21, respectively. As can be seen, while the steady-state currents of the facilitated transfers increase with increasing of bulk concentration of the chiral ligands (Eq. 4.4), there is no obvious change in the half-wave potential (Figure 4.18c, 4.19c, 4.20c and 4.21c). These results further support that the facilitated ion transfer is limited by the spherical diffusion of AcαCD and AcβCD toward the aqueous|1,2-DCE micro interface from the organic phase. Also, no change at the half-wave transfer potential with the changing in concentration of ligand suggests that the facilitated chiral ion transfer occurs with the complexation having 1:1 stoichiometry (according to Eq. 2.57). Experiments at the higher concentrations caused inaccurate results and no well-defined peaks of the facilitated transfer in the CVs were observed.
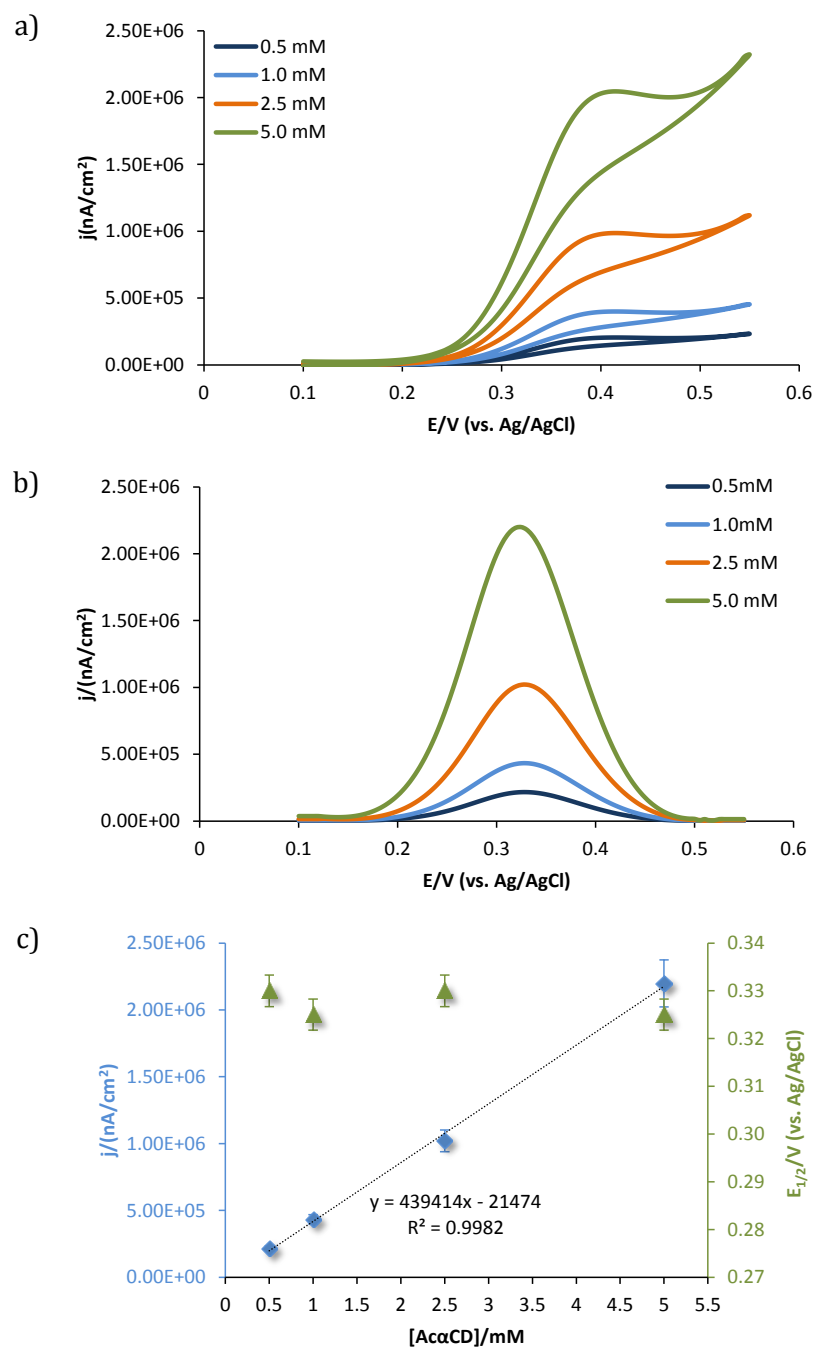
Figure 4.18 – a) CV and b) DPV voltammograms of the facilitated transfer of (+)EPH+ (5 mM) by AcαCD across the aqueous|1,2-DCE micro interface. c) Dependence of current and half-wave potential on the variation of [AcαCD]. Scan rate:10 mV s-1; pulse amplitude 0.05 V, sampling with 0.060 s, step height 0.005 V. Micropipette tip radius 7±1 μm. When not visible, the error bars are smaller than the symbols.
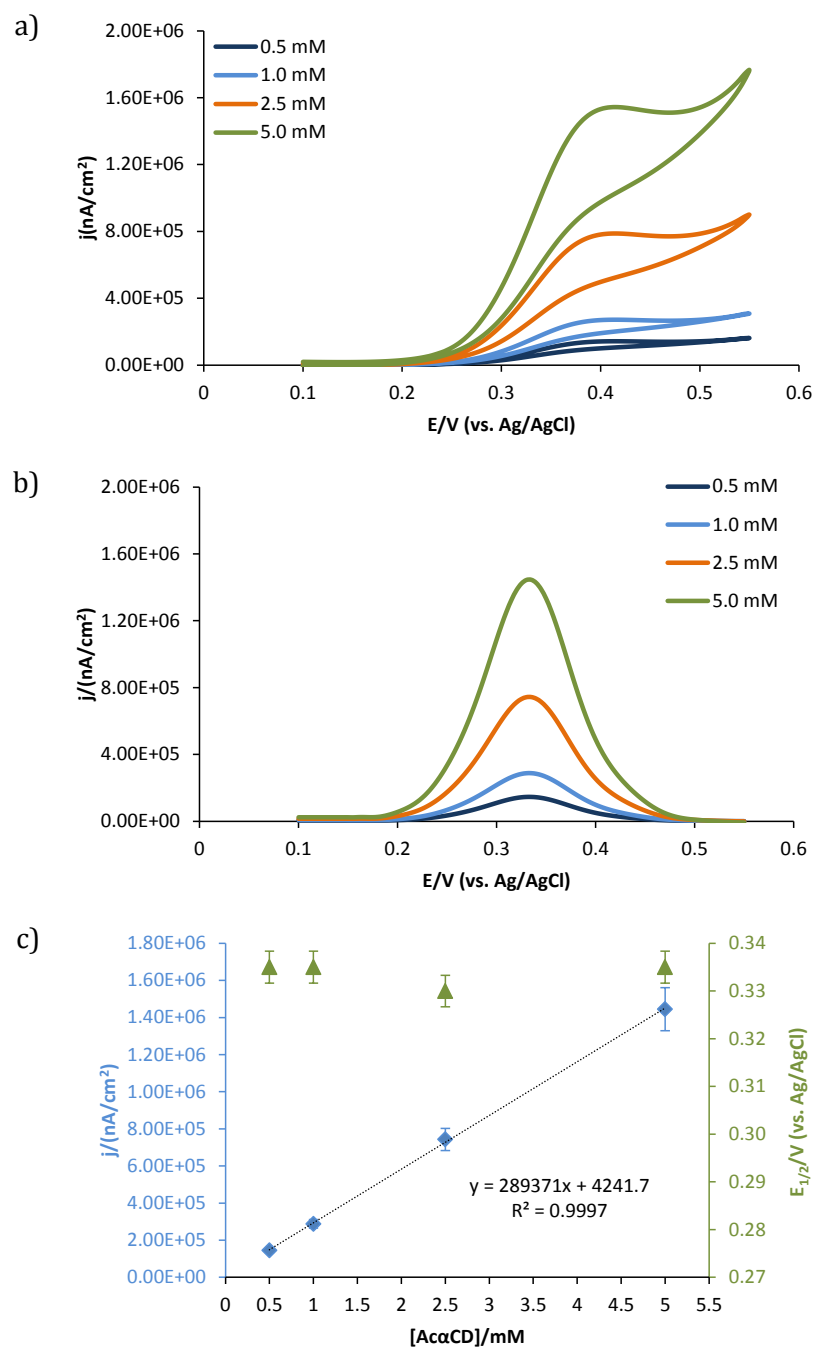
Figure 4.19 – a) CV and b) DPV voltammograms of the facilitated transfer of (-)EPH+ (5 mM) by AcαCD across the aqueous|1,2-DCE micro interface. c) Dependence of current and half-wave potential on the variation of [AcαCD]. Scan rate:10 mV s-1; pulse amplitude 0.05 V, sampling with 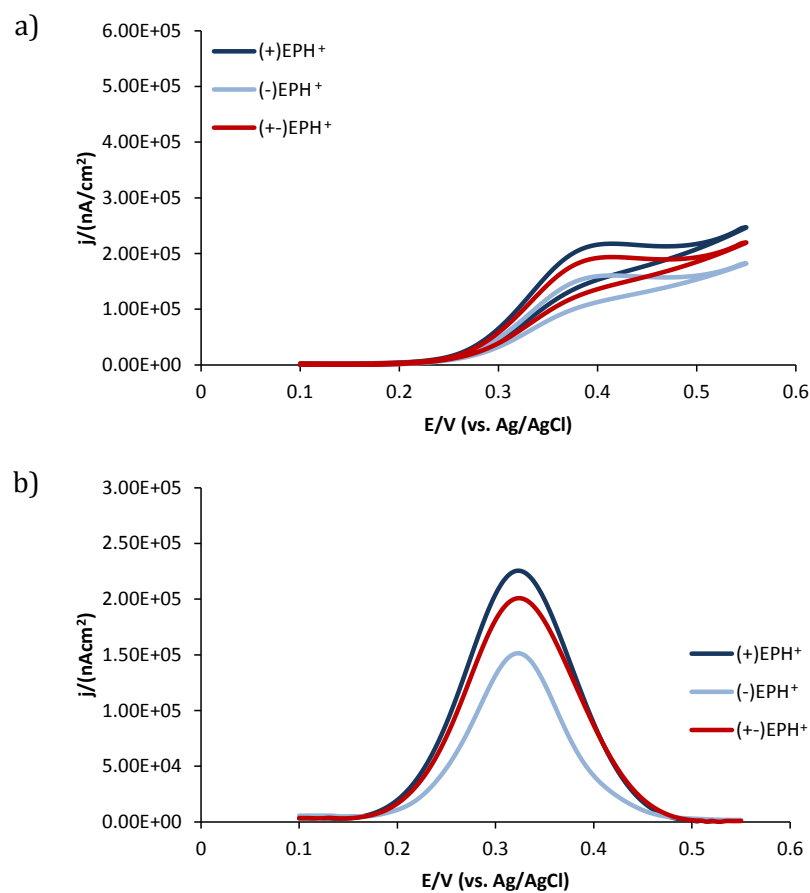0.060 s, step hight 0.005 V. Micropipette tip radius 7±1 μm. When not visible, the error bars are smaller than the symbols.
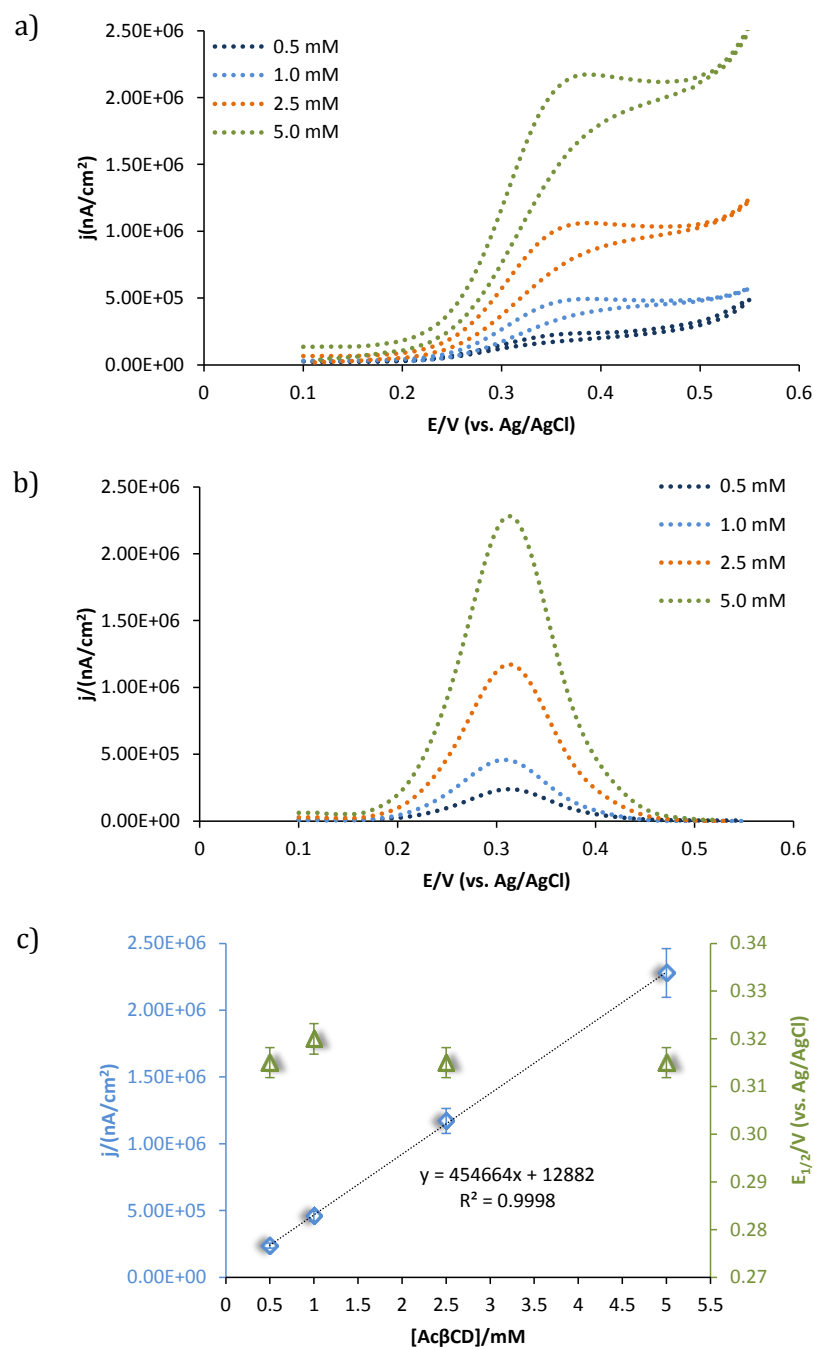
Figure 4.20 – a) CV and b) DPV voltammograms of the facilitated transfer of (+)EPH⁺ (5 mM) by AcβCD across the aqueous|1,2-DCE micro interface. c) Dependence of current and half-wave potential on the variation of [AcβCD]. Scan rate:10 mV s⁻¹; pulse amplitude 0.05 V, sampling with 0.060 s, step height 0.005 V. Micropipette tip radius 7±1 μm. When not visible, the error bars are smaller than the symbols.
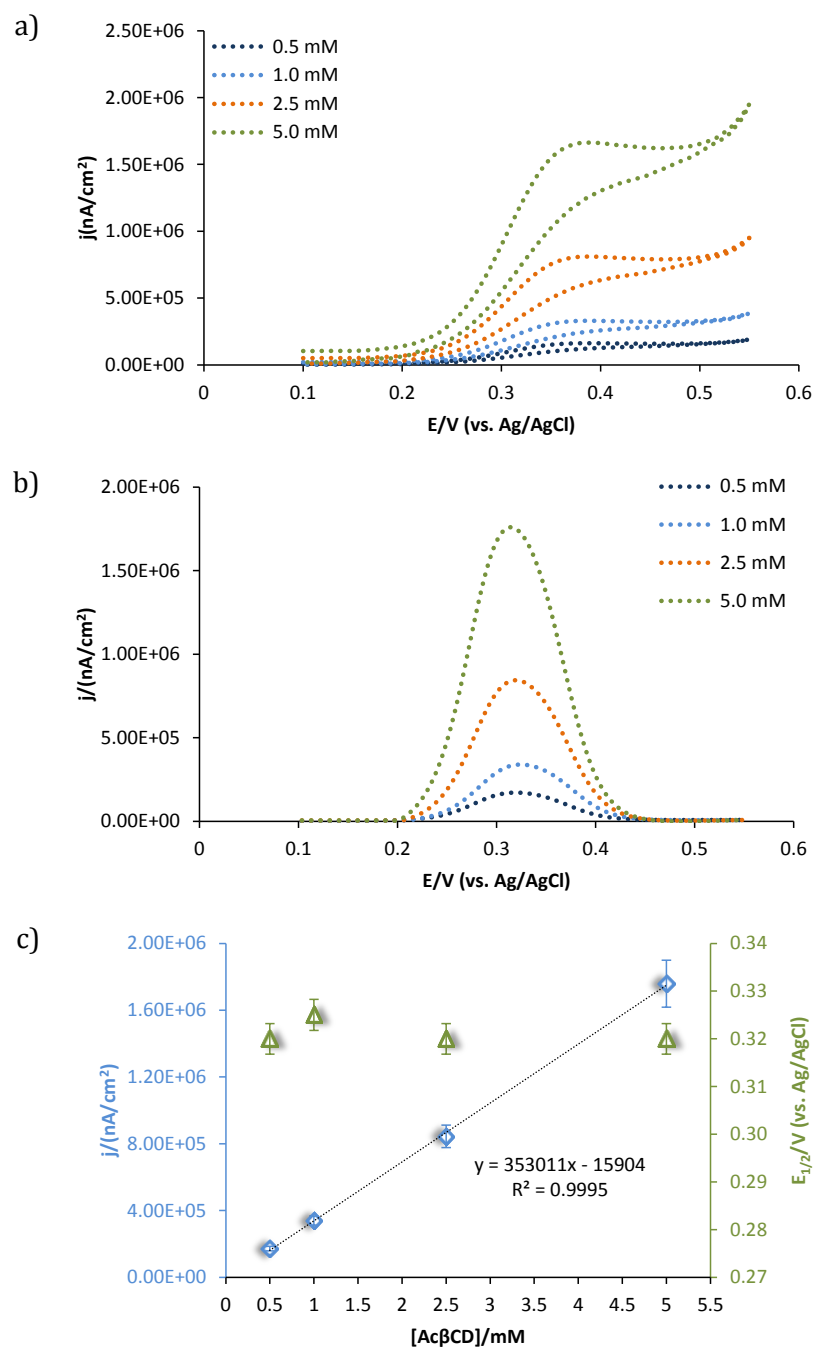
Figure 4.21 – a) CV and b) DPV voltammograms of the facilitated transfer of (-)EPH$^+$ (5 mM) by AcβCD across the aqueous|1,2-DCE micro interface. c) Dependence of current and half-wave potential on the variation of [AcβCD]. Scan rate:10 mV s^{-1}; pulse amplitude 0.05 V, sampling with 0.060 s, step height 0.005 V. Micropipette tip radius 7±1 μm. When not visible, the error bars are smaller than the symbols.

Figures 18c, 19c, 20c and 21c show that the limiting current obtained in the CVs were proportional to the concentration of the chiral ligands in the presence of an excess of (+)-EPH$^+$ and (-)-EPH$^+$. The differences observed in the half-wave potentials, when the transfer of the chiral ions are facilitated by the two ligands, indicates that AcβCD has higher chiral selectivity compared to AcαCD (Table 4.2). Additionally, the transfer of (+)-EPH$^+$ seems to be the more facile process to occur upon complexation with ligands, its potential of transfer occurs at slightly is smaller potentials, when compared to (-)-EPH$^+$. This is also an indication of different binding constants for the interaction between the EPH$^+$ ions with the chiral ligands.[69] Previous studies have shown that stereodifferentiation of ephedrine[61] and its congeners as guest of CD host arises from a difference in $\overset{+}{N}H \ldots O$ hydrogen bonding. As mentioned previously, the (-)-EPH$^+$ has unfavourable steric interactions which may be responsible for the formation of a weaker complex compared to (+)-EPH$^+$ ion. Although these differences cannot be directly proved electrochemically, we believe that is a combination of these effects that manifests as the difference observed in this study.

As we were unable to obtain a complete voltammogram for the unassisted transfer of ephedrine ions, only a rough estimate for the binding constant is available from this study. The estimated values, for the free Gibbs energy of transfer and binding constant, related to the facilitated chiral ions transfer are presented in table 4.3.

The results obtained (figure 4.18 to figure 4.21) indicate that the current response is limited by the diffusion of the ligand (AcαCD or AcβCD) to the interface and by the diffusion of the complex away from it. It is also plausible that the complexation between the ephedrine enantiomers and the modified CD is determined by kinetic control. This means that the FIT process can be limited by the rate of the complex formation.

Table 4.3 – Enantioselective differentiation of ephedrine enantiomers [5mM] using AcαCD and AcβCD [0.5mM] as chiral stationary phases at a micro aqueous|1,2-DCE interface.

	(+)-EPH+	(-)-EPH+	$\Delta(\Delta G)_{chiral}$/J mol^{-1}	ΔK
$E^{1/2}_{(Ac\alpha CDEPH^+)}$/mV	328±3	333±3	-482.4	0.71±0.1
$E^{1/2}_{(Ac\beta CDEPH^+)}$/mV	315±3	323±3	-771.8	0.83±0.1

4.3 Conclusion

Chiral stationary phases based on acetylated CDs, AcαCD and AcβCD, were used to facilitate and differentiate chiral ion transfer at a micro liquid|liquid interface. The results obtained show that the performance of CDs as chiral selectors is due to the molecular interaction based on the inclusion of the chiral analyte into the hydrophobic cavity, hydrogen bonds or dipole-dipole interactions with the acetyl groups of the CDs. The size of the chiral selector (Table 4.1) seems to influence strongly the selectivity of the analyte, as the chiral responses using AcβCD and AcαCD showed a significantly different response towards the selectivity of the ephedrinium ions. The use is a bigger macrocycle, AcβCD, proved to be more favourable for the chiral discriminations of ephedrinium ions.

The values obtained for the variation of stability constants using AcβCD (0.83±0.1) and AcαCD (0.71±0.1) were modest; however, they prove that the ephedrinium ions interact differently with the chiral selectors and those differences can be detected electrochemically. Although the present approach has not been yet applied for the separation of ephedrines, it can constitute a rapid and simple alternative to other methods for the analysis of pure chiral compounds requiring small volumes and non-destructive of samples.

References

(1)   Biot, D. *Anales de Chemie et de Physique* **1820**, *15*, 222–223.

(2)   Beesley, T. E.; Scott, R. P. W. *Chiral Chromatography*; 1st ed.; Wiley, 1999.

(3)   Gal, J. In *Chirality in Drug Research, Volume 33*; Francotte, E.; Lindner, W., Eds.; Wiley-VCH Verlag GmbH & Co. KGaA, 2006; pp. 1–26.

(4)   Pasteur, L. *Ann. Chim. Phys.* **1848**, *24*, 442–459.

(5)   Aboul-Enein, H. Y.; Wainer, I. W. *The impact of stereochemistry on drug development and use*; Wiley, 1997.

(6)   Le Bell, J. A. *Bull. Soc. Chim. Paris* **1874**, *22*, 337–347.

(7)   van't Hoff, J. H. *Arch. Neerl. Sci. Exactes Natur.* **1874**, *9*, 445–454.

(8)   Baer, E.; Fisher, H. O. L. *Science* **1938**, *88*, 108–108.

(9)   Reddy, I. K.; Mehvar, R. *Chirality in drug design and development*; CRC Press, 2004.

(10)   Del Valle, E. M. M. *Process Biochem.* **2004**, *39*, 1033–1046.

(11)   Stella, V. J.; He, Q. *Toxicol. Pathol.* **2008**, *36*, 30–42.

(12)   Harada, A.; Furue, M.; Nozakura, S.-I. *J. Polymer. Sci.* **1978**, *16*, 189–196.

(13)   Armstrong, D. W. *J. Liq. Chromatogr.* **1980**, *6*, 895–900.

(14)   Schneiderman, E.; Stalcup, a M. *J. Chromatogr. B* **2000**, *745*, 83–102.

(15)   Szejtli, J. *Chem. Rev.* **1998**, *98*, 1743–1754.

(16)   Shahgaldian, P.; Pieles, U. *Sensors* **2006**, *6*, 593–615.

(17)   Szejtli, J. *Pure Appl. Chem.* **2004**, *76*, 1825–1845.

(18)   Ogoshi, T.; Harada, A. *Sensors* **2008**, *8*, 4961–4982.

(19)   Loftsson, T.; Brewster, M. E. *J. Pharm. Sci.* **1996**, *85*, 1017–1025.

(20)   Atwood, J. L.; Lehn, J.-M. *Comprehensive Supramolecular Chemistry: Cyclodextrins*; Pergamon, 1996.

(21)   Roux, M.; Perly, B.; Djedaïni-Pilard, F. *Eur. Biophys. J.* **2007**, *36*, 861–867.

(22)   Loftsson, T.; Duchêne, D. *Int. J. of Pharm.* **2007**, *329*, 1–11.

(23)   Uekama, K.; Hirayama, F.; Irie, T. *Chem. Rev.* **1998**, *98*, 2045–2076.

(24)   Singh, M.; Sharma, R.; Banerjee, U. C. *Biotechnol. Adv.* **2002**, *20*, 341–59.

(25)   Fanali, S. *J. Chromatogr. A* **1989**, *474*, 441–446.

(26)   Juvancz, Z.; Kendrovics, R. B.; Iványi, R.; Szente, L. *Electrophoresis* **2008**, *29*, 1701–1712.

(27)   Blanco, M.; Valverde, I. *TrAC* **2003**, *22*, 428–439.

(28)   Szemaán, J.; Ganzler, K. *J. Chromatogr. A* **1994**, *668*, 509–517.

(29)   Schmitt, T.; Engelhardt, H. *Chromatographia* **1993**, *37*, 475–481.

(30)   Salvatore, F. *J. Chromatogr. A* **2000**, *875*, 89–122.

(31)   Subramanian, G. *Chiral separation techniques: a practical approach*; Wiley-VCH, 2007.

(32)   Schurig, V.; Nowotny, H.-P. *Angew. Chem. Int. Edit.* **1990**, *29*, 939–957.

(33)   Holzgrabe, U.; Mallwitz, H.; Branch, S. K.; Jefferies, T. M.; Wiese, M. *Chirality* **1997**, *9*, 211–219.

(34)   Ndou, T. T.; Mukundan, S.; Warner, I. M. *J. Incl. Phenom. Macro.* **1993**, *15*, 9–25.

(35)   Hellriegel, C.; Händel, H.; Wedig, M.; Steinhauer, S.; Sörgel, F.; Albert, K.; Holzgrabe, U. *J. Chromatogr. A* **2001**, *914*, 315–324.

(36)   Tanaka, Y. *Chromatography* **2002**, *23*, 13–23.

(37)   Kataky, R.; Bates, P. S.; Parker, D. *Analyst* **1992**, *117*, 1313–1317.

(38)   Bates, P. S.; Kataky, R.; Parker, D. *J. Chem. Soc., Chem. Commun.* **1992**, 153–155.

(39)   Ozoemena, K. I.; Stefan, R.-I.; Staden, J. F. V.; Aboul-Enein, H. Y. *Sensor. Actuat. B-Chem.* **2005**, *105*, 425–429.

(40)   Stefan, R.; Staden, J. F. V.; Aboul-Enein, H. Y. *Crystal Engineering* **2001**, *4*, 113–118.

(41)   Easton, C. J.; Lincoln, S. F. *Chem. Soc. Rev.* **1996**, *25*, 163–170.

(42)   Gübitz, G.; Schmid, M. G. *Chiral separations: methods and protocols*; Humana Press, 2004.

(43)   Bikádi, Z.; Iványi, R.; Szente, L.; Ilisz, I.; Hazai, E. *Curr. Drug Discov. Tech.* **2007**, *4*, 282–294.

(44)   Dalgliesh, C. E. *J. Chem. Soc.* **1952**, 3940–3942.

(45)   Armstrong, D. W.; Ward, T. J.; Armstrong, R. D.; Beesley, T. E. *Science* **1986**, *232*, 1132–1135.

(46)   Rekharsky, M. V.; Inoue, Y. *Chem. Rev.* **1998**, *98*, 1875–1918.

(47)   Harada, A. *Acc. Chem. Res.* **2001**, *34*, 456–464.

(48)   Schänzer, W. *Recent Advances in Doping Analysis*; Sport und Buch Strauß: Germany, 2001; Vol. 9.

(49)   Shekelle, P. G.; Hardy, M. L.; Morton, S. C.; Maglione, M.; Mojica, W. A.; Suttorp, M. J.; Rhodes, S. L.; Jungvig, L.; Gagne, J. *JAMA* **2003**, *289*, 1537–1545.

(50)   LeBelle, M. J.; Savard, C.; Dawson, B. A.; Black, D. B.; Katyal, L. K.; Zrcek, F.; By, A. W. *Forensic Sci. Int.* **1995**, *71*, 215–223.

(51)   Zhang, L.; Han, D.; Song, X.; Wang, H.; Wang, K.; Liu, Z. *ORL* **2008**, *70*, 91–96.

(52)   Vansal, S. S.; Feller, D. R. *Biochem. Pharmacol.* **1999**, *58*, 807–810.

(53)   Rekharsky, M. V.; Goldberg, R. N.; Schwarz, F. P.; Tewari, Y. B.; Ross, P. D.; Yamashoji, Y.; Inoue, Y. *J. Am. Chem. Soc.* **1995**, *117*, 8830–8840.

(54)   Noggle, F. T.; DeRuiter, J.; Clark, C. R. *Anal. Chem.* **1986**, *58*, 1643–1648.

(55)   Herráez-hernández, R.; Campins-Faco, P. *Anal. Chim. Acta* **2001**, *434*, 315–324.

(56)   Marusza, W.; Trojanowicz, M.; Margasińska, M.; Engelhardt, H. *J. Chromatogr. A* **2001**, *926*, 327–236.

(57)   Ševčík, J.; Stránský, Z.; Ingelse, B. A.; Lemr, K. *J. Pharmaceut. Biomed. Anal.* **1996**, *14*, 1089–1094.

(58)   Mularz, E. A.; Cline-Love, L. J.; Petersheim, M. *Anal. Chem.* **1988**, *60*, 2751–2755.

(59)   Li, S.; Purdy, W. C. *Anal. Chem.* **1992**, *64*, 1405–1412.

(60)   Kataky, R.; Parker, D.; Kelly, P. M. *Scand. J. Clin. Lab. Invest.* **1995**, *55*, 409–419.

(61)   Gafni, A.; Cohen, Y.; Kataky, R.; Palmer, S.; Parker, D. *J. Chem. Soc. Farad. T. 2* **1998**, 19–24.

(62)   Bates, P. S.; Kataky, R.; Parker, D. *J. Chem. Soc. Farad. T. 2* **1994**, 669–675.

(63)   Qian, Q.; Wilson, G. S.; Bowman-James, K.; Girault, H. H. *Anal. Chem.* **2001**, *73*, 497–503.

(64)   Ribeiro, J. A.; Silva, F.; Pereira, C. M. *Talanta* **2012**, *88*, 54–60.

(65)   Su, B. *Chin. Sci. Bull.* **2002**, *47*, 1325–1329.

(66)   Shao, Y.; Stewart, A. A.; Girault, H. H. *J. Chem. Soc Faraday Trans.* **1991**, *87*, 2593–2597.

(67)   Kataky, R.; Lopes, P. *Chem. Commun.* **2009**, 1490–1492.

(68)   Zhan, D.; Xiao, Y.; Yuan, Y.; He, Y.; Wu, B. *J. Electroanal. Chem.* **2003**, *553*, 43–48.

(69)   Matsuda, H.; Yamada, Y.; Kanamori, K.; Kudo, Y.; Takeda, Y. *Bull. Chem. Soc. Jpn.* **1991**, *64*, 1497–1508.

Chapter 5

Binding of drug molecules with

α_1-acid glycoprotein at a μ-liquid|liquid interface

The investigation of interactions of drugs, particularly chiral drugs with plasma proteins, is of fundamental importance for drug efficacy and toxicity studies. In this chapter, the interaction between propranolol, procaine and lidocaine hydrochloride with a chiral acute phase plasma protein, α_1-acid-glycoprotein (AGP) at a micro liquid-liquid interface was studied. The binding of these basic drugs to the protein was studied using electrochemical techniques such as cyclic voltammetric (CV) and differential pulse voltammetric (DPV). The interaction between the AGP and the drugs was shown as a decrease in the CV and DPV current responses, corresponding to the decrease in the transfer of the drugs at the liquid|liquid interface. The bound concentration of propranolol (R- and S- enantiomers), procaine and lidocaine to AGP was estimated based on the responses obtained in the presence and absence of the protein. Scatchard analysis was employed to calculate the association constant and the number of binding sites of the drugs with AGP. It was proved that AGP has different affinity for different basic drugs which was reflected in the calculated association constants 2.7×10^5 M^{-1} for S- and 1.3×10^5 M^{-1} for R-propranolol, 1.2×10^4 M^{-1} for lidocaine and 8.4×10^3 M^{-1} for procaine.

5.1 Introduction

The study of the binding interactions between drug molecules and plasma proteins is of crucial importance since it affects the transportation and distribution of pharmaceutical agents in the body.[1,2] Binding of drugs to plasma proteins can be both a help and hindrance to the distribution of drugs through the body. They can help the drugs to reach regions remote from the site of administration but, because the rate of distribution of drug into to the tissue is controlled by the concentration gradient of the unbound drug, the drug-protein binding can affect both the duration and intensity of drug action.[2-4]

When a drug is dosed to the body, it enters in the bloodstream, where it quickly reaches binding equilibrium with plasma proteins. However, the total drug concentration exists in two forms, the fraction bound to plasma proteins and the free or unbound fraction. The unbound fraction is usually ionic and transfers freely across the biological membranes, reaching the drug receptor site to produce the pharmacological effect and must be easily metabolized for elimination from the body to prevent potential toxicity (scheme 5.1). On the other hand, the bound drug fraction is prevented from passing through the blood vessel walls, as the drug-protein complex becomes too large for easy diffusion.[5,6]

The drug-protein binding is influenced by a number of important factors which includes, i) the drug: its physicochemical properties and concentration in the body, ii) the plasma protein, the quantity of protein available for drug-protein binding, iii) the affinity between drug and protein, which includes the association constant, iv) drug interactions: competition for the drug by other substances at the protein binding site and v) the pathophysiologic condition of the patient, because the drug-protein binding may be altered according to the health of the patient.
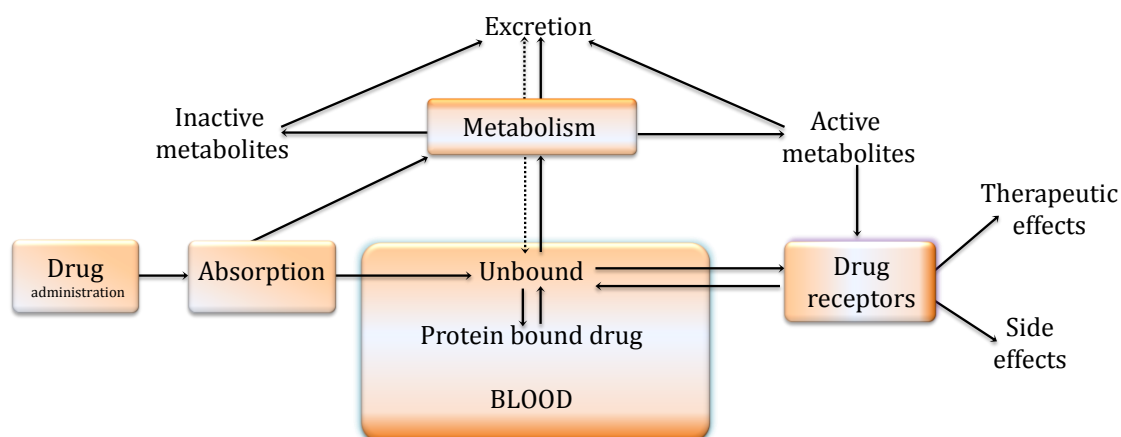
Scheme 5.1 – Schematic representation of protein binding and drug disposition.

5.1.1 Kinetics of protein binding

The interaction of most drugs with plasma proteins is characterised by a dynamic, reversible process with dissociation of bound drug molecules from the drug-protein complex occurring very rapidly (probably within milliseconds or less).[4,7] Quantitatively, the kinetics of reversible drug-protein binding can be described by the law of mass action, as follows:

$$[\text{Protein}] + [\text{unbound drug}] \rightleftarrows [\text{drug} - \text{protein}]_{complex}$$

or

$$[P] + [D] \rightleftarrows [PD] \qquad (5.1)$$
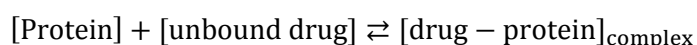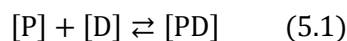
From Eq. (5.1), an association constant, K_a can be expressed as the ratio of the concentration of the drug-protein complex [PD] and the concentration of the drug [D] and protein [P]. The extent of the drug-protein complex formed is dependent on the equilibrium association constant, K_a, given by Eq. (5.2),

$$K_a = \frac{[PD]}{[P][D]} \qquad (5.2)$$

Accordingly, drugs that strongly bind to proteins have a very large K_a and exist mostly as the drug-protein complex. In these circumstances a large dose may be needed in order to obtain a reasonable therapeutic concentration of the drug. Drug-protein binding may also be expressed in terms of dissociation constant (K_d), which is the reciprocal of affinity and is equal to K_2/K_1. Experimentally, the free drug [D] and the protein-bounded drug [PD], as well as the total protein concentration [P]+[PD], can be determined. Another term frequently used is the free fraction, fu, of the drug in plasma,[8,9] which is defined by:

$$fu = \frac{[D]}{[D] + [PD]} = \frac{[D]}{[D]_{tot}} \qquad (5.3)$$

where $[D]_{tot}$ is the total drug concentration in the plasma, fu presents values between 0 and 1, or from 0 to 100%. The free fraction of the drug in plasma depends on the magnitude of the equilibrium constant, the total drug concentration and the protein concentration. In order to study the binding behaviour of drugs, a ratio r, Eq. (5.4), must be considered

$$r = \frac{\text{moles of drug bound}}{\text{total moles of protein}} \qquad (5.4)$$

where r determines the extent to which the binding sites in protein are occupied by the drug. The moles of drug bound is defined as [PD] and the total moles of protein is [PD] + [P], the Eq. (5.5) becomes

$$r = \frac{[PD]}{[PD] + [P]} \qquad (5.5)$$

According to Eq. (5.2), [PD]=k$_a$[P][D], substituting into Eq.(5.5)

$$r = \frac{K_a[P][D]}{K_a[P][D] + [P]} \qquad (5.6)$$

which yields,

$$r = \frac{K_a[D]}{1 + K_a[D]} \qquad (5.7)$$

Eq. (5.7) describes the simplest situation, in which 1 mole of drug binds to a mole of protein in a 1:1 complex. In this case, it is assumed only one binding site for each molecule of drug. However, if there are n identical independent binding sites in the protein, then the following is used:

$$r = \frac{nK_a[D]}{1 + nK_a[D]} \qquad (5.8)$$

In terms of K_d, Eq. (5.8) becomes:

$$r = \frac{n[D]}{nK_d + [D]} \qquad (5.9)$$

The values for the association constant, K_a, and the number of binding sites, n, are obtained by various graphic methods. A graphic technique called Scatchard plot, gives an estimation of the binding constants and binding sites for such a system. From Eq. (5.8), is obtainable:

$$r + nK_a[D] = nK_a[D]$$

$$r = nK_a[D] - rK_a[D]$$

$$\frac{r}{[D]} = nK_a - rK_a \qquad (5.10)$$

Plotting $\frac{r}{[D]}$ versus r yields a straight line as shown in Figure 5.1. The intercept of this plot gives the number of the binding sites and the slope is the negative value of the association constant.
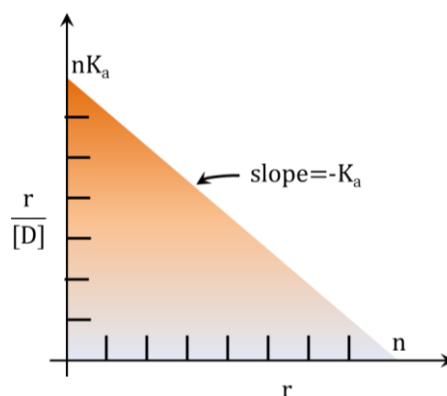
Figure 5.1 – Example of Scatchard plot where K_a is the association equilibrium constant, n is number of binding sites, and [D] corresponds to the free or unbound drug concentration.

5.1.2 Plasma proteins

5.1.2.1 α_1-acid-gycoprotein

Albumin, α_1-acid-gycoprotein (AGP) and lipoproteins are the three major proteins to which drugs bind in plasma.[5,7] The binding properties of these plasma proteins are different from each other and their plasma concentrations may vary depending on gender, age and/or disease state of patients.[5]

The concentration of AGP in blood (1g/L)[5,10] is about 30 times less than that of albumin, which is the most abundant plasma protein in blood (approximately 60% of the total plasma protein).[7] While albumin binds mainly with acidic-type molecules, AGP is known as the principal binding protein for a wide variety of basic and neutral drugs, with significant clinical implications.[11,12] Human AGP is produced mainly in the liver but extrahepatic synthesis has also been reported,[13] is one of the major acute phase proteins of human blood.[14] The binding of several drugs has been shown to increase following surgical interventions, inflammation and stress and this increased binding is due to an

increase in plasma concentration of AGP.[15,16] Thus changes in the level of AGP in plasma during physiological and pathological conditions can have a profound effect on drug disposition and pharmacological activity, which may result in treatment failure, due to higher binding and the resultant lower concentration of the free drug.[11]

AGP (Figure 5.2), also called orosomucoid, is a negatively charged (pI=2.7-3.2)[17] acidic (pKa=2.6)[14] glycoprotein, due to the presence of sialic acids (12% of the carbohydrate moiety). It is a highly heterogeneous, extensively glycosilated (Mw≈41,000), with a carbohydrate content of 45% (w/w). It is composed of a single polypeptide chain of 183 amino acids with up to five carbohydrate moieties attached to the protein core via five N-linked glycans.[11,14,17,18] It has been estimated that there are between 12 and 20 different forms[19] of AGP in serum due to variations in its amino acid sequence and the types and numbers of carbohydrate groups attached to its polypeptide chain. These carbohydrate moieties are thought to be located on the outside of this protein, giving it a hydrophobic core and a hydrophilic exterior.[20]
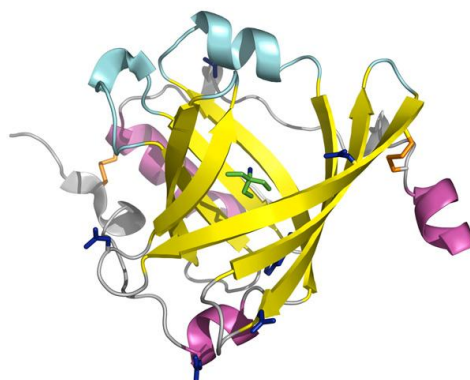
Figure 5.2 – Crystal structure of human α_1-acid-gycoprotein at 1.8 Å resolution.[21] The secondary structure is represented in yellow (β-strands), pink (α-helix), and grey (coils). Reproduced from Schönfeld et al.,[21] with permission.

5.1.2.2 Binding properties of α₁-acid-gycoprotein

The drug-protein binding is the result of multiple interactions between the two molecules, some of which are fairly weak (such as van der Waal's forces) and some of which are extremely strong (such as covalent bonding). Hydrogen bonding, ionic interactions and the hydrophobic effect between the molecule and protein also play a role on the favourability of a drug-protein interaction. Rarely a drug-protein binding is caused by a single type of interaction; rather it is a combination of binding interactions that provides drugs and proteins with the necessary forces, specificity and affinity to form a drug-protein complex.

The molecular structure of the drug strongly dictates the physical and chemical properties that contribute to its specific binding to the protein. Important factors include hydrophobicity, ionization state (pK_a), conformation, and stereochemistry of the drug molecule. The protein binding site, often referred as microenvironment, is highly specific, thus small changes in the drug can have a great effect on the affinity of the drug-protein interaction.

In the case of AGP, the nature of drug binding is still not clearly understood, however, it has been characterised mainly, by hydrophobic interactions, due to the hydrophobic residues near the AGP binding site. Hydrogen bonding, van der Waal's forces and electrostatic interactions have also been mentioned as participants in the binding interactions.[1,2,11,14,15,22] Kaliszan et al.[23] proposed an asymmetric and a negative charge distribution for the binding site for antihistamine drugs on AGP, that later would contribute for the studies of enantioselective binding. They suggested that the binding site is formed by a conical pocket that contains lipophilic regions at the base of the cone and an anionic region, close to the spike of the cone, which interacts with protonated aliphatic

nitrogen within a basic drug (Figure 5.3). The hydrophobic moieties provide anchoring for the drug molecule in the binding site of the protein,[23] and the steric restriction prevents the molecule from plunging into the binding site.
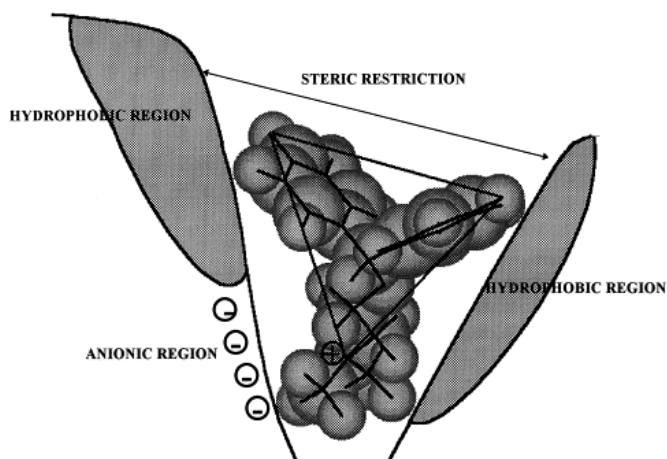
Figure 5.3 – Structural feature of the binding site for basic drugs on AGP. The AGP site is occupied by an exemplary drug (pheniramine). Reproduced from R. Kaliszan[24] with permission.

Additionally, it has been demonstrated that AGP has the ability to stereoselectively bind of enantiomers of widely different character.[25–27] The binding interaction takes place in the chiral sites of the protein, which appear to be located both in the peptide chain and in the carbohydrate units.[25] This peptide chain is composed of several different chiral groups, beside the hydrophobic groups, hydrogen bonding amides and anionic and cationic groups. On the other hand, the carbohydrate units are built up of sialic acid, hexosamine and neutral hexoses, and all contain chiral carbons, which appear to be involved in the retention of enantiomers.[28,29]

AGP has an extremely broad applicability, with the binding of drugs being examined by a wide range of techniques. Examples include equilibrium dialysis,[30,31] capillary electrophoresis,[28] high performance liquid chromatography (HPLC)[26,29,32] and various spectroscopic methods.[10,33–35]

5.1.2.3 Binding of propranolol, lidocaine and procaine to AGP

Since AGP is acidic, it is the main binding protein of basic (cationic) drugs, such as β-adrenergic receptor blockers and local anaesthetics.[2,3,22] The extent of binding of local anaesthetics ranges from 6% (procaine) to 95% (bupivacaine).[36] In table 5.1 are listed the drugs which binding to AGP was studied in this work.

Table 5.1 – Properties of basic drugs that interact with AGP.

Drugs	pK$_a$ (298K)	Log(P)$_{oct}$	Drug binding (%) to AGP
Procaine (anaesthetic)	8.6-8.9[37]	1.87[38]	6[36]
Lidocaine (anaesthetic)	7.7-8.1[37]	2.26[38]	65[36]
Propranolol (antiarrhythmic)	9.3-9.5[39]	3.56[38]	80[36]

Local anaesthetics are drugs that provide a reversible regional loss of sensation, reducing the pain and therefore facilitating surgical procedures. The site of action is believed to be the nerve membrane. In nerve cells, action potentials are created by the influx of sodium ions from the surrounding tissues.[40] These action potentials result in the conduction of nerve impulses that produce sensations (including pain). Local anaesthetics prevent the conduction of impulses by decreasing the permeability of nerve membranes to sodium ions. This reversible block of impulses, prevents excitation along a neural pathway and gives rise to anesthesia.[40,41]

The clinically useful local anaesthetics agents have been classified as either amino-esters, such as procaine (Figure 5.4 a) possessing an ester linkage between the benzene ring and the intermediate chain, or amino-amides, like lidocaine (Figure 5.4 b) possessing an amide link between the benzene ring and intermediate chain. Depending on physical and

chemical properties, such as lipid solubility, protein-binding and pK_a, these agents exert their anaesthetic effect by acting on the highly lipid nerve membranes.[42] Lidocaine is known to bind strongly to AGP, with an association constant in the range of $3.2(\pm 0.2) \times 10^4$ (determined by capillary electrophoresis/frontal analysis, $25^\circ C$ and pH 7.4) up to $1.0 \times 10^5 M^{-1}$.[43] Lidocaine is also believed to bind weakly to HSA with an estimated K_a of $2.3 \times 10^2 M^{-1}$ (measured at $25^\circ C$ and pH 7.4 by equilibrium dialysis).[44,45]

β-blockers comprise a group of drugs that are mostly used to treat cardiovascular disorders such as hypertension, angina pectoris and cardiac arrhythmias.[39,46] Each of these drugs possesses at least one chiral centre, and an inherent high degree of enantioselectivity in binding plasma proteins in blood.[47] Propranolol (Figure 5.4 c) is known to stereoselectively bind to both whole plasma and individual serum proteins.[46,48,49] The first stereoselectivity of propranolol was established by Walle et al. using equilibrium dialysis.[46,50,51] They demonstrated that plasma binding of the propranolol enantiomers differed with the unbound fraction, with (S)-(-)-propranolol (22$\pm$2%) being smaller than that of (R)-(+)-propranolol (25.3$\pm$1.9%), meaning that the binding of AGP was stereoselective for (S)-(-)-propranolol. They also demonstrated that the stereoselectivity in the binding of propranolol enantiomers to HSA revealed to be the opposite of that observed for human AGP.[46,52]

The binding of propranolol to AGP has been studied using various analytical techniques, encompassing fluorescence spectrophotometry,[53] circular dichroism,[54] NMR,[35] HPLC,[54] ultrafiltration[2] and equilibrium dialysis,[30] among others. The binding parameters of propranolol enantiomers binding to AGP have been estimated to be $2.62 \times 10^5 M^{-1}$ and $8.57 \times 10^5 M^{-1}$ with a binding site number of 0.41 and 1.17 for R- and S-propranolol, respectively, at 17°C using fluorescence spectrophotometry.[53] Using ultrafiltration,[2] the

dissociation constant of $1.58 \times 10^6 M^{-1}$ and $2.65 \times 10^6 M^{-1}$, with n=0.78 and 0.63 were determined for S- and R-propranolol at 37°C, respectively.
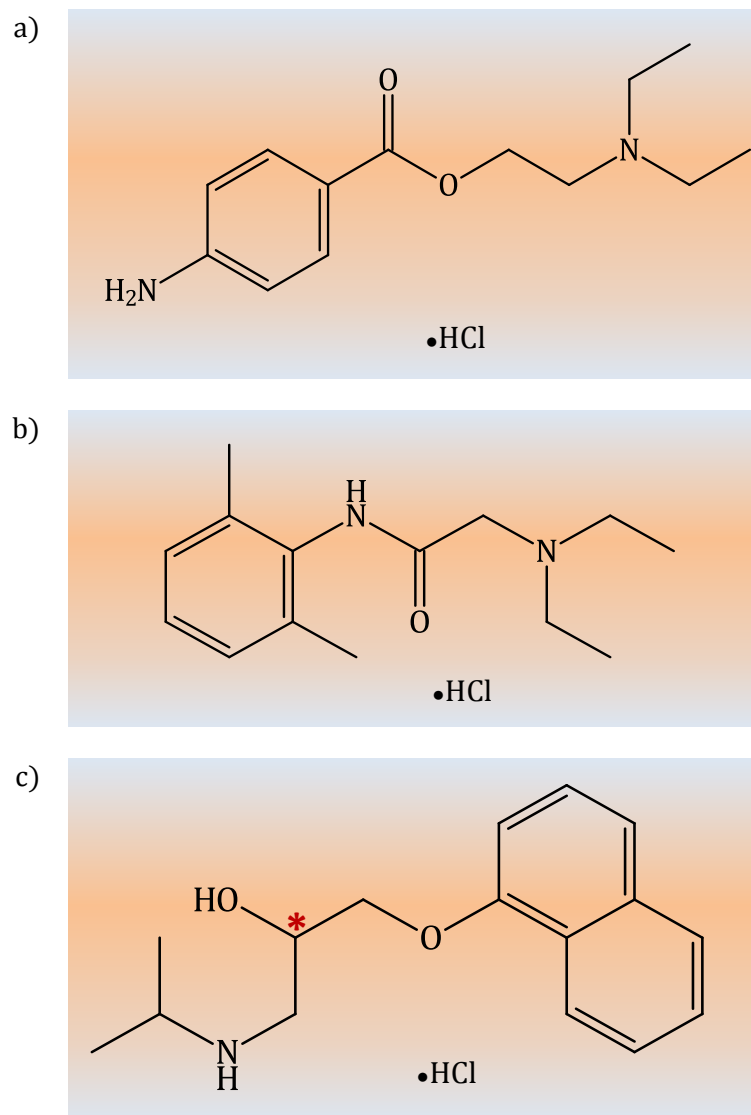
Figure 5.4 – Chemical structures of a) procaine hydrochloride, 2-(diethylamino)ethyl 4-aminobenzoate hydrochloride, b) lidocaine, 2-(diethylamino)-N-(2,6-dimethyl-phenyl)-acetamide hydrochloride and c) (±)-propranolol hydrochloride, (±)-1-isopropylamino-3-(1-naphthyoxy)-2-propranolol hydrochloride (asterisk denotes the chiral carbon).

5.2 Results and Discussion

The basic drugs studied, procaine, lidocaine and propranolol, have pK_a values between 7.8 and 9.5 (Table 5.1). Procaine and lidocaine, like the majority of anaesthetic drugs, have a pK_a value close to the normal extracellular pH of 7.4, thus they exist in two forms in solution, the uncharged (deprotonated) basic form (B) and the charged (protonated) form (BH+), according to the equilibrium:

$$BH^+ \Leftrightarrow B + H^+ \qquad (5.11)$$
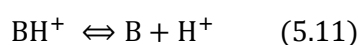
The importance of the pK_a-pH relationship is that this knowledge allows the calculation of the relative amounts of these two forms, by the use of the Henderson-Hasselbach equation:

$$pH = pK_a - \log \frac{[BH^+]}{[B]} \qquad (5.12)$$

When the pH is equal to the drug's pK_a, 50% of the drug is in the uncharged form, and 50% is in the charged form. At physiological pH, procaine, lidocaine and propranolol present an ionization of 96.9, 83.4 and 99.2%, respectively. In order to study the drug-protein interactions, two solutions of phosphate buffer (pH=7.4) were prepared: one without AGP and another with 50µM of AGP. A simple two electrode arrangement (as described in section 3.1.2, Figure 3.5) was used to perform the voltammetric measurements. The electrochemical cell can be represented by the following scheme:

| Ag\|AgCl(s) | 1mMBTPACl
10mMLiCl
(aq.) | 10mMBTPPATPBCl
(1,2-DCE) | 10mMLiCl+ χµM PH+
with /without 50µM AGP
Buffer (aq.) | Ag\|AgCl(s) |
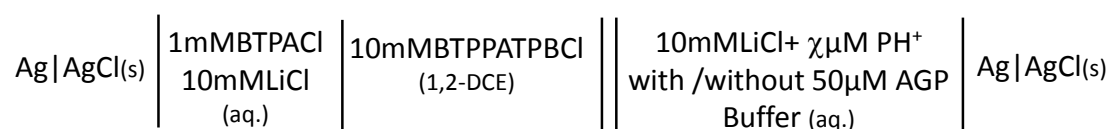
Scheme 5.2 – Cell configuration used, where PH+ is the protonated drug cations, procaine, lidocaine, (R)-(+)- and (S)-(-)-propranolol, where χ= 100, 87.5, 75.0, 62.5, 37.5 µM.

Initial experiments were focused towards establishing whether the addition of AGP would create changes in the potential window, which is limited by the background electrolytes transfer at extremes of the potentials. Figure 5.5 shows the potential range of the electrochemical system, which is about 600mV, in the presence (dashed line) and absence (dotted line) of the protein, in phosphate buffer at pH7.4.
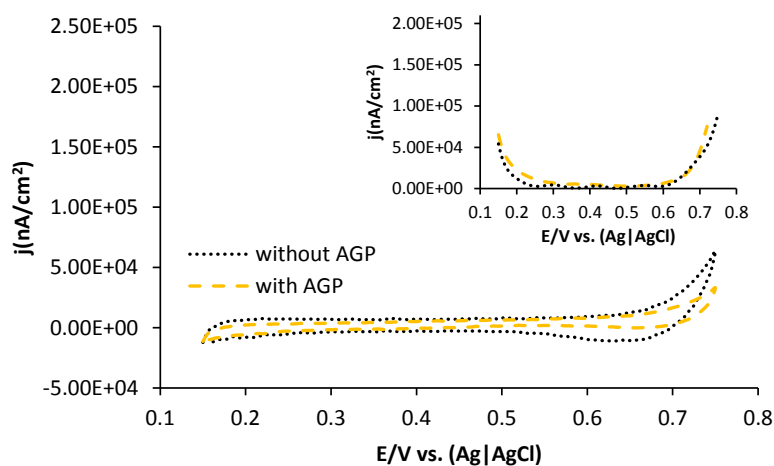
Figure 5.5 – CV (inset DPV) of the supporting electrolyte without AGP (dotted line) and in the presence of AGP (dashed line) at physiological pH. Scan rate: 10mV s^{-1}, micropipette radius = 10±1μm.

As can be seen in Figure 5.5, there is no marked effect on the potential window when the protein is added, meaning that there is no significant contribution to the increasing of the charging current. This is corroborated by the findings of Vanysek and Sun,[55] where in the study of bovine serum albumin adsorption at water-nitrobenzene interface, they showed that the capacitance increases for pHs below the isolelectic point and that at more basic pHs, the opposite occurs.

At physiological pH, AGP bears a negative overall charge and the drugs have a charge of +1 (i.e. the amine group is protonated) which makes the binding complex very likely to occur. The drugs are mainly ionized and can be strongly retained by ionic bonding to the anionic groups in the binding site of the protein. Ravis et al.[30] have shown that the

composition of the buffer and pH can have a great effect in the drug-protein binding. Using equilibrium dialysis, they found that in the case of propranolol the binding to AGP was greater when the protein was initially dissolved at pH 7.4, compared with pH 7.2 as well as with phosphate buffers than with a physiological buffer. It has also been demonstrated that pH values near the isoelectric point of the protein, lower the degree of its negative charge and thus decreases the retention of the cationic drug.[29]

Initially the transfer of the cationic drugs was characterised in the absence of AGP, using both CV and DPV, at pH 7.4 (Figures 5.6 to 5.9), and a linear concentration dependence was observed within the range studied, 0.0375-0.10mM.
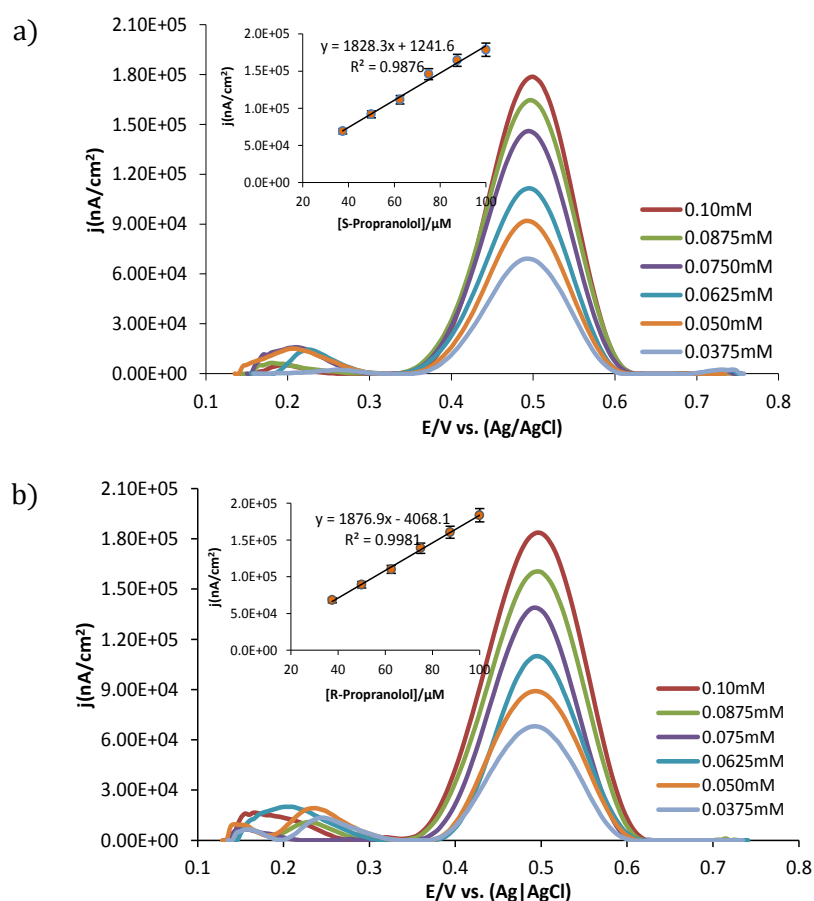
Figure 5.6 – DPV of increasing concentrations of a) S-propranolol and b) R-propranolol in the absence of AGP (pulse amplitude 0.05 V, sampling with 0.060 s, step height 0.005 V). Insets: calibration curve of peak current vs. concentration, ($\emptyset = 20 \pm 1 \mu m$).
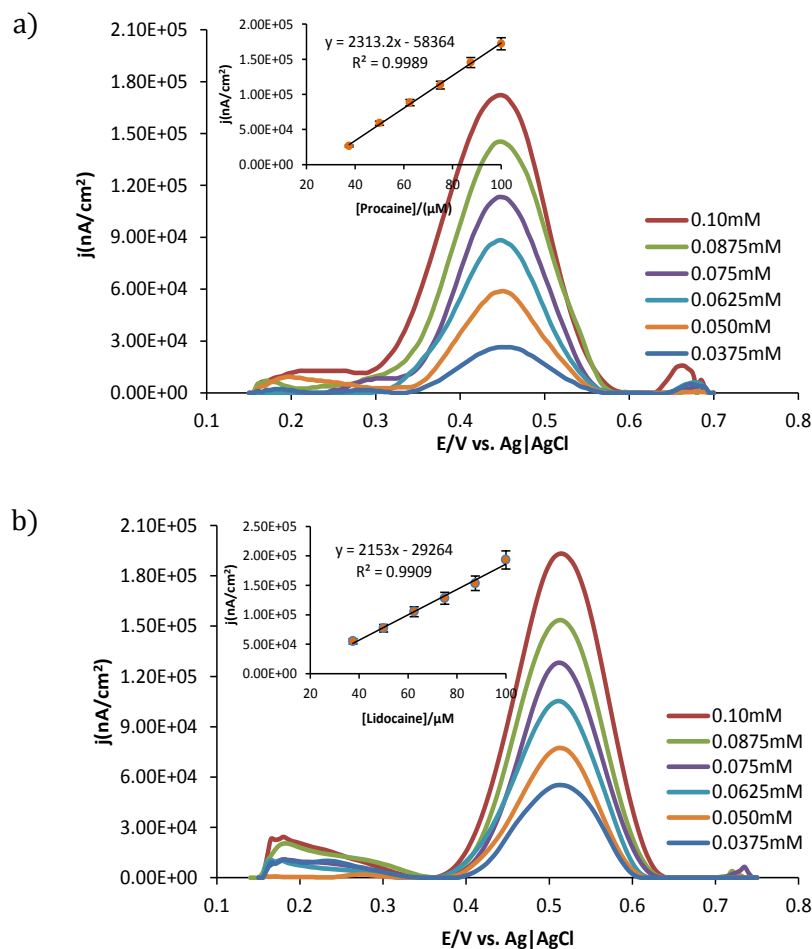
Figure 5.7 – DPV of increasing concentrations of a) procaine and b) lidocaine in the absence of AGP (pulse amplitude 0.05 V, sampling with 0.060 s, step height 0.005 V. Insets: calibration curve of peak current vs. concentration, ($\emptyset = 20 \pm 1 \mu m$).

The CV response of propranolol enantiomers (Figure 5.8), and the local anaesthetics, procaine and lidocaine (Figure 5.9) produced an asymmetric shape with an apparent steady-state on the forward scan, corresponding to transfer and ingress of the cationic drugs into the organic phase and a peak-shaped response on the reverse scan, corresponding to the transfer and egress of the propranolol from the organic phase to the aqueous phase.

This type of diffusion regime was pioneered by Shao et al.[56] who observed a pseudo-steady state wave (spherical diffusion) when the ion transfer process was controlled by the species entering the micropipette and a peak-shaped voltammogram (linear diffusion) occurred when the transfer process was controlled by the species leaving the micropipette. Therefore, the apparent steady-state in the forward scan and the peak observed in the reverse scan, are due to the transfer of the protonated drugs, consistent with the different diffusion fields on either side of the micro interface.[56,57]
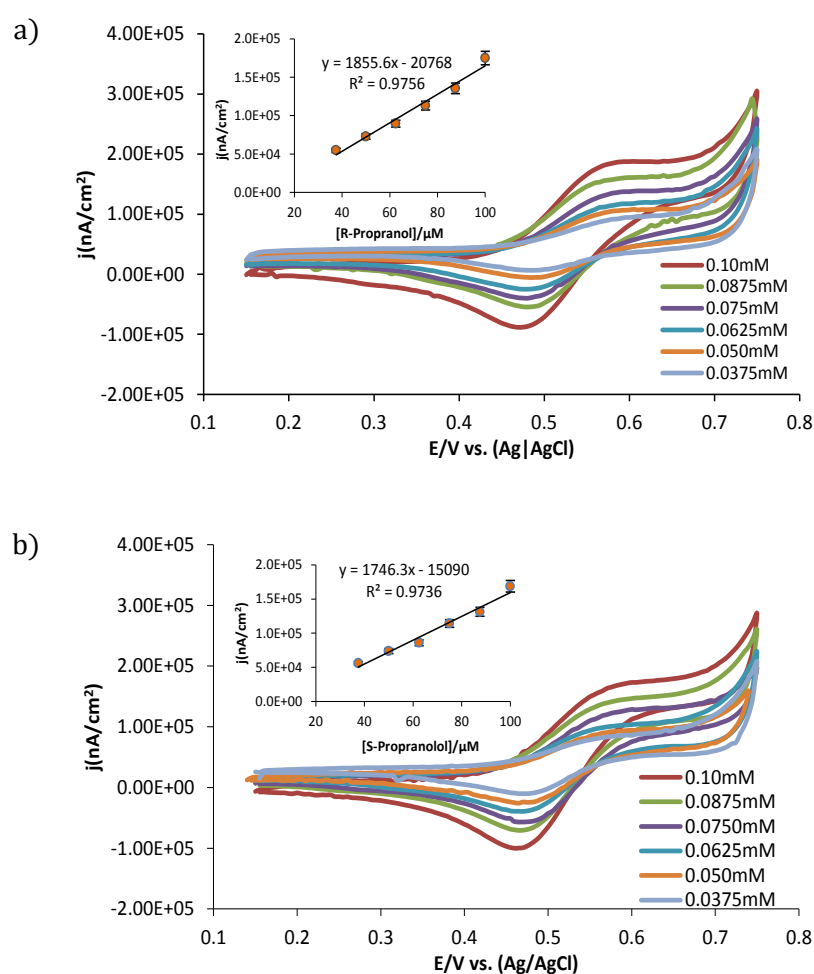
Figure 5.8 – CV of increasing concentrations of a) R-propranolol and b) S-propranolol in the absence of AGP, scan rate: 10mV s^{-1}. Insets: calibration curve of steady-state current vs. concentration, ($\varnothing = 20\pm1\mu$m).
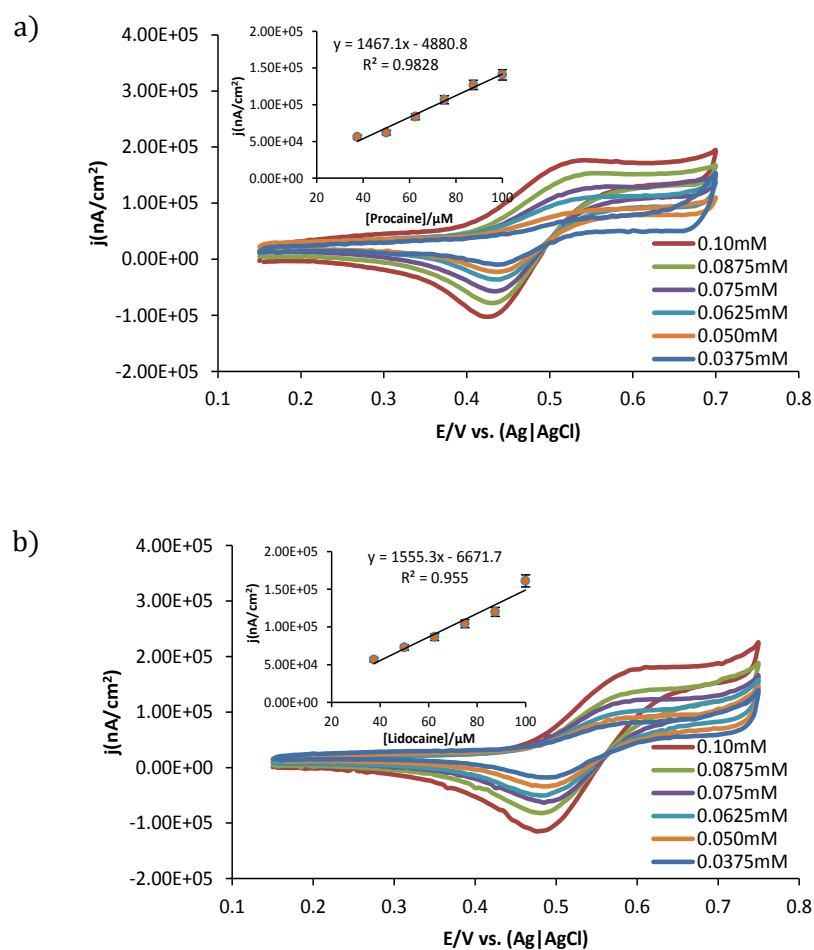
Figure 5.9 – CV of increasing concentrations of a) procaine and b) lidocaine in the absence of AGP, scan rate: 10mV s^{-1}. Insets: calibration curve of steady-state current vs. concentration, $(\varnothing = 20\pm 1\mu m)$.

The standard potential of transfer of the drugs under study was determined from the CV experiments, and referred to an internal reference ion, TEA$^+$, according to Eq.5.13,

$$E_{BH^+}^{1/2} - \Delta_o^w\phi_{BH^+}^{o'} = E_{TEA^+}^{1/2} - \Delta_o^w\phi_{TEA^+}^{o'} \qquad (5.13)$$

where $\Delta_o^w\phi_{TMA^+}^{o'} = 52$ mV,[58,59] is the standard transfer potential of TEA$^+$ across the water|1,2-dichloroethane interface. $E_{BH^+}^{1/2}$ and $E_{TEA^+}^{1/2}$ are the experimental half-wave

potentials drug cations and TEA+, respectively. A value for the free Gibbs energy of transfer, $\Delta G_{tr,BH^+}^{0,w\rightarrow o}$, was calculated using the Eq.(5.14),

$$\Delta G_{tr,BH^+}^{0,w\rightarrow o} = z_i F \times \Delta_o^w \phi_{BH^+}^{o'} \qquad (5.14)$$

The standard potential of the propranolol enantiomers, $\Delta_o^w \phi_i^{o'}$, was found to be the same and equal to 197±5 mV and the free Gibbs energy of transfer equal to 18.0±0.5 kJ mol^{-1}. These values are in reasonable agreement with values already reported in the literature,[60] $\Delta_o^w \phi_i^{o'}$ =197±5 mV vs. $E_{TEA^+}^{1/2}$ and $\Delta G_{tr,i}^{0,w\rightarrow o}$ = 12.6±0.5 kJ mol^{-1}. For procaine and lidocaine, $\Delta_o^w \phi_i^{o'}$ was found to be 142±5 and 207±5 mV with a correspondent free Gibbs energy of transfer of 13.7 and 19.0±0.5 kJ mol^{-1}, respectively. These values could not be easily compared with literature values as their exact values are not well known.

The organic|aqueous interface at a DCE filled micropipette has been shown to be essentially planar under normal conditions (absence of applied potential), thus the steady-state plateau current can be described by Eq.(5.15)[61]

$$I_{ss} = A\pi z_i aFDC \qquad (5.15)$$

where I_{ss} is the limiting current, D the diffusion coefficient, C is the concentration of the protonated drugs in the outer solution, a is the radius of the micropipette tip (10±1 μm), and the empirical factor A is 4, assuming that the micro interface displays current response similar to a disk-shaped ITIES.[57,61] The diffusion coefficient of the protonated drugs were determined using Eq.(5.15), and the limiting currents were taken from the CVs responses (Figures 5.8 and 5.9). For S- and R-propranolol were found to be 1.6x10^{-6}±0.1 and 1.5x10^{-6}±0.1 cm^2 s^{-1}, respectively, which are in good agreement with those reported by Fantini et al.[60] for a nongellified interface, table 5.2. The diffusion coefficients of procaine and lidocaine could not be compared with the literature values, as

well as the Gibbs free energy of transfer and formal potential due to the lack of studies that at a water|1,2-DCE interface.

Table 5.2 – Thermodynamic and transport parameters of the transfer of the protonated propranolol enantiomers, procaine and lidocaine across the aqueous 1,2-DCE micro liquid|liquid interface.

Drugs	$\Delta_o^w \phi_i^{o\prime}/V$	$\Delta G_{tr,i}^{0,w \rightarrow o}/kJ\ mol^{-1}$	$D/cm^2\ s^{-1}$
Procaine	142$\pm$4	13.7$\pm$0.5	1.4 x10^{-6}$\pm$0.1
Lidocaine	207$\pm$4	19.0$\pm$0.5	1.1 x10^{-6}$\pm$0.1
(R)-(+)-propranolol	197$\pm$4	12.6$\pm$0.5	1.5x10^{-6}$\pm$0.1
(S)-(-)-propranolol	197$\pm$4	12.6$\pm$0.5	1.6x10^{-6}$\pm$0.1

It was expected that, on the addition of AGP to the aqueous phase, the ionized drug molecules would bind to the protein in the aqueous phase and that the binding would influence its transfer across the interface. As mentioned previously, the binding of drugs to plasma proteins is a reversible and rapid reaction. The uncomplexed/unbounded drug is able to diffuse through the interface into the organic phase, whereas the bound one is retained by the protein (Figure 5.10). The reaction that occurs in solution can be described by Eq. (5.16) and (5.17).

$$[\text{Protonated Drug}]_{unbound(w)} \rightleftharpoons [\text{Protonated Drug}]_{unbound(o)} \qquad (5.16)$$

$$[\text{Protonated Drug} \cdot \text{AGP}]_{complex(w)} \nrightleftharpoons [\text{Protonated Drug} \cdot \text{AGP}]_{complex(o)} \quad (5.17)$$

The subscripts unbound and complex refer to non-complexed and complexed drug, respectively, and (w) and (o) refer to the locations of the species in the aqueous and organic phase, respectively.
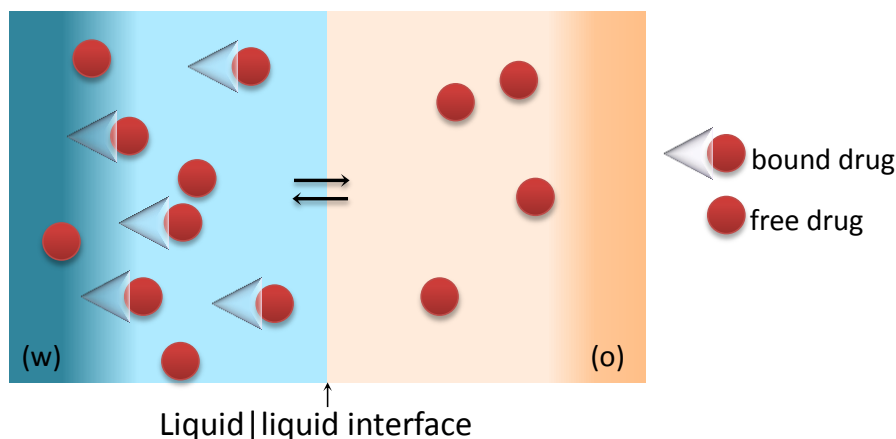
Figure 5.10 – Schematic representation of the drug-protein equilibrium at the liquid|liquid interface.

To understand the effect of AGP on procaine, lidocaine and propranolol enantiomers transfer across the micro interface, a constant concentration (50 µM) of AGP was added to aqueous solution containing different concentrations of the ionized drugs, under the same conditions (PBS buffer, pH 7.4). A decrease in current in the CV and DPV responses was observed in the presence of AGP, due to the binding of the drug molecules to AGP, which suppressed its transfer across the interface. Similar findings were obtained by Horrocks et al.[62] in the binding study of a cation, N-methylphenanthroline, to DNA. In one of the approaches developed, where the cation is initially present in the aqueous phase, they also found that, upon the addition of high molecular weight DNA to the aqueous phase that the concentration of free cation decreases which resulted in a decrease in the ion transfer current.

The CV and DPV responses obtained for the binding of R-propranolol, S-propranolol, procaine and lidocaine to AGP are presented in figures 5.11, to 5.14, respectively. The DPV response provided a more sensitive detection signal at lower concentrations for the transfer of the unbounded drugs in comparison with CV. It was observed that the peak current intensity for the DPV, in the presence of AGP, was in average about 33% and 52% smaller for R- and S -propranolol, respectively, when compared to the measurements in the absence of AGP. For procaine and lidocaine a decrease of 7.4% and 26%, respectively, was observed. CVs revealed steady-state currents on forward sweep, but these were decreased relative to that in the absence of AGP.
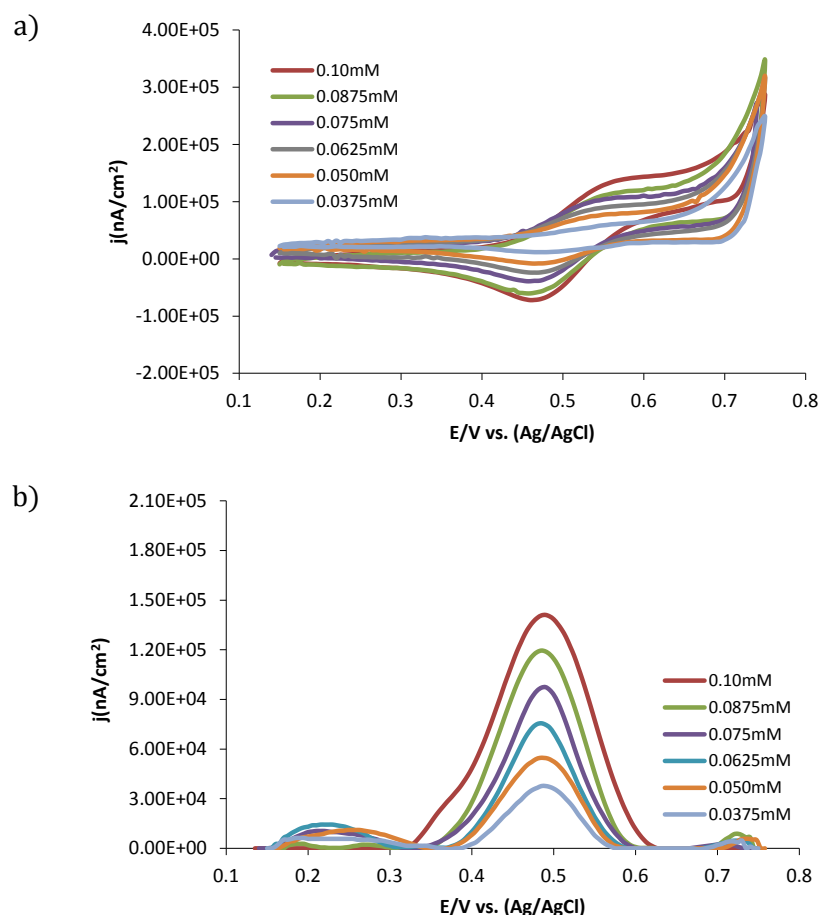
Figure 5.11– a) CV and b) DPV at different concentrations of R-propranolol in the presence of AGP (50μM), scan rate: 10 mV s^{-1}; pulse amplitude 0.05 V, sampling with 0.060 s, step height 0.005 V, (∅ = 20±1μm).

a)

b)
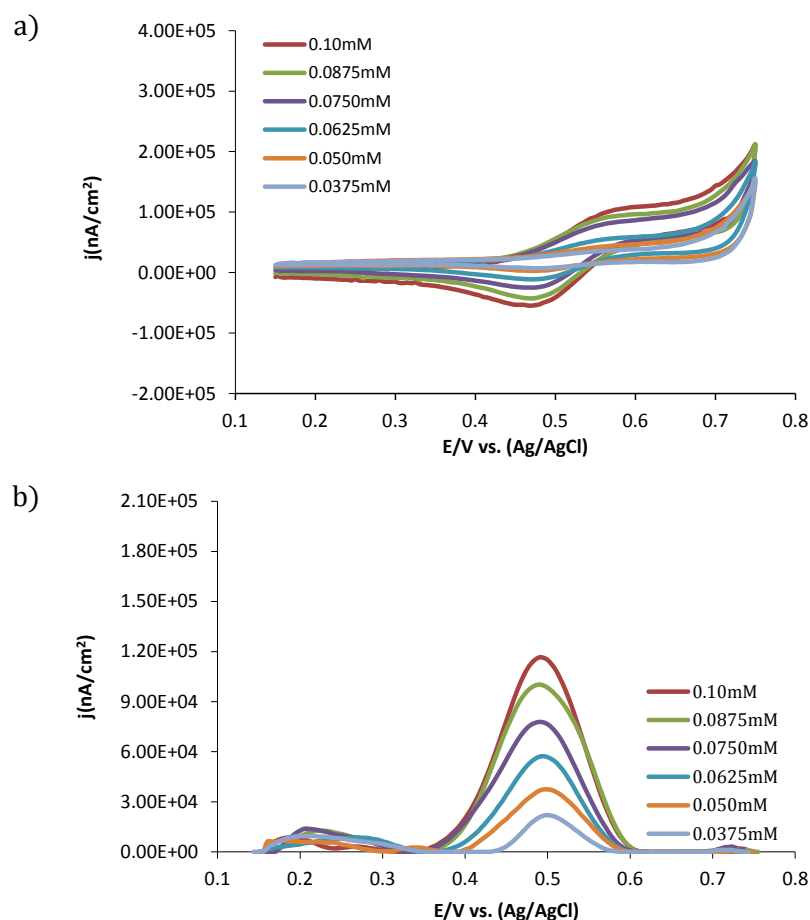
Figure 5.12 – a) CV and b) DPV at different concentrations of S-propranolol in the presence of AGP (50μM), scan rate: 10 mV s^{-1}; pulse amplitude 0.05 V, sampling with 0.060 s, step height 0.005 V, ($\emptyset = 20\pm1\mu$m).

When compared the responses obtained for the interactions of AGP with R- and S-propranolol, figures 5.11 and 5.12, the peak in DPV and the apparent steady-state in CV are clearly of lower current intensity in the case for S-propranolol. This suggests that the drug-protein binding is stronger in the case of the S-propranolol enantiomer.
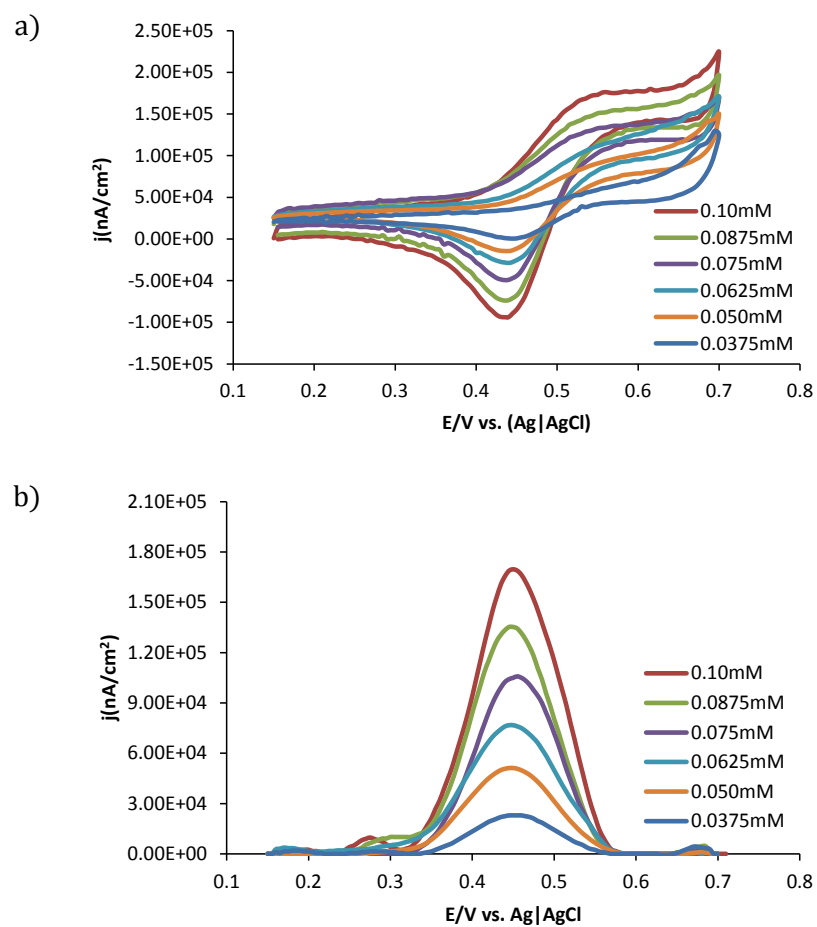
Figure 5.13 – a) CV and b) DPV at different concentrations of procaine in the presence of AGP (50μM), scan rate: 10 mV s^{-1}; pulse amplitude 0.05 V, sampling with 0.060 s, step height 0.005 V, (Ø = 20±1μm).
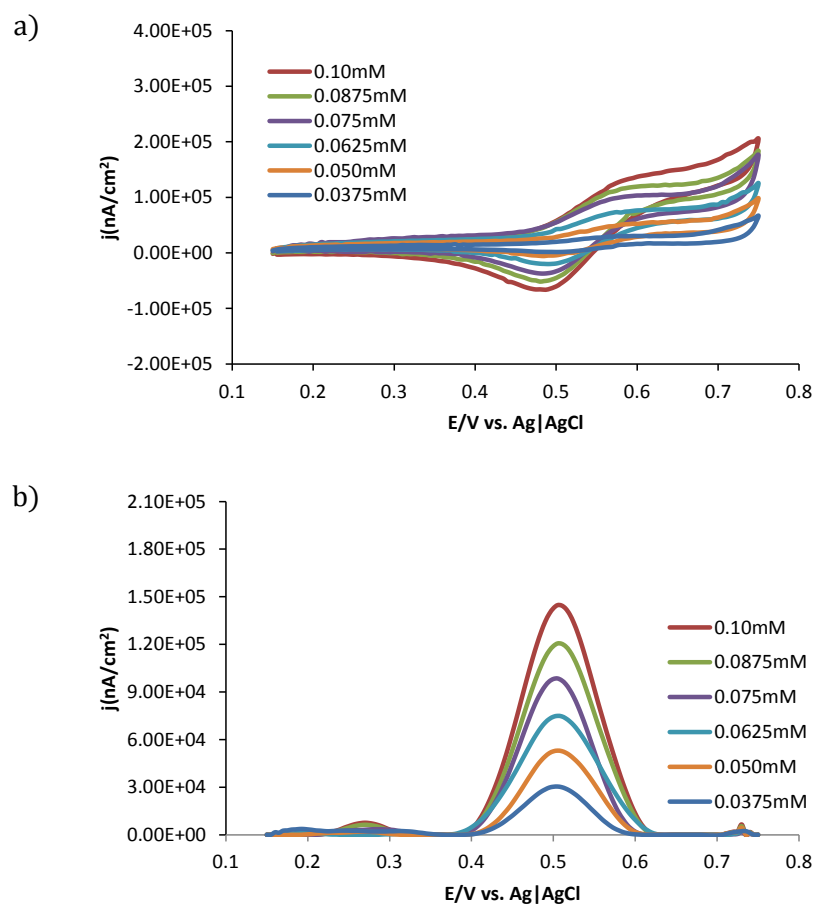
Figure 5.14 – a) CV and b) DPV at different concentrations of lidocaine in the presence of AGP (50μM), scan rate: 10 mV s^{-1}; pulse amplitude 0.05 V, sampling with 0.060 s, step height 0.005 V, ($\varnothing = 20\pm1\mu$m).

As it can be seen in Figures 5.13 and 5.14 AGP interacts more strongly with lidocaine than with procaine, which was reflected as a more significant decrease in current.

For an equilibrium system, the binding sites (n), bound and free drug can be calculated according to the Scatchard model (Eq. (5.9)), as mentioned earlier. The Scatchard plots, for S-and R-propranolol are presented in Figure 5.15 a) and b), respectively.
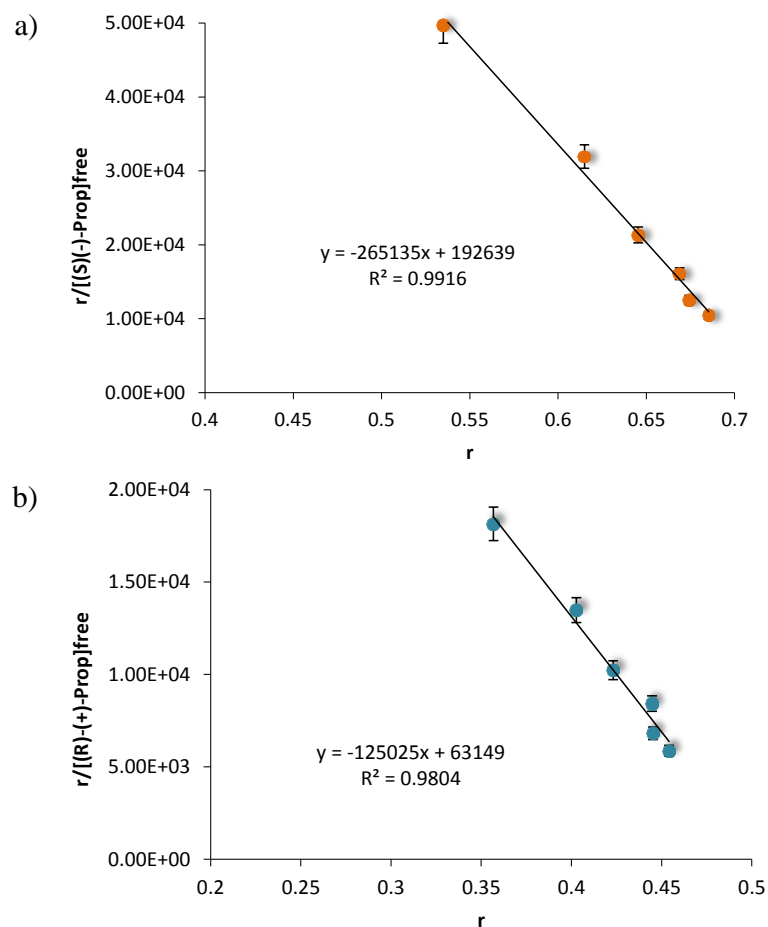
Figure 5.15 – Scatchard plot for the binding of AGP to a) S- and b) R-propranolol (according to Eq. 5.10). The data points are expressed as mean of three separate experiments.

From these plots, the binding parameters of K_a and n, for the interactions of the enantiomers of propranolol with AGP, can be easily calculated using Eq.(5.9). The difference in the binding parameters 2.7 x10^{5}M^{-1}, n=0.73 and 1.3 x10^{5}M^{-1}, n=0.50, for S- and R-propranolol respectively, clearly shows a chiral selective binding for the two enantiomers with AGP, with the S- enantiomer having a higher affinity compared to R-propranolol. The difference obtained is due to the chiral interactions of AGP with propranolol enantiomers. The number of binding sites, n, on AGP molecules is less than the unity for both enantiomers, which means that both bind at the same place in the

protein, but in a dissimilar way. Accordingly, a higher amount of S-propranolol is bounded to AGP, as it can be seen in figure 5.16, for the same [propranolol]/[AGP] ratios.
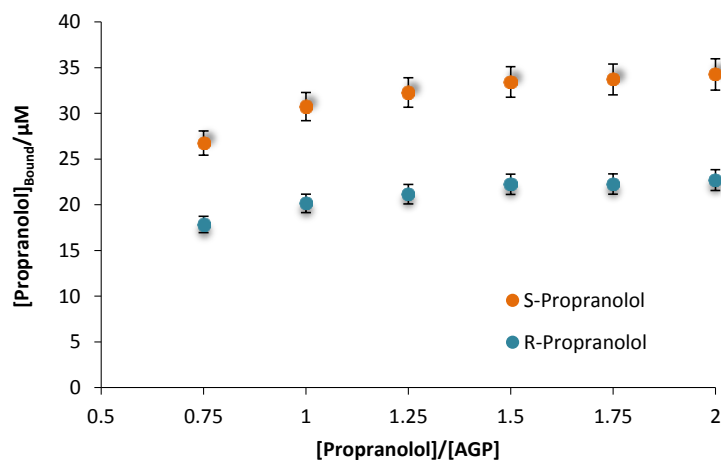
Figure 5.16 – Relation between bound concentration of S- and R-propranolol to AGP, for the same [propranolol]/[AGP] ratios. The [Propranolol]$_{Bound}$ was determined based on the responses obtained in the presence and absence of protein. The data points are expressed as mean of three separate experiments.

The Scatchard plots obtained for procaine and lidocaine are presented Figure 5.17a) and 5.17b), respectively. The binding parameters of the two anaesthetic drugs were significantly different, 8.4 x10^3M^{-1}, n=0.24 and 1.2 x10^4M^{-1}, n=0.76 for procaine and lidocaine, respectively. These values indicate that the affinity of AGP for lidocaine is much higher in comparison with procaine, which appears to form a very weak complex. Thus, lidocaine presents a higher amount of drug bounded to AGP for the same ratio [Drug]/[AGP].
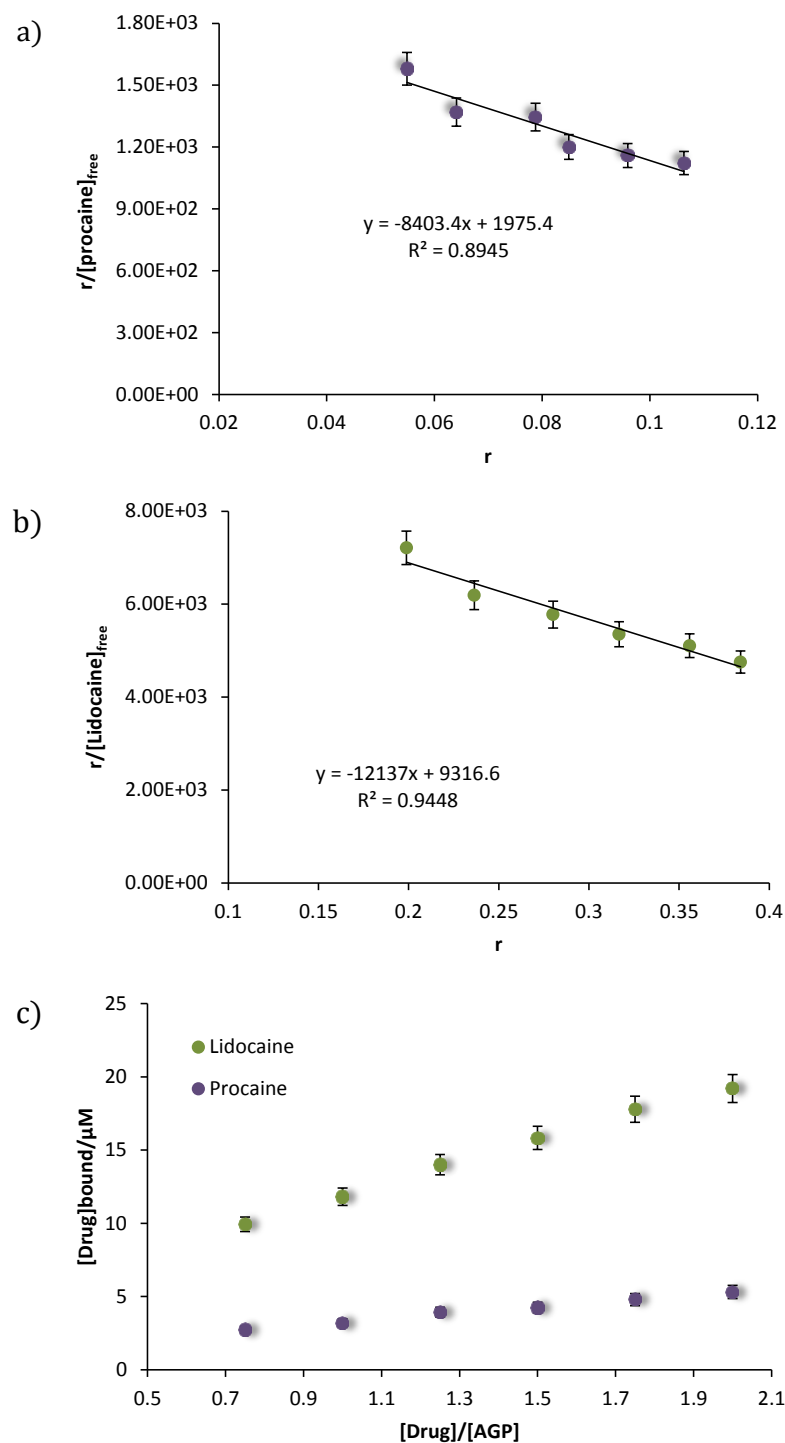
Figure 5.17 – Scatchard plot for the binding of AGP to a) procaine, b) lidocaine; c) relation between bound concentration of procaine and lidocaine to AGP, for the same [propranolol]/[AGP] ratios. The data points are expressed as mean of three separate experiments.

An evaluation of the free Gibbs energy of binding between the drugs studied and AGP can be determined using the following:

$$\Delta G_{(Drug \cdot Protein)} = -RTlnK_{a(Drug \cdot protein)} \qquad (5.16)$$

where K_a(Drug·AGP) is the stability constant of the complexes formed (calculated from the Scatchard plot), R the gas constant (8.314 J.mol^{-1}.K^{-1}) and T, the temperature (K). The ΔG value represents the free energy of the reactions 1 and 2 (Figure 5.10 b), respectively. In the case of propranolol, the enantioselectivity of the protein can be given by:

$$\Delta(\Delta G)_{chiral} = \Delta G(S \cdot AGP) - \Delta G(R \cdot AGP) \qquad (5.18)$$

The estimated binding parameters, number of binding sites and the free energy for the drug-protein binding interaction are presented in Table 1.

Table 5.3 – Binding parameters of S- and R-propranolol, procaine and lidocaine with α_1-acid glycoprotein at pH=7.4, T=21°C.

	K_a (M^{-1})	n	$\Delta G_{(Drug \cdot Protein)}$ (kJ.mol^{-1})	$\Delta(\Delta G)_{chiral}$ (kJ.mol^{-1})
(S)-Propranolol	2.7×10^5	0.73	-30.1	
				-1.8
(R)-Propranolol	1.3×10^5	0.50	-29.2	
Procaine	8.4×10^3	0.12	-22.1	
Lidocaine	1.2×10^4	0.76	-23.3	

5.3 Conclusion

In this chapter is demonstrated a simple and effective method for studying interactions of drugs and proteins. It was shown that using a micro liquid|liquid interface the affinity of propranolol enantiomers, lidocaine and procaine to AGP can be quantitatively evaluated. The presence of AGP in the aqueous phase lead to the formation of a complex between the protonated drugs and the protein, which was reflected as a decrease in the detection signal, once only the unbound drug is able to transfer across the interface.

The three drugs bound to AGP with different affinities, which were reflected in the values of association constants and number of binding sites. The association constant for S- propranolol (2.7×10^5 M^{-1}) was found two times bigger than of R-propranolol (1.3×10^5 M^{-1}), which proves that AGP can be a very effective chiral selector at liquid|liquid interface. The calculated values are in good agreement with the literature, where it was found that S-propranolol is significantly more bound to AGP than R-propranolol.[2,31,53]

On the other hand the two anaesthetic drugs studied, procaine and lidocaine also revealed to have very different affinities with AGP. The interactions of procaine and lidocaine with AGP led to association constants of 1.2×10^4 M^{-1} and 8.4×10^3 M^{-1}, respectively. Procaine was the less bounded drug studied and therefore having the smallest association constant value.

Based on the results presented in this chapter, it is shown that interaction between drugs and plasma proteins can be studied using electrochemical methods, which can offer rapid, simple and alternative analysis for these types of studies.

References

(1)   Rodriguez Rosas, M. E.; Shibukawa, A.; Yoshikawa, Y.; Kuroda, Y.; Nakagawa, T. *Anal. Biochem.* **1999**, *274*, 27–33.

(2)   Hanada, K.; Ohta, T.; Hirai, M.; Arai, M.; Ogata, H. *J. Pharm. Sci.* **2000**, *89*, 751–757.

(3)   Kishino, S.; Itoh, S.; Nakagawa, S.; Miyazaki, S. *Eur. J. Clin. Pharmacol.* **2001**, *57*, 583–587.

(4)   Lindup, W. E.; Orme, M. C. L. *Br. Med. J.* **1981**, *282*, 212–214.

(5)   Tomlin, M. E. *Pharmacology and Pharmacokinetics*; Springer-Verlag London Limited: London, 2010.

(6)   Brocks, D.; Mehvar, R. In *Chirality in Drug Design and Development*; Reddy, I.; Mehvar, R., Eds.; CRC Press, 2004.

(7)   Wood, M. *Anesth. Analg.* **1986**, *65*, 786–804.

(8)   Foye, W. O.; Lemke, T. L.; Williams, D. A. *Foye's principles of medicinal chemistry*; Lippincott Williams & Wilkins, 2007.

(9)   Toutain, P. L.; Bousquet-Melou, A. *J. vet. Pharmacol. Therap.* **2002**, *25*, 460–463.

(10)   Zsila, F.; Molnár, P.; Deli, J.; Lockwood, S. F. *Bioorganic Chemistry* **2005**, *33*, 298–309.

(11)   Israili, Z. H.; Dayton, P. G. *Drug Metab. Rev.* **2001**, *33*, 161–235.

(12)   Otagiri, M.; Yamamichi, R.; Maruyama, T.; Imai, T.; Suenaga, A.; Imamura, Y.; Kimachi, K. *Pharm. Res.* **1989**, *6*, 156–159.

(13)   Sörensson, J.; Matejka, G. L.; Ohlson, M.; Haraldsson, B. *Am. J. Physiol-Heart C* **1999**, *276*, H530 –H534.

(14)   Fournier, T.; Medjoubi-N, N.; Porquet, D. *Biochim. Biophys. Acta* **2000**, *1482*, 157–171.

(15)   Routledge, P. a *Brit. J. Clin. Pharmaco.* **1986**, *22*, 499–506.

(16)   Grandison, M. K.; Boudinot, F. D. *Clin. Pharmacokinet.* **2000**, *38*, 271–290.

(17)   Hochepied, T.; Berger, F. G.; Baumann, H.; Libert, C. *Cytokine Growth Factor Rev.* **2003**, *14*, 25–34.

(18)   Yoshima, H.; Matsumoto, A.; Mizuochi, T.; Kawasaki, T.; Kobata, A. *J. Biol. Chem.* **1981**, *256*, 8476 –8484.

(19)   Xuan, H.; Hage, D. S. *Anal. Biochem.* **2005**, *346*, 300–310.

(20)   Aubert, J.-P.; Biserte, G.; Loucheux-Lefebvre, M.-H. *Arch. Biochem. Biophys.* **1976**, *175*, 410–418.

(21)   Schönfeld, D. L.; Ravelli, R. B. G.; Mueller, U.; Skerra, A. *J. Mol. Biol.* **2008**, *384*, 393–405.

(22)   Verbeeck, R.; Cardinal, J.; Wallace, S. *Eur. J. Clin. Pharmacol.* **1984**, *27*, 91–97.

(23)   Kaliszan, R.; Nasal, A.; Turowski, M. *J. Chromatogr. A* **1996**, *722*, 25–32.

(24)   Kaliszan, R. *J. Chromatogr. B* **1998**, *715*, 229–244.

(25)   Enquist, M.; Hermansson, J. *J. Chromatogr. A* **1990**, *519*, 271–283.

(26)   Hermansson, J.; Hermansson, I. *J. Chromatogr. A* **1994**, *666*, 181–191.

(27)   de Vries, J. X.; Schmitz-Kummer, E. *J. Chromatogr. A* **1993**, *644*, 315–320.

(28)   Li, S.; Lloyd, D. K. *Chirality* **1993**, *65*, 3684–3690.

(29)   Hermansson, J.; Grahn, A. *J. Chromatogr. A* **1995**, *694*, 57–69.

(30)   Ravis, W. R.; Parsons, D. L.; Wang, S. J. *J. Pharm. Pharmacol.* **1988**, *40*, 459–463.

(31)   Albani, F.; Riva, R.; Contin, M.; Baruzzi, A. *Brit. J. Clin. Pharmaco.* **1984**, *18*, 244–246.

(32)   Armstrong, D. W.; Zhang, B. *Anal. Chem.* **2001**, *73*, 557 A–561 A.

(33)   Zsila, F.; Iwao, Y. *Biochim. Biophys. Acta* **2007**, *1770*, 797–809.

(34)   Zsila, F.; Bikádi, Z.; Simonyi, M. *Bioorgan. Med. Chem.* **2004**, *12*, 3239–45.

(35)   Becker, B. a; Larive, C. K. *J. Phys. Chem. B* **2008**, *112*, 13581–13587.

(36) Sear, J. *Anaesth. Intens. Care* **2011**, *12*, 160–165.

(37) Vacanti, C. A.; Sikka, P. K.; Urman, R. D. *Essential Clinical Anesthesia*; Cambridge University Press, 2011.

(38) *Comprehensive medicinal chemistry: The rational design, mechanistic study & therapeutic application of chemical compounds*; Hansch, C., Ed.; 1st ed.; Pergamon, 1990.

(39) Caron, G.; Steyaert, G.; Pagliara, A.; Reymond, F.; Crivori, P.; Gaillard, P.; Carrupt, P.; Avdeef, A.; Comer, J.; Box, K. J.; Girault, H. H.; Testa, B. *Helv. Chim. Acta* **1999**, *82*, 1211–1222.

(40) Yagiela, J. A. Y. D.; Neidle, E. A.; Dowd, F. J. *Pharmacology and Therapeutics for Dentistry*; 1998.

(41) Isen, D.; Hawkins, J. M. *Ont Dent* **1995**, *72*, 18–22.

(42) Arthur, G. R.; Covino, B. G. *Bailliere Clin. Anaes.* **1991**, *5*, 635–658.

(43) Jia, Z.; Ramstad, T.; Zhong, M. *J. Pharm. Biomed. Anal.* **2002**, *30*, 405–413.

(44) Krauss, E.; Polnaszek, C.; Scheeler, D.; Halsall, H.; Eckfeldt, J.; Holtzman, J. *J. Pharmacol. Exp. Ther.* **1986**, *239*, 754–759.

(45) Soman, S.; Yoo, M. J.; Jang, Y. J.; Hage, D. S. *J. Chromatogr. B. Analyt. Technol. Biomed. Life Sci.* **2010**, *878*, 705–708.

(46) Mehvar, R.; Brocks, D. R. *J. Pharm. Pharmaceut. Sci.* **2001**, *4*, 185–200.

(47) Zahra, R.; Ahmad, R.; Asghar, M. S. A.; Ali, A.; Soghra, K. *Indian J. Clinica Bioelectrochem.* **2006**, *21*, 121–125.

(48) Ray, K.; Trawick, W. G.; Mullins, R. E. *Clin. Chem.* **1985**, *31*, 131–134.

(49) Reddy, I. K.; Mehvar, R. *Chirality in drug design and development*; CRC Press, 2004.

(50) Walle, U. K.; Fagan, T. C.; Topmiller, M. J.; Conradi, E. C.; Walle, T. *Br. J. Clin. Pharmacol.* **1994**, *37*, 21–25.

(51) Simonyi, M.; Fitos, I.; Visy, J. *Trends in Pharmacological Sciences* **1986**, *7*, 112–116.

(52) Walle, U. K.; Walle, T.; Bai, S. A.; Olanoff, L. S. *Clin. Pharm. Ther.* **1983**, *34*, 718–723.

(53) Zhang, F.; Du, Y.; Ye, B.; Li, P. *J. Photoch. Photobio. B* **2007**, *86*, 246–251.

(54) Oravcová, J.; Bystricky, S.; Trnovec, T. *Biochem. Pharmacol.* **1989**, *38*, 2575–2579.

(55) Vanýsek, P.; Sun, Z. *Bioelectrochem. Bioener.* **1990**, *298*, 177–194.

(56) Shao, Y.; Osborne, M. D.; Girault, H. H. *J. Electroanal. Chem.* **1991**, *318*, 101–109.

(57) Liu, B.; Mirkin, M. V. *Electroanal.* **2000**, *12*, 1433–1446.

(58) Zhang, M.; Sun, P.; Chen, Y.; Li, F.; Gao, Z.; Shao, Y. *Chin. Sci. Bull.* **2003**, *48*, 1234–1239.

(59) Reymond, F.; Chopineaux-Courtois, V.; Steyaert, G.; Bouchard, G.; Carrupt, P.-A.; Testa, B.; Girault, H. H. *J. Electroanal. Chem.* **1999**, *462*, 235–250.

(60) Fantini, S.; Clohessy, J.; Gorgy, K.; Fusalba, F.; Johans, C.; Kontturi, K.; Cunnane, V. J. *Eur. J. Pharm Sci.* **2003**, *18*, 251–257.

(61) Shao, Y.; Mirkin, M. V. *Anal. Chem.* **1998**, *70*, 3155–3161.

(62) Horrocks, B. R.; Mirkin, M. V. *Anal. Chem.* **1998**, *70*, 4653–4660.

Chapter 6

Chiral ion transfer

across the liquid|liquid interface

coupled to electrochemical redox reaction

This chapter describes the chiral discrimination of mandelic acid (MAH) enantiomers, by the use of a thick organic film modified electrode. The transfer of the chiral ions was achieved in a unique arrangement that consisted of a small volume of an organic phase immobilized at the surface of a glassy carbon electrode. The organic film contained an ethylated ferrocene cyclodextrin (EtCDFc) which has a dual role, a redox moiety and a cyclodextrin moiety which is able to form chiral complexes with a variety of compounds. The modified electrode was immersed in aqueous solutions containing mandelic acid ions (R- or S-MAH) and aqueous electrolyte. The redox reaction of EtCDFc is accompanied by the complexation of the MAH enantiomers with the cyclodextrin part of EtCDFc. The coupled reaction led to the formation of diastereoisomers complexes between the enantiomers and EtCDFc. The effect of the concentration and ionization state of MAH ions was analysed at different pHs (2, 3.4 and 7). The S-MAH showed preferential enantiomeric interactions with EtCDFc. At pH of 3.4 the chiral discrimination between R- and S-MAH was the most pronounced.

6.1 Introduction

Electrochemical processes of a redox compound accompanied by the simultaneous transfer of ions from the adjacent electrolyte solution are considered very interesting from the viewpoints of the energy transformation at biological membranes, the active transport and selective transport of ions or electrons, etc.[1,2] Besides their fundamental interest, as they comprise both an electron and an ion transfer reaction,[3,4] they can also be very important for various potential applications, such as energy storage,[5] charge storage[6] and ion sensing and detection.[7]

The four electrode system has been a popular choice, for the determination of ion partition coefficients between two immiscible phases. The partition coefficient is a very important molecular parameter used in different areas of chemistry, medicine and pharmacology for predicting interactions with biological receptors, and biological effects in general. The four electrode system is only to polarizable phase boundaries, at which, relatively narrow potential ranges are available. Nonetheless, its shortcoming limits wider applications in the determination of ion transfer. Girault et al.[8,9] introduced liquid|liquid interface supported on a metallic electrode for the study of ion and electron transfer. The system was composed of an aqueous droplet (where a highly concentrated redox coupled was dissolved together with a small amount of the target ion) supported on a platinum disc electrode which was immersed into an organic electrolyte solution. Analogously, Shao et al.[10,11] constructed another water droplet modified electrode by depositing an aqueous electrolyte solution on to a solid reference electrode for the study of various ionic species, such as biological molecules.[10,11] These methodologies have the benefit of not requiring special instrumentation, however they still present limitations for the study of extreme ion transfer, in the sense that only ionic analytes with formal potentials that fall within the potential window can be readily and precisely determined.

A new era of ion transfer based on electrochemically induced redox processes accompanied by the simultaneous transfer of ions was started by Compton,[12–14] Marken,[15–17] and Scholz et.al.[3,18,19] They created a concept of ion transfer voltammetry, named three-phase electrode, with the development of new approaches for the deposition of oil microdroplets on suitable electrode surfaces.

Marken et al.[13,16,17] were the first to note the importance and consequences of ion transfer from one liquid phase to another at a three-phase electrode. They deposited an oily electroactive compound (N,N,N',N'-tetrahexylphenylene diamine, THPD) in the form of several droplets on a graphite electrode surface and immersed this composition into aqueous solutions of different inorganic salts. Oxidation of THPD proceeded at voltammetric potentials dependent on the hydrophilic properties of the anions from the aqueous solution. Scholz et al.[3,18,20,21] developed new approaches to measure the lipophilicity of ions by employing highly-hydrophobic paraffin-impregnated graphite electrodes (PIGE) and replaced the pure organic phase with a solution of selected electroactive compound (e.g., decamethylferrocene) in organic solvents such as nitrobenzene,[3,21,22] n-octanol,[23,24] menthol[25] and 2-nitrophenyloctyl ether.[26] The authors assigned the observed potential shifts to the differences in the Gibbs energies of transfer of the ions being transferred across the interface of the two immiscible liquids, leading to significant progress in the determination of the lipophilicity of a variety of inorganic and organic ions.[20,21,27,28] In the three-phase electrode no electrolyte is dissolved in the organic phase and, as a result, the electrode reaction occurs exclusively at the three-phase junction, which is the junction water| solid electrode| organic phase, e.g., on the rim of an organic droplet set on a solid surface in contact with an aqueous electrolyte. Only there the electrochemical reaction can proceed and advance into the organic solvent droplet,

regardless of the electrical conductivity of the organic phase. This was experimentally proved by employing a microelectrode probe.[29]

Ion transfer voltammograms can also be obtained when a thin layer is used to cover the electrode surface, partially. This is exemplified by the work developed by Opallo and co-workers,[30] who recently investigated the ion transfer across liquid|liquid interfaces of the type: aqueous solution|solution of electroactive compound in polar organic solvent supported on a hydrophobic silicate carbon composite. They also encapsulated the organic phase in a ceramic carbon material composed of carbon particles and hydrophobic silicate, prepared via the sol-gel chemistry from methyltrimetoxysilane-based sol.[30,31]

In another approach, Shi and Anson[32–34] showed that when the droplet of the organic phase is replaced with a thin film of this solvent, containing a dissolved electroactive compound, the system becomes analytical applicable. In this case, the layer of organic solvent may require the addition of supporting electrolyte. The thin film-modified electrodes have shown to be particularly effective for the study of electron transfer across the liquid interface,[34,35] and the measurement of kinetics of ion transfer.[36]

Thin-organic film modified and three-phase electrodes are closely related. Both systems couple the electron transfer at the electrode|organic solution interface with the ion transfer at an organic|aqueous solution interface. When these modified electrodes are placed in contact with an aqueous electrolyte solution, ion exchange will occur (an anion for the oxidation or cation for the reduction of the molecule) in order to compensate the charge neutrality required during the course of the voltammetric experiments. The ion transfer is related to the hydrophobicity and thus can be monitored as a function of electrode potential.

The thin film electrode configuration circumvents some of the physical problems associated with three-phase electrodes with immobilized droplets such as irreproducibility of the drop size and the need of using a graphite substrate due to the instability of organic droplets on metal surfaces.

The redox probes employed must strictly fulfil the following requirements: (i) they must remain in the organic phase and have very low affinity for water; (ii) both the redox probes and their generated products, should be chemically very stable and should not react with the included ions; (iii) the bonding effects between the generated products of the redox probes and the included ions should not be significant enough to be worth considering. In this sense, the development of a suitable redox probe can be a difficult task. For instance, the transfer of the ferrocenium ion, Fc^+, from organic solvents to water is known to occur easily which makes it not suitable for such studies. On the hand, decamethylferrocene (DMFc) with a higher lipophilicity is a frequently used probe and has the ability of being dissolved in most organic solvents, however in the presence of highly hydrophilic ion transfers, $DMFc^+$ can become chemically unstable.[37] High lipophilicity is therefore an essential characteristic, as the redox products of the molecules must also stay in the organic phase and not participate in the ion exchange across the interface.

In previous publications, it has been shown that a method to increase the stability of the ferrocene (Fc) and its derivatives at the electrode surface is by the formation of inclusion complexes with cyclodextrins (CDs), a class of toridally shaped cycloamyloses, with a hydrophilic outer surface and a hydrophobic inner cavity.[38,39] Fc is spherical shaped and can be accommodated as guest for β-cyclodextrin (β-CD). Breslow[40] reported that Fc forms a 1:2 complexation ratios with α-cyclodextrin and 1:1 with β- and γ-cyclodextrin even in organic solvents. He also found that the binding of substrates by β-CD in

nonaqueous solvents were not as strong as in water, however strong enough to permit complete binding by cyclodextrin of nonpolar species which could fit into the cavity.[40,41] The formation of β-CD and Fc inclusion complex greatly decreases the solubility of the Fc^+ in water and correspondingly improves its retention in a non-aqueous phase on the electrode.[38]

In the work reported in this chapter, a β-CD-linked ferrocene (EtCDFc)[42] was used as redox probe to improve the retainment of Fc on the electrode surface. EtCDFc consists of an ethylated β-CD, composed of 7 glucose units with a linked ferroceneacetamido group (Figure 6.1). EtCDFc is characterized by being a highly lipophilic organic compound, reversibly oxidizable, soluble in organic solvents and almost insoluble in water.
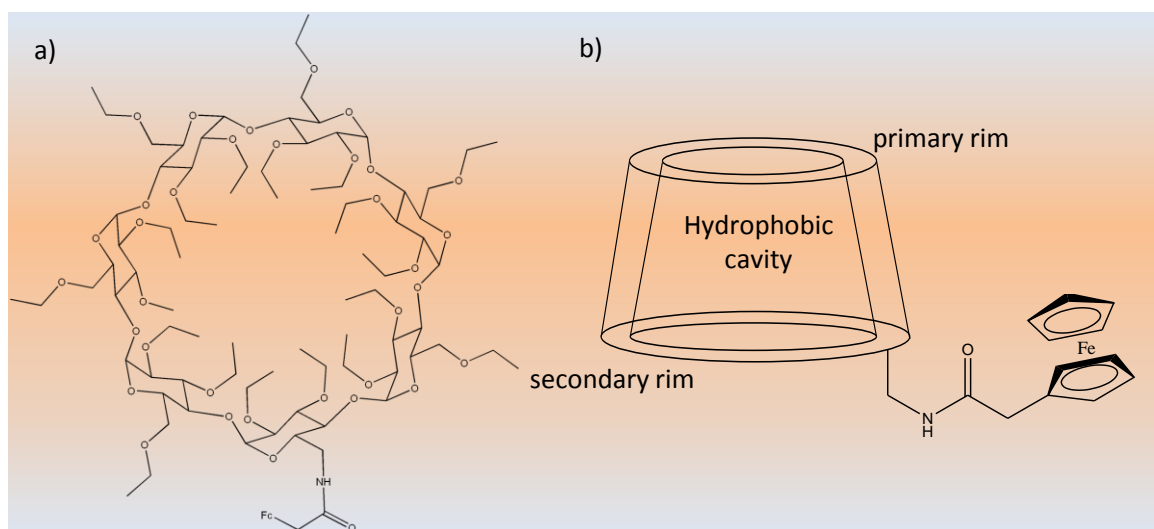
Figure 6.1 – a) Molecular structure of the EtCDFc,[42] b) conical representation showing the hydrophobic and rims of the cyclodextrin.

An additional benefit of the system used in this work, arises from the fact that the relatively thick film ensures that the generated product of the molecular probe, $EtCDFc^+$, is retained within a limited diffusion layer and is kept far away from the aqueous|organic solvent interface. Also, bis(triphenylphosphoranylidene) ammonium ($BTPPA^+$) ions from

the electrolyte bis(triphenylphosphoranylidene) ammonium tetrakis (4-chlorophenyl)borate (BTPPATPBCl) (see section 2.4.1.2), dissolved in the organic film are highly hydrophobic and this will ensure they will not be excluded from the organic film. For these reasons, EtCDFc$^+$ and BTPPA$^+$ will not partake in the ion exchange across the interface and the charge compensation/neutrality in the organic film is only maintained by the injection of ions in the aqueous phase.

6.2 Study of chiral ion transfer using modified electrodes

Electrochemical reactions can exhibit stereoselectivity when performed in chiral solvents,[25,43] in the presence of chiral agents,[44–46] or on electrodes with a chiral surface.[47,48] Using a three-phase system, Scholz and co-workers,[25] reported for the first time Gibbs energies of transfer of chiral anions. The three-phase arrangement system consisted of a droplet of decamethylferrocene in a chiral liquid, D- and L-2-menthol, which was attached to a graphite electrode, when immersed in aqueous solution containing chiral anions, D- and L-trypotphan, the determination of the energetic differences of Gibbs energy of transfer is possible. Later, the same group reported the quantification of Gibbs energies of transfer of D-phenylalanine and L-phenylalanine anions across the water|chiral solvent (D- and L-2-octanol) using a similar three-phase system. They suggested that the differences obtained between D-phenylalanine and L-phenylalanine anions were probably due to the formation of diastereomeric complexes with one solvent molecule.[49] It is known that when the organic phase is not chiral, one cannot expect measurable differences in the standard Gibbs energies of transfer of the enantiomers of the chiral ion. However, using a chiral liquid phase these differences should be detectable.[25]

In this work, an ethylated ferrocene cyclodextrin is dissolved in 1,2-dichloroethane which will make the organic phase chiral. EtCDFc was chosen as a chiral selector, as one of the main interest in CDs lies in their ability to form inclusion complexes with several compounds.[50-52] The lipophilic cavity of the CDs molecules provides a microenvironment into which appropriately sized non-polar moieties can enter and form inclusion complexes. The enantioselectivity of the molecular interaction is based on the inclusion of the chiral analyte into the hydrophobic cavity (internal selectivity) of the cyclodextrin and on various interactions involving Van der Waals, dispersive forces, dipole-dipole interactions, electrostatic forces and hydrogen bonding between the guest molecules with the groups on the cyclodextrin rim (external enantioselectivity). This type of interaction is obviously affected by the arrangement, size and type of ions bound to the external chain of the CD.[53] On this basis, it is expected that the redox properties combined with the enantioselective capabilities, characteristic of a cyclodextrin, will make EtCDFc a very suitable compound, capable of sensing chiral molecules, such as mandelic acid (MAH) enantiomers. The chirality selective inclusion of MAH in the CD cavity of EtCDFc should affect the redox properties of EtCDFc and the generated electrochemical signal used to transduce the interaction between the two molecules.

Ueno et al.[54] prepared a ferrocene-appended β-cyclodextrin (similar to the one represented in figure 6.1) and examine its induced circular dichroism (i.c.d.) spectra in organic solvents. He found that the i.c.d. intensity decreases upon guest addition, and that the analysis of the guest-induced intensity variations gives binding constants of 1:1 host-guest stoichiometry.[41] In figure 6.2 is shown a schematic representation associated with induced-fit type complexation proposed by Ueno et al.[54]
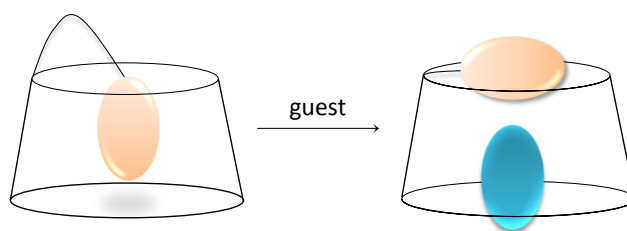
Figure 6.2 – Induced-fit type of complexation for a ferrocene-appended cyclodextrin.[41]

MAH (Figure 6.3), the chiral analyte chosen in this study, is considered a major metabolite of styrene[55,56] and an important fine chemical. MAH and its derivatives are widely used in the chemical and pharmaceutical industries. Enantiopure MAH is an important chiral synthetic intermediate, an important chiral determination reagent in nuclear magnetic resonance (NMR), and a useful reagent in chromatography.[57,58] It is present in certain skin care products and used as a precursor in the manufacture of certain dyes.[59] R-MAH for instance is applied as precursor for the synthesis of cephalosporin and penicillin.[60,61] It is also used as a chiral resolving agent and chiral synthon for the synthesis of anti-tumour and anti-obesity agent.[62,60] The S-MAH is used to synthesise substituted cyclopentenones and commercial drugs, including the nonsteroidal anti-inflammatory drugs.[63,64]
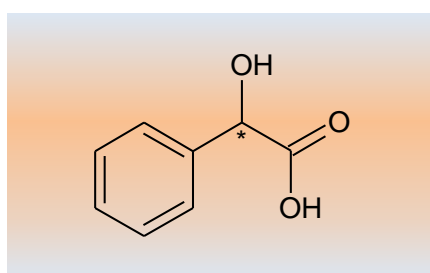
Figure 6.3 – Chemical structure of mandelic acid, * represents the chiral centre.

6.3 Coupled electron and ion transfer reactions

Coupled electron and ion transfer reactions, combines the electron transfer at the solid electrode|organic solvent (E|O) interface with the ion transfer at the organic solvent|water (O|W) interface. The solid electrode (electron conductor) serves as a source of electrons; the organic phase provides the redox active material and the aqueous phase supplies the charge compensating ions. Upon oxidation or reduction, the electroneutrality of the organic phase is unbalanced, promoting an ion transfer reaction which has to occur to maintain the electroneutrality in both liquid phases.

The electrochemical process at the thick film modified electrode (Figure 6.3) couple electron transfer Eq.(6.1) at the E|O with the ion transfer Eq.(6.2) at the O|W interface:

$$Red^0_{(o)} \rightleftarrows Ox^+_{(o)} + e^- \qquad (6.1)$$

$$A^{n-}_{(w)} \rightleftarrows A^{n-}_{(o)} \qquad (6.2)$$
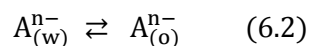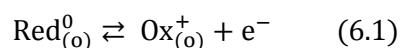
Although the ion transfer follows the electron transfer reaction, these two electrochemical processes cannot be separately identified, and in the potential window of the voltammetric experiments they proceed simultaneously at two different interfaces,[36,65–67] appearing as a single overall process Eq.(6.3).

$$Red^0_{(o)} + A^-_{(w)} \rightleftarrows Ox^+_{(o)} + A^-_{(o)} + e^- \qquad (6.3)$$
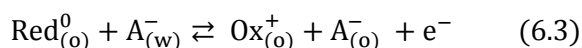
In Eq. (6.3), $Red^0_{(o)}$ and $Ox^+_{(o)}$ denotes EtCDFc and EtCDFc$^+$, respectively, and A$^-$ stands for the transferring anions of MAH. Figure 6.4 shows a schematic representation of the mechanism involved in the coupled electron and ion transfer reaction. The redox reaction of the EtCDFc takes place at the surface of the thick film modified electrode, whereas the transfer of the anion A$^-$ occurs at the organic|aqueous interface.
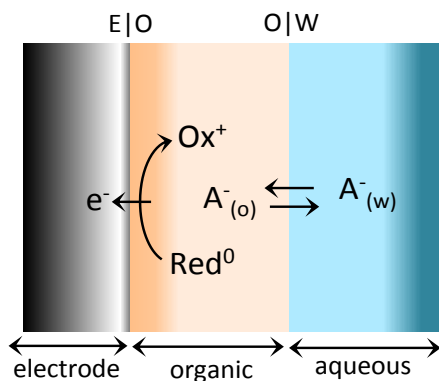
Figure 6.4 – Schematic representation of coupled anion and electron transfer reaction using a thick film modified electrode.

The potential difference between the working electrode and the reference electrode in aqueous electrolyte (E|W) i.e., that is potentiostatically controlled, is given by the sum of the potential at the electrode|organic (E|O) interface and the potential across the organic|aqueous (O|W) interface, corresponding to the potential of the coupled reaction:

$$E_{E|W} = E_{E|O} + E_{O|W} = E_{E|O} + \Delta_w^o \phi \qquad (6.4)$$

where $E_{E|O}$ and $\Delta_w^o \phi$ are given by:

$$E_{E|O} = E^0_{EtCDFc^+_{(o)}|EtCDFc_{(o)}} + \frac{RT}{nF} \ln \left(\frac{a_{EtCDFc^+_{(o)}}}{a_{EtCDFc_{(o)}}} \right) \qquad (6.5)$$

$$\Delta_w^o \phi = \Delta_w^o \phi_{A^-}^0 + \frac{RT}{Fz_{A^-}} \ln \left(\frac{a_{A^-_{(o)}}}{a_{A^-_{(w)}}} \right) \qquad (6.6)$$

$E_{E|O}$ and $E_{O|W}$ are the potentials differences at the electrode and organic film and organic|aqueous interface, respectively. At the equilibrium, the potential of the coupled reaction $E_c^{0\prime}$ is defined as follows:

$$E_c^{0\prime} = E^0_{EtCDFc^+_{(o)}|EtCDFc_{(o)}} + \Delta_w^o \phi_{A^-_{(w)}}^{0\prime} + \frac{RT}{nF} \ln \left(\frac{C_{EtCDFc^+_{(o)}}}{C_{EtCDFc_{(o)}}} \right) + \frac{RT}{F} \left(\frac{C_{A^-_{(o)}}}{C_{A^-_{(w)}}} \right) \qquad (6.7)$$

In a first approximation, the activities in the Nernst equation Eq. (6.5) and (6.6) can be replaced by concentrations. Since the concentration of the anions in the aqueous phase is kept in excess in comparison to $C_{EtCDFc_{(o)}}$, and does not change significantly during the experiments. In Eq. (6.7), the $E^0_{EtCDFc^+_{(o)}/EtCDFc_{(o)}}$ is the standard redox potential of the redox couple EtCDFc$^+$|EtCDFc in the organic solvent (vs. Ag|AgCl), n is the number of the exchanged electrons (n = 1 in the case of EtCDFc), F is the Faraday constant (96485 C mol^{-1}), R is the gas constant (8.314 J mol^{-1} K^{-1}), and T the temperature (K). $C_{EtCDFc^+_{(o)}}$ and $C_{EtCDFc_{(o)}}$ are, respectively, the concentrations of EtCDFc$^+$ and EtCDFc in the organic phase. $\Delta^o_w\phi^{0'}_{A^-_{(w)}}$ is the standard potential of transfer of anions A$^-$ from the aqueous phase to the organic phase, while $C_{A^-_{(o)}}$ and $C_{A^-_{(w)}}$ are the concentrations of the studied anion in, respectively, the organic and aqueous phases. Eq.(6.7) shows that the formal potential of the voltammograms that portray the coupled electron and ion transfer processes depend on the nature of the anions in the aqueous phase via the values $\Delta^o_w\phi^{0'}_{A^-_{(w)}}$. Generally, the more lipophilic the anions are the more negative the value of $\Delta^o_w\phi^0_{A^-_{(w)}}$ is. Consequently, the oxidation of the compound Red in the organic phase will be shifted towards more negative potentials when the lipophilicity of the transferrable anions increases.

In our study the coupled electron and ion transfer reactions is rather more complicated as the EtCDFc combines the function of a redox probe and ligand in simultaneous. In this case, a fast equilibrium must be considered in which the anion $MA^-_{(o)}$ is forming a complex with $EtCDFc^+_{(o)}$, as represented by Eq. 6.8

$$EtCDFc^0_{(o)} + MA^-_{(w)} \rightleftharpoons [EtCDFc^+_{(o)} - MA^-_{(o)}] + e^- \qquad (6.8)$$

If both forms of MAH, carboxylic acid (MAH) and carboxylate ion (MA⁻) are able to form a complex with EtCDFc, the equilibria presented in scheme 6.1 has to be considered.

$$\text{MAH} \quad \underset{}{\overset{K_a}{\rightleftharpoons}} \quad H^+ + MA^-$$

$$+ \qquad\qquad +$$

$$\text{EtCDFc}^+ \qquad\qquad \text{EtCDFc}^+$$

$$K_{HA} \updownarrow \qquad\qquad \updownarrow K_A$$

$$[MAH - EtCDFc^+] \quad \overset{K_a'}{\rightleftharpoons} \quad H^+ + [MA^- - EtCDFc^+]$$
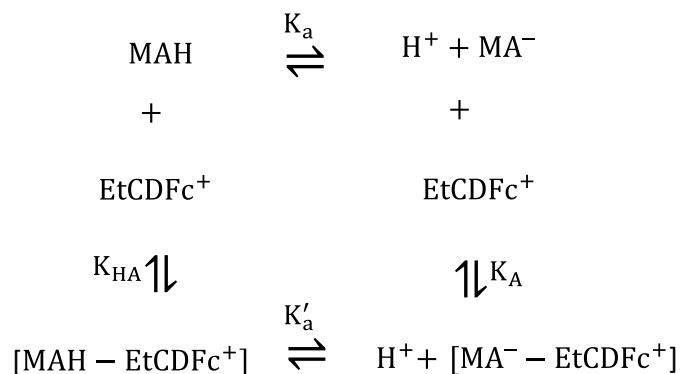
Scheme 6.1 – Equilibria for the complex of MAH and MA⁻ with EtCDFc⁺. K_a and K_a' represent the acid dissociation constants in the free state and in the complex respectively. K_{HA} and K_A represent the complexation of the protonated and ionized form of the acid.

The stability constant of the complex formed, is related to the standard free energy change for the complex formation by:

$$\Delta G = -RT\ln K \qquad (6.9)$$

The units of ΔG are determined by the units of R, but the magnitude of ΔG is also controlled by the concentration units in which K is expressed (Eq. 6.10)

$$K = \frac{[\text{complex}]}{[\text{host}][\text{guest}]} \qquad (6.10)$$

The system then manifests its enantioselectivity through the differential interaction of the chiral selector with the two enantiomers to be resolved. This enantioselectivity is thermodynamic in origin and is due to the different stability of the diastereomeric species formed by the two enantiomers and the chiral selector. In the absence of achiral interactions the enantioselectivity is related to the Gibbs energy difference by Eq. (6.11)

$$\Delta\Delta_{R,S} = \Delta G_R - \Delta G_S = -RTlnK_{R,S} \qquad (6.11)$$

Where $\Delta\Delta_{R,S}$ is the difference in the Gibbs free energy between the two enantiomers and the chiral selector.

6.4 Results and discussion

6.4.1 Characterisation of EtCDFc

In order to study the electrochemical response of EtCDFc by means of a thick organic film modified electrode, its response was first analysed using a classical three-electrode system and compared to Fc. Cyclic voltammetric measurements were carried out in 1,2-DCE solution with BTPPATPBCl (0.02M) as the supporting organic electrolyte. A fresh polished glassy carbon was used as a working electrode (A=0.07cm^2), a platinum flag and platinum wire were used as a counter and pseudo reference electrodes, respectively. Figure 6.5 shows cyclic voltammograms of the oxidation of EtCDFc to EtCDFc$^+$ (Figure 6.5a) and Fc to Fc$^+$ (Figure 6.5b), 1mM each at different scan rates. It can be seen on the voltammograms that both, EtCDFc and Fc show a well-defined and reversible one-electron response.
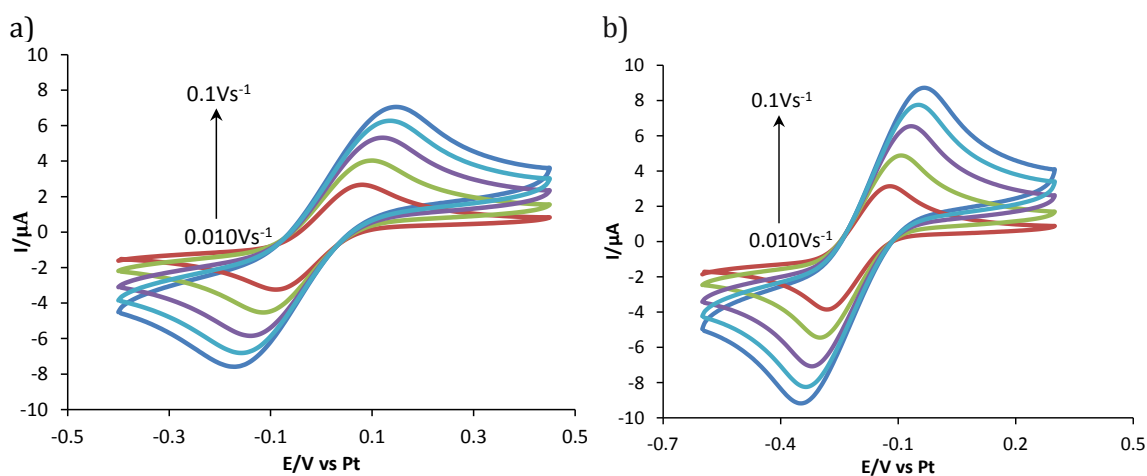
Figure 6.5 – Cyclic voltammograms of 1mM of a) EtCDFc and b) Fc at different scan rates (10, 25, 50, 75, 100 mV s^{-1}).

Ideally, the two redox couples should exhibit a peak separation of 0.057V, however the separation between voltammetric peaks ($\Delta E_p = E_{pc} - E_{pa}$), increases slightly with the increase of scan rate. This behaviour suggests slow electron transfer at the electrode surface, meaning that the potential applied does not result in the generation of the concentrations at the electrode surface as predicted by the Nernst equation, due to the kinetics of the reaction the equilibrium is not established rapidly. A large ΔE_p value can be also attributed to the uncompensated resistance effect, as was previously observed by other researchers.[68,69] Nonetheless, a plot of the anodic (i_{pa}) and the cathodic peak current (i_{pc}) against the square root of the scan rate ($v^{1/2}$) resulted in a straight line with a slope proportional to the square root of the scan rate ($v^{1/2}$), as given by the Randles-Sevcik equation[70] (Figure 6.5 a) and b), and the i_{pa}/i_{pc} ratios were equal to the unit for the two ferrocenes.

a)

b)
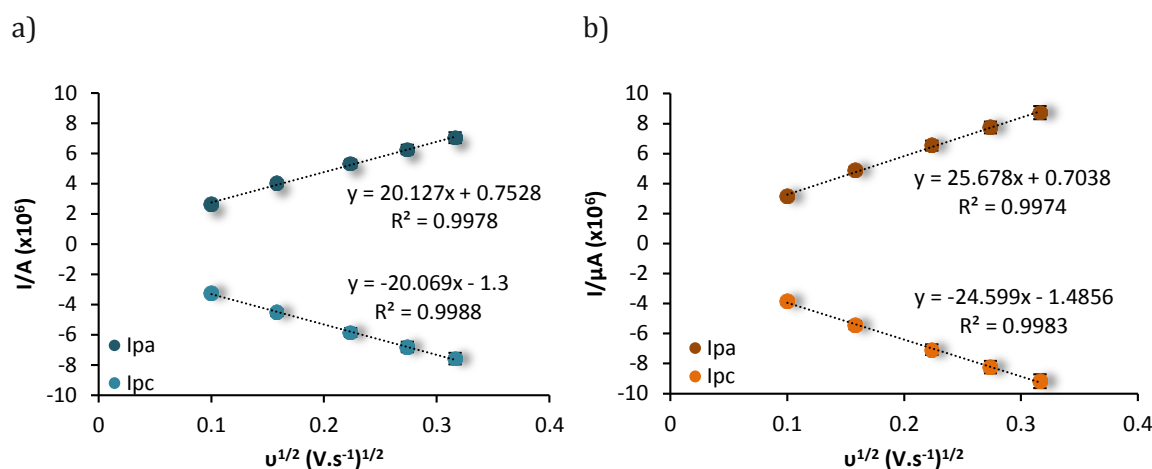
Figure 6.6 – Plots of peak current vs. square root of scan rate a) EtCDFc and b) Fc in the range from 10mV s^{-1} to 100mV s^{-1}. When not visible, the error bars are smaller than the symbols.

This linearity between the examined scan rates indicates that the oxidation process of both ferrocenes is reversible and diffusion controlled in the investigated solvent media at room temperature (295 ± 2K). On this basis the diffusion coefficients were calculated and

found equal to 1.12×10^{-6} and 1.81×10^{-6} cm^2 s^{-1} for EtCDFc and Fc, respectively. A difference in the diffusion coefficients was expected having in account the structure of the redox species under study. EtCDFc has a CD in its structure (Figure 6.2) and this should, empirically, decrease the velocity at which the molecule moves in the media; hence a lower diffusion coefficient. This was observed but the difference between Fc and EtCDFc was smaller than that predicted; the reason for this might lie in the fact that the diffusion coefficient determined from figure 6.6 is one order of magnitude higher than the value reported in the literature (2.1×10^{-5} cm^2 s^{-2}).[71]

6.4.1 Stability of the thick modified electrode

In order to verify the stability of the thick film used, the oxidation of EtCDFc to EtCDFc$^+$ was examined under consecutive voltammograms at a fixed scan rate (50mV s^{-1}), as depicted in Figure 6.6. In contrast with previous reports[3,49,72] where it has been shown that the organic phase does not contain any deliberately added supporting electrolyte, the organic phase was made sufficiently conductive by the incorporation of a hydrophobic salt. A small volume (25μL, corresponding to 1.3mm thickness) of the organic solution was placed on the surface of a glassy carbon working electrode. A silicon support at the end of the working electrode was used to immobilize the organic phase (see section 3.4.1). The working electrode was then immersed in an aqueous solution containing LiCl (20mM), according to the following electrochemical cell:

GC	20mMBTPPATPBCl 1mM ETCDFc	20mMLiCl	Ag|AgCl(s)
WE	1,2-DCE	Aqueous	RE
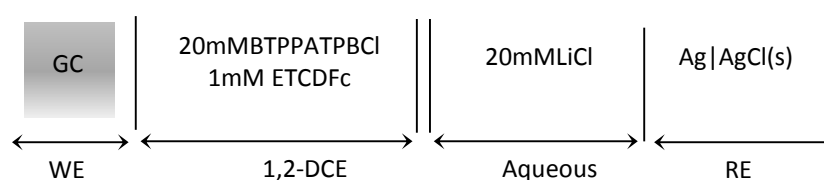
Scheme 6.2 – Electrochemical cell for the study of the stability of the thick film modified electrode.

It is clearly shown (Figure 6.7) that the voltammograms are fully reversible and the current magnitude remained virtually unchanged after 30 cycles. The reproducibility of the voltammograms reveals the stability of the redox probe during the electrochemical transformations within the thick layer, meaning that there is no leaching of the reactants (EtCDFc+) from the organic film to the aqueous solution. In this way, the charge compensation process can only occur by the transfer of Cl- into the organic film. This fact is easy to understand as the thickness of the diffusion layer of EtCDFc within the organic film is considerably smaller than that of the thick organic film.
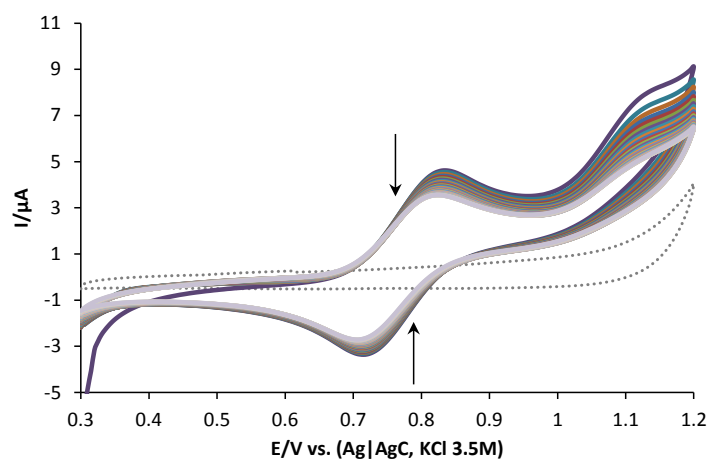
Figure 6.7 – 30 consecutive cycling of CV at a constant scan rate (0.5mVs-1) using 1mM of EtCDFc as redox probe and 20mM of LiCl in the aqueous phase. The dotted line shows the background response (absence of EtCDFc).

6.3.1 Electrochemical response of the redox couple EtCDFC|EtCDFc$^+$ in the presence of different aqueous anions

The voltammetric response of the thick film modified electrode was inspected in a series of different aqueous anions solutions, using CV and DPV (Figures 6.8a and 6.8b). As it was expected, the reduction and oxidation of EtCDFc is accompanied by the transfer of the anions from the aqueous phase to the organic film, and thus sensitive to the type of aqueous ions. Figure 6.8 b) shows clearly the position of the half-wave potential of each

anion on the potential axis, which follows a reasonable sequence reflecting their affinities towards the organic phase. The shift in the midpoint potential may be attributed to the Gibbs free energy, which is responsible for the transfer of the anion from the aqueous to the organic phase in this system.
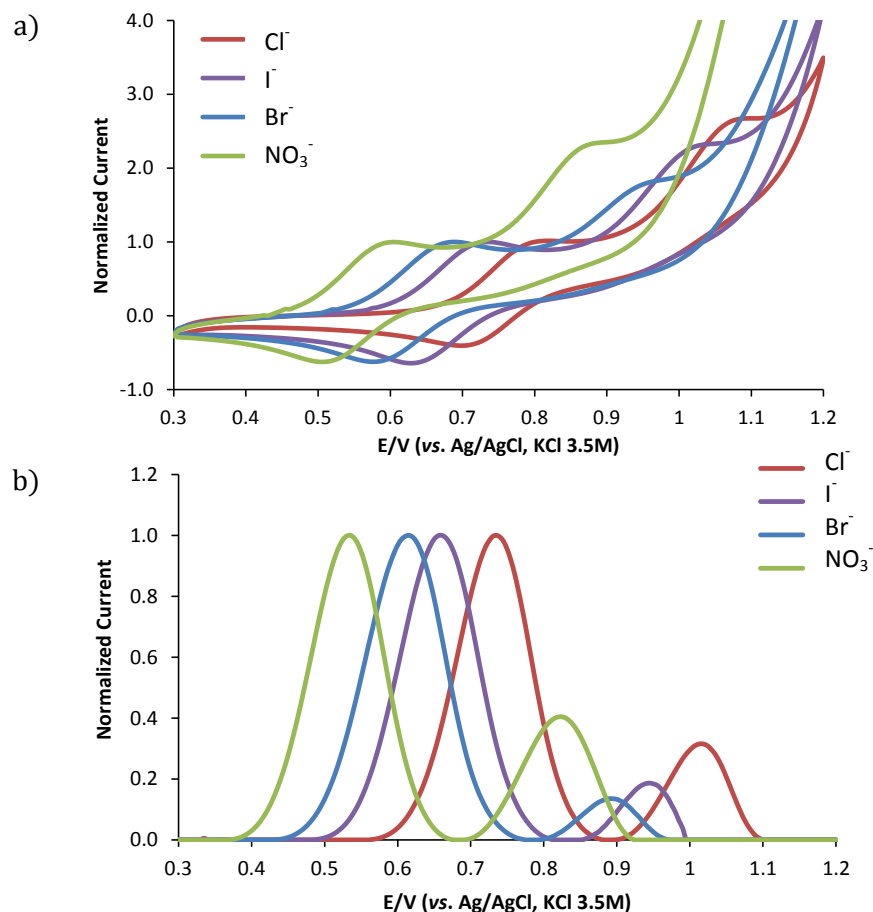
Figure 6.8 – a) CV and b) DPV voltammograms (normalized currents) of EtCDFc (1mM) at the thick film modified electrode coupled to the transfer of the anions of different electrolytes, KI, KNO$_3$, KBr and KCl, across water|1,2-DCE interface. The concentration of the aqueous electrolytes was 0.02M. Scan rate:50mVs^{-1}; pulse amplitude 0.05V, sampling with 0.060s, step height 0.005 V.

From figure 6.8 a second peak of lower intensity, which also shifts according to the anion in solution, can also be seen. The explanation may lie in a two-step process, migration of ion and complexation of ion with EtCDFc, as all the experimental conditions, (concentration, temperature and pH) were kept constant. It has been shown previously,

using spectrophotometric and ultrasonic relaxation techniques, that these anions complex with βCD,[41,73] with the stability constants being dependent on the lipophilicity of the anions.

Since the voltammetric systems measured in such experiments possess all the features of electrochemical reversibility and the transfer coefficients can be assumed to be near 0.5, it is reasonable to take the mid-peak potentials as the formal potential of the system. $E_c^{0\prime}$ can then be derived from the cyclic voltammograms as $E_c^{0\prime} = \frac{1}{2}(E_{pa} + E_{pc})$ where E_{pa} and E_{pc} are the anodic and cathodic peak potentials respectively, or from differential pulse voltammograms according to $E_c^{0\prime} = E_{p,DPV}$ where $E_{p,DPV}$ is the peak at the half-wave potential.[74] One can rationalize the potential shift by plotting the measured peak potentials as a function of $\Delta_w^o \phi_{A-}^0$, as this parameter describes the ability of the anion to be transferred across the water-organic solvent interface and therefore its hydrophobicity. Some of the properties of the studied anions, such as standard Gibbs free energy of transfer ($\Delta_w^o G^0$/KJ mol^{-1}), standard ion transfer potential($\Delta_w^o \phi_{A-}^0$/V) from water to 1,2-DCE, and radii of ions (r/nm) together with the mid-peak potentials obtained with CV and DPV are listed in Table 6.1.

Table 6.1 – Standard transfer potentials, standard Gibbs energy of transfer, radius and transfer half-wave potentials of the studied anions ([Anion]=20mM, [EtCDFc]=1mM).

	$\Delta_w^o \phi_{A-}^0$/V	$\Delta_w^o G^0$/KJmol^{-1}	r/nm	$E_c^{0\prime}$/V[a]	$E_c^{0\prime}$/V[b]
Cl^-	0.481[75]	54[75]	0.167[75]	0.74	0.75
I^-	0.274[75]	25[75]	0.206[75]	0.54	0.55
Br^-	0.400[75]	38[75]	0.182[75]	0.66	0.68
NO_3^-	0.330[75]	34[75]	0.189[75]	0.62	0.63

[a] CV measurements, [b] DPV measurements.

The y-intercept obtained in the linear relationship between the half-wave potential and $\Delta_w^o \phi_{A^-}^0$ is depicted in figure 6.9 using CV (a) and DPV (b), and can be related to $E_{EtCDFc_{(o)}^+|EtCDFc_{(o)}}^0$ according to Eq.(6.7). It can be seen that the relationship is linear, with a slope of approximately one for both measurements, which is in good agreement with Eq.(6.7).

a)   b)
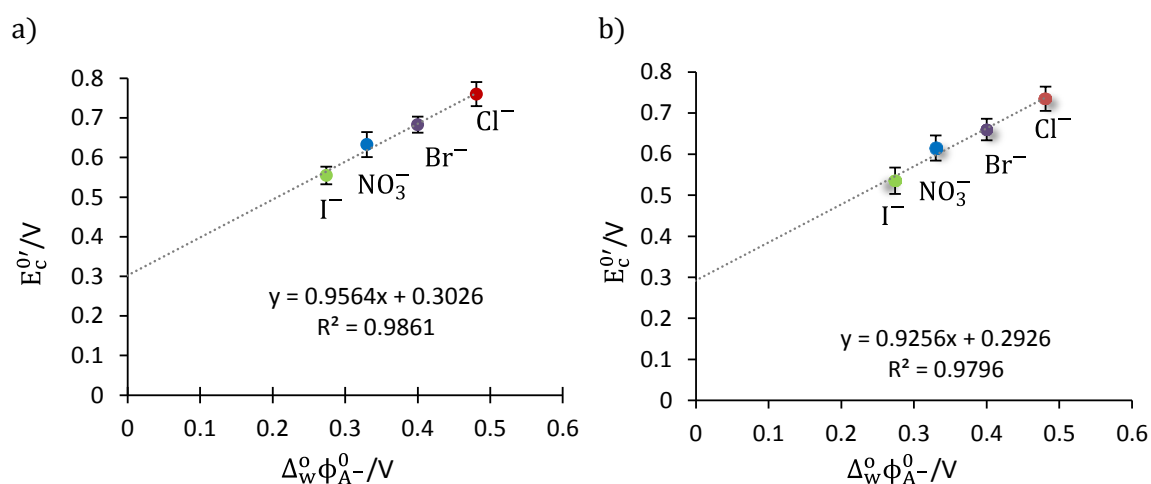
Figure 6.9 – Dependence of the half-wave potentials of a) CV and b) DPV of 1mM EtCDFc in 1,2-DCE in the presence of 20mM aqueous solution of KI, KNO₃, KBr and KCl, with the standard Galvani potential differences[75] of anions of the aqueous electrolytes (average values).

Considering the intercept of the straight line in figure 6.9, the standard potential of EtCDFc/EtCDFc+ couple in 1,2-DCE was found to be 0.30 ± 0.01 V (vs. Ag|AgCl) using CV and DPV.

The ion transfer depends both on the nature of the solvent and on the ionic radius. Figure 6.10 shows the half-wave potentials of transfer versus the ion radius at the water|1,2-DCE interface. As can be seen from the figure 6.10 the ion distribution potential decreases linearly with the increasing of ionic ion radii.[75]

a)

b)
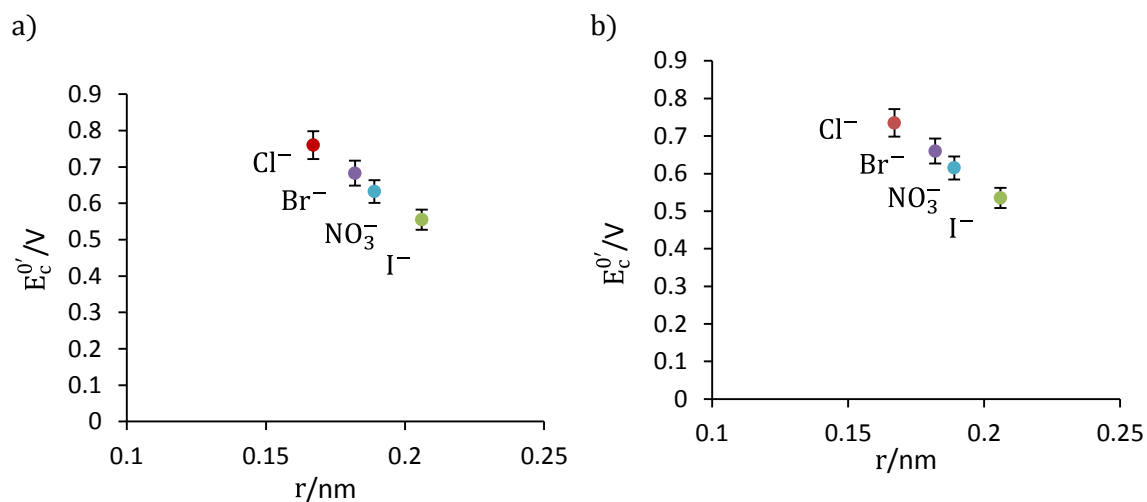
Figure 6.10 – Dependence of the half-wave potentials of a)CV and b)DPV of 1mM EtCDFc in 1,2-DCE versus the ion radii.[75]

6.3.2 Transfer of mandelic acid chiral anions at a thick film modified electrode

Previous studies using different chromatographic systems and enantioselective crystallization have shown that the enantiomeric discrimination and separation of mandelic acid and its derivatives can be done using CD as chiral selector.[52,76] A prerequisite for chiral recognition[77] was assumed to be the inclusion complex formation with the tightest fit of the complex and the interaction of the groups at the cyclodextrin cavity entrance with the chiral centre of the guest molecule. However, contradictory evidence also exists indicating that a tight fit implies the formation of strong complexes that can be unfavourable for the enantiomeric differentiation.[78] Nonetheless, the cavity size of the CD needs to be suitable to accommodate a guest of particular size.

We expect that the recognition of the MAH enantiomers by EtCDFc at the modified thick film electrode couples the complexation process to the redox reaction, i.e. the two reactions will mutually influence each other. The insertion (reduction) or withdrawal (oxidation) of an electron from the EtCDFc molecule will change the stability of the

complexed formed, leading to a change on its redox potential. Furthermore, the interaction of MAH with EtCDFc will depended on its relative hydrophobicity-hydrophilicity, which depends on the pH of the aqueous phase. The equilibrium equation for the protonation (unionized) and deprotonation (ionized) (scheme 6.3) of MAH is as follows:
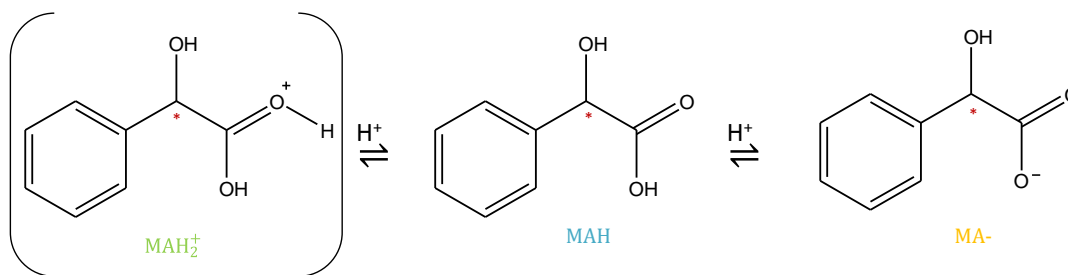
The association constant at the pK_a value can be described as:

$$K_a = \frac{[MA^-][H^+]}{[MAH]} \qquad (6.12)$$

where MAH and MA^- represent the unionized and anionic forms of R or S-MAH, respectively. The concentration of the ionic moiety of the acid increases with increasing pH of the aqueous solution, as shown in the Henderson-Hasselbalch equation:

$$pH = \log\frac{[MA^-]}{[MAH]} + pK_a \qquad (6.13)$$

According to Eq. (6.13), at pH=2 the MAH is ionized only 3.83% ([MAH]>>[MA$^-$]) meaning that it is mainly in its protonated (unionized) form; at pH=3.4, MAH is 50% ionized, protonated and anionic forms exist in equal quantity ([MAH]=[MA$^-$]); at pH=7, the anionic (ionized) form of the MAH is dominant in solution with 99.97% ionization ([MA$^-$]>>[MAH]). The effects of the protonated, neutral and ionized forms of MAH in the redox reaction of EtCDFc were studied using the electrochemical cells represented in scheme 6.3.
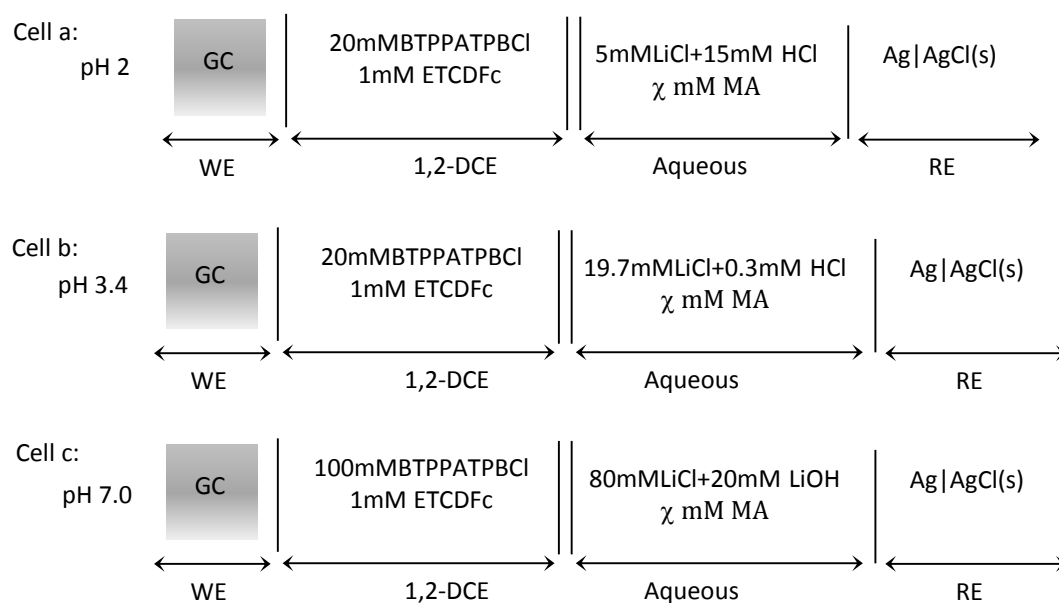
Scheme 6.3 – Cell configurations used, where χ is the concentration of MAH enantiomers, 0mM≤[MAH] ≤20mM.

The modified thick film electrode was first analysed in the absence of both, chiral redox probe and analyte, i.e only in the presence of aqueous and organic background electrolytes (Figure 6.11, dashed line). No redox or ion transfer behaviour was observed within the potential window. In order to observe if a detection signal corresponding to the MAH transfer could be seen, its transfer was studied in the absence of EtCDFc in the organic film. As it can be seen from figure 6.11 (dotted line) the CV and DPV responses were very similar to ones obtained in the presence of the aqueous and organic electrolytes. This indicates that no transfer of MAH can be detected without the redox probe in the organic film.

a)

b)
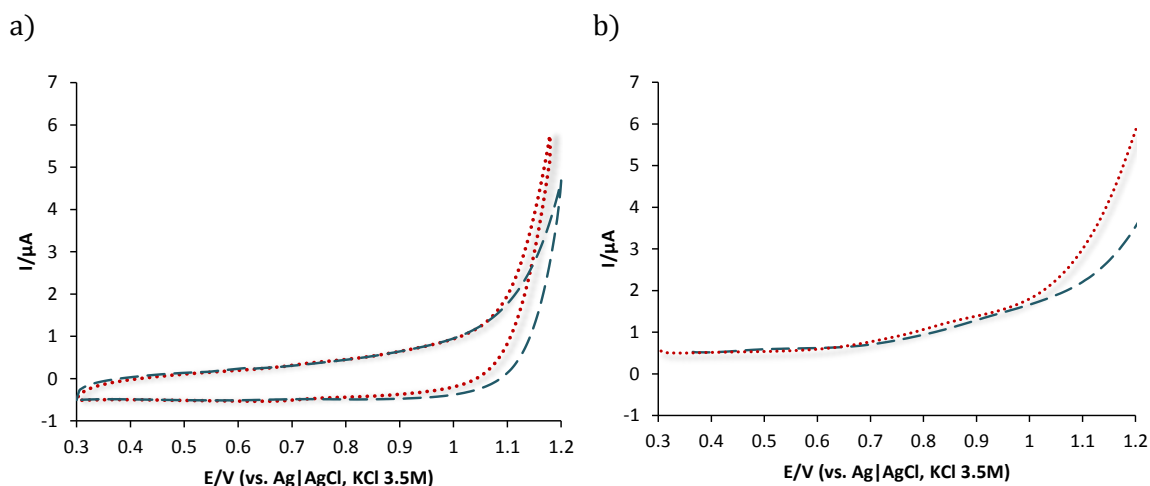
Figure 6.11 – a)CV and b)DPV response of the thick modified electrode in the absence of MAH and EtCDFc (dashed line), and in the absence of EtCDFc (dotted line). Scan rate:50 mV s^{-1}; pulse amplitude 0.05 V, sampling with 0.060 s, step height 0.005 V.

In the three pH ranges studied it was observed that when the concentration of the MAH enantiomers is below the concentration of EtCDFc, there is little effect on the response (Figures 6.12, 6.13 and 6.14). However, when the concentration of R- and S-MAH enantiomers increases and becomes higher than that of EtCDFc, a more noticeable effect is observed as both oxidation and reduction peak potentials on the CV and peak potential on DPV shift towards to negative potentials (Figures 6.12, 6.13, 6.14). It can also be seen from the same figures that the current response decreases with the increase of MAH enantiomers concentration. The presence of enantiomers of MAH in solution lowered the I_p values of the EtCDFc redox waves and shifted their peak potentials to less positive values, with the peak-to-peak separation ΔE_p increasing. This behaviour may be explained with the formation of inclusion complexes between the cyclodextrin moiety of the EtCDFc and the MAH enantiomers. The oxidation of EtCDFc to EtCDFc$^+$ becomes more difficult to occur as the concentration of free EtCDFc in the organic phase decreases, as a consequence a reduction in the current responses is observed.

As mentioned previously, the complex formation between the MAH enantiomers and EtCDFc will be strongly influenced by electrostatic interactions, Van de Waals interactions, hydrophobic interactions and hydrogen bonding.[79] Altering the charge state of the analyte by changing the pH of the aqueous solution will affect the enantioselectivity of the inclusion complex.

At pH=2 (Figure 6.12), as the MAH enantiomers are protonated, the phenyl ring of MAH will interact easily with the hydrophobic cavity of the cyclodextrin. On the other hand, at pH=3.4 (Figure 6.13), as MAH and MA⁻ enantiomers will be in equilibrium in solution, both will compete in the complex formation with EtCDFc. At pH=7 (Figure 6.14), the MAH enantiomers are mainly ionised carrying a negative charge. As EtCDFc becomes positively charged upon its oxidation, the MA⁻ anions migrate to the 1,2-DCE phase, to maintain electroneutrality and due to complexation with the CD cavity.

a)

b)

c)

d)
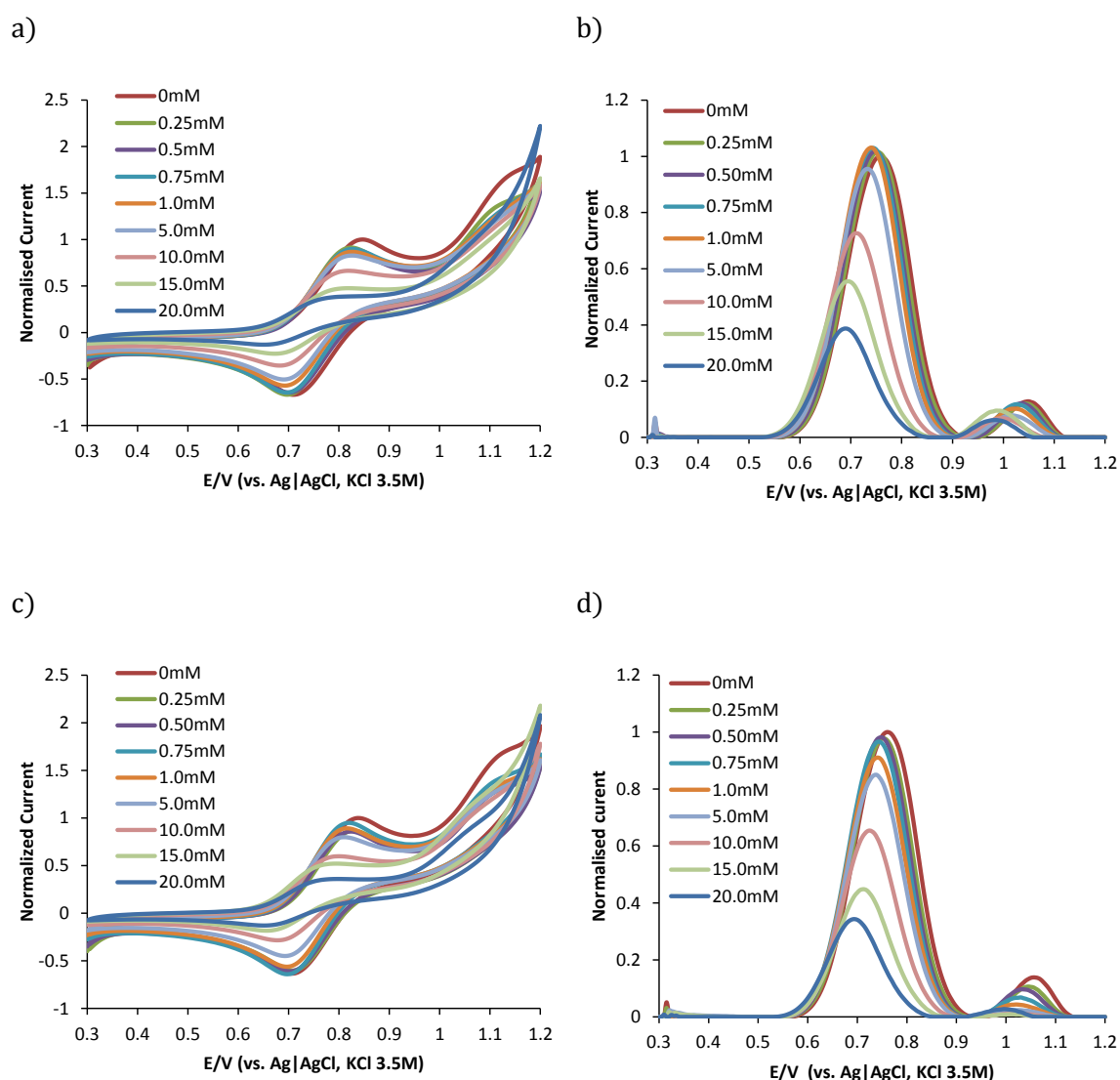
Figure 6.12 –CV and DPV responses at pH=2.0 for R (graphs a and b) and S (graphs b and c), according to cell 1 (scheme 6.3). Scan rate:50m Vs^{-1}; pulse amplitude 0.05 V, sampling with 0.060 s, step height 0.005 V. The variation of current, for all the concentrations studied, at different scan rates is shown in appendix (A1).
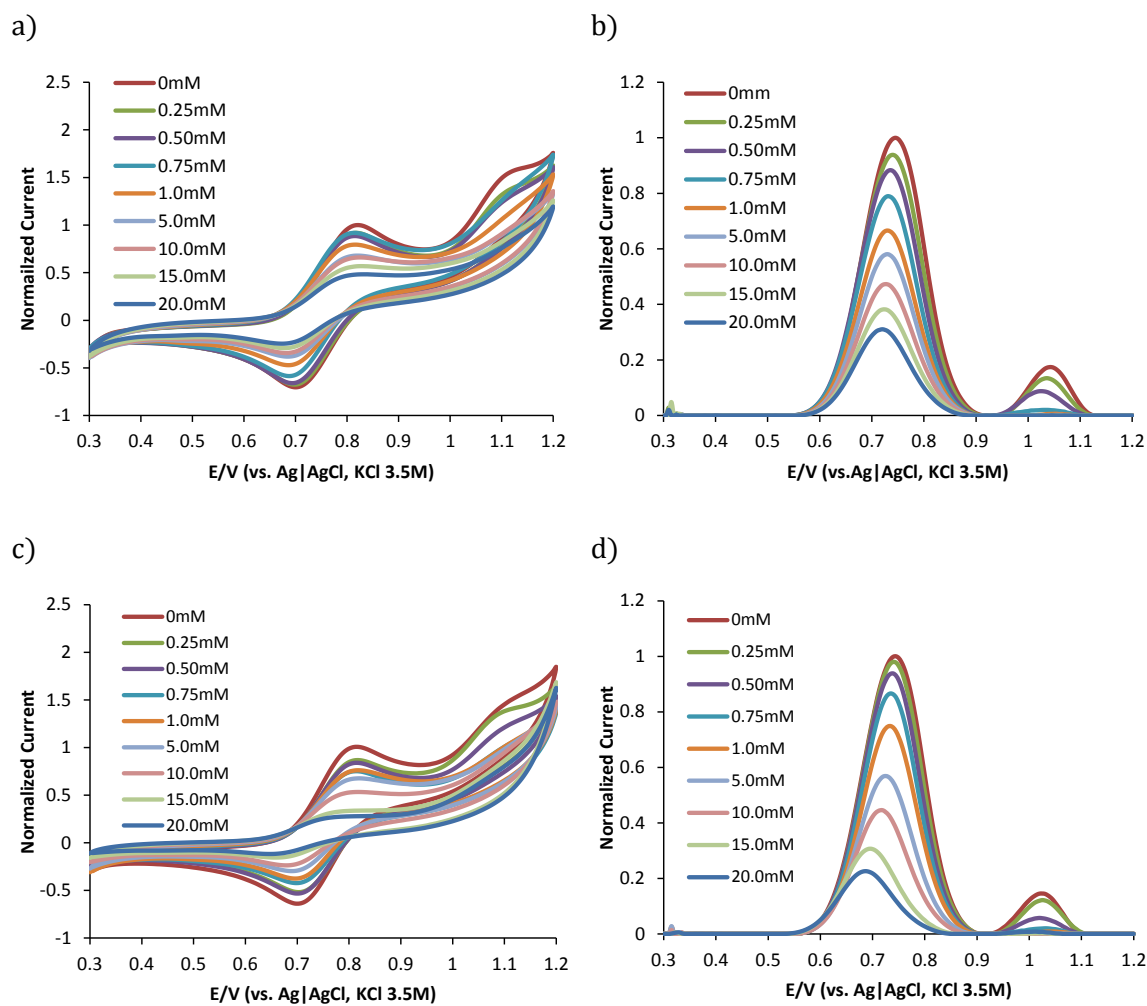
Figure 6.13 –CV and DPV responses at pH=3.4 for R (graphs a and b) and S (graphs b and c), according to cell 2 (scheme 6.3). Scan rate:50m Vs⁻¹; pulse amplitude 0.05 V, sampling with 0.060 s, step height 0.005 V. The variation of current, for all the concentrations studied, at different scan rates is shown in appendix (A1).

a)

b)

c)

d)
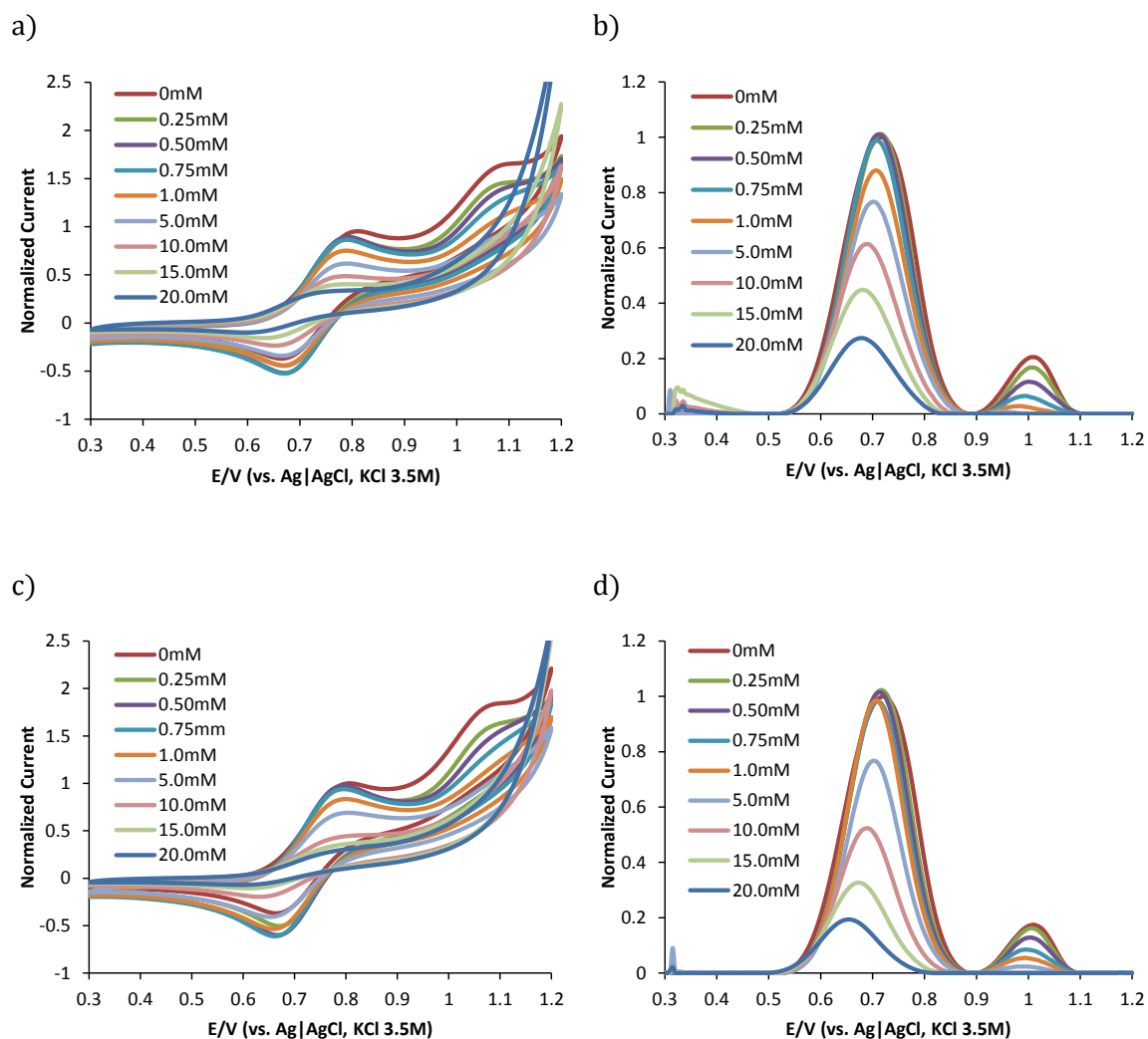
Figure 6.14 – CV and DPV responses at pH=7.0 for R (graphs a and b) and S (graphs b and c), according to cell 3 (scheme 6.3). Scan rate:50m Vs^{-1}; pulse amplitude 0.05 V, sampling with 0.060 s, step height 0.005 V. The variation of current, for all the concentrations studied, at different scan rates is shown in appendix (A1).

The discrimination between the enantiomers is easily observed in the DPV voltammograms, as the response is a well-defined peak shape. A second peak of lower intensity is observed in the three pHs studied and again it is believed to be due the complexation of EtCDFc with the chloride ions also present in solution. This parallel reaction does not seem to affect the enantioselectivity of the MAH enantiomers. Figure

6.14 shows the variation in peak potentials and normalized currents with the concentration of MAH for the three pH ranges studied.
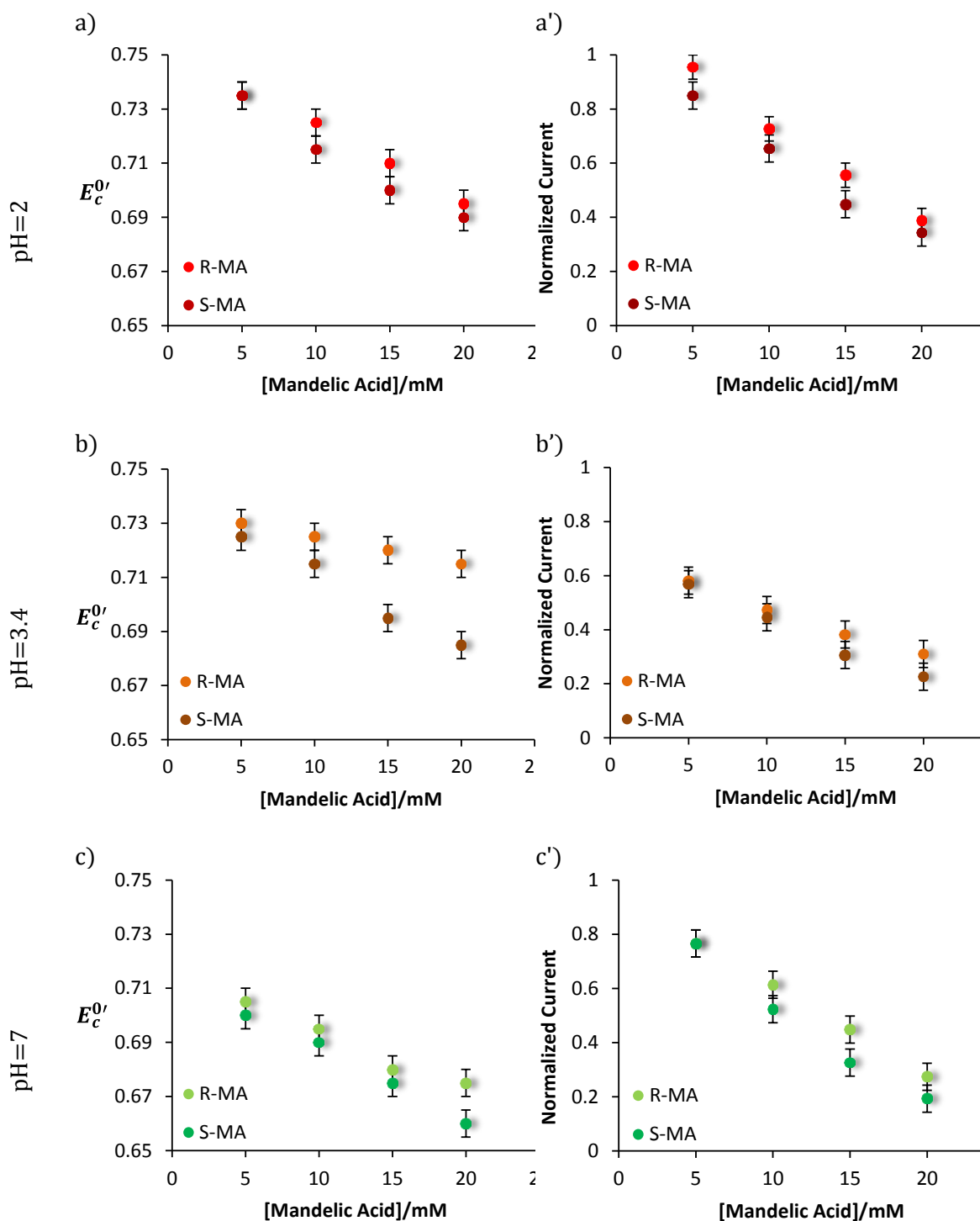
Figure 6.15 – Plot of the half-wave potentials (a), b) and c)) and current (a'), b') and c')) *vs.*, concentration of MAH enantiomers obtained from DPV at pH=2, b) pH=3.4 and pH=7.

Initially, the higher chiral differentiation was expected to be at pH 7 due to the strong interactions between EtCDFc and MAH enantiomers (EtCDFc is positively charged upon its oxidation and MAH is 99.97% ionized), but this was not the case. The strong electrostatic interactions between the two molecules lead to a difference of, at most, 15±2mV. This pH was not the one that presented higher difference in the potential for the coupled reaction between MAH enantiomers and EtCDFc; 30±2mV were observed in the case of pH 3.4. At pH 3.4 there are electrostatic and hydrophobic interactions involved in the complex formation. The hydrophobic interactions are stronger at pH 2, as the MAH is almost unionized (3.83% ionized), the hydrophobicity of the MAH enantiomers at this pH will make its entrance in the cavity of the cyclodextrin more favourable, however the difference detected in the response of S- and R-MAH was approximately 10mV±2mV.

From the experiments performed at the three pH ranges, it seems that the combination of electrostatic and hydrophobic interactions and the maintenance of electroneutrality are needed to achieve a better chiral differentiation. For the different concentrations analysed, the S- enantiomer showed consistently lower current intensities indicating that there is a preferential interaction with this enantiomer with EtCDFc.

The possibility of a pre-equilibration process with the anions of mandelic acid exchanging the chloride needs also to be considered for an alternative interpretation.

6.4 Conclusion

The present study shows that a thick film modified electrode can be used as an alternative system for the study of ion transfer. It was demonstrated that the redox probe, EtCDFc, is sensitive to the nature of the aqueous solution, as its redox potential shifted according to the hydrophobicity of the ions in solution. A good linear correlation was found between the mid-peak potential of cyclic and differential pulse voltammograms of EtCDFc and the

standard Galvani potential differences of the anions present in the aqueous solution. For Br-, Cl- and NO$_3^-$ ions the relationship was linear, which made possible to estimate the standard redox potential of EtCDFc in 1,2-DCE of 0.0853$\pm$0.005V, using DPV.

Due to its unique structure EtCDFc was also used as a chiral selector for the discrimination of mandelic acid enantiomers. The oxidation of the EtCDFc was accompanied by the charge compensating of MAH anions from the aqueous to the organic phase. This coupled reaction led to the formation of diastereomeric complexes. It was found that the recognition of mandelic acid anions using EtCDFc strongly depends on the pH of the aqueous solution which determines the intermolecular forces that participate in the complex formation. In the three pHs studied (2.0, 3.4 and 7.0) the S- enantiomer showed to be more favourable to complex with EtCDFc as the potential of the global reaction occurred at more negative potentials. Also, the results obtained at pH 3.4 showed better chiral discrimination between R- and S-MAH.

Using a thick film modified electrode, is demonstrated that electrochemically driven transfer of chiral mandelic acid ions can be differentiated using a compound that can be both redox active and chiral selector. Redox probes such as EtCDFc can be very promising as they simplify the number of compounds used in such system. Research on the differentiation of chiral anions can be continued and optimized using simple and alternative systems as the one described in this chapter.

References

(1)   Watarai, H.; Teramae, N.; Sawada, T. *Interfacial nanochemistry: molecular science and engineering at liquid-liquid interfaces*; Springer, 2005.

(2)   Volkov, A. G. *Liquid Interfaces in Chemical, Biological, and Pharmaceutical Applications*; 1st ed.; CRC Press, 2001.

(3)   Scholz, F.; Komorsky-Lovrić, Š.; Lovrić, M. *Electrochem. Commun.* **2000**, *2*, 112–118.

(4)   Scholz, F.; Meyer, B. *Chem. Soc. Rev.* **1994**, *23*, 341–347.

(5)   Shouji, E.; Buttry, D. A. *Langmuir* **1999**, *15*, 669–673.

(6)   Laforgue, A.; Simon, P.; Sarrazin, C.; Fauvarque, J.-F. *J. Power Sources* **1999**, *80*, 142–148.

(7)   Hermes, M.; Scholz, F. *J. Solid State Electrochem.* **1997**, *1*, 215–220.

(8)   Gobry, V.; Ulmeanu, S.; Reymond, F.; Bouchard, G.; Carrupt, P.-A.; Testa, B.; Girault, H. H. *J. Am. Chem. Soc.* **2001**, *123*, 10684–10690.

(9)   Ulmeanu, S.; Lee, H. J.; Fermin, D. J.; Girault, H. H.; Shao, Y. *Electrochem. Commun.* **2001**, *3*, 219–223.

(10)   Zhan, D.; Mao, S.; Zhao, Q.; Chen, Z.; Hu, H.; Jing, P.; Zhang, M.; Zhu, Z.; Shao, Y. *Anal. Chem.* **2004**, *76*, 4128–4136.

(11)   Zhang, M.; Sun, P.; Chen, Y.; Li, F.; Gao, Z.; Shao, Y. *Anal. Chem.* **2003**, *75*, 4341–4345.

(12)   Davies, T. J.; Wilkins, S. J.; Compton, R. G. *Journal of Electroanalytical Chemistry* **2006**, *586*, 260–275.

(13)   Banks, C. E.; Davies, T. J.; Evans, R. G.; Hignett, G.; Wain, A. J.; Lawrence, N. S.; Wadhawan, J. D.; Marken, F.; Compton, R. G. *Phys. Chem. Chem. Phys. 5*, 4053–4069.

(14)   Rayner, D.; Fietkau, N.; Streeter, I.; Marken, F.; Buckley, B. R.; BulmanPage, P. C.; delCampo, J.; Mas, R.; Munoz, F. X.; Compton, R. G. *J. Phys. Chem.* **2007**, *111*, 9992–10002.

(15)   Marken, F.; Blythe, A. N.; Wadhawan, J. D.; Compton, R. G.; Bull, S. D.; Aplin, R. T.; Davies, S. G. *J. Solid State Electrochem.* **2001**, *5*, 17–22.

(16)   Marken, F.; Compton, R. G.; Goeting, C. H.; Foord, J. S.; Bull, S. D.; Davies, S. G. *Electroanalysis* **1998**, *10*, 821–826.

(17)   Marken, F.; Webster, R. D.; Bull, S. D.; Davies, S. G. *J. Electroanal. Chem.* **1997**, *437*, 209–218.

(18)   Scholz, F.; Gulaboski, R.; Caban, K. *Electrochem. Commun.* **2003**, *5*, 929–934.

(19)   Scholz, F. *Annu. Rep. C* **2006**, *102*, 43–70.

(20)   Komorsky-Lovrić, Š.; Riedl, K.; Gulaboski, R.; Mirčeski, V.; Scholz, F. *Langmuir* **2002**, *18*, 8000–8005.

(21)   Gulaboski, R.; Riedl, K.; Scholz, F. *Phys. Chem. Chem. Phys.* **2003**, *5*, 1284–1289.

(22)   Gulaboski, R.; Mirčeski, V.; Scholz, F. *Amino Acids* **2003**, *24*, 149–154.

(23)   Gulaboski, R.; Mirčeski, V.; Scholz, F. *Electrochem. Commun.* **2002**, *4*, 277–283.

(24)   Bouchard, G.; Galland, A.; Carrupt, P.-A.; Gulaboski, R.; Mirčeski, V.; Scholz, F.; Girault, H. H. *Phys. Chem. Chem. Phys.* **2003**, *5*, 3748–3751.

(25)   Scholz, F.; Gulaboski, R.; Mirčeski, V.; Langer, P. *Electrochem. Commun.* **2002**, *4*, 659–662.

(26)   Gulaboski, R.; Galland, A.; Bouchard, G.; Caban, K.; Kretschmer, A.; Carrupt, P.-A.; Stojek, Z.; Girault, H. H.; Scholz, F. *J. Phys. Chem. B* **2004**, *108*, 4565–4572.

(27)   Komorsky-Lovrić, Š.; Riedl, K.; Gulaboski, R.; Mirčeski, V.; Scholz, F. *Langmuir* **2003**, *19*, 3090–3090.

(28)   Gulaboski, R.; Scholz, F. *J. Phys. Chem. B* **2003**, *107*, 5650–5657.

(29) Donten, M.; Stojek, Z.; Scholz, F. *Electrochem. Commun.* **2002**, *4*, 324–329.

(30) Shul, G.; Opallo, M.; Marken, F. *Electrochim. Acta* **2005**, *50*, 2315–2322.

(31) Shul, G.; Murphy, M.; Wilcox, G.; Marken, F.; Opallo, M. *J. Solid State Electrochem.* **2005**, *9*, 874–881.

(32) Shi, C.; Anson, F. C. *Anal. Chem.* **1998**, *70*, 3114–3118.

(33) Shi, C.; Anson, F. C. *J. Phys. Chem. B* **1998**, *102*, 9850–9854.

(34) Shi, C.; Anson, F. C. *J. Phys. Chem. B* **1999**, *103*, 6283–6289.

(35) Barker, A. L.; Unwin, P. R. *J. Phys. Chem. B* **2000**, *104*, 2330–2340.

(36) Quentel, F.; Mirčeski, V.; L'Her, M. *Anal. Chem.* **2005**, *77*, 1940–1949.

(37) Charreteur, K.; Quentel, F.; Elleouet, C.; L'Her, M. *Anal. Chem.* **2008**, *80*, 5065–5070.

(38) Guorong, Z.; Xiaolei, W.; Xingwang, S.; Tianling, S. *Talanta* **2000**, *51*, 1019–1025.

(39) Luong, J. H. T.; Male, K. B.; Zhao, S. S. *Anal. Biochem.* **1993**, *212*, 269–276.

(40) Siegel, B.; Breslow, R. *J. Am. Chem. Soc.* **1975**, *97*, 6869–6870.

(41) Atwood, J. L.; Lehn, J.-M. *Comprehensive Supramolecular Chemistry: Cyclodextrins*; Pergamon, 1996.

(42) Kataky, R.; Dell, R.; Senanayake, P. K. *Analyst* **2001**, *126*, 2015–2019.

(43) Kuhn, A.; Anson, F. C. *J. Electroanal. Chem.* **1996**, *410*, 243–246.

(44) Lopes, P.; Kataky, R. *Anal. Chem.* **2012**, *84*, 2299–2304.

(45) Kataky, R.; Lopes, P. *Chem. Commun.* **2009**, 1490–1492.

(46) Gao, C.; Ding, S.; Tan, Q.; Gu, L.-Q. *Anal. Chem.* **2009**, *81*, 80–86.

(47) Zhou, J.; Chen, Q.; Wang, L.; Wang, Y.; Fu, Y. *Int. J. Electrochem. Electrochem.* **2011**, *2011*, 1–6.

(48) Schulte, B.; Pleus, S. *J. Solid State Electrochem.* **2001**, *5*, 522–530.

(49) Scholz, F.; Gulaboski, R. *Faraday Discuss.* **2005**, *129*, 169–177.

(50) Del Valle, E. M. M. *Process Biochem.* **2004**, *39*, 1033–1046.

(51) Schneiderman, E.; Stalcup, a M. *J. Chromatogr. B* **2000**, *745*, 83–102.

(52) Novák, C.; Végh, A.; Marokházi, S.; Pokol, G.; Szente, L. *J. Therm. Anal.* **1994**, *41*, 181–190.

(53) Izake, E. L. *J. Pharm. Sci.* **2007**, *96*, 1659–1676.

(54) Ueno, A.; Moriwaki, F.; Matsue, T.; Osa, T.; Hamada, F.; Murai, K. *Makromol. Chem. Rapid Commun.* **1985**, *6*, 231–233.

(55) Utkin, I. b.; Yakimov, M. m.; Matveeva, L. n.; Kozlyak, E. i.; Rogozhin, I. s.; Solomon, Z. g.; Bezborodov, A. m. *FEMS Microbiol. Lett.* **1991**, *77*, 237–242.

(56) Linhart, I.; Smejkal, J.; Mládková, I. *Toxicol. Lett.* **1998**, *94*, 127–135.

(57) Amoroso, R.; Bettoni, G.; Tricca, M. L.; Loiodice, F.; Ferorelli, S. *Il Farmaco* **1998**, *53*, 73–79.

(58) Chataigner, I.; Lebreton, J.; Durand, D.; Guingant, A.; Villiéras, J. *Tetrahedron Lett.* **1998**, *39*, 1759–1762.

(59) Taran, F.; Gauchet, C.; Mohar, B.; Meunier, S.; Valleix, A.; Renard, P. Y.; Créminon, C.; Grassi, J.; Wagner, A.; Mioskowski, C. *Angew. Chem. Int. Ed.* **2002**, *41*, 124–127.

(60) Yamamoto, K.; Oishi, K.; Fujimatsu, I.; Komatsu, K. *Appl. Environ. Microbiol.* **1991**, *57*, 3028–3032.

(61) Kaul, P.; Banerjee, A.; Mayilraj, S.; Banerjee, U. C. *Tetrahedron: Asymmetry* **2004**, *15*, 207–211.

(62) Allenmark, S.; Bomgren, B.; Borén, H. *J. Chromatogr. A* **1983**, *264*, 63–68.

(63) Mateo, C.; Chmura, A.; Rustler, S.; van Rantwijk, F.; Stolz, A.; Sheldon, R. A. *Tetrahedron: Asymmetry* **2006**, *17*, 320–323.

(64) Blay, G.; Fernández, I.; Molina, E.; Muñoz, M. C.; Pedro, J. R.; Vila, C. *Tetrahedron* **2006**, *62*, 8069–8076.

(65) Gulaboski, R.; Mirćeski, V.; Pereira, C. M.; Cordeiro, M. N. D. S.; Silva, A. F.; Quentel, F.; L'Her, M.; Lovrić, M. *Langmuir* **2006**, *22*, 3404–3412.

(66) Mirčeski, V.; Quentel, F.; L'Her, M.; Pondaven, A. *Electrochem. Commun.* **2005**, *7*, 1122–1128.

(67) Mirčeski, V. *J. Phys. Chem. B* **2004**, *108*, 13719–13725.

(68) Bond, A. M.; Oldham, K. B.; Snook, G. A. *Anal. Chem.* **2000**, *72*, 3492–3496.

(69) Ranchet, D.; Tommasino, J. B.; Vittori, O.; Fabre, P. L. *J. Solution Chem.* **1998**, *27*, 979–991.

(70) Bard, A. J.; Faulkner, L. *Electrochemical Methods: Fundamentals and Applications*; 2nd ed.; John Wiley & Sons, 2001.

(71) Janisch, J.; Ruff, A.; Speiser, B.; Wolff, C.; Zigelli, J.; Benthin, S.; Feldmann, V.; Mayer, H. A. *Journal of Solid State Electrochemistry* **2011**, *15*, 2083–2094.

(72) Scholz, F.; Gulaboski, R. *ChemPhysChem* **2005**, *6*, 16–28.

(73) Rohrbach, R. P.; Rodriguez, L. J.; Eyring, E. M.; Wojcik, J. F. *J. Phys. Chem.* **1977**, *81*, 944–948.

(74) Scholz, F. *Electroanalytical Methods: Guide to Experiments and Applications*; Springer, 2010.

(75) Volkov, A. G. *Liquid Interfaces in Chemistry and Biology*; Wiley: New York, 1998.

(76) Nardi, A.; Eliseev, A.; Boček, P.; Fanali, S. *J. Chromatogr. A* **1993**, *638*, 247–253.

(77) Bikádi, Z.; Iványi, R.; Szente, L.; Ilisz, I.; Hazai, E. *Curr. Drug Discov. Tech.* **2007**, *4*, 282–294.

(78) Asztemborska M.; Nowakowski R.; Sybilska D. *J. Chromatogr. A* **2000**, *902*, 381–387.

(79) Liu, L. E. I.; Guo, Q. *J. Incl. Phenom. Macro.* **2002**, *42*, 1–14.

Chapter 7

Conclusion

and Further work

New approaches for the study of chiral molecules and interaction at liquid|liquid interface have been presented. In this thesis, it is shown how chiral stationary phases made of lipophilic cyclodextrins and plasma proteins can contribute to the enhancement of applications for chiral studies. The electrochemical techniques allow qualitative and quantitative differentiation between the enantiomers studied. The chiral differentiation obtained in the different systems used is comparable to that shown by other techniques with the advantage that it involves significant less costs, simple instrumentation and rapid analysis. It seems, therefore, that the conversion of chiral discrimination from other formats (e.g. chromatographic, spectroscopic etc.) to the format of a sensing electrochemical system deserves an increasing attention in the current analytical research.

Initially the study of chiral detection and discrimination at liquid|liquid interface was done using lipophilic cyclodextrins, such as AcαCD and AcβCD. This study was performed in order to enable us to understand the nature of analyte recognition by the lipophilic cyclodextrins using electrochemical techniques. The chiral stationary phases used proved to be successful for the study of chiral interaction and differentiation at liquid|liquid interface. The results indicate that acetylated cyclodextrins provide a size-selective cavity

for the binding and detection of ephedrinium ions. The differences obtained in the responses of the two enantiomers, suggest that (+)EPH+ and (-)-EPH+ enantiomers of ephedrine fit differently in the cavity of the cyclodextrins which may result from their different orientation. In both cyclodextrins, the (+)EPH+ enantiomer was transferred at less positive potentials than (-)-EPH+ and with a higher magnitude of response, suggesting that this is the enantiomer that more strongly bounds to the chiral selectors and is more feasible to be transferred across the interface. Although the values obtained for the variation in stability constants using AcβCD (1.41 ± 0.1 M^{-1}) and AcαCD (1.20 ± 0.1 M^{-1}) were modest, they proved to be sufficient to differentiate between the enantiomers of ephedrine.

In the study of the interaction between the basic drugs, propranolol, lidocaine and procaine, with the acute phase plasma protein, it was found that the three drugs studied bound to AGP with different affinities. The interaction and the formation of complex between the AGP and the drugs lead a decrease in the detection signal, as only the unbound or free drug was able to be transferred across the interface. The differences in the detection signal in the presence of AGP made possible the differentiation between the enantiomers of propranolol hydrochloride. No substantial difference was observed in the transfer of lidocaine in the presence of AGP, indicating that there is a weak interaction between the two molecules. The differences observed in the affinities of the drugs and protein was reflected in the values of association constants. The association constant of S-propranolol was found to be 2.7×10^5 M^{-1}, whereas for R-propranolol the value was about two times smaller, 1.3×10^5 M^{-1}. On the other hand the two anaesthetic drugs studied, procaine and lidocaine also revealed to have very different affinities with AGP, which lead to association constants of 1.2×10^4 M^{-1} and 8.4×10^3 M^{-1}, respectively. Procaine was the less bounded drug studied and therefore having the smallest association constant value.

A thick film electrode modified with an ethylated ferrocene cyclodextrin, EfCDFc, was used as additional system for the study of chiral ion transfer. The chiral selector used has a dual role, a redox active moiety and a cyclodextrin moiety which was able to form enantioselective complexes the enantiomers of mandelic acid. The oxidation of the EtCDFc accompanied by the charge compensating of MA anions from the aqueous to the organic phase led to the formation of diastereomeric complexes, which depended on the pH of the aqueous solution. This simultaneous reaction made possible the differentiation of the enantiomers of mandelic acid.

The work presented in this thesis can/should be developed further. In the case of the chiral detection and discrimination with lipophilic cyclodextrins, further studies can be focused on other chiral analytes of pharmacological interest in order to extend the application of chiral discrimination at liquid|liquid interface. The use of more efficient chiral selectors, such as those negatively charged, can also be considered. For instance, sulfated CDs offer the possibility of formation of stronger interactions, such as ion-ion interactions between the positively charged nitrogens of ephedrines and the negatively charged groups of the CD. The formation of stronger interactions may lead to a better chiral differentiation. In seeking further to understand in detailed the mechanism by which the enantiomeric discrimination occurs, a systematic variation of both, the structure of the chiral analyte and of the CD host can be undertaken.

The study of the interaction between chiral and non-chiral drugs with plasma proteins can be done using other type of proteins such as albumin which according to the literature[1,2] is more suitable to bind with acid drugs, extending the application of the system used and the number of the drugs studied.

In the thick film modified electrode, a more deep study has to be done as the system is more complex with two reactions occurring simultaneously. A redox chiral selector which
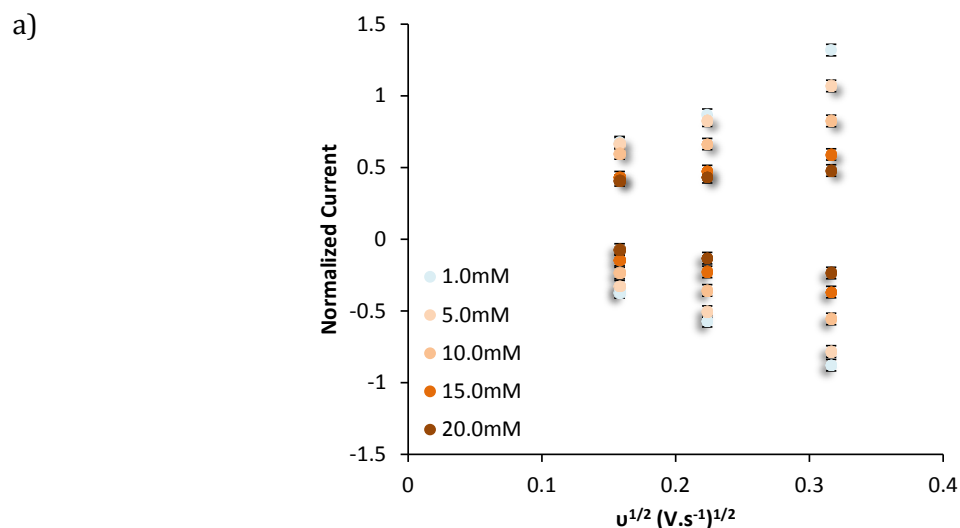
is able to differentiate enantiomeric molecules seems to be a very promising way of studying chiral acidic compounds.

References

(1)   Tajmir-Riahi, H. A. *Scientia Iranica* **2007**, *14*, 87–95.

(2)   Zhu, X.; Ding, Y.; Lin, B.; Jakob, A.; Koppenhoefer, B. *Proteins* **1999**, *20*, 1869–1877.

Appendix

A1 – Variation of current with scan rate at different concentrations of mandelic acid

a)

b)

[R-MA]/mM	i_{pa}	i_{pc}
0	y = 3.9305x + 0.1055	y = -3.8265x + 0.1749
	R² = 0.9981	R² = 0.999
0.25	y = 3.3705x + 0.144	y = -3.5435x + 0.1214
	R² = 0.9865	R² = 1
0.5	y = 3.3661x + 0.1135	y = -3.5907x + 0.1516
	R² = 0.9999	R² = 0.9997
0.75	y = 3.3311x + 0.1557	y = -3.555x + 0.1442
	R² = 0.9999	R² = 0.9998
1	y = 4.1151x - 0.0032	y = -3.2127x + 0.141
	R² = 0.9832	R² = 0.9995
5	y = 2.5294x + 0.2664	y = -2.8931x + 0.1352
	R² = 0.9996	R² = 0.9994
10	y = 1.4542x + 0.357	y = -2.0446x + 0.0936
	R² = 0.9815	R² = 0.9982
15	y = 1.0221x + 0.2624	y = -1.4109x + 0.0812
	R² = 0.9763	R² = 0.9976
20	y = 0.4438x + 0.3377	y = -1.0455x + 0.0976
	R² = 0.9908	R² = 0.9968

Figure A1.1 – a) Relation between anodic (i_{pa}) and cathodic (i_{pc}) peak currents and the square root of scan rate ($\upsilon^{1/2}$) at different concentrations of R-MA, b) linear regression of the data points, at pH 2.

a)
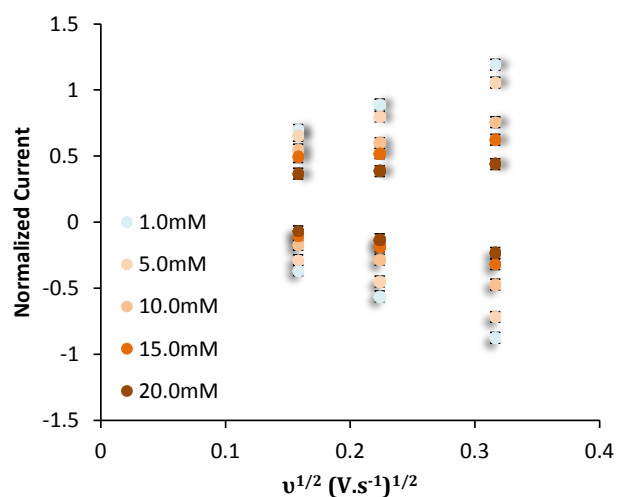
b)

[S-MA]/mM	i_{pa}	i_{pc}
0	y = 3.7043x + 0.142	y = -3.5674x + 0.1694
	R^2 = 0.9924	R^2 = 0.9998
0.25	y = 3.271x + 0.1463	y = -3.3734x + 0.1477
	R^2 = 0.9989	R^2 = 0.9996
0.5	y = 3.6295x + 0.0528	y = -3.5781x + 0.184
	R^2 = 0.9996	R^2 = 0.9995
0.75	y = 3.6461x + 0.1347	y = -3.6513x + 0.1702
	R^2 = 1	R^2 = 0.9996
1	y = 3.1236x + 0.201	y = 2.5624x + 0.2402
	R^2 = 0.9993	R^2 = 0.9963
5	y = 2.5624x + 0.2402	y = -2.7265x + 0.1504
	R^2 = 0.9963	R^2 = 0.9981
10	y = 1.3343x + 0.3249	y = -1.9021x + 0.1337
	R^2 = 0.9607	R^2 = 0.9977
15	y = 0.8485x + 0.3487	y = -1.3615x + 0.1153
	R^2 = 0.9538	R^2 = 0.9973
20	y = 0.4704x + 0.2885	y = -1.0371x + 0.0985
	R^2 = 0.9774	R^2 = 0.9974

Figure A1.2 – a) Relation between anodic (i_{pa}) and cathodic (i_{pc}) peak currents and the square root of scan rate ($\upsilon^{1/2}$) at different concentrations of S-MA, b) linear regression of the data points at pH 2.

a)

b)

[R-MA]/mM	i_{pa}	i_{pc}
0	y = 3.7242x + 0.1742	y = -3.9177x + 0.1697
	R^2 = 0.9996	R^2 = 1
0.25	y = 3.4113x + 0.1644	y = -3.6613x + 0.1379
	R^2 = 0.9992	R^2 = 0.9997
0.5	y = 3.3072x + 0.1495	y = -3.6325x + 0.1469
	R^2 = 0.9998	R^2 = 0.9998
0.75	y = 3.0689x + 0.2013	y = -2.992x + 0.0756
	R^2 = 0.9881	R^2 = 0.9992
1	y = 2.412x + 0.2534	y = -2.6266x + 0.108
	R^2 = 0.9999	R^2 = 0.9989
5	y = 1.7746x + 0.2832	y = -2.1277x + 0.0883
	R^2 = 1	R^2 = 0.9991
10	y = 1.8668x + 0.2263	y = -2.0722x + 0.1183
	R^2 = 0.9907	R^2 = 1
15	y = 1.3018x + 0.2829	y = -1.7332x + 0.0926
	R^2 = 0.9981	R^2 = 0.9997
20	y = 1.0379x + 0.2588	y = -1.4584x + 0.0775
	R^2 = 0.9929	R^2 = 0.9995

Figure A1.3 – a) Relation between anodic (i_{pa}) and cathodic (i_{pc}) peak currents and the square root of scan rate ($\upsilon^{1/2}$) at different concentrations of R-MA, b) linear regression of the data points at pH 3.4.
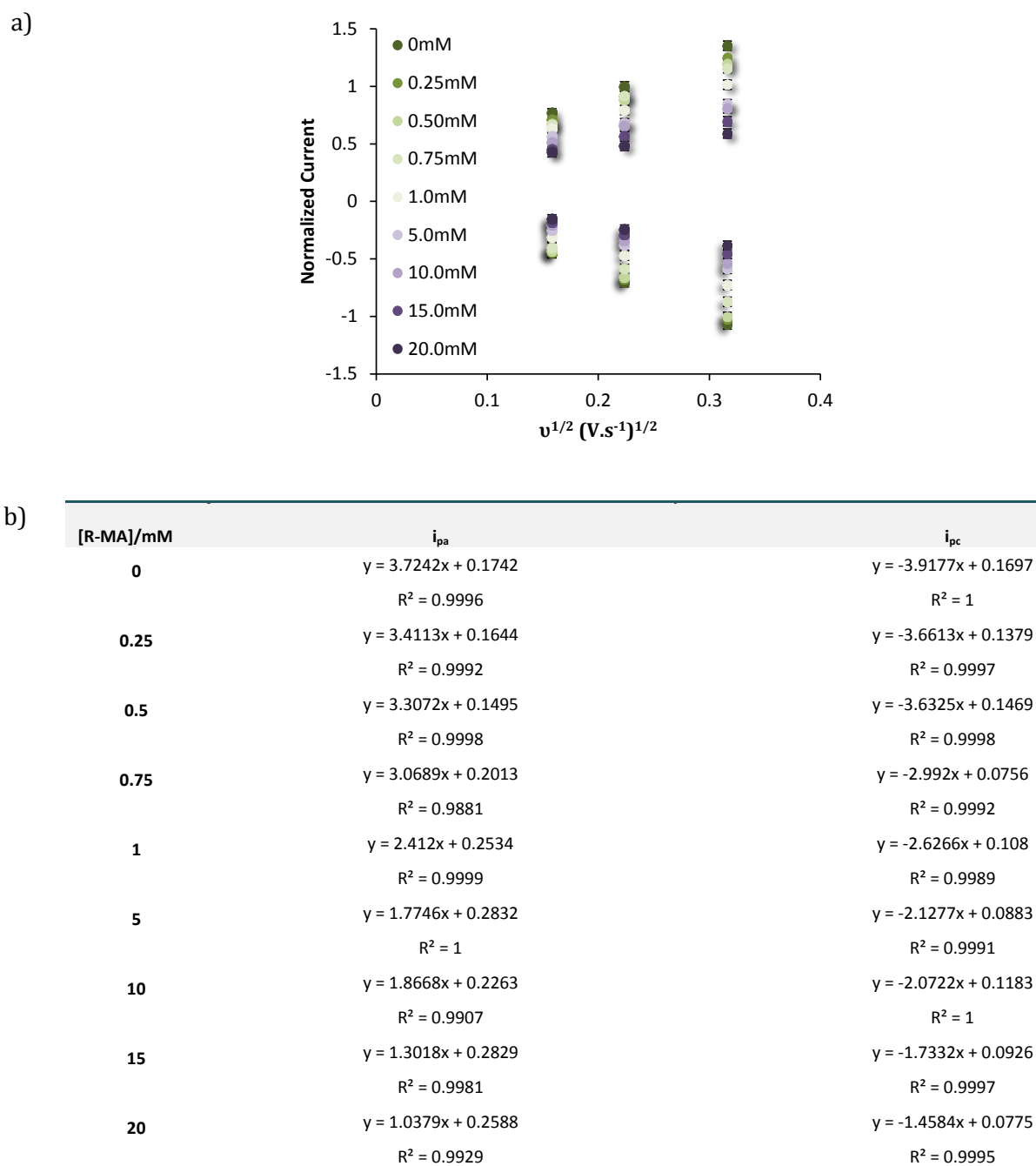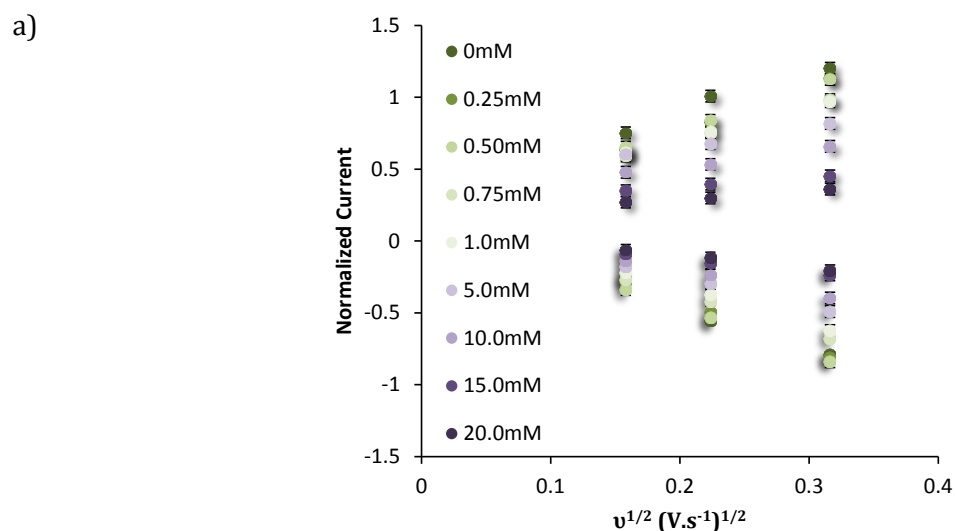
a)

b)

[S-MA]/mM	i_{pa}	i_{pc}
0	y = 2.7959x + 0.3376	y = -3.3648x + 0.2505
	R^2 = 0.9696	R^2 = 0.9667
0.25	y = 3.1641x + 0.1297	y = -3.3492x + 0.2491
	R^2 = 0.9988	R^2 = 0.9995
0.5	y = 2.9908x + 0.1776	y = -3.195x + 0.1736
	R^2 = 0.9995	R^2 = 0.9992
0.75	y = 2.4875x + 0.1974	y = -2.5903x + 0.1462
	R^2 = 1	R^2 = 0.998
1	y = 2.2376x + 0.2623	y = -2.5516x + 0.1871
	R^2 = 1	R^2 = 0.9988
5	y = 1.3687x + 0.3814	y = -1.9763x + 0.1379
	R^2 = 0.9935	R^2 = 0.9983
10	y = 1.1483x + 0.29	y = -1.6488x + 0.1267
	R^2 = 0.9847	R^2 = 0.9988
15	y = 0.6495x + 0.2489	y = -0.916x + 0.0528
	R^2 = 0.9993	R^2 = 0.999
20	y = 0.5852x + 0.1748	y = -0.9086x + 0.0823
	R^2 = 0.9889	R^2 = 0.9978

Figure A1.4 – a) Relation between anodic (i_{pa}) and cathodic (i_{pc}) peak currents and the square root of scan rate ($\upsilon^{1/2}$) at different concentrations of S-MA, b) linear regression of the data points at pH 3.4.
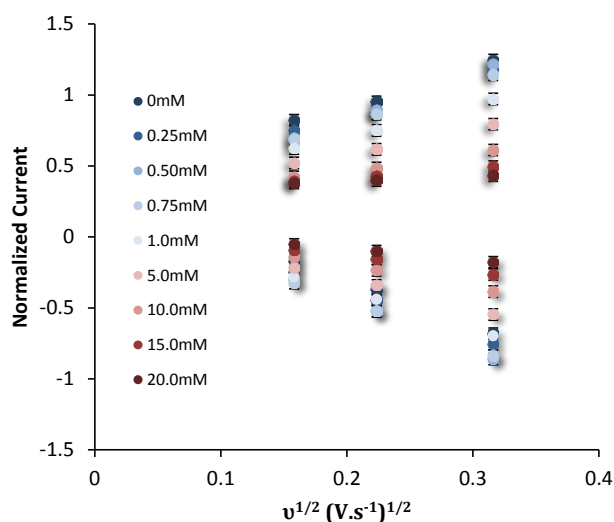
a)

b)

[R-MA]/mM	i_{pa}	i_{pc}
0	y = 2.7209x + 0.3738	y = -3.2234x + 0.3422
	R² = 0.9858	R² = 0.9991
0.25	y = 2.7209x + 0.301	y = -3.2234x + 0.2672
	R² = 0.9858	R² = 0.9991
0.5	y = 3.4013x + 0.1406	y = -3.5459x + 0.2641
	R² = 0.9993	R² = 0.9993
0.75	y = 2.8521x + 0.2363	y = -3.2298x + 0.1894
	R² = 0.9986	R² = 0.9993
1	y = 2.2254x + 0.2642	y = -2.6354x + 0.1403
	R² = 0.9971	R² = 0.9987
5	y= 1.7363x + 0.2406	y = -2.0983x + 0.1201
	R² = 0.9947	R² = 0.9983
10	y = 1.199x + 0.2289	y = -1.5285x + 0.1005
	R² = 0.9907	R² = 0.998
15	y = 0.6448x + 0.2882	y = -1.1042x + 0.0857
	R² = 0.9882	R² = 0.998
20	y = 0.3207x + 0.3282	y = -0.797x + 0.0757
	R² = 0.9902	R² = 0.9979

Figure A1.5 – a) Relation between anodic (i_{pa}) and cathodic (i_{pc}) peak currents and the square root of scan rate ($\upsilon^{1/2}$) at different concentrations of R-MA, b) linear regression of the data points at pH 7.0.
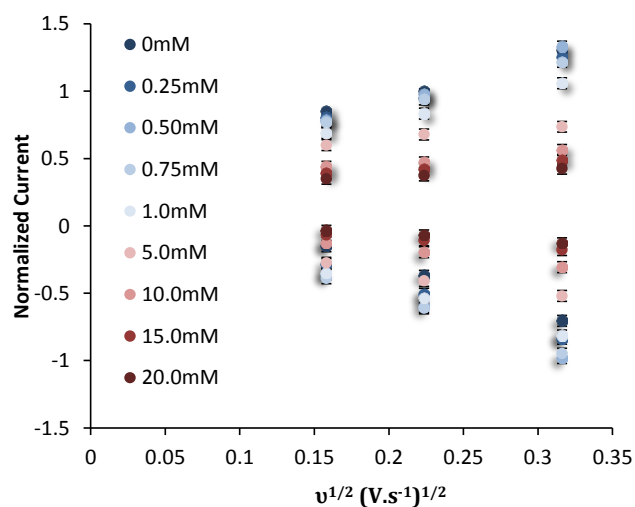
a)

b)

[S-MA]/mM	ipa	ipc
0	y = 2.8791x + 0.3824	y = -3.5109x + 0.4082
	R^2 = 0.9902	R^2 = 0.9995
0.25	y = 2.8791x + 0.3316	y = -3.5109x + 0.2744
	R^2 = 0.9902	R^2 = 0.9995
0.5	y = 3.4991x + 0.2161	y = -3.9288x + 0.2665
	R^2 = 0.9957	R^2 = 0.9989
0.75	y = 2.8507x + 0.3121	y = -3.5378x + 0.1733
	R^2 = 0.9983	R^2 = 0.9997
1	y = 2.3405x + 0.3166	y = -2.9295x + 0.1143
	R^2 = 0.9993	R^2 = 0.9996
5	y = 0.8439x + 0.4753	y = -1.5314x - 0.045
	R^2 = 0.9636	R^2 = 0.9773
10	y = 0.7919x + 0.3074	y = -1.1477x + 0.0578
	R^2 = 0.9705	R^2 = 0.9993
15	y = 0.6534x + 0.2814	y = -0.7076x + 0.0467
	R^2 = 0.9878	R^2 = 0.9952
20	y = 0.4785x + 0.2717	y = -0.5887x + 0.0585
	R^2 = 0.9892	R^2 = 0.9975

Figure A1.6 – a) Relation between anodic (i_{pa}) and cathodic (i_{pc}) peak currents and the square root of scan rate ($\upsilon^{1/2}$) at different concentrations of S-MA, b) linear regression of the data points at pH7.0.

A2 – Curriculum Vitae

Publications

"Chiral interaction of the drug propranolol and α_1-acid-glycoprotein at a micro liquid|liquid interface". Paula Lopes and Ritu Kataky, *Anal. Chem.*, **2012**, 84 (5), 2299–2304.

"Chiral detection at liquid|liquid interface" Ritu Kataky and Paula Lopes; *Chem. Comm.*, **2009**, 1490-1492.

"Chiral resolution of (R)- and (S)-1-phenylethanol on glassy carbon electrodes" R. Kataky, L. Murphy, A. Delcourt-Lançon, S. Kalakunta and P. Lopes, *Electroanal. Chem.*, **2009**, 663, 57-62.

Oral presentations

"Probing chirality electrochemically", 42nd IUPAC congress, 2-7 August 2009, Glasgow UK.

"Binding of chiral biomolecules at a micro liquid|liquid interface", Electrochem 2011, 5-6 September 2011, Bath UK.

Poster presentations

"Electrochemical chiral sensing at liquid|liquid interface", Analytical Research Forum (ARF) 2008, 21-23 July, Hull University, UK.

"Electrochemical chiral sensing at liquid|liquid interface by modified cyclodextrins", ARF 2009, 13-15 July, Kent University, UK.

"Electrochemical method for chiral detection at a micro ITIES", 216th ECS annual meeting, 4-9 October 2009, Vienna, Austria.

"Detection of chiral molecules at a micro liquid|liquid interface", 61st ISE annual meeting, Nice, France.

"Detection of potassium and chiral discrimination of drugs at a liquid|liquid interface", 9th ISE spring meeting, 8-11 May 2011, Turku, Finland.

Awards

Poster prize at Electrochem. 2009 with the poster entitled "Chiral detection by modified cyclodextrins at liquid-liquid interface".